



This work is protected by copyright and other intellectual property rights and duplication or sale of all or part is not permitted, except that material may be duplicated by you for research, private study, criticism/review or educational purposes. Electronic or print copies are for your own personal, non-commercial use and shall not be passed to any other individual. No quotation may be published without proper acknowledgement. For any other use, or to quote extensively from the work, permission must be obtained from the copyright holder/s.

MECHANISMS OF SHEAR ZONE DEFORMATION

Peter Richard Attfield, B.Sc.

Thesis submitted in accordance with the requirements of the
University of Keele for the degree of Doctor of Philosophy.

December 1988.



IMAGING SERVICES NORTH

Boston Spa, Wetherby
West Yorkshire, LS23 7BQ
www.bl.uk

The following has been excluded at the request of the university:

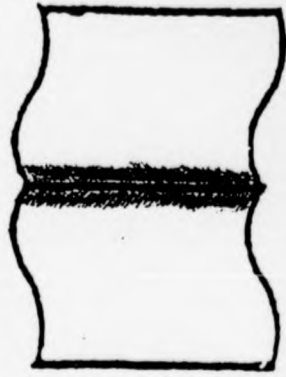
Fig 1.5 (after pg 13)

Fig 1.10 (after pg 31)

Please contact the university for further information.

THIS VOLUME HAS A

VERY TIGHT BINDING



ABSTRACT

The accommodation of displacement within discrete zones of ductile deformation is a feature of many metamorphic rocks. The mechanisms by which the deformation becomes concentrated within these shear zones, as opposed to being equally distributed throughout the rock, are the subject of this study.

A model is presented based on the analogy of a brittle crack propagating in an elastic medium. This is then used to define the stress field around the tip of a propagating ductile shear zone. The patterns of stress, strain and the resulting stress release at the tip are examined. The consistency of the model is investigated by determining the ratio of driving stress to stress release at the tip. The model predicts that shear zones will only propagate in materials where the power (n) to which the stress is raised is ≤ 3 . Using this conclusion it is possible to determine the interrelationships between the temperature, propagation velocity, length and applied stress for the shear zone.

The model is then developed to include displacement on the zone and the orientation of foliation around the tip. It is found that variations in propagation velocity are required to accommodate changes in the shear zone length and changes in rheology.

The model is then applied to examples of shear zones from the Lewisian and estimates of propagation velocity and applied stress are obtained for specific shear zones. Conclusions from the model regarding increased displacement associated with higher temperatures are confirmed from the fieldwork, and it is concluded that the displacement/width ratio is a function of the local P/T conditions. It is proposed that the majority of shear zones develop by propagation

but an element of localization is necessary in the initial stages. The nature of this nucleation event is of importance in determining the final dimensions of the shear zone.

Acknowledgements

This study was carried out during the tenure of a N.E.R.C. research studentship at the University of Keele. I would like to thank all members of the Department of Geology for their help during the last "few" years.

The work was supervised by Dr R.G.Park and Prof. N.J.Kusznir who both gave invaluable guidance. Special thanks must also go to Dr M.G.Norton and Dr T.G.Blenkinsop for help developing the model and Dr A.W.Shelton without whose help and encouragement this thesis would never have been written. Thanks too to the technical staff of the department for photographic work, thin sections and all the general backup they have provided.

I am deeply indebted to all the research students, past and present, for providing continual distractions, entertainment and discussion on all subjects. Many thanks too to Malcolm et al. at the Park Inn, Burslem for providing employment and liquid inspiration for the past six years.

Finally thanks to my parents and parents-in-law for financial and moral support and, most of all, to Liz for putting up with me.

CONTENTS

CHAPTER 1

1.I	Introduction	1
1.I.1	Aims and methods of this study	1
1.II	Literature review	2
1.II.1	Shear zone: a definition	2
1.II.2	General aspects of shear zones	3
1.II.2.a	Occurrence of shear zones	3
1.II.2.b	Fabrics in shear zones	4
1.II.2.c	Shear zone networks	5
1.II.2.d	Rock types associated with shear zones	6
1.II.2.e	Strain states in shear zones	7
1.II.3	Deformation mechanisms	9
1.II.3.a	Factors affecting rock deformation	9
1.II.3.b	Flow laws	10
1.II.3.c	Steady state creep	11
1.II.3.d	Rheological parameters	13
1.II.4	Localization of deformation	14
1.II.4.a	Instability and localization	14
1.II.5	Strain softening (s.l.)	16
1.II.5.a	Geometrical softening	16
1.II.5.b	Structural softening	18
1.II.5.c	Strain softening (s.s.)	19
1.II.5.d	Strain rate softening	20
1.II.5.e	Shear heating	20
1.II.5.f	Other strain softening mechanisms	22

1.II.5.g	The relative importance of the strain softening mechanisms	24
1.III	Previous models of shear zone formation	25
1.III.1	Localization versus propagation	25
1.III.2	Localization models	26
1.III.2.a	Shear heating models	26
1.III.2.b	Other localization models	33
1.III.3	Propagation models	36
1.III.4	Conclusions	41
 CHAPTER 2		
2.I	Introduction to fieldwork	43
2.I.1	Objectives of the fieldwork	43
2.II	The Canisp Shear Zone	43
2.II.1	Introduction	43
2.II.1.a	History of research	43
2.II.1.b	Aims of the present study	45
2.II.2	General description and structural setting	45
2.II.3	Description of rock types	46
2.II.3.a	The gneisses	46
2.II.3.b	The intrusive bodies	51
2.II.4	Description of structures and tectono- metamorphic history	54
2.II.5	Discussion	61
2.III	The small scale shear zones	62
2.III.1	Introduction	62
2.III.1.a	Aims and objectives	62

2.III.1.b	Methods of approach	62
2.III.2	The data	63
2.III.2.a	Methods	63
2.III.2.b	Description of selected zones	64
2.III.2.c	Limitations of the data	72
2.III.3	Summary of results and discussion	73
2.IV	Conclusions	75
2.IV.1	Fieldwork: conclusions and relevance to modelling	75

CHAPTER 3

3.I	The crack tip analogy model	78
3.I.1	Reasons for this approach	78
3.I.2	The crack tip analogy: fundamental theory and assumptions	78
3.I.3	Strain distribution	84
3.I.4	Self consistency test of the model	87
3.I.5	The importance of the factor n	88
3.II	The pre-multiplier relationships	89
3.II.1	Derivation of the pre-multiplier relationships	89
3.II.2	The interrelationship equations	91
3.III	Results and conclusions	92
3.III.1	Results from the interrelationship equations	92
3.III.2	Discussion and conclusions	95

CHAPTER 4

4.I	Development of the model	97
-----	--------------------------	----

4.I.1	Introduction	97
4.I.2	Strain distribution	97
4.I.2.a	Initial theory	97
4.I.2.b	The effect of the boundary conditions	98
4.I.2.c	The effect of rheological change	100
4.I.2.d	Theoretical foliation orientations	101
4.I.3	Displacement fields	102
4.I.3.a	Initial theory and assumptions	102
4.I.3.b	The effect of the boundary conditions	103
4.II	Application of the model	104
4.II.1	Theory and methods	104
4.II.1.a	Problems of application	104
4.II.1.b	Theory of application	105
4.II.2	Application to zones from the NW Highlands	106
4.II.2.a	The stress/temperature/propagation velocity diagrams	106
4.II.2.b	Comparison of strain profiles	109
4.II.2.c	Foliation orientations	110
4.III	Conclusions	111
 CHAPTER 5		
5.I	Conclusions	113
5.I.1	Initiation	113
5.I.2	Localization versus propagation	113
5.I.3	Relationships between the boundary conditions	114
5.I.4	The importance of the factor n	114
5.I.5	Variation in propagation velocity	114

5.I.6	Application to natural examples	115
5.I.7	Final size and displacement	115
5.I.8	Displacement/width relationships	116
5.I.9	Tip zones	116
5.I.10	Justification of the approach to modelling	117
5.II	Limitations	117
5.II.1	Limitations of the approach	117

References

Appendices

CHAPTER 1

1.1 INTRODUCTION

1.1.1 Aims and methods of this study.

The aim of this study is to present a model for the development and propagation of shear zones. Natural examples of shear zones from the N.W.Highlands of Scotland were studied in order to evaluate the relative importance of the controls on shear zone morphology and development. From the field data and the literature, factors critical to the initiation of shear zones were isolated so that these could be incorporated and tested in a model. The question as to whether shear zones localize on pre-existing material heterogeneities, or propagate in a direction controlled by the local stress field was examined. The conclusions drawn from the field evidence were then used as the basis for a model, which could be used to examine the relationships between the controlling factors for shear zone development, and establish a range of conditions that would favour shear zone propagation.

The structure of this thesis is chronological in that it follows the order in which the work progressed. Firstly a literature review of recent work on shear zones and their development is presented, this is followed by a description of the field work undertaken and the conclusions drawn from it. The field work is in two distinct sections, a description of a major shear zone in the Lewisian of the N.W.Highlands of Scotland, and then the work done on a data set of over fifty small (cm-scale) shear zones from the mainland Lewisian outcrop. The questions and constraints arising from the field studies are incorporated into the computer model described in the latter part of the thesis. The model presented uses a crack tip analogy for shear

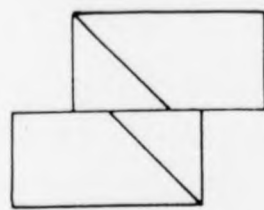
zone development and demonstrates the interrelationships between shear zone length, applied stress, ambient temperature, and propagation velocity. The effects of rheology are also shown. The conclusions drawn from the model and their relationship to the field data is discussed in the last chapter. The computer programmes used for the model are presented in the appendices.

1.II LITERATURE REVIEW

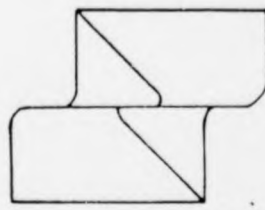
1.II.1 Shear zone: a definition.

Prior to any discussion of shear zones, a working definition of the term must be established. Shear zones are approximately tabular regions of heterogeneously high strain due to dominantly simple shear deformation, in which ductile deformation mechanisms have predominated at the grain scale. They mark areas that have undergone localized strain softening, the degree of which depends on the mechanical properties of the rock (White, et al. 1980, Norton 1982). Ramsay (1980) extends the term to include brittle faults and makes a three-fold division into brittle shear zones, brittle-ductile shear zones and ductile shear zones (Fig 1.1). Cataclasis is a ductile mechanism on the scale of a fault zone, but the term "shear zone" implies continuous deformation and so it is considered inappropriate in the description of faulting.

Fig 1.1



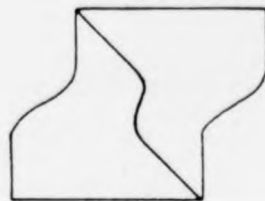
a. brittle



b. brittle-ductile



c. brittle-ductile



d. ductile

Fig 1.1 Subdivision of shear zone types. After Ramsay (1980).

1.II.2 General aspects of shear zones.

1.II.2.a Occurrence of shear zones.

Shear zones occur on all scales from sub-microscopic shear bands and slip planes in metals, up to major zones of intense deformation tens of kilometres wide. They are a characteristic feature of rocks deforming in a ductile manner where there is no mechanically active layering present likely to lead to buckling (Norton 1982). Thus crystalline rocks tend to favour the development of shear zones, and as a result most recent publications deal with shear zones in either igneous or metamorphic rocks.

The major shear zones in the Archean and Proterozoic rocks of Greenland have been described by Bak *et al.* (1975), Escher *et al.* (1975) and Grocott & Watterson (1980). Other major zones in metamorphic terrains have been described, for example, the South Armorican Shear Zone (Jegouzo 1980), the shear zones in the Precambrian of Southern Africa (Coward 1980) and the major shear zones in the Lewisian of N.W.Scotland (Beach 1973; 1976; 1980, Coward & Park 1987, Attfield 1987). Work on smaller shear zones, centimetre to metre scale, has been restricted mainly to igneous rocks, for example, Ramsay & Graham (1970), in meta-gabbro and granite, Burg & Laurent (1978), granodiorite, Ramsay & Allison (1979), granitic basement and Simpson (1980), in granite.

Shear zones have also been reported from sedimentary rocks, (Ramsay & Graham 1970, Knipe & White 1979). Here the shear zones are of the "en-echelon tension-gash" type corresponding to the brittle-ductile type C of Ramsay (1980) (Fig 1.1), and occur in folded, massive limestone and sandstone units.

1.11.2.b Fabrics in shear zones.

The use of crystallographic fabrics and their relation to deformation within shear zones, has been studied in detail by Lister & Williams (1979), who conclude that the kinematic framework controls the orientation of crystallographic fabrics developed in plastically deformed quartzites. Burg et al. (1986) used ice deformation experiments to show that crystallographic orientation is due to the reorientation of grains for easy slip and continuing dynamic recrystallization. Asymmetric quartz c-axis patterns allow determination of the movement sense of a shear zone, but the pattern of preferred orientations is sensitive to the closing stages of deformation. Thus the relationship of fabrics to early shearing episodes must be viewed in the light of any subsequent deformation. The asymmetry of intensity distribution is less susceptible to modification than the asymmetry of the fabric distribution, and so may be used to determine shear sense in rocks that have undergone subsequent co-axial deformation. The problems associated with crystallographic fabric analysis in shear zones are related to the initial population of grain orientations and the influence of recrystallisation and grain growth. There is also the problem of scale, extrapolating from a few hundred grains to the bulk deformation. It is possible that the individual quartz grains could be subjected to a dominantly co-axial deformation, whereas the overall bulk deformation is progressive simple shear (Lister & Williams 1979).

Several authors have used quartz c-axis patterns to determine movement sense on shear zones, for example, in the Central Himalayas (Boucher & Pecher 1976), and in the Canisp Shear Zone in the Lewisian of N.W.Scotland (Jensen 1984). C-axis patterns have also been used to measure strain (Laurent & Etcheocopar 1976) and to infer the strain state in shear zones (Johnson 1967). The use of the technique in this

way causes problems in interpretation, due to the tendency of quartz fabrics to reflect the closing stages of deformation. The problem of the rotation of early fabrics and their deformation history must be taken into account to obtain a full understanding of the observed phenomena.

1.II.2.c Shear zone networks.

Shear zones developing in an isotropic rock tend to form anastomosing networks of high strain zones enclosing blocks or "augen" of relatively low strain. This general principle breaks down when the form of the zone is controlled by pre-existing features within the rock, such as dyke boundaries (Escher et al. 1975), or isolated thrust planes.

Shear zone networks occur on all scales from a few metres (Coward 1976, Ramsay & Allison 1979, Mitra 1979), up to several hundreds of metres (Sibson 1977, Attfield 1987), and there are several theories on their possible origins. Coward (1976) considers the tendency to form networks as evidence for the non-planar propagation of shear zones, and proposed that the relationship between propagation velocity and displacement rate dictated the degree of curvature (see 1.III.3). Sibson (1979) considers that small-scale material inhomogeneities, such as metabasite pods, within the gneisses of the Outer Hebrides Thrust Zone, have led to the "mesh structure" present there. Flinn (1977) suggests that the need to accommodate large-scale asperities or fault zone curvature accounts for the network associated with the Walls Boundary Fault in Shetland. Mitra (1979) has proposed that shear zone networks develop due to conjugate sets of shear zones becoming progressively rotated into sub-parallelism and thus coalescing.

It is possible for two or more sets of shear zones with different senses of movement to develop simultaneously in an area, and thus form a continuous network. Coward (1976) and Mitra (1979) have both suggested that the zone may then deform by a block-sliding mechanism analogous to grain boundary sliding on a micro-scale.

An understanding of the way in which shear zone networks develop is of considerable significance to the study of the propagation and kinematics of these zones, and the way in which they can accommodate large displacements.

1.II.2.d Rock types associated with shear zones.

The dominant rock type found in shear zones is mylonite, although in some areas of higher metamorphic grade, schists are the product of shear zone activity (Teall 1885), or gneisses in high-grade areas where igneous rocks are deformed. Since the term mylonite was introduced by Lapworth (1885) it has been the subject of major controversy amongst geologists, mainly due to a recent change in the understanding of the deformation mechanisms responsible for mylonite formation. The initial use of the term implied grain size reduction by brittle processes and the recrystallized texture of many mylonites was thought to be due to post-tectonic grain growth of the "milled" fragments. Recent studies have shown however that the recrystallization was syntectonic (Bell & Etheridge 1973, Lister et al. 1977). This led to a clear division between cataclasites, where grain refinement was by cataclastic processes, and sliding and rotation of the fragments, and mylonites, where recrystallization was the dominant mechanism and ductile processes predominated. Sibson (1977) presents a terminology which has no genetic connotations and which is still probably the most widely accepted.

The change in rock chemistry within a shear zone was first noted by Teall (1885) who recorded an increase in silica and Fe_2O_3 . Beach & Fyfe (1972) and Beach (1973) described large-scale metasomatism in the Laxfordian shear zones at Scourie, N.W.Scotland. Their analyses showed increases in K_2O and H_2O but a decrease in CaO and silica, and they postulated that large volumes of low-pH fluids had moved through the zone, either from the mantle or from the relatively cold Laxfordian granites.

Recent work on shear zone geochemistry has focussed on whether or not the deformation within a shear zone is isochemical. Kerrich *et al.* (1977) described a small shear zone in adamellite from the Swiss Alps and concluded that deformation was both isochemical and isovolumetric. Brodie (1981) reached similar conclusions for a 5m wide zone in metagabbro. Kerrich *et al.* (1980) studied a major shear zone at Mieville, Switzerland, and presented evidence to show that deformation was isochemical and that little or no fluid flow occurred. These studies suggest that the role of fluids in shear zone processes is dependant on the presence of a fluid source, and that not all shear zones act as pathways for fluid migration.

1.II.2.e Strain states in shear zones.

The strain state in shear zones has been the subject of debate in recent years. In particular the relative importance of pure-shear versus simple-shear. This question is fundamental to an understanding of the formation of shear zones.

Initially it was thought that the strain state in shear zones was one of heterogeneous simple shear (Ramsay & Graham 1970, Ramsay 1980), but recent evidence suggests that there is a component of pure shear present in most zones. Coward (1976) relates the initial propagation episode to pure shear, but with simple shear becoming

dominant immediately after. However Goldstein (1980), using magnetic susceptibility anisotropy on the Lake Char mylonites, considered the propagation event to be associated with simple shear and the later stages to be related to a flattening deformation. Johnson (1967) considered mylonite foliation to be analogous to slaty cleavage and thus best represented by heterogeneous flattening, whereas Ross (1973) used the evidence of symmetry of deformation inside and outside the zones of high strain to postulate a pure shear mechanism. More recently Bell (1981) has again suggested that heterogeneous flattening is the dominant deformation mechanism. It is apparent from these studies that the relative importance of pure-shear and simple-shear mechanisms must vary between individual zones. This is particularly the case when a shear zone is localized on a pre-existing material heterogeneity; here the initial orientation of the zone with respect to the local stress field will govern the dominant strain mechanism.

The measurement of strain profiles across shear zones is normally carried out under the assumption of heterogeneous simple shear. The first study of this type was done by Ramsay & Graham (1970) who showed that strain profiles could be used to calculate the displacements on shear zones (Fig 1.2). Most of the strain profiles published by Ramsay & Graham (*op. cit.*) and Ramsay & Allison (1979), show a normal distribution of strain across the zone, whereas more recent publications (Watterson 1979) tend to show flat-topped profiles as being more prevalent. The 13 Km-long strain profile across the Ikertoq shear belt in West Greenland (Grocott & Watterson 1980) shows a very irregular distribution of strain, with a succession of low and high-strain zones. This may however be partly due to the class system used for determining strain. Strain profiles across a zone are not always symmetrical and this is obviously the case with shear zones developed along lithological boundaries (Bell & Etheridge 1976). The

Fig 1.2

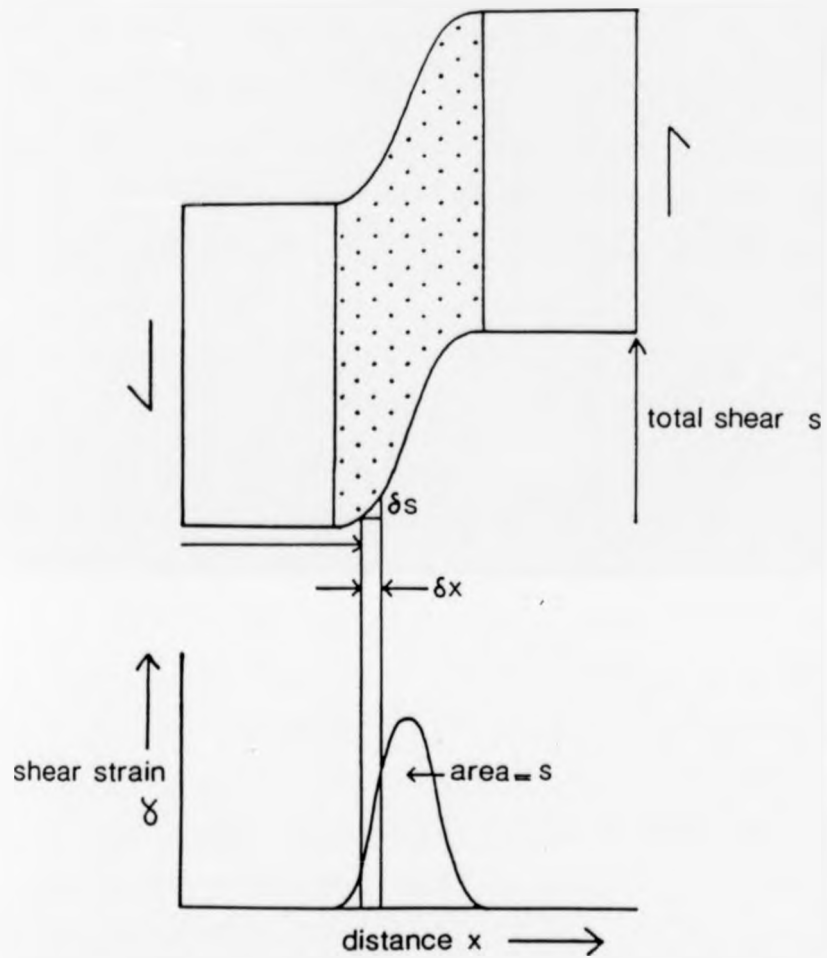


Fig 1.2 Calculation of displacement from a shear zone strain profile by summation of small elements δs . After Ramsay & Graham (1970).

accuracy of any strain profile is dependent on the method used to measure strain, and as not all shear zones conform to the ideal parallel-sided slab of heterogeneously high strain, inaccuracy of measurement can be substantial. Also the work of Burg *et al.* (1986) on polycrystalline ice shows that the shape fabric of recrystallised grains does not correspond to the theoretical foliation, and therefore estimates of strain from mineral grain orientation are unreliable in high-temperature shear zones.

1.II.3 Deformation mechanisms.

1.II.3.a Factors affecting rock deformation.

Studies of the behaviour of solid materials at particular pressures, temperatures and applied stresses, were first carried out using ice. This enabled experiments to be conducted either under laboratory conditions (Glen 1953) or in the field (Gerrard *et al.* 1952). The object of these studies was to relate strain rate to the applied stress with an equation of the form:

$$\dot{\epsilon} = f(\sigma) \quad (1.1)$$

where: $\dot{\epsilon}$ - is the strain rate

σ - is the applied stress

Measurements of strain from natural rocks in laboratory experiments show that large volume changes are rare and the effects of lithostatic stress are not highly significant in terms of deformation. This means that that only the deviatoric components of stress and strain need be considered (Brun & Cobbold 1980). Other factors that will affect the flow properties of a rock are the ambient temperature

and the rheological properties of the rock itself, ie. grain size, mineral composition, degree of order, state of imperfection, homogeneity and anisotropy (Heard 1976). Most laboratory studies have been confined to monomineralic samples, either polycrystalline aggregates (Post & Griggs 1973) or single crystals (Kohlstedt *et al.* 1976) such simplifications remove most of the rheological variables.

1.II.3.b Flow laws.

There are three principal types of creep observed in laboratory tests (Fig 1.3) (Weertman & Weertman 1975). The large scale movement and multiplication of crystal dislocations occurs above a critical stress σ_c given by:

$$\sigma_c = \mu b \sqrt{\rho} \quad (1.2)$$

where: μ - is the shear modulus

b - is the length of the burgers vector of crystal dislocations

ρ - is the dislocation density prior to stress application

(i) Low temperature creep:- $T < T_m/3$ (T_m = melting temperature)

In this state the dislocations within crystals move only in their glide planes, there is very little dislocation climb perpendicular to the glide planes, as diffusional processes are too slow at low temperatures.

(ii) High temperature creep:- $T > T_m/3$

At values of σ above σ_c dislocation climb becomes important and there may be recovery due to dislocations of opposite sense moving towards each other and being annihilated. A steady state is reached when the production of dislocations is equal to the rate at which they

Fig 1.3

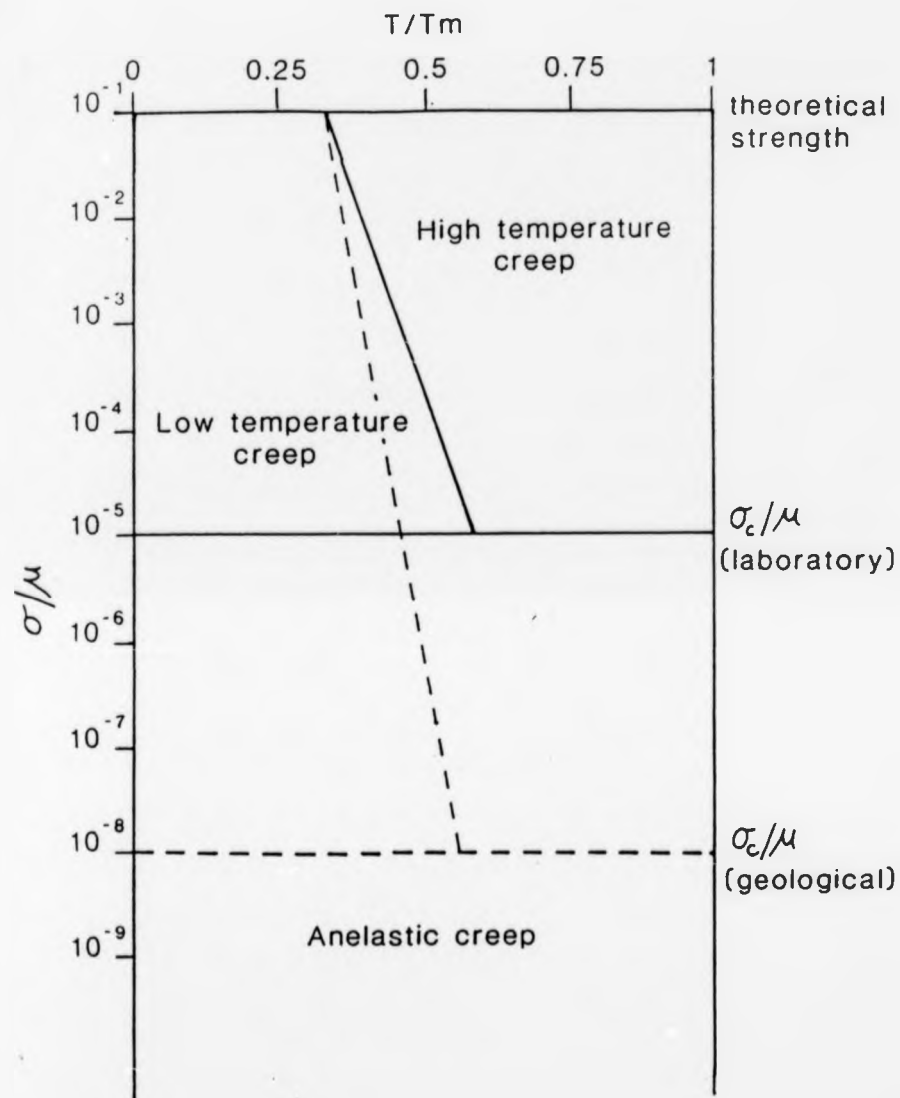


Fig 1.3 Creep diagram for the three principal types of creep. T/T_m - homologous temperature, σ/μ - normalized stress. Solid lines are for laboratory experiments, dashed lines for geological strain rates. After Weertman & Weertman (1975).

cancel each other, so creep rate $\dot{\epsilon}$ does not vary with time. Before the steady state is reached there is a transient creep phase where $\dot{\epsilon}$ varies with time. If the material had a low initial dislocation density the creep rate accelerates; if the initial dislocation density was high then the creep rate will decelerate (Fig 1.4).

(iii) Anelastic creep.

This type of creep is recoverable, ie. if the stress is removed then the creep decreases in value to zero.

1.II.3.c Steady state creep.

For geological purposes steady state creep (see (ii) above) is the most important, this can be accomplished by several mechanisms, which are summarised here.

Power law creep (dislocation creep).

This type of steady state creep can be controlled either by the glide velocity of dislocations or by dislocation climb. For glide controlled creep the general equation is of the form;

$$\dot{\epsilon} = \alpha (D/b^2) \cdot (\mu\Omega/kT) \cdot (\sigma/\mu)^3 \quad (1.3)$$

where α - is a dimensionless constant

D - is the diffusion constant

b - is the length of the Burgers vector

μ - is the shear modulus

Ω - is the atomic volume

Fig 1.4

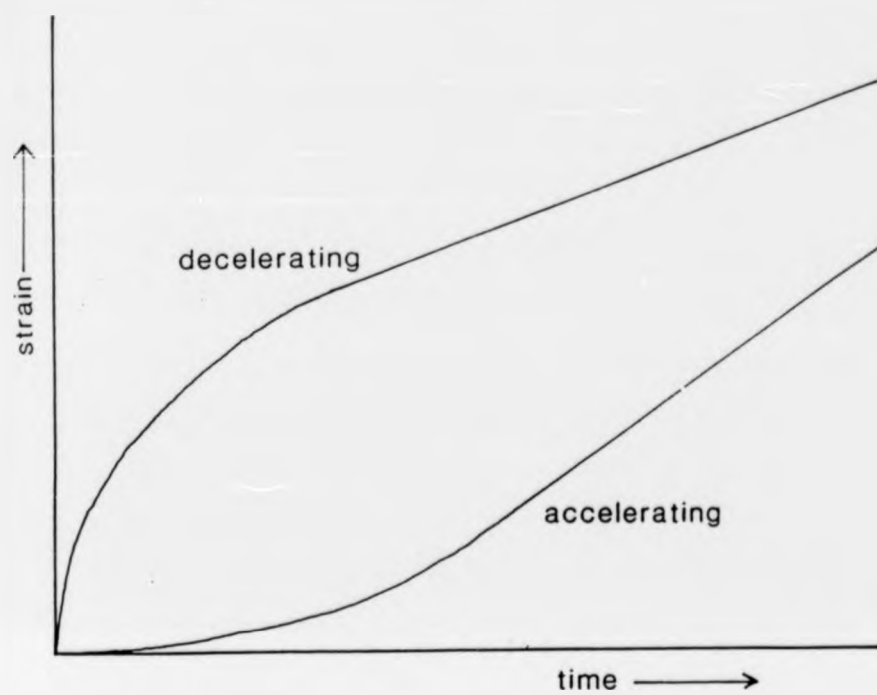


Fig 1.4 Schematic creep curves for strain versus time for transient creep. After Weertman & Weertman (1975).

k - is Boltzman's constant

T - is temperature

If creep is controlled by dislocation climb the general equation is;

$$\dot{\epsilon} = \beta (D/b^{3.5} M^{0.5}) \cdot (\mu\Omega/kT) \cdot (\sigma/\mu)^{4.5} \quad (1.4)$$

where M - is the number of dislocation sources per unit volume

β - is a dimensionless constant

Nabbaro-Herring creep.

This is steady state creep due to the diffusional mass transport of atoms across grain boundaries and has the general equation;

$$\dot{\epsilon} = \gamma (D/L^2) \cdot (\sigma\mu/kT) \quad (1.5)$$

where L - is the average grain diameter

γ - is a dimensionless constant

(Weertman & Weertman 1975)

Coble creep (grain size sensitive creep)

The grain-size sensitivity of creep under certain conditions is due to the fact that fully recrystallised small grains are softer than the coarse-grained starting material at certain differential stresses (Goetze 1978). Schwenn & Goetze (1977) presented an equation of the form;

$$\dot{\epsilon} = \delta \cdot \sigma \cdot G_s^{-3} \exp(-Q/RT) \quad (1.6)$$

where δ - is a dimensionless constant

G_s - is the grain size

Q - is the activation energy

R - is the Gas Constant

The effects of temperature and pressure on power-law creep and Nabarro-Herring creep are governed by the diffusion co-efficient (D) in equations 1.3, 1.4 & 1.5. For material containing only one atomic species the diffusion co-efficient is given by;

$$D = D_0 \exp(-Q/kT) \exp(-PV/kT) \quad (1.7)$$

where P - is hydrostatic pressure

D_0 - is a constant

V - is the activation volume for diffusion

(Weertman & Weertman 1975)

These deformation laws have been linked by Stocker & Ashby (1973) to form deformation maps relating temperature and shear stress for the conditions of operation for each type of creep mechanism (Fig 1.5).

1.II.3.d Rheological parameters.

Most recent studies of creep measurement in rocks have used a power-law type flow law of the form;

$$\dot{\epsilon} = A \exp(-Q/RT) (\sigma_1 - \sigma_3)^n \quad (1.8)$$



Fig 1.5 Deformation map for olivine, the narrow lines are for different values of strain rate. From Stocker & Ashby (1973).

where A & n are material constants

The parameters A, Q and n are determined experimentally for any given rock type or mineral. Table 1.1 gives recently published values for a variety of rheologies. Some studies however have shown that these constants may vary with temperature. Franssen *et al.* (1987) record a decrease from 6 to 2 for n at temperatures of 400°C and 550°C respectively, for experiments using polycrystalline halite in simple shear. Such examples however are scarce and models must rely on the available published data. R, the Universal Gas Constant, is 1.98 cal/K° and temperature is the absolute temperature in K°. In order to study the stress release resulting from strain in a rock it is necessary to know the Young's Modulus (E) of the material, values of which are given in table 1.2.

1.II.4 Localization of deformation.

1.II.4.a Instability and localization.

Shear zone formation is dependent on the initiation of a discrete zone of high strain. This can be achieved either by localization of the deformation due to initial inherent material heterogeneities or by the deformation becoming formally unstable. The onset of instability can be defined as the loss of load-carrying capacity under constant strain rate, or by the negative slope of the stress-strain curve (Bowden 1970).

Bowden (*op. cit.*) developed a model for localization of deformation, in which the material has a certain volume fraction (F) of embryonic bands whose strain was "fortuitously" larger than the matrix by $\Delta\epsilon$. The model can be demonstrated by examining a portion of the flow stress surface shown in Fig 1.6 projected onto a surface in the plane of strain-strain rate (Fig 1.7). The starting points (b =

Fig 1.6

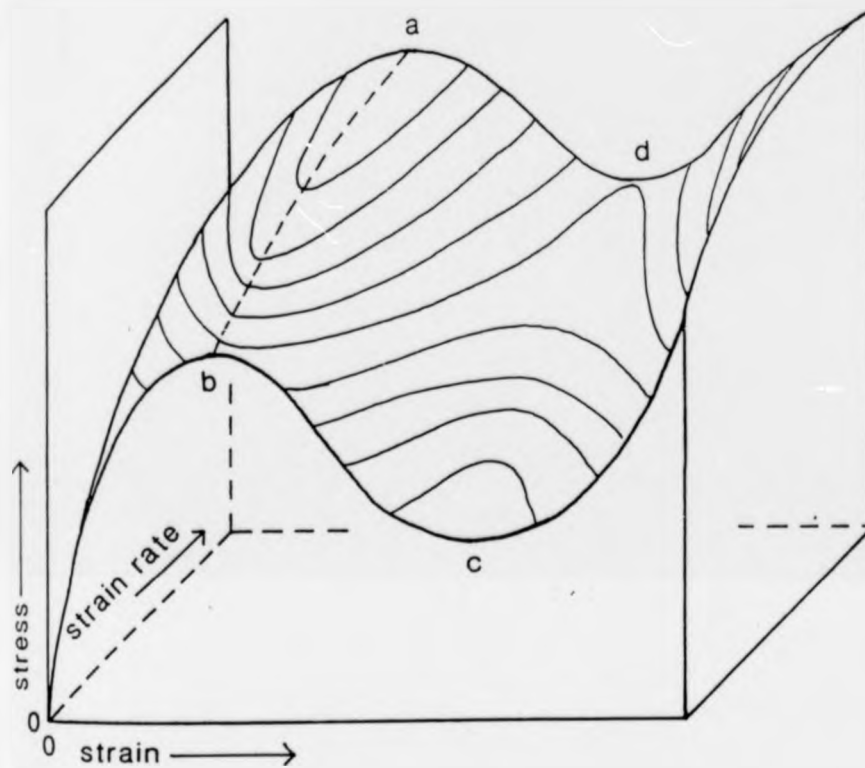


Fig 1.6 Flow stress surface in stress, strain, strain rate space, the portion of negative slope is labelled a,b,c,d. After Bowden (1973).

Fig 1.7

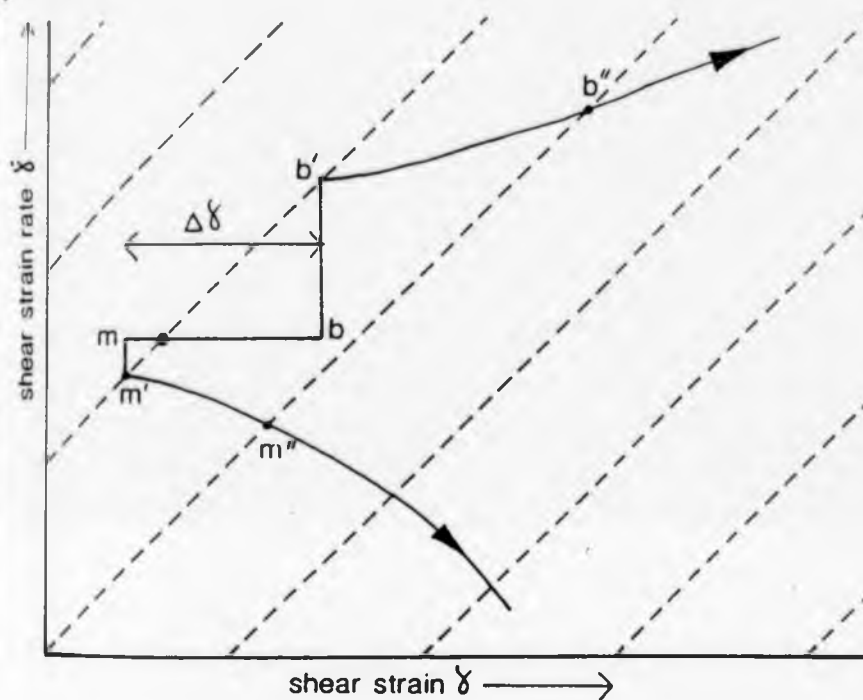


Fig 1.7 A portion of the negative slope region in fig 1.6 viewed in the strain, strain rate plane, showing the divergence of strain rate between the bands (b) and matrix (m) after an initial strain perturbation $\Delta\gamma$. The dashed lines are stress contours and the stress gradient is assumed to be constant. After Bowden (1973).

TABLE 1.1
RHEOLOGICAL PARAMETERS FOR EQUATION 1.8

Rock type	Source	A (Kb ⁻ⁿ s ⁻¹)	Q (Kcal/mol)	n
Polycrystalline Dry Olivine	Carter & Ave'Lallement (1970)	1.2 x 10 ¹⁰	119.8	4.8
	Goetze & Kohlstedt (1973)		140.0	
	Post (1977)	4.3 x 10 ⁸	126	3.0
	Goetze (1978)	7.0 x 10 ¹⁰	122.0	3.0
	Bodine et al. (1981)	7.0 x 10 ¹⁰	122.0	3.0
Polycrystalline Wet Olivine	Zeuch (1983)	3.4 x 10 ¹¹	130.0	3.5
	Post & Griggs (1973)	3.4 x 10 ⁸	93.1	3.18
	Post (1977)	4.3 x 10 ⁸	93.8	3.0
Single Crystal Dry Olivine	Bodine et al. (1981)	7 x 10 ¹⁰	105.0	3.0
	Kohlstedt & Goetze (1974)		126.0	
Diabase	Kohlstedt et al. (1976)		125.0	3.0
	Caristan (1982)	7.7 x 10 ⁴	66.0	3.05
Wet Quartz	Shelton & Tullis (1981)	1.4 x 10 ³	62.0	3.4
	Koch et al. (1980)	4.36	38.2	2.44
Dry Quartz	Koch et al. (1980)	0.126	36.0	2.86
Wet Quartzite	Shelton & Tullis (1981)	11.0	40.0	2.0
	Turcotte & Schubert (1982)	7000.0	55.0	2.6
Dry Quartzite	Turcotte & Schubert (1982)	67.0	64.1	6.5

TABLE 1.1 CONTINUED

Albite	Shelton & Tullis (1981)	151.1	56.0	3.9
Anorthosite	Shelton & Tullis (1981)	820.2	57.0	3.2
Granite	Carter <u>et al.</u> (1981)	1.4×10^{-9}	25.4	2.9

TABLE 1.2

YOUNG'S MODULI FOR SOME ROCK TYPES

Rock Type	Young's modulus (Kb)
Quartz	100.0
Dry olivine	1000.0
Dunite	1500.0
Anorthosite	830.0

Young's Moduli for some dominant minerals in important rock types.
After Turcotte & Schubert (1982).

bands, m = matrix) are a distance $\Delta\gamma$ apart. From there the strain rate of the bands increases instantaneously to b' and the strain rate of the matrix decreases instantaneously to m' such that both b' and m' still lie on the same stress contour. Bowden (1970) then goes on to derive equations for the change in strain rate with strain in both bands and matrix in terms of the initial strain rate, the volume fraction of the bands, the gradient of the stress contours and the initial strain perturbation $\Delta\gamma$. From this it can be shown that for small values of $\Delta\gamma$ the divergence in strain rate between the bands and matrix is small, but with increasing $\Delta\gamma$, the strain rate of the matrix becomes very slow relative to that of the bands, and so the divergence in rate increases.

An alternative for instability due to localization was presented by Poirier (1980) using a general equation for deformation in shear;

$$\frac{(1+n+m) \cdot dM}{M} + \frac{1 \cdot d\tau_0}{\tau_0} + \frac{n}{\gamma} + \frac{m \cdot d\dot{\gamma}}{\dot{\gamma}} - \frac{mQ \cdot dT}{RT} = \frac{1 \cdot d\tau}{\tau} \quad (1.9)$$

where M - is the Taylor factor, which depends on the orientation of the active slip systems.

n - is the strain sensitivity of stress

m - is the strain rate sensitivity of stress

γ - is the shear strain

τ_0 - is the effect of structural changes

$\dot{\gamma}$ - is the strain rate

Q - is the activation energy

R - is the Universal Gas Constant

T - is temperature

τ - is the resolved shear stress

In which the requirement for instability in this equation is that $\frac{d\tau}{d\gamma} \leq 0$

1.II.5 Strain softening (s.l.)

Each term in the general deformation equation (1.9) represents a mechanism of strain softening. This can be defined as a reduction in flow stress at constant strain rate and/or with increasing strain. Stress is usually regarded as constant across an area, so local strain softening is expressed as a variation in strain rate. Using Poirier's (1980) system there are five principal strain softening (s.l.) mechanisms, all of which, apart from shear heating, may also be hardening mechanisms.

- (a) Geometrical softening
- (b) Structural softening
- (c) Strain softening (s.s)
- (d) Strain-rate softening
- (e) Shear heating

1.II.5.a Geometrical softening $\frac{(1+n+m) \cdot dM}{M \quad d\gamma}$

Geometrical softening can be divided into two types, rotation softening and fabric softening.

Rotation softening relates to the bulk anisotropy of the rock, and is only important if the rock contains a strong planar anisotropy. Kink-band formation is thought to be due to the effects of rotation softening, as deformation within the band is accomplished by finite rotation of the foliation, and individual layers undergo little internal strain but slide past one another (Cobbold 1977a). Shear bands in phyllonites and ribbon mylonites (White et al. 1980) only form when a strong planar anisotropy is present and so appear to be the result of rotation softening (Norton 1982).

Fabric softening occurs due to the rotation of the active slip-planes in the constituent minerals towards the orientation in which the resolved shear stress is higher for a constant applied stress (Poirier 1980). This is best envisaged as the increased resolved shear stress for intragranular slip on a given plane as it rotates into parallelism with the shear zone walls, and as the direction of slip rotates into parallelism with the stretching lineation. The extent of fabric softening will depend on the starting fabric and its orientation to the shear plane and shear direction. Dillamore et al. (1979) attributed the formation of shear bands in heavily rolled cubic metals to fabric softening. The number of slip systems available in a material and their relative ease of slip will govern the importance of fabric softening. The more slip systems available, the less important fabric softening will be, assuming they are all of approximately equal ease of movement (Norton 1982). Most geological materials have only one or two dominant slip systems and will therefore favour fabric softening. The data from Burrows et al. (1979) for polycrystalline magnesium gives some indication of the degree of softening possible for a polycrystalline material. The flow stress after softening is independent of temperature but the degree of softening is temperature dependent. This is due to the presence of

more pronounced fabrics at lower temperatures. Fabric softening has been reported in experiments with ice deforming in simple shear (Burg *et al.* 1986). They showed that intracrystalline glide, grain rotation and dynamic recrystallization operate to accommodate the large strains by producing fabrics that favour glide on the basal plane of ice crystals. Grains with an initial orientation that favours glide will rotate towards the shear direction and then become highly elongate. Grains with initial orientations that do not favour glide will undergo irregular rotation and then kink or bend to produce sub-grains and deformation bands, so the microstructure evolves towards a more deformable state. It has been suggested (White *et al.* 1980) that fabric softening is the single most important softening process associated with mylonite formation (see also Williams & Dixon 1982).

1.II.5.b Structural softening

$$\frac{1.d\tau_0}{\tau_0 d\delta}$$

There are three main causes of structural softening, phase transformations, metamorphic reactions and dynamic recrystallization; these may all lead to the production of softer more deformable phases and/or more deformable grains.

Phase transformation can lead directly to the production of a weaker phase, eg. α -quartz to β -quartz (Norton 1982), or alternatively, volume changes can occur due to the production of a more or less dense phase with associated weakening of the material.

Metamorphic reactions can soften a material by producing a new mineral with a smaller grain size. This will lead to an increase in grain boundary sliding and in addition diffusive mass transfer processes such as Nabarro-Herring creep and Coble creep will be enhanced. The new grains produced by such a metamorphic reaction will also be soft strain-free grains and hence more easily deformed.

Metamorphic reactions can also change hard phases such as feldspar to weaker assemblages such as quartz and sericite (White *et al.* 1980). If the reaction is concurrent with deformation then there is a weakening effect due to "transformational superplasticity" (White & Knipe 1978, Dixon & Williams 1983). This is due to the stresses and strains associated with volume changes and the increased diffusion rates during reaction. Dehydration reactions can liberate lattice-held water thus increasing pore fluid pressure and reducing the effective stress, and so assist deformation (Williams & Dixon 1982).

Dynamic recrystallization also produces small strain-free grains which soften the material due to increased grain boundary sliding and diffusive mass transfer processes. Dynamic recrystallization is favoured by higher temperatures (Burg *et al.* 1986, Fransen *et al.* 1987), and can start at strains as low as 2-3%. It also prevents strain hardening of the material by the build up and tangling of dislocations in "old" grains. The data of Burrows *et al.* (1979) includes a degree of dynamic recrystallization, but this is probably of less significance than the geometrical softening.

1.II.5.c. Strain softening (s.s.) $\frac{n}{\gamma}$

This occurs when n , the strain sensitivity of stress, is less than zero. This is unlikely to be common but there may be some true strain softening in the early stages of deformation caused by the avalanching of dislocations that were pinned by impurities, and allowing entangled dislocations to pass (Norton 1982). Strain softening (s.s.) is favoured by very high temperatures and large stresses when $n \rightarrow 0$ as the material behaves as an ideally plastic solid, so that even if no strain softening (s.s.) occurs, n is not appreciably larger than zero and so there is no strain hardening

(Poirier 1980).

1.II.5.d. Strain-rate softening $\frac{m \cdot d\dot{\gamma}}{\dot{\gamma} d\delta}$

The value of m , the strain rate sensitivity of stress, is important in that for values of $m < 1$ localization of deformation is more likely. But the strain rate softening term is always positive and therefore represents strain hardening which must be balanced out by the other terms in equation 1.9. Weijmars (1987) however considers that a type of strain-rate softening is important in the deformation of the Palomares shear zone in Spain. He states that strain-rate softening could result from structural and thermal softening and uses this to explain variations in effective viscosity within the zone. This however appears to be a sort of "secondary" strain-rate softening, resulting from shear heating and structural softening, rather than "true" strain-rate softening as defined by Poirier (1980).

1.II.5.e. Shear heating $\frac{-mQ \cdot dT}{RT^2 d\delta}$

Shear heating is the result of the conversion of mechanical energy into heat during progressive deformation, and its effect is always to soften a material. The relative importance of shear heating in the overall strain softening equation is largely dependent on the size of the shear zone. In small shear zones the small amount of heat produced is quickly conducted away by the surrounding rock and so temperatures within the zone do not increase significantly. In large continental shear zones however, such as the deep levels of transcurrent faults and possibly along the base of large thrust sheets, shear heating is probably of major significance (Brun & Cobbold 1980).

The effect of shear heating has been widely used in the modelling of shear zone development, eg. Yuen *et al.* (1978), Flietout & Froideveaux (1980) and Lockett & Kusznir (1982). The general equation for shear heating is given by Yuen *et al.* (1978) and Brun & Cobbold (1980), for a steady state ie. $\frac{dT}{dt} = 0$

$$K \frac{d^2T}{dy^2} + \sigma_s^{(n+1)} \cdot (2A/T) \cdot \exp(-Q/RT) = 0 \quad (1.10)$$

where K - is the thermal conductivity

T - is the temperature

y - is the distance from the centre of the shear zone perpendicular to the walls

σ_s - is the applied stress

R - is the Universal Gas Constant

n, A and Q are rheological constants (see 1.II.3.)

Solutions to this equation (Yuen *et al.* 1978, Schubert & Yuen 1978) have identified three branches on the shear stress / shear rate graph (Fig 1.8). The cold or subcritical branch, the intermediate or supercritical branch and the hot branch. On the cold branch heat production is negligible until at a certain critical value of shear-rate, heat is produced faster than it can be conducted away, the material softens and there is a resulting drop in shear stress. Beyond another critical value the term $(2A/T) \cdot \exp(-Q/RT)$ tends to a limiting value and stress starts to rise again with shear rate.

Geological evidence for shear heating is not abundant. Lockett & Kusznir (1982) show that temperatures achieved in constant velocity shear zone models should be sufficient for partial melting to occur. The association of diapiric granites with shear zones has been used as

Fig 1.8

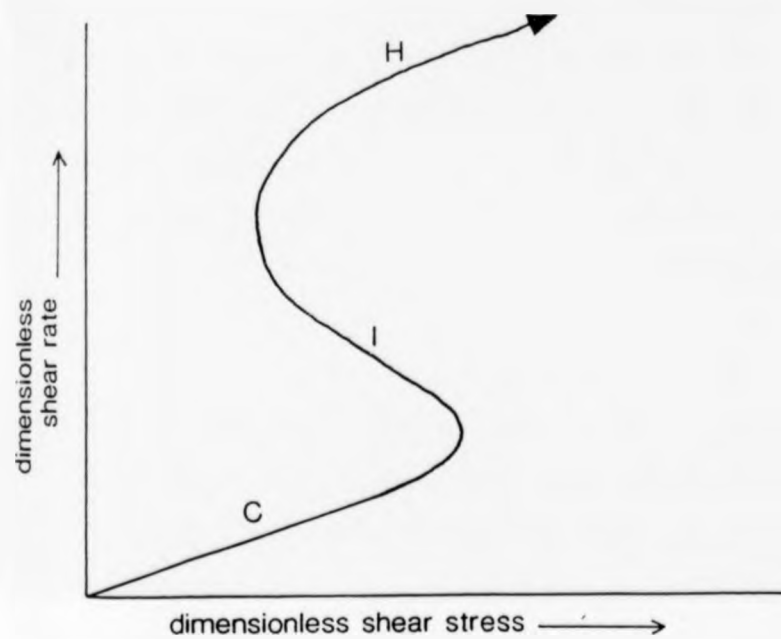


Fig 1.8 Sketch of the steady state solution for shear heating models.
C - cold or subcritical branch, I - intermediate or supercritical
branch, H - hot branch. After Brun & Cobbold (1980).

evidence to demonstrate partial melting in shear zones (Brun & Cobbold 1980), but Poirier et al. (1979) have argued however that the presence of rising plutons would thermally soften the host rock sufficiently to allow localization of a major shear zone, so the evidence is equivocal. The widening of shear zones with depth (Bak et al. 1975) has also been attributed to shear heating effects and successfully modelled by Lockett & Kusznir (1982). There is very little evidence for shear heating in small (<100m) shear zones and this agrees with the predictions from the theory. Brun & Cobbold (1980) calculated the critical widths for shear zones deforming by shear heating and concluded that "thermal runaway" was only possible for zones of 1km or more in width, or for very high differential stresses (>1Kb) which are unlikely under geological conditions. Slight shear heating may be of importance when the shear zone is operating at a temperature just below that of a critical phase change or metamorphic reaction, it could also assist dynamic recrystallization and hence enhance the effects of structural softening.

1.11.5.f. Other strain softening mechanisms.

White et al. (1980) used a slightly different classification of strain softening mechanisms to that of Poirier (1980)

Change of deformation mechanism

Geometric or fabric softening

Continual recrystallization

Reaction softening

Chemical softening

Pore fluid effects

Shear heating

Geometric softening and shear heating have already been discussed here (1.II.5.a & 1.II.5.f) and continual recrystallization and reaction softening have been discussed under structural softening (1.II.5.b.)

A change in deformation mechanism can occur as the grain size is reduced due to dynamic recrystallization. A warm or hot working mechanism will change to one in which grain boundary sliding dominates or, if there are fluids present, pressure solution can be favoured. The general requirement of a fine grain size means that these mechanisms are favoured by low temperatures and high initial stresses. In addition the presence of a second phase (eg. mica), which can inhibit grain growth will enhance the effects.

Trace elements present in the lattice of minerals can effectively weaken them (eg. water in quartz), so chemical softening could result from the ingress of water into a deforming shear zone, where the quartz in a mylonite could take up a small quantity of the fluid present. The weakening effect of even small quantities of lattice-bound water in quartz can be substantial (White *et al.* 1980). Pore fluid effects can also weaken a rock significantly, this can occur by both mechanical and physiochemical effects. Mechanically, there is a lowering of the effective stress due to the presence of pore fluids, which will lead to cataclasis, and secondly there is an increase in ductility due to the Rebinder effect. This occurs under loading, when the electronic structure of dislocations and lattice point defects, such as vacancies and impurity ions, can become altered. This leads to a change in the nature of the interaction between the dislocations and such impurities, thereby affecting dislocation mobility and hence local ductility (Westwood *et al.* 1967). Also there can be a lowering of the interfacial tension between

crystals. This reduces the work-hardening component due to the pile-up of dislocations at the crystal-fluid interface, and increases the probability of the emergence of dislocations onto the crystal faces, leading to a reduction in the dislocation density and allowing the crystal to accommodate further strain (Rutter 1972).

1.II.5.g The relative importance of the strain softening mechanisms.

The dominant mechanism of strain softening operating at any given time in a shear zone will be a function of the physical, mechanical and chemical properties of that zone, so it is difficult to generalise on the importance of individual mechanisms. White *et al.* (1980) considered geometrical softening and dynamic recrystallization to be the dominant processes in mylonite formation from the evidence of well-defined crystallographic fabrics. They also noted that the comparative scarcity of weak or random fabrics suggests that superplasticity, due to reaction softening and grain boundary sliding, may not be of great importance. This is in agreement with the experimental work of Burg *et al.* (1986) who consider that high-temperature shear zones will deform by dominantly crystal-plastic processes. The effect of shear heating may be of considerable significance in the deformation of very large shear zones, but is probably of little importance in smaller zones. The presence of initial fabrics will favour fabric softening, and for a rock with a strong initial fabric this will probably be the single most important mechanism. Strain softening (s.s.) and strain-rate softening are unlikely to be of importance, and will give rise to strain hardening in most cases. Chemical softening and pore fluid effects can be of significance, but only under certain conditions, as not all shear zones act as fluid channels (Kerrich *et al.* 1980). The dominant strain softening mechanism may also change with time. Weijmars (1987)

recorded a change from initial geometrical softening, through a stage of continued geometrical softening with structural softening at depth, to a final state of shear heating and strain rate softening for the Palomares Shear Zone in southern Spain. Some form of evolution for the softening mechanisms is probably the case with most naturally occurring shear zones.

The relationship of deformation mechanisms to the strain softening mechanisms is summarised in table 1.3. Taking the example of dislocation glide; in the undeformed material there are few dislocations present, if stress is then applied, the existing dislocations can propagate, new ones may nucleate and the material will flow. If conditions are favourable dislocations may multiply and the flow rate may temporarily increase, the material is now softer. However a stage is reached where the dislocations tangle and interact with each other causing the material to harden (Cobbold 1977 (b)).

1.III PREVIOUS MODELS OF SHEAR ZONE FORMATION

1.III.1 Localization versus propagation

Models of shear zone formation and development can be divided into two main types: localization models and propagation models. In the localization model a pre-existing tabular region of weaker material is used to localize the deformation and subsequent development of the shear zone. In propagation models the tip region of a growing shear zone is considered and the deformation in front and behind the propagating tip is modelled. This section contains a description of the important shear zone models divided into localization and propagation classes.

TABLE 1.3

**STRAIN SOFTENING MECHANISMS FOR THE OPERATION OF ONE
DOMINANT DEFORMATION MECHANISM.**

Deformation mechanism	Causes of strain softening
Grain boundary sliding	<ul style="list-style-type: none"> - loss of cohesion and overcoming of friction - alignment of neighbouring boundaries
Microfracturing and cataclasis	<ul style="list-style-type: none"> - fracture propagation and multiplication - sliding on new grain boundaries
Dislocation glide	<ul style="list-style-type: none"> - multiplication of dislocations
Dislocation creep	<ul style="list-style-type: none"> - dynamic recrystallization of grains
Pressure solution with possible mass transport	<ul style="list-style-type: none"> - change in grain shape configuration - increase in proportion of catalyzing impurities
Nabarro-Herring creep with possible mass transfer	<ul style="list-style-type: none"> - change in bulk chemical composition - solid state phase transformations - change in distribution of inert grains

After Cobbold (1977(b))

The evidence for both types of shear zone model is equivocal, and it is probable that both localization and propagation effects are important in the development of shear zones. General observation tends to favour propagation models, as shear zones are commonly found in isotropic rocks which have no large scale material heterogeneities on which shear zones could localize. However shear zones formed at depth in transcurrent faults on a plate tectonic scale are constrained in their morphology and can be regarded in terms of a localization model.

1.III.2 Localization models.

1.III.2.a Shear heating models.

Many of the localization models for shear zone formation have used shear heating to soften the material inside the shear zone and hence localize the deformation (see 1.II.5.e). Brun & Cobbold (1980) have recently reviewed the approaches to shear heating models. The basis for the models is the energy balance equation,

$$C \frac{\delta T}{\delta t} = KV^2T + E \quad (1.11)$$

Where C - is the volumetric specific heat

T - is the temperature

t - is time

KV^2T - is the heat lost by conduction

E - is the rate of energy dissipation per unit volume

C and K are assumed to be constant (Brun & Cobbold (1980)).

In the case of simple shear (see fig 1.9)

$$E = \sigma_s \dot{\gamma} = \sigma_s \frac{\partial u}{\partial y} \quad (1.12)$$

Where $\dot{\gamma}$ - is the strain rate

σ_s - is the applied stress

u - is the relative velocity of the two blocks

y - is the distance from the centre of the shear zone
perpendicular to the plane of shear

By considering only one dimension eqn. 1.11 can be written,

$$C \frac{\partial T}{\partial t} = K \frac{\partial^2 T}{\partial y^2} + E \quad (1.13)$$

and substituting from eqn. 1.12,

$$C \frac{\partial T}{\partial t} = K \frac{\partial^2 T}{\partial y^2} + \sigma_s \frac{\partial u}{\partial y} \quad (1.14)$$

Equation 1.13 can be solved for the following three conditions,
each assuming that one of the terms is equal to zero.

i/ Steady state; no increase of temperature with time $\frac{\partial T}{\partial t} = 0$

$$K \frac{\partial^2 T}{\partial y^2} = -E \quad (1.15)$$

Fig 1.9

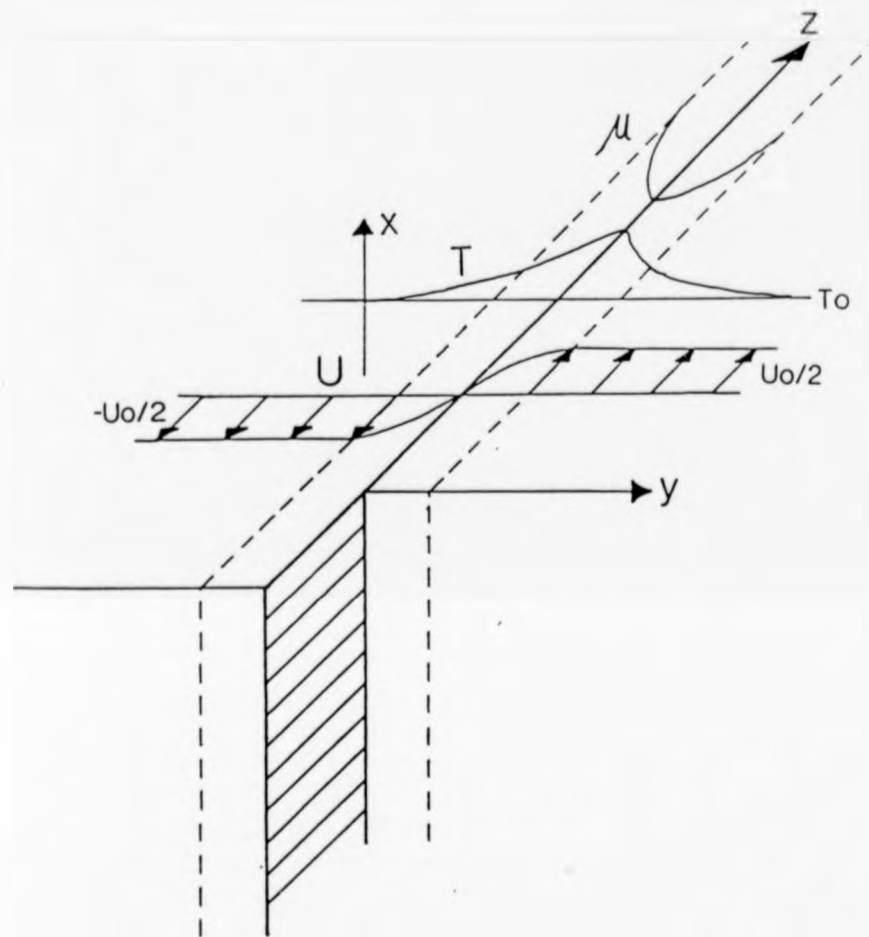


Fig 1.9 General situation for shear heating models giving the co-ordinate frame. T - temperature, u - velocity, μ - effective viscosity, T_0 - ambient temperature, u_0 - boundary velocity. After Yuen *et al.* (1978).

This is the most common form used in shear heating models and assumes E is constant for a steady state.

ii/ No heat conduction through the material $K \frac{\partial^2 T}{\partial y^2} = 0$

$$C \frac{\partial T}{\partial t} = E \quad (1.16)$$

This situation can never actually occur but it can be used as an approximation for materials with very low thermal conductivity, or when thermal gradients are very low.

iii/ Zero heat source $E = 0$

$$C \frac{\partial T}{\partial t} = K \frac{\partial^2 T}{\partial y^2} \quad (1.17)$$

This is the equation for heat conduction in one dimension, and can be used to show the effect if deformation ceases.

Substituting 1.12 into 1.15,

$$K \frac{d^2 T}{dy^2} + \sigma_s \frac{du}{dy} = 0 \quad (1.18)$$

A rheological flow law is introduced at this point, generally a power law of the form of eqn. 1.8. Substituting into 1.18 for $\frac{du}{dy} = \dot{\epsilon}$ gives (see 1.10),

$$K \frac{d^2 T}{dy^2} + \sigma_s^{n+1} A \exp(-Q/RT) = 0 \quad (1.19)$$

which is the general equation for shear heating models (Brun & Cobbold 1980).

Yuen *et al.* (1978) use a shear heating type of localization model to demonstrate the development of shear zones several kilometres wide. Their model uses a viscous deformation, the magnitude of shear stress and the width of the zone being derived internally from the model. The first models use two blocks with contrasting rheologies and examine the development of a shear zone at the interface between the two blocks. The rheology used for the hard block is that of olivine, whereas the soft block has the combined rheology of diabase, quartz and limestone. They found that the shear zone localizes in the soft block close to the boundary, and that the actual morphology of the zone depends on the amount of heat transfer between the two blocks. The model is then applied to a situation where the two blocks are identical. Using a power law creep equation, the relationship between the viscosity, ambient temperature and velocity profiles is examined. The model shows that the region of intense shear is an order of magnitude less extensive than the associated thermal anomaly. They conclude that the ambient temperature outside the zone has little effect on the shape of the thermal anomaly due to the zone, and that

the viscosity inside the shear zone is almost independent of the rheology. They show that increasing the ambient temperature widens the velocity and viscosity profiles across the shear zone. The boundary velocity, applied to the margins of the two blocks, has little effect on the temperature structure or the velocity profile inside the zone, but for low boundary velocities at low ambient temperatures the applied stresses need to be very high as the shear zone cannot produce sufficient heat to soften the zone adequately. This model and others like it only consider the heat flow perpendicular to the shear zone boundaries, and so are essentially one-dimensional models.

Flietout & Froidevaux (1980) used a similar model, based on equation 1.14, to examine the development of a thermo-mechanical shear zone with time. In the initial stages of development the shearing occurs across the whole zone, after which the deformation becomes concentrated into a narrow zone. With continued deformation the zone broadens gradually and the temperature anomaly flattens. In general, for lower ambient temperatures, the model predicts narrower zones, higher initial stresses and a shorter initiation period, but no real effect on the long term behaviour of the zone. For smaller boundary velocities the zone will be colder and the viscosities higher. If a temperature perturbation of 10°C is introduced at the centre of the zone, the initiation stage is more rapid and the deformation is concentrated into a narrower zone. The model is then applied to small (cm- to m-scale) shear zones, assuming deformation to be confined by strong inhomogeneities in the host rock. A high temperature perturbation is necessary to avoid the build up of large stresses leading to brittle failure. The values used for modelling the small shear zones are: width 20 m, ambient temperature 800°C and boundary velocity of 10 cm/a. It is calculated that a zone of these dimensions could produce temperatures high enough for partial melting, but the

resulting thermal anomaly would be 10 Km wide which is geologically unreasonable. They calculate that for a cm-scale shear zone with initial stresses as high as 5 Kb and displacement rates of 10 cm/a, a temperature rise of only 100°C would require 3000 years and a displacement of 300 m. If a more realistic velocity value of 1 cm/a is used, then 30 Ma and 30 Km displacement are the results. These are obviously unrealistic and force Flietout & Froidevaux to conclude that small shear zones do not deform by shear heating.

Flietout & Froidevaux (1980) also investigated the effect of a shear zone that cuts a boundary between a hard and soft medium. In such a situation, it is possible that the temperature in the hard rock will reach sufficient values to produce partial melting in the softer rock. The two rheologies are wet quartzite for the soft half, and wet olivine for the hard half, these are then deformed at an ambient temperature of 600°C, at a boundary velocity of 10 cm/a. The temperatures produced in the quartzite layer reached 900°C, which is sufficient for partial melting. This is in contrast to the results for a homogeneous rock which does not reach temperatures high enough for migmatization when sheared at values comparable with plate motions.

Shear heating models using constant shear stress and constant boundary velocity for a viscous medium are presented by Lockett & Kuszniir (1982). For the constant velocity models the initial assumption is that of a constant velocity gradient across the shear zone, not a step-like Heaviside function as used by Yuen et al. (1978). The models show that for the constant shear stress situation, thermal runaway, leading to temperatures high enough for partial melting, is possible. For lower ambient temperatures, higher stresses are required to produce runaway. The constant velocity models show that shear zones broaden more rapidly at higher ambient temperatures, and this is used to explain the broadening of shear zones with depth,

Fig 1.10

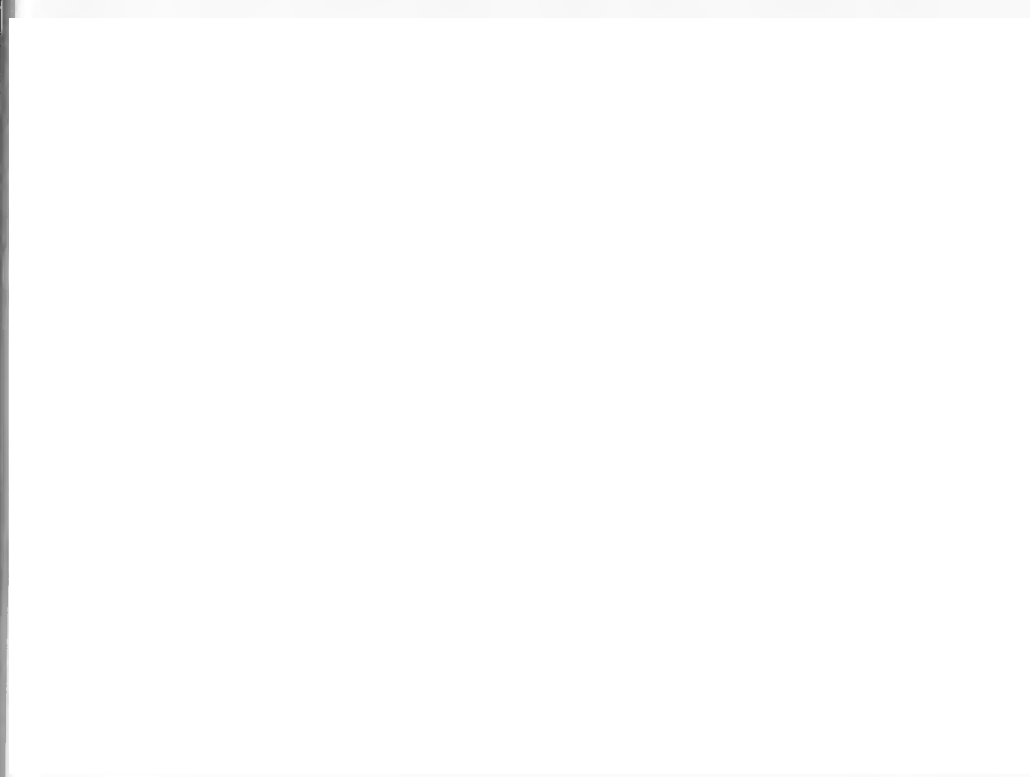


Fig 1.10 Typical shear heating model results for temperature and velocity profiles at various times after the onset of shearing. The dashed lines are the shear zone boundaries. Variations of T_{max} (dashed line), minimum effective viscosity and stress are shown in the insets. From Flitout & Froidevaux (1980).

as observed in the field. The merging of two parallel shear zones over a period of time is also investigated.

The most recent model to make use of shear heating has been developed by Pavlis (1987) who has applied models developed from Yuen *et al.* (1978) and Brun & Cobbold (1980), to the evolution of crustal "megathrust" systems. It involves using a steady state solution to equation 1.11, and the model shows a two-stage evolution for the development of the shear zones. In the initial stages, dry lower crust/upper mantle rocks are deformed in a ductile shear zone, the temperature achieved within this zone being dependent on the rheology of the deforming material, and almost independent of the ambient temperature. Low ambient temperatures thus give rise to high thermal anomalies, and high ambient temperatures will have small thermal anomalies. Because of this, shear heating acts as a thermal buffer, such that when hanging-wall rocks arrive at mid- to upper-crustal levels, their temperature is controlled by the rheology rather than their initial thermal state. As "wet" upper crustal rocks are emplaced below the preheated hanging wall, partial melting of the footwall metasediments may result. Stresses in excess of 0.5 Kb are required for temperature increases of $>100^{\circ}\text{C}$, and the maximum temperature achieved by the model is almost independent of depth and velocity, provided that these are not extreme. This model agrees with those of Yuen *et al.* (1978) and Flietout & Froidevaux (1980) in that a rheological contrast, either wet/dry or hard/soft is required to produce partial melting as a result of shear heating.

The general conclusions from all shear heating models are broadly similar as regards the relationships between ambient temperature, boundary velocity and applied stress. The principal disagreement is on the conditions necessary for shear zones deforming by shear heating to reach temperatures high enough for partial

melting. The main problem with these models is their inability to model the development of small shear zones realistically, but the conclusions relating to large zones are probably similar to the actual mechanisms involved for the deformation on these zones.

1.III.2.b Other localization models.

The model developed by Bowden (1970) for inhomogeneous plastic deformation has been described in a previous section (1.II.4.a). In this model the deformation was localized in the bands by use of a strain difference $\Delta\gamma$ between the bands and the matrix. He concluded that for deformation bands to form in a material, the applied strain necessary for the strain rate in the bands to double needs to be small, so the initial strain defect $\Delta\gamma$ must be large. The analysis presented assumes that inhomogeneous deformation can only occur on the negative slope of the stress-strain curve (see fig 1.6) as then the strain increases with decreasing stress.

Poirier et al. (1979) and Poirier (1980) use a model based on the general deformation equation (eqn 1.9). They assume a perfectly plastic rheology with a constant imposed strain rate, i.e. a constant boundary velocity, and no variation of shear stress in the y direction. A strain gradient is then introduced along the y axis, and the deformation is considered to become unstable if the strain gradient increases with strain, causing the deformation to become more localized. The shear zone is initiated using an initial strength defect τ_0 . The model uses a granite rheology and the principal softening mechanisms of structural softening and shear heating, the structural softening being achieved by decreasing τ_0 in equation 1.9 with each step of the calculation. The important effect of structural softening is to localize the deformation and give a "clean cut" shear zone; if there is no structural softening, the strain in the zone

merely increases linearly with the homogeneous strain outside the zone. The angle between the foliation inside the zone and the shear zone walls decreases with increased structural softening; thus in order to obtain the low angles observed in most shear zones, structural softening must be an important factor.

The shear heating component used in the models is not important when a constant strain rate is imposed, and Poirier *et al.* (1979) conclude that thermal runaway is unlikely under geological strain rates. This may be due to the assumption of a constant strain rate, a situation that is unlikely to occur naturally. The model requires an initial strength defect in order to activate the shear zone, and the larger this defect, the more enhanced the shear rate becomes. The model also predicts that shear heating will not be important below lower amphibolite facies conditions, and that migmatization due to shear heating is unlikely.

A model for the development of a shear zone, based on the elastic stress distribution around a lithospheric fault, was proposed by Watterson (1979). He used the relationship between width and displacement to obtain values of strain rate from observed field data, which were then used to constrain the model. The elastic stress field on the fault gave the initial stress distribution and this was then used, with a dislocation creep flow law, to obtain the initial ductile strains. The model predicts that a steady state for stress will first be achieved in the centre of the zone, and that this will then widen with time. This model is further developed using a stress-related grain-size reduction mechanism, combined with a diffusion creep flow law, to further soften the centre of the zone. The introduction of these additional softening mechanisms results in increased strain rate at constant stress, which prevents the zone widening to the initial elastic stress profile. The model is used to predict the observed

widening of shear zones with depth, and demonstrates several of the principal features of shear zones observed in the field.

The shear zone model developed by Casey (1980) can be used to explain brittle failure in shear, second order faulting and en-echelon tension gash arrays. The model is based on the principle of minimum energy and assumes that rocks have linear isotropic viscous or elastic rheology. The deformation is localized within the zone by using a region with a lower elasticity or viscosity modulus, and the stresses within the zone are calculated for various orientations of the applied stress relative to the shear zone walls. For a shear zone in a homogeneous material not to increase the total stored strain energy, the material inside the zone must be weaker than the host. The shear zone is assumed to be a planar region of infinite extent with a lower Young's Modulus than the host and, in addition, the boundary between the shear zone and the host is assumed to be cohesive. The variation of stress components in the weak zone with variation of the angle ϕ (Fig 1.11) are calculated, and it is shown that for $\phi = 45^\circ$ the stresses in the zone and the matrix are the same. For $\phi < 45^\circ$ the stress in the zone is less compressive than in the matrix, and for $\phi > 45^\circ$ it is more compressive, a maximum is achieved at $\phi = 60^\circ$. The position of these points is independent of the Young's Modulus of the zone, but the stress difference between the zone and matrix increases as the zone gets weaker. With increased weakening of the zone the principal stresses within the zone rotate so as to be at 45° to the shear zone walls for all values of ϕ except 0° and 90° . Casey (1980) considers that, in ductile zones, weakening due to transformation or reaction-enhanced ductility is the dominant softening process. Stress concentration could cause local metamorphic reactions, and if any of these local regions are elongate with their long axes at angles of 45° or more to the matrix σ_1 , then a shear zone could initiate. The

Fig 1.11

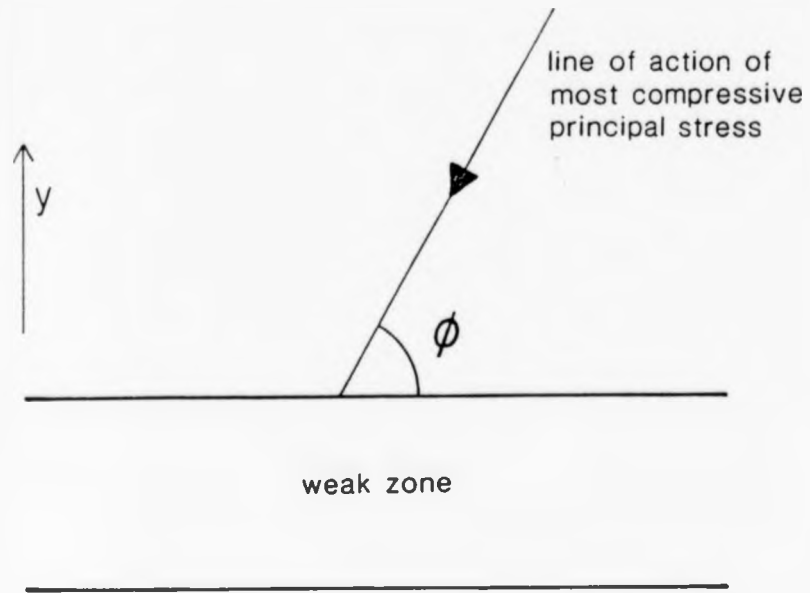


Fig 1.11 Geometry of the shear zone model presented by Casey (1980).

weakening caused by a local phase change results in an increase in mean stress which will further promote the phase change. Such a mechanism may be important in the very early stages of shear zone development, but after the initiation stage it is probable that geometrical softening and other mechanisms of structural softening, e.g. dynamic recrystallization, will take over.

These localization models demonstrate many of the features observed in shear zones, the shear heating models being only appropriate to zones of several kilometres width. A feature common to most of the models is that, the larger the initial perturbation of temperature, strain, Young's Modulus etc., the more pronounced the later development of the zone becomes. As many shear zones can be found in rocks where there are no strong initial material heterogeneities or other types of "localizing feature", there are obviously aspects of shear zone development that these models do not explain. However, it is difficult to be certain that shear zones in apparently homogeneous material did not localize on heterogeneities that are now obscured by the presence of the shear zones, but it seems unlikely that shear zones would obliterate all traces of every heterogeneity in an otherwise homogeneous medium.

1.III.3 Propagation models.

One of the first propagation models developed was that used to investigate the propagation of a shear crack by Palmer & Rice (1973) for the failure of overconsolidated clays. They used the J integral technique to derive the conditions for propagation of a concentrated shear band. The basis of the model is the cohesive force models for tensile cracks and Palmer & Rice (*op. cit.*) regard the shear band as a surface discontinuity on which there exists a relationship between shear stress τ and displacement d . They found that shear bands will

propagate once a certain critical load is attained, as then the energy surplus at the tip just balances the energy used to dissipate the shear stresses in the back region of the zone, behind the tip, above the residual stress in the band. The propagation of the band reduces the "energy density" around the tip if the boundaries remain fixed. The stress field used to drive the model is derived from the type presented by Paris & Sih (1965), modified to take into account the normal and shear stresses transmitted across the band. A problem exists at the band tip, in that the stress field becomes a singularity. Palmer & Rice (1973) therefore consider that there is an end region of small but finite size embedded at the tip which will deform plastically. There is a strong size effect predicted by the model, in that a shear band will grow slowly from an initial stress concentration and will then propagate more quickly once a certain critical length is reached. The critical lengths and load stresses necessary for shear band propagation are calculated. This model is a good analogy for shear zone development, in that a degree of cohesiveness across the discontinuity is maintained, and that stresses are transmitted across the plane of shear as would be the case with a true shear zone.

The model proposed by Coward (1976) is based on the assumption that, in the initial stages of shear zone development, the small zone will be subject to boundary conditions at each end. The strain state around the zone may then deviate from a simple shear mechanism, with areas of compression and extension near the ends of the developing zone and a region of simple shear in the centre (Fig 1.12). The model goes on to assume that deformation is by plane strain with no change in length of the shear zone and no displacement at the boundaries of the region. The curvature of the zone will depend on the balance between the amount of flattening strain taken up at the ends of the

Fig 1.12

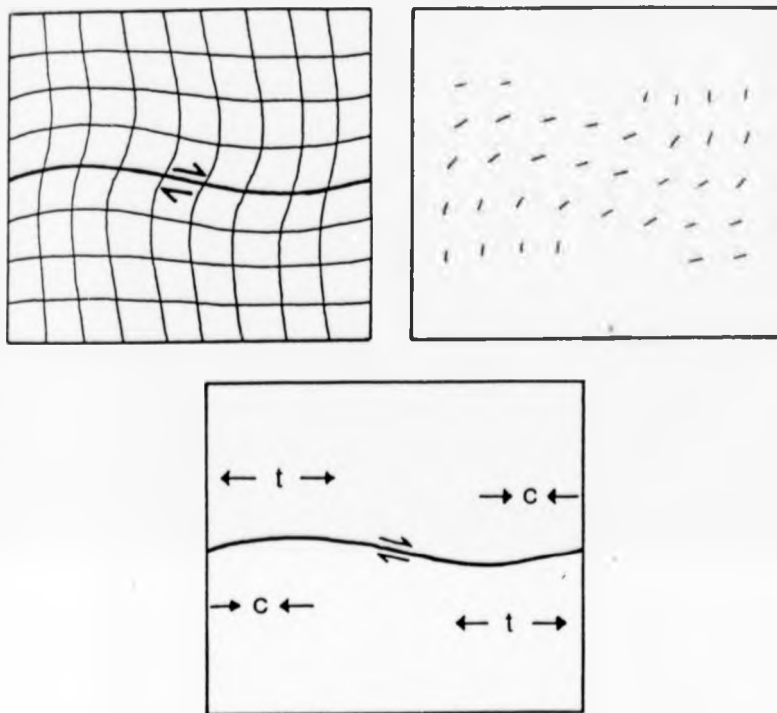


Fig 1.12 Diagrammatic representation of a shear zone deforming with fixed boundaries giving rise to areas of compression (c) and tension (t) around the ends, with simple shear in the central region. After Coward (1976).

zone and that taken up along its length. If the strain rate $\dot{\gamma}$ (displacement velocity) is very low relative to the propagation rate \dot{d} , then flat planar zones will result, if however $\dot{\gamma}$ is similar to \dot{d} then the zones will have a mild degree of curvature. As $\dot{\gamma} \rightarrow \dot{d}$, i.e. a high $\dot{\gamma}/\dot{d}$ ratio, the zones will suffer more flattening strain, and for zones with a low $\dot{\gamma}/\dot{d}$ ratio there will be less flattening strains; these strains are however still present and cannot be removed by later simple shear deformation. Several closely spaced zones with high $\dot{\gamma}/\dot{d}$ ratios will curve and coalesce to form networks. The lozenge-shaped augen in between represent areas of pure shear, and have a tectonic fabric at a high angle to the shear zones. Coward (1976) concludes that the strain path of a deforming shear zone is not one of simple shear alone, but that there will be an area of pure shear at the leading edge of shear zones. Field evidence of strain measurements using mineral cluster axial ratios and magnetic susceptibility anisotropy is presented to support this model.

Another model based on the stress distribution around a propagating crack was developed by Ball (1980). He modelled a thin disc-shaped crack filled with very fine grained material that could deform superplastically. A concentrated region of shear stress around the perimeter of the crack promotes dynamic recrystallization ahead of the propagating tip at temperatures greater than half the melting temperature (T_m). The concentrated stress field around the crack is a function of the diameter of the crack such that:

$$\tau_c = \tau_0(c/2r)^{0.5} \quad (1.20)$$

where c - is the crack radius

r - is the distance ahead of the crack tip

τ_c - is the concentrated stress

τ_0 - is the applied stress

When τ_c reaches τ_y , the yield stress, a toroidal volume of plastic rock is formed around the crack tip. Within this zone, if the temperature (T) is high enough ($T > 0.6 T_m$) dynamic recrystallization may take place such that the grain size remains in equilibrium with τ_c . The model therefore predicts a contrast in grain size from the host rock going into the tip region, deformation within the zone being accommodated by grain boundary sliding. Values calculated for τ_c are around 5 Kb (For $\tau_0 = 100$ bar and $T = 1000^\circ\text{K}$), this gives a recrystallized grain size of $10\ \mu\text{m}$ and strain rates of $10^{-12}\ \text{s}^{-1}$ for grain boundary sliding, or $10^{-19}\ \text{s}^{-1}$ for dislocation creep. These values demonstrate the very large softening effect that results from a change from dislocation creep to grain boundary sliding superplasticity. The theoretical material used for these calculations is not given, but the values appear to be consistent with an olivine rheology. The energy build up before propagation is then related to the crack radius (c), and the model predicts that a crack must be of the order of 100 - 1000 Km long before self propagation of the crack can occur ($\tau_0 = 0.1 - 1\text{Kb}$, crack width of the order of 1 Km). These values appear to be unrealistically large. The model also predicts that the growth of the crack will be subject to periods of acceleration and deceleration due to the rate of propagation exceeding the ability of the dynamic recrystallization to accommodate the strain. This would then lead to brittle failure and could explain the occurrence of periodic earthquakes. The conclusions from this model are of general interest but some of the initial assumptions appear to be geologically unreasonable. The use of a $10\ \mu\text{m}$ grain size in the

crack is not consistent with the published data, as grain sizes this small are uncommon; also the temperatures $> 0.6 T_m$ used are probably unrealistically high. The model predicts that the grain size along a shear zone should change as τ_c increases with c due to propagation, and this has not been recorded from field evidence.

Norton (1982) proposed a model that again uses the crack tip analogy for a propagating shear zone. Like Palmer & Rice (1973) he uses the crack tip theory to predict the stress distribution at a shear zone tip, with modifications based on palaeostress estimates from field examples. The model predicts flat-topped strain profiles with a maximum value of $\gamma = 50$ and concludes that this is probably not due to strain hardening (c.f. Cobbold 1977 (a & b)) as the observed microstructures from natural examples show a steady state from $\gamma = 2$. Norton's (1982) model makes the following assumptions:

- i/ Propagation rate is constant.
- ii/ Stress distribution has a "saw tooth" form.
- iii/ The host becomes part of the shear zone at an arbitrary critical strain γ_c .
- iv/ The deformation is accommodated by dislocation creep with power-law flow.
- v/ A parabolic law is used for the effect of strain softening.

This model is constrained using field evidence for stress intensification levels and the degree of strain softening. It is used principally to calculate the propagation rate of shear zones for various stress intensification factors, temperatures and widths. When propagation rate is compared to displacement rate the propagation rate is found to be one or two orders of magnitude larger, and the results suggest that the propagation rate is proportional to the width of the zone. The observation that shear zones in the field tend to have a

constant aspect ratio (length : width) of about 500 : 1, is used to support the propagation rate - width relationship. Assuming that all shear zones in a particular area form over a given period of time, then the large zones must propagate faster. The model is used to predict the time taken for a shear zone to reach this final aspect ratio and this is then compared with the time taken to reach a strain of $\gamma = 50$. The calculated values depend on the temperature, stress intensification and the degree of strain softening. Time taken to reach the final aspect ratio is estimated at between 2.8×10^{14} and 5.3×10^{11} seconds (9 Ma - 17 Ka), and so shear zone development should represent a considerable time span in an orogenic episode

1.III.4 Conclusions

The models discussed cover a variety of approaches to the study of shear zone development. The shear heating models are only applicable to the large zones and do not explain much of the finer detail of the development of small shear zones, but given this limitation, these models give realistic results and are of considerable significance. Of the other localization models, that of Watterson (1979) is perhaps the most realistic in that it uses a changing deformation mechanism through the life of the zone. The model of Casey (1980) is chiefly concerned with the brittle features of shear zones and does not deal in any detail with the development of a true ductile shear zone. The propagation models have an advantage in that they appear to be more useful in explaining the cm- to m-scale shear zones that are easily observable in the field. The basis for most of these models is the calculation of the stress field around a growing crack tip. This has been modified by Palmer & Rice (1973) to take into account the stresses transmitted across the shear band in order to give a more acceptable approximation to the natural case.

Norton (1982) also modified the calculated stress field by using data from palaeostress estimates and strain profiles. The model presented by Ball (1980) suffers from the the use of unrealistic values as input parameters, which may have led to over-estimates in the results. One aspect common to all the models is the need for improved data constraints, both from field studies and experimental work in order to enable the models to be properly calibrated, and to enable the relevance of the results to be assessed.

CHAPTER 2

2.1 INTRODUCTION TO FIELDWORK

2.1.1 Objectives of the fieldwork.

The fieldwork undertaken had two principal objectives; to provide a data set that could be used to test and constrain a model of shear zone development, and to obtain information on the way in which shear zones initiate and develop that could be used as the basis for the approach to the shear zone modelling.

Shear zones of all scales were examined from 0.75 km to less than 1 cm in width and in a variety of rheologies. All the examples used were taken from the Lewisian of the North West Highlands of Scotland. The account of the fieldwork is divided into three parts; a description and analysis of a major crustal shear zone - the Canisp Shear Zone, the collection of data from over fifty cm-scale shear zones between Torridon and Laxford, and the results and conclusions from the fieldwork and their relevance to the development of a model for the initiation and operation of a shear zone.

2.11 THE CANISP SHEAR ZONE

2.11.1 Introduction

2.11.1.a History of research.

The Lewisian of the Assynt region was first mapped by Peach *et al.* (1907), who noted the major shear structure to the N of Lochinver and followed it inland to Glen Canisp (Fig 2.1).

Fig 2.1

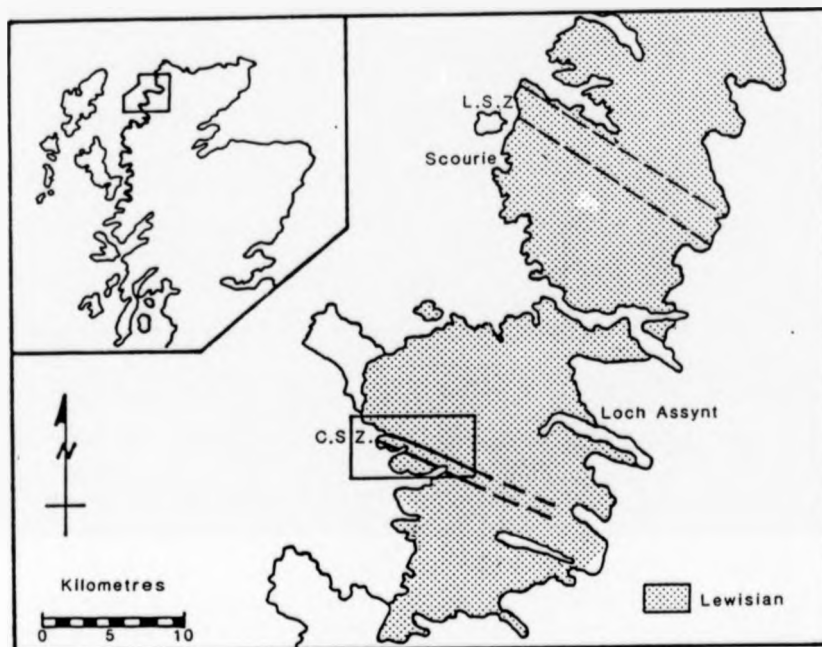


Fig 2.1 Location map showing study area. CSZ - Canisp Shear Zone, LSZ - Laxford Shear Zone.

Work in the Lochinver area by Evans (1965) led to the recognition of the Inverian metamorphic event. This is a pre-Scourie dyke, amphibolite-facies event of higher grade than the later Laxfordian, and post dating the intrusion of a suite of pegmatites, which were emplaced after the Scourian granulite-facies metamorphism.

Following the chronology of Park & Tarney (1987), the first event recognised is the Badcallian granulite-facies metamorphism at c. 2700 Ma. This was followed by intrusion of potassium-rich pegmatites (Evans & Lambert 1974). The Inverian deformation and metamorphism occurred between c. 2600 and 2400 Ma. with the emplacement of the Scourie dykes into hot country rock (Tarney 1963), between 2400 and 1900 Ma. The boundary between the Inverian and the Laxfordian is not well defined. Evans & Lambert (1974) considered that the dyke emplacement was associated with the end of the Inverian, rather than with a period of quiescence between two separate tectono-metamorphic episodes. The time of peak Laxfordian metamorphism was around 1850 Ma. (Lambert & Holland, 1972).

A major study of the Assynt region was made by Sheraton *et al.* (1973a,b). On the evidence of the folding they postulated a N-side-up movement for the Canisp Shear Zone during the Laxfordian, following the N-side-down sense of movement implied by the Lochinver monoform.

Beach (1974), in a paper dealing primarily with the Laxford shear zones, suggested a dextral N-side-up sense of movement, perpendicular to the principal lineation. He was however, unable to calculate a displacement across this zone, due to the absence of well-exposed dykes oblique to the zone, such as those at Tarbet.

A sinistral S-side-up sense of movement was adduced by Evans & Lambert (1974) for the Laxfordian shearing on the Canisp Shear Zone. They also referred to the "intensely deformed gneiss of the major Inverian structures" but did not specifically mention a period of

Inverian shearing.

In the most recent work on the Lochinver area, Jensen (1984) used the quartz microstructures to obtain a dextral, S-side-up sense for the Laxfordian movements, but did not consider the earlier Inverian movements.

2.II.1.b Aims of the present study.

The aim of this part of the fieldwork was to produce a detailed map of the western end of the Canisp Shear Zone including the important coastal exposure between Achmelvich and Clachtoll. Particular emphasis was placed on the distribution of strain within the zone and several traverses were done on a sub-metre scale across the zone at points along its length. Detailed mapping of small areas was combined with logging of critical sections; this enabled a complete picture of the development of a large crustal shear zone to be constructed.

2.II.2 General description and structural setting

The Canisp shear zone outcrops on the coast at Achmelvich Bay, 3 km NW of Lochinver, and trends ESE inland to Glen Canisp where it disappears beneath a cover of younger rock. The portion of the zone which has been mapped for this study extends from the coast to grid line 210 E, 5 km inland (Fig 2.2). The shear zone is sub-vertical at outcrop and approximately 0.75 km in width at its widest point. To the south of the shear zone the foliation in the gneisses is flat lying; this is folded by the Lochinver monocline, becoming steeply N-dipping in the N limb (Figs 2.3 & 2.4). This steep N-dipping foliation is cut by steeply S-dipping high-strain rocks that strike slightly obliquely to the axial trace of the Lochinver monocline. Within the shear zone

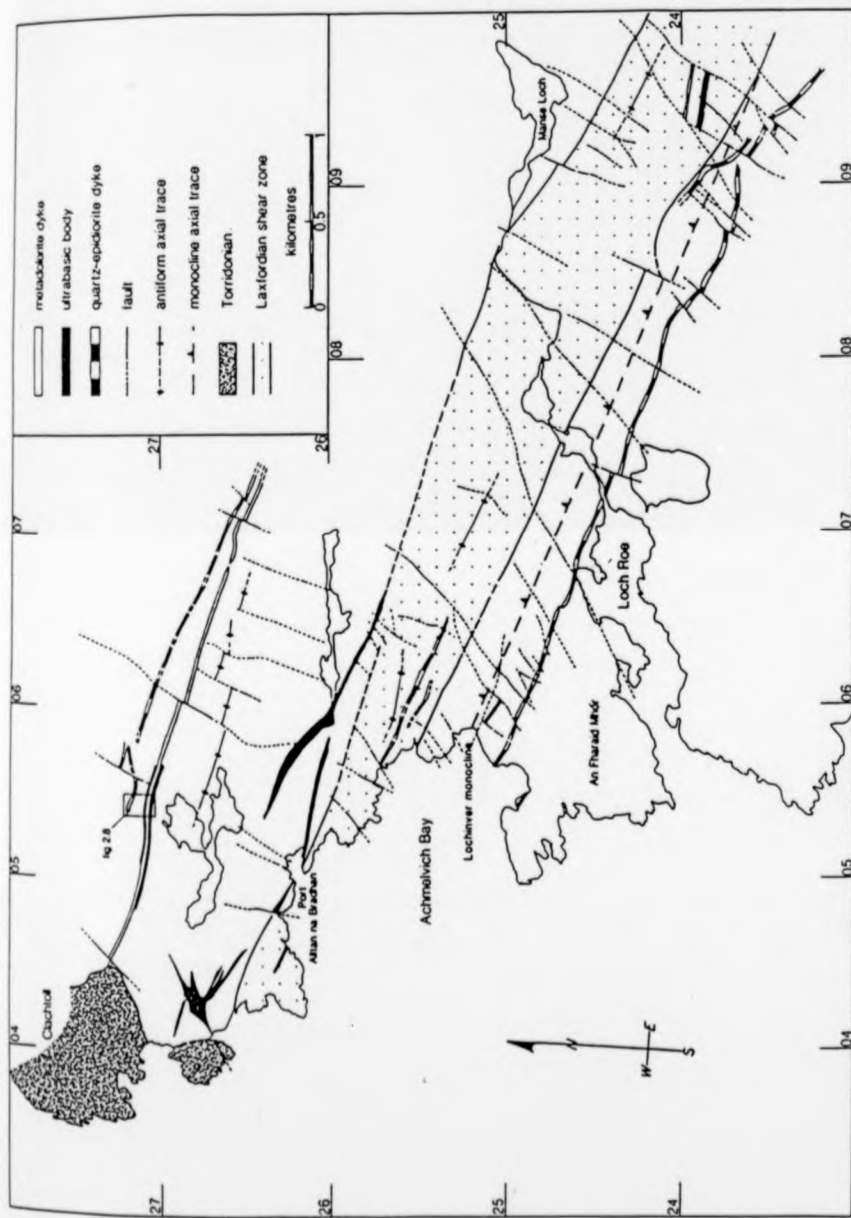


Fig 2.2

Fig 2.2 General geological map of the NW end of the Canisp Shear Zone showing the location of Fig 2.8

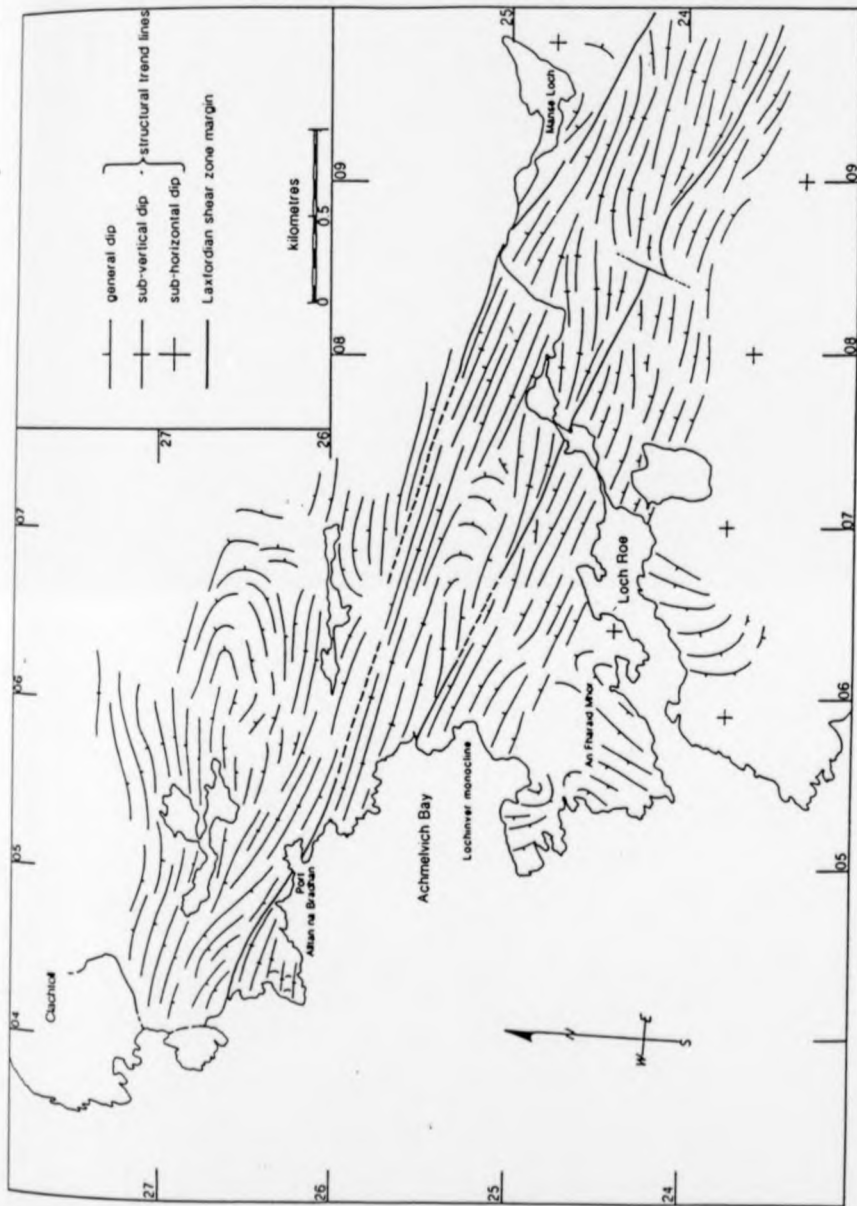


Fig 2.3

Fig 2.3 Structural trend map of the NW end of the Canisp Shear Zone including some data from Jensen (1984).

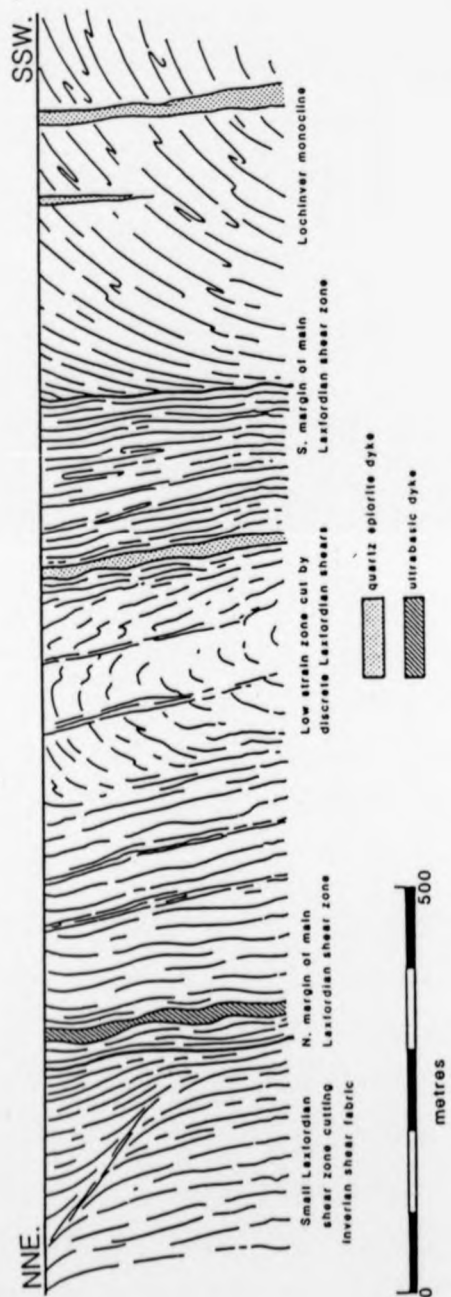


Fig 2.4 Schematic cross section through the NW end of the Canisp Shear Zone showing the main structural relationships.

Fig 2.4

the rocks vary from mylonites to relatively undeformed gneisses similar to those to the S of the zone; the foliation within the zone is generally sub-vertical. At the E end of the area the gneisses to the N of the zone dip gently NE and the boundary to the shear zone is well defined. At the western end of the zone the N boundary is less well defined due to a series of folds with E-W trending axes and associated shears. There are numerous dykes in the area, all sub-vertical and striking sub-parallel to the shear zone.

2.II.3 Description of rock types

2.II.3.a The gneisses.

Selective aspects of the petrography relevant to the present study are described in this section; more comprehensive studies of the petrology, geochemistry and microstructure are presented by Peach et al. (1907), Khoury (1968), Sheraton et al. (1973a) and Jensen (1984).

The gneisses of the mapped area are broadly tonalitic in composition (Fig 2.5) and have been variably deformed. To describe them, it is convenient to examine the lowest-strain gneiss from the area and then document the changes that occur with increasing strain.

The lowest-strain gneisses occur to the S of the Canisp Shear Zone and to the N of the zone at the eastern end of the area. They have a good mineralogical banding; the individual layers, varying in composition from acid to mafic or ultramafic, are parallel to the weak foliation. The layers are laterally discontinuous and cannot be followed for more than a few m. The banding is locally folded by isoclinal intrafolial folds. Ultramafic pods, now consisting almost entirely of amphibole, occur within the gneisses; they are flattened in the plane of the foliation and their long axes vary from a few cm to several m in length.

Fig 2.5

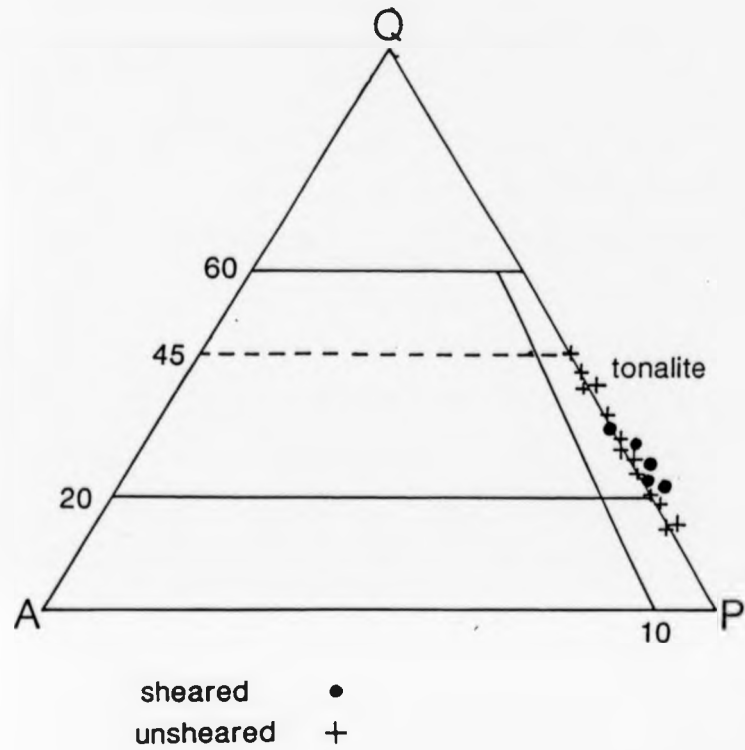


Fig 2.5 Composition of the gneisses, from Jensen (1984), showing the same modal composition for both sheared and unsheared gneiss.

Fig 2.5

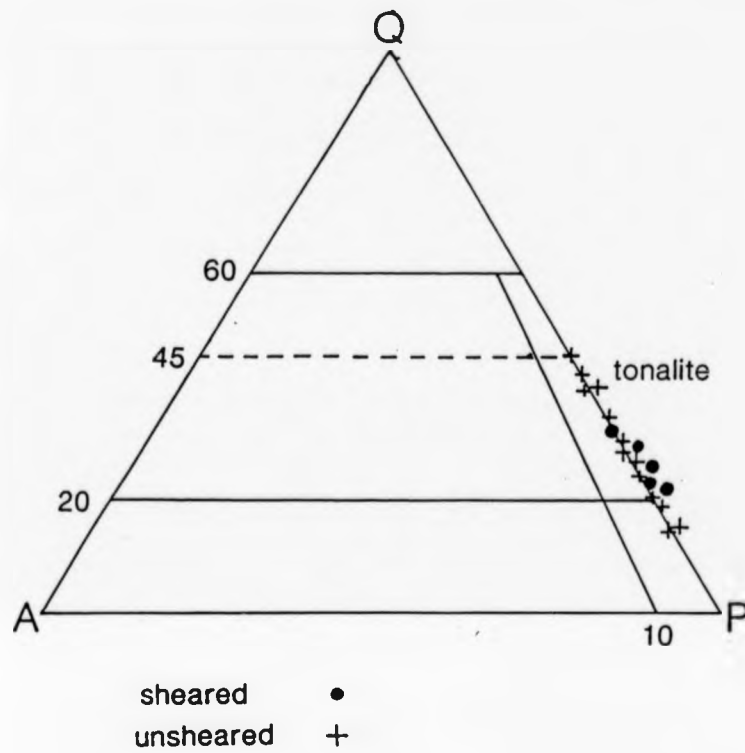


Fig 2.5 Composition of the gneisses, from Jensen (1984), showing the same modal composition for both sheared and unsheared gneiss.

Mineralogically the gneisses consist of plagioclase (An 25-35), quartz and hornblende, with variable amounts of biotite, epidote and opaque ore minerals. Most samples show a division into quartz-plagioclase and hornblende-biotite rich domains corresponding to the mineral layering seen in hand specimen. The boundaries to these domains can be quite sharp but in general the low-strain gneisses show a diffuse gradation between felsic and mafic layers. The variation in the composition of the gneisses is shown in Table 2.1. A weak fabric parallel to the mineral banding is defined by the preferred orientation of hornblende laths. The grain size within the low-strain gneisses is variable, the average being between 0.1 and 0.3 mm, but individual grains may be as large as 5 mm. The larger grains are porphyroclasts of plagioclase and hornblende, have strongly embayed margins and exhibit a variable degree of alteration. The hornblende porphyroclasts often have numerous inclusions of small rounded quartz grains producing a "sieve" texture. The plagioclase porphyroclasts are often heavily sericitised and may have small inclusions of epidote; twinning is infrequent both in the porphyroclasts and in the plagioclase in the groundmass. The groundmass consists mainly of small- to medium-sized anhedral, equant plagioclase and quartz grains and the feldspar is often sericitised. The quartz grains show little evidence of strain and have an annealed texture; they are confined almost entirely to the felsic domains. Rare quartz segregations are present which contain fresher quartz with some strain features such as undulose extinction. Biotite occurs as small lath shaped grains within the mafic layers, usually aligned parallel to the foliation/banding; occasionally irregular sheaves of biotite occur representing a later phase of biotite growth. The low-strain gneisses show considerable evidence of late-stage alteration. As well as the sericitization of plagioclase already described, the hornblende grains are often heavily

TABLE 2.1

COMPOSITION OF THE GNEISSES

Mineral	Average Content	Range of Content	Standard Deviation	N
Plagioclase	50.0	20.3 - 68.7	11.6	18
Quartz	20.7	1.1 - 35.4	9.4	18
Biotite	5.6	0.0 - 17.8	5.2	16
Hornblende	22.1	0.0 - 67.7	14.9	14
Chlorite	0.5	0.0 - 2.9	0.8	11
Epidote	2.2	0.3 - 5.6	1.3	18
Opaque	0.9	0.0 - 1.7	0.5	16
Accessories	0.9	0.0 - 3.8	0.9	16
An in plag.	29.0	25.0 - 32.0	2.1	68

Taken from Jensen (1984) Table 1

clouded and show alteration rims. There may also be biotite growth along the cleavage planes of the larger hornblende crystals. Quartz and plagioclase grains often show late fracturing.

The first indication of increasing strain on the microstructure of the gneisses is an increase in the preferred orientation of the smaller hornblende laths and also biotite laths where present. Quartz grains exhibit strain features such as undulose extinction and sub-graining, and the grain size decreases. There is a small amount of newer, strain-free hornblende and an increase in the amount of granular epidote which appears to be associated with the larger hornblende porphyroclasts. The mineral layering is still present and there is an increase in the sharpness of the boundaries to the individual layers. The felsic layers exhibit little evidence of any shape fabric to the grains. In some samples there is a slightly stronger fabric defined by small prismatic hornblendes cross cutting the mineral banding at a low angle.

At high strains the gneisses have a strong foliation parallel to the mineral layering. It is not possible at this degree of deformation to tell whether the mineral layering is a completely new feature, or whether it is a modified and transposed relic of the low-strain gneissose banding. These gneisses often exhibit a strong penetrative lineation formed by quartz rods, and may also show a non-penetrative lineation on the foliation surfaces defined by the alignment of prismatic hornblendes. In places there is random growth of amphibole on the foliation surfaces occasionally becoming rosette shaped. Microstructurally there is an extremely strong preferred orientation to all the prismatic hornblende and biotite crystals. These form discrete surfaces, often grouped together with very thin felsic domains between. There is very little felsic material in the mafic layers and the layer boundaries are extremely sharp. There is a

moderate preferred shape orientation of quartz and feldspar grains in the felsic layers. The quartz grains are recrystallized and annealed, exhibiting curved boundaries, undulose extinction, subgraining and subgrain rotation. In the felsic layers there is development of quartz ribbons, within which the individual grains show a slightly larger grain size than those in the groundmass. The presence of subgrains and quartz ribbons indicates temperatures in excess of 400°C. There is an overall decrease in the grain size, particularly marked in the quartz grains, which show a decrease of up to 50% of the median grain size (Jensen 1984). The feldspar grains are sericitized and often show an alteration to fine white mica along the grain boundaries. There are few porphyroclasts present in the high-strain gneisses, but where they do occur, the fabric deflects around them and they are heavily altered. Some plagioclase porphyroclasts have retrogressed totally to random aggregates of white mica. Very few of the porphyroclasts show twinning. Where present, biotite is of a very uniform size and has a very strong preferred orientation. There are a few grains of earlier biotite within the rock, these have strongly embayed margins and are retrogressing to chlorite.

The highest strain rocks in the area are quartz-feldspar mylonites. These are composed of quartz and feldspar with accessory mica and amphibole. There is marked reduction in grain size and a good preferred shape orientation to all grains. Ribbon quartz development is common and all grains show strain features and a strongly annealed texture. A few feldspar porphyroclasts survive but these are smaller than in the less deformed gneisses and are heavily sericitized, as is the feldspar in the groundmass. The more quartz-rich mylonites contain up to 5% of late prismatic white mica grains that cross cut the fabric with random orientations. Biotite occurs in discrete thin planes within the mylonites, but these are rare and the biotite is

retrogressing to chlorite. There are also a small number of hornblende porphyroclasts which survive only as fragments of crystals in the felsic groundmass, but maintain optical continuity.

The ultramafic pods occur within the gneisses throughout the area, even in the strongly deformed areas (c.f. Jensen 1984), but are not seen in the mylonites. There is no apparent mineralogical change in their composition from the low to the high deformation areas; they all consist almost entirely of hornblende in various stages of alteration. Some of the fresher grains have sieve-textured centres with inclusions of epidote and feldspar. The majority of the grains are clouded and have strongly embayed margins, and there are rare euhedral grains. Unfortunately, the shape of the ultramafic pods cannot be used as a strain marker to assess the distribution of strain within the zone. Even in the low-strain areas outside the shear zone the pods may be strongly flattened, whereas within some of the highest strain gneisses there are examples of almost spherical pods.

No evidence for an early high-grade metamorphism was found within the mapped area but this has been well documented elsewhere by Evans (1965), Evans & Lambert (1974) and Sheraton *et al.* (1973 a & b). The rocks within the mapped area are all of amphibolite-facies metamorphic grade, the stable paragenesis inside and outside the shear zone being plagioclase-quartz-hornblende-biotite-epidote. This gives a temperature interval of 500°- 600°C (Dickinson & Watson 1976) but no indication of pressure. The presence of fresh hornblende and white mica within the sheared gneisses indicates that amphibolite-facies conditions outlasted the final shearing event.

2.11.3.b Intrusive bodies.

There are several types of intrusive body in the study area, the most numerous of which are the quartz-epidiorite "Scourie" dykes. The term quartz-epidiorite is used here as no unmetamorphosed examples exist within the area, and so a term implying an original igneous composition is avoided. Tarney (1973) called these dykes the "early dolerites" and described unaltered examples from near Loch Assynt to the E of the area. Within the mapped area the quartz-epidiorite dykes vary from 20 m to a few tens of cm in width, the largest being traceable for over 6 km. All the quartz-epidiorite dykes in the area are sub-parallel to the main shear zone. The dykes consist of hornblende, plagioclase, epidote and quartz. The felsic components occur in approximately spherical aggregates which give the rock a speckled appearance in hand sample. As the rock deforms these aggregates act as strain markers and their axial ratios may be used to determine the strain at any point within the dyke. The quartz-epidiorites in the area deform in a characteristic way, the strain becoming localised into a network of discrete shear zones within the dyke. These shear zones form an anastomosing pattern surrounding blocks of relatively undeformed material. In the less deformed dykes, the strain is concentrated into shear zones at the margins of the dyke.

The undeformed quartz epidiorites have a large variation in grain size and are typically composed of hornblende (55%), plagioclase (An 19-33)(25%), quartz (10%) and epidote (8%) plus opaques and accessory minerals (2%). The hornblende occurs as both large anhedral sieve-textured grains with quartz inclusions and embayed margins, and as small prismatic grains within the groundmass, the smaller prismatic grains often showing a moderate preferred shape orientation. The plagioclase in the groundmass occurs as small anhedral grains usually

heavily sericitized. There is some indication that there may have been feldspar phenocrysts or porphyroclasts but these are very rare. Quartz is present as concentrations of 5 - 10 grains or as blebby inclusions within the larger hornblende grains. The rock as a whole has a granular texture in thin section and contains quite large amounts of epidote. The felsic aggregates are composed of plagioclase, quartz, sericite and epidote, all as small, anhedral, equant grains. Some quartz grains show strain features such as undulose extinction and sub-graining.

With increasing deformation, the preferred orientation of the prismatic hornblendes increases, the felsic aggregates become flattened in the plane of the foliation, and the epidote content decreases. The number of large sieve-textured hornblendes decreases leaving only a few hornblende porphyroclasts, usually approximately $\times 10$ the average grain size in the groundmass. The foliation deflects around these porphyroclasts and there may be growth of new quartz and opaques in the pressure shadows. The prismatic hornblendes are of a very uniform size and there is an increase in the segregation of mafic and felsic phases, very few quartz and feldspar grains occurring in the mafic domains. Within the felsic aggregates there is a weak preferred shape orientation of quartz and feldspar grains, the quartz grains exhibit subgraining and there is evidence of grain size reduction by progressive subgrain rotation. The felsic aggregates appear to be slightly more competent than the groundmass as the foliation deflects around them. Occasionally late rosettes of anthophyllite cross-cut the foliation.

With further increases in deformation the quartz-epidiorites take on a striped appearance as the felsic aggregates are further flattened in the plane of the foliation. The thin sections have a banded appearance with planar felsic and mafic domains. Feldspar is

dominant in the felsic domains occurring as lightly sericitized, small, equant grains. The quartz appears annealed and has a moderate preferred shape orientation parallel to the banding. The mafic domains consist of extremely uniform small prismatic hornblendes with a very strong preferred orientation. Epidote is almost absent in the highest strain portions of the dykes and there is a decrease in the amount of opaque ore minerals. As with the gneisses, there appears to be no change in the bulk composition between the quartz-epidiorite dykes outside the shear zone and those within it.

The other common intrusive bodies in the area are irregular ultrabasic intrusions mapped as picrites by Tarney (1973). Within the study area these have been severely altered and show none of their original mineralogy; unaltered examples however do occur to the E away from the shear zone. The mapped bodies consist of talc, chlorite, carbonate, actinolite and epidote, in various proportions depending on the degree of alteration. In hand specimen the rocks are extremely soft and highly sheared. The degree of alteration, metamorphism and deformation within these samples means that they are of little use in determining the structural history of the area.

A fine-grained amphibolite dyke outcrops on the coast at Altan na Bradhan, consisting of hornblende altering to anthophyllite, some epidote and accessory feldspar. There is a weak fabric visible in the thin section due to the moderate preferred orientation of small prismatic hornblendes, but in general the rock has a granular texture.

In the N of the area to the E of Clachtoll a dyke of similar appearance to the quartz-epidiorites is intruded along the centre of an ultrabasic dyke, thus post-dating it. This dyke however contains relict phenocrysts of plagioclase, now heavily sericitized, rather than the felsic aggregates of the quartz-epidiorites, and it is these that give the dyke a similar speckled appearance. The groundmass is

mainly hornblende, some large anhedral grains containing inclusions of quartz, together with quartz and plagioclase. To avoid confusion with the quartz-epidiorites this dyke has been termed a metadolerite as it retains some of the original igneous textures.

2.II.4 Description of structures and tectonometamorphic history.

In addition to mapping on a 1:10,000 scale, detailed maps on a 1:200 scale were constructed for areas of particular interest. Sections that were not suitable for mapping were logged on a cm scale and detailed traverses across the shear zone were logged on a sub-metre scale. Examination of the Canisp Shear Zone at these different scales has enabled a complete record of the structural history to be established.

The early history of the Assynt area including the Canisp Shear Zone has been discussed in detail by Sheraton *et al.* (1973a,b). They propose that the early flat-lying foliation, as seen in the S of the study area, is the result of the transposition of a previous layering at the crust/mantle interface, possibly due to a degree of decoupling at the base of the crust. The abundance of early intrafolial folds and the truncation of banding in certain basic gneiss bodies, are used as evidence to support this suggestion. At this time extreme boudinage of early ultramafic layers led to the formation of the ultramafic pods within the gneiss and partially flattened them in the plane of the foliation.

The early foliation has been locally folded by NE-SW trending folds, this is well demonstrated on the An Fharaid Mhor peninsula (Fig 2.3) where a mafic/ultramafic body has been folded into a synform which plunges gently to the SW (Tarney 1978). Sheraton *et al.* (1973) also recognised a series of early monoclinial folds with axes trending 230° and plunging gently to the SW. These events took place under

granulite-facies conditions during the Badcallian.

The beginning of the Inverian episode is marked by the onset of amphibolite-facies conditions causing retrogression of the granulite-facies Badcallian gneisses throughout the area. The main Inverian structures in the area are the Lochinver Monocline and a belt of sub-vertical well foliated gneisses to the N of the monocline (Figs 2.3 & 2.4). The Lochinver Monocline folds the flat-lying Badcallian foliation along an approximately horizontal axis trending ESE-WNW the S limb being horizontal and the N limb dipping steeply N. There is an attenuation of the fabric within the N limb of the monocline. On the coast to the S of Clachtoll the Inverian gneisses are best exposed (Fig 2.6), they are strongly deformed with a good sub-vertical foliation and a weak, steeply SE-plunging lineation, which is also present in the N limb of the Lochinver Monocline. In the N of the area the transition back into Badcallian structure is more complicated than to the S as small relict areas of Badcallian gneiss, now retrogressed to amphibolite grade, are surrounded by Inverian and Laxfordian structures. The Lochinver Monocline and the belt of high-strain gneisses are taken to represent a major shear zone, approximately 1 km wide, that was operating during the Inverian, the steeply SE-plunging lineation representing the movement direction within this zone. The geometry of the Lochinver Monocline indicates a downward movement of the northern block relative to the stable flat-lying gneisses in the S of the area, and, in conjunction with the lineation, a dominantly dip-slip movement with a small dextral component.

Following the Inverian was a period of dyke emplacement. Probably the earliest dyke in the area is the fine-grained amphibolite dyke that outcrops on the coast at Altan na Bradhan (Fig 2.7) (see 2.II.3.b). This is a small dyke that is only exposed over a few m. The dyke cross cuts the Inverian shear foliation, thus dating the fabric

Fig 2.6



Fig 2.6 Inverian shear foliation to the S of Clachtoll (GR 04162660).

Fig 2.7



Fig 2.7 Fine grained amphibolite dyke cutting Inverian shear foliation and subsequently folded during the Laxfordian with formation of a weak axial planar fabric within the dyke. Port Alltan na Bradhan (GR 05122612).

in this area, and has been subsequently folded with the formation of a weak axial-planar fabric. There is no direct evidence for the age of this dyke relative to the other intrusive bodies, but field relations and the degree of alteration suggest it is early in the sequence, possibly associated more with the end of the Inverian than the other dykes.

Evidence for the relative age of the other dykes is not present within the area as no cross cutting relationships between the quartz-epidiorites and the ultrabasic bodies are seen. Tarney (1973) established that the "early dolerites" (quartz-epidiorites) pre-date the "picrites" (ultrabasics) from evidence to the E of the present study area. The quartz-epidiorites were emplaced parallel to the Inverian shear zone along planes of weakness formed during the shearing. This is evident from the large dyke that cuts the Lochinver Monocline (Figs 2.2 & 2.4) outcropping on the coast at Achmelvich and continuing inland to E of Lochinver. Despite being outside the later Laxfordian shear zone the dyke still parallels the zone, thus reorientation of the quartz-epidiorites due to the later shearing has been negligible, and therefore they cannot be used to estimate the displacement on the zone (c.f. Jensen 1984).

The ultrabasic bodies are of variable shape, some being extremely irregular in outcrop while others are relatively planar dykes. The irregular outcrops may be due to later modification of the relatively soft rock during the Laxfordian deformation, but the nature of the outcrop makes this impossible to verify. The only definitive dyke relationship within the area is to the E of Clachtoll where a metadolerite dyke (see 2.11.3.b) is intruded along the centre of an ultrabasic body (Fig 2.8). Due to erosion the contact between the two is not visible and so the implied relationship cannot be supported by evidence from chilled margins. The emplacement of the

Fig 2.8

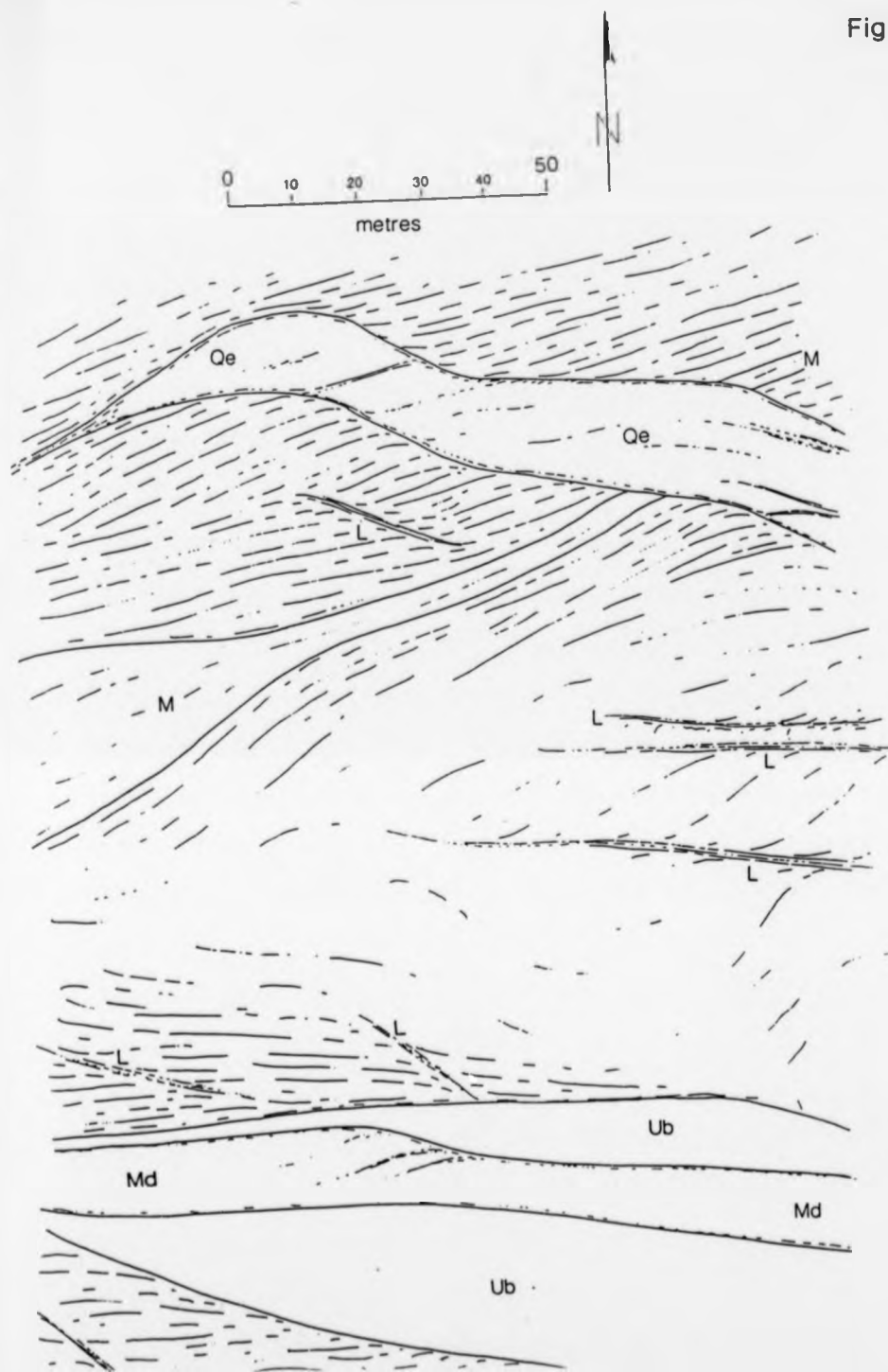


Fig 2.8 Large scale map of an area to the E of Clachtoll (GR 054271) showing the relationships between the phases of dyke emplacement and the principal tectonic episodes. M - ultramafic layer in gneiss, Qe - quartz-epidiorite, Ub - ultrabasic body, Md - metadolerite, L - Laxfordian shear zones.

quartz-epidiorites appears to have been dilational and therefore associated with a period of N-S extension in the area. To the E of Clachtoll a distinctive ultramafic band within the gneisses is offset where it is cut by a quartz-epidiorite dyke. The offset of the ultramafic band has been modified by later Laxfordian shearing on the margins of the quartz-epidiorite, but restoring this the initial offset indicates extension perpendicular to the dyke walls.

Following this period of dyke emplacement the shear zone was reactivated during the Laxfordian episode. The margins to the Laxfordian shearing are well exposed on the coast at Achmelvich and to the S of Clachtoll. In the S a band of steeply S-dipping mylonites (Fig 2.9) cut the Inverian foliation in the N limb of the Lochinver Monocline (Fig 2.4) giving clear evidence of a second phase of shearing. Within these mylonites there is a strong penetrative lineation that plunges at approximately 20° to the SE (Fig 2.10). This lineation is also present in the high-strain gneisses that occur close to the margins and at places within the zone. The plunge of the lineation within the gneisses is used to distinguish areas of dominantly Inverian structure from those with a dominantly Laxfordian fabric, as the foliation planes are often parallel (Fig 2.11). This approach is supported by the occurrence of discrete small shear zones in the area (Figs 2.12 & 2.13). These only occur in areas where there is a steeply plunging lineation. Thus the small shear zones are Laxfordian in age and the steep lineation is Inverian. The Laxfordian deformation within the zone is concentrated in discrete planes up to $\times 10$ m in width. This is illustrated by the data from the traverses taken across the zone. On these the strain within the gneisses was quantified using various parameters. As there are no definitive strain markers within these rocks that can be used in the field, a class system was constructed based on the width and definition of the

Fig 2.9



Fig 2.9 Laxfordian mylonites, S margin Canisp Shear Zone (GR 05732550).

Fig 2.10

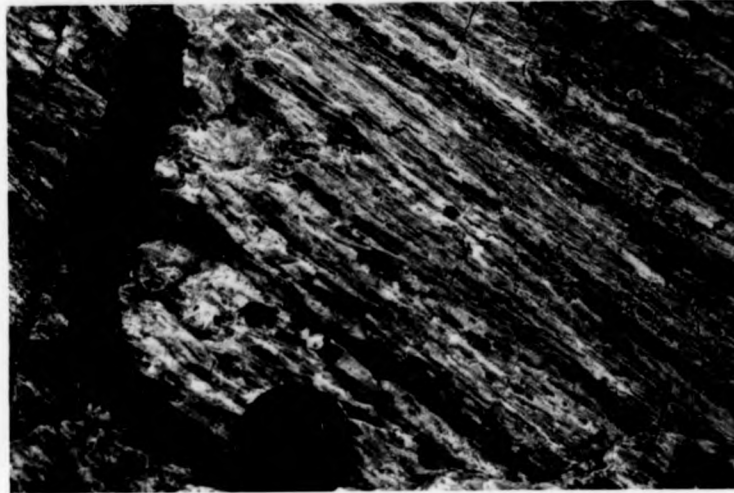
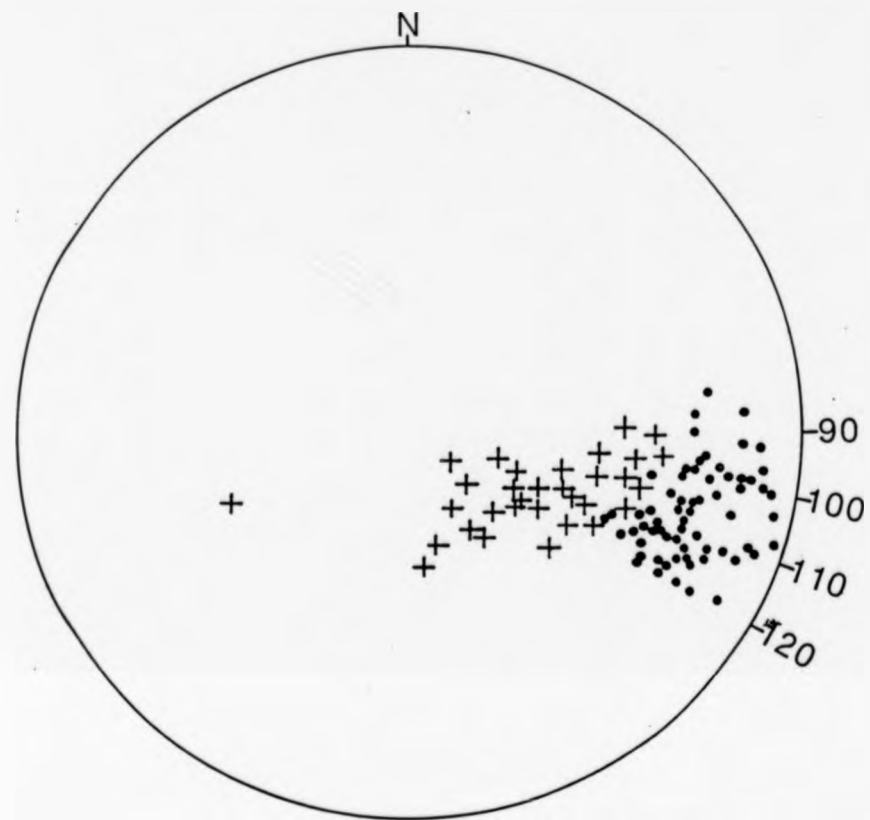


Fig 2.10 Laxfordian lineation within Canisp Shear Zone (GR 05742555).

Fig 2.11



+ Lineations from areas of low Laxfordian strain
• Lineations from areas of high Laxfordian strain

Fig 2.11 Stereoplot of lineations showing the division between areas of high Laxfordian strain and areas relatively unaffected by the Laxfordian deformation.

Fig 2.12



Fig 2.12 Laxfordian shear zone cutting Inverian gneisses (GR 07592554).

Fig 2.13



Fig 2.13 Laxfordian shear zone cutting Inverian gneisses (GR 04162660).

banding and the development of the foliation (Fig 2.14). Class 1 corresponds to the lowest strain gneisses seen in the area with only a diffuse mineral layering and a very weak foliation. Classes 2 - 4 represent an increase from a weak foliation with moderately well defined banding to a strongly deformed gneiss with fine clearly defined banding and a strong foliation. Class 5 is a true mylonite. Figs 2.15 - 2.17 show the qualitative variation in strain across the shear zone highlighting the extremely heterogeneous nature of the deformation, and the way in which the Laxfordian shearing is concentrated into narrow high-strain mylonite zones.

The Laxfordian deformation is associated with both the formation of a completely new fabric, as in the mylonites of the S margin of the zone, and the modification of the earlier Inverian shear fabric. This means that unless a lineation is present it is impossible to separate the two episodes in areas of moderate deformation. In places there is modification and refolding of Inverian structures. Folds within the zone have small interlimb angles and highly attenuated limbs, some showing a transition to shear zones along the fold limbs (Fig 2.18). These are interpreted as Inverian folds that have been tightened and sheared during the Laxfordian. In areas of high Laxfordian deformation there has also been rotation of the fold axes into parallelism with the strong Laxfordian stretching lineation. Refolding of folds occurs throughout the area especially at Port Alltan na Bradhan where Inverian folding of a heavily modified Badcallian banding has been refolded during the Laxfordian along axes parallel to the Laxfordian lineation (Fig 2.19).

The Laxfordian shearing also affects the dykes in the area, both inside and outside the shear zone. Outside the zone the deformation within the dykes is confined to narrow shear zones along the dyke margins. These may be up to 0.5 m in width within the dyke

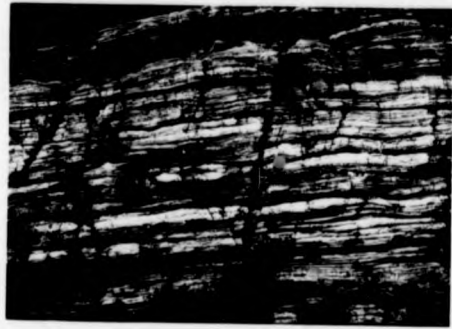
Fig 2.14



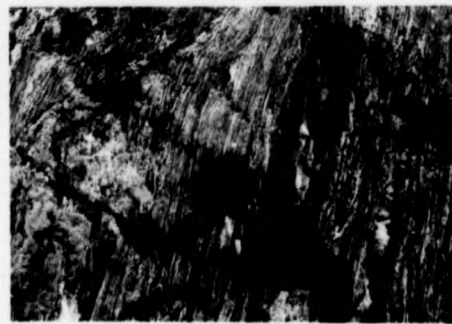
Class 1



Class 2



Class 3



Class 4



Class 5

Fig 2.14 Class system used to qualitatively assess strain in the field.

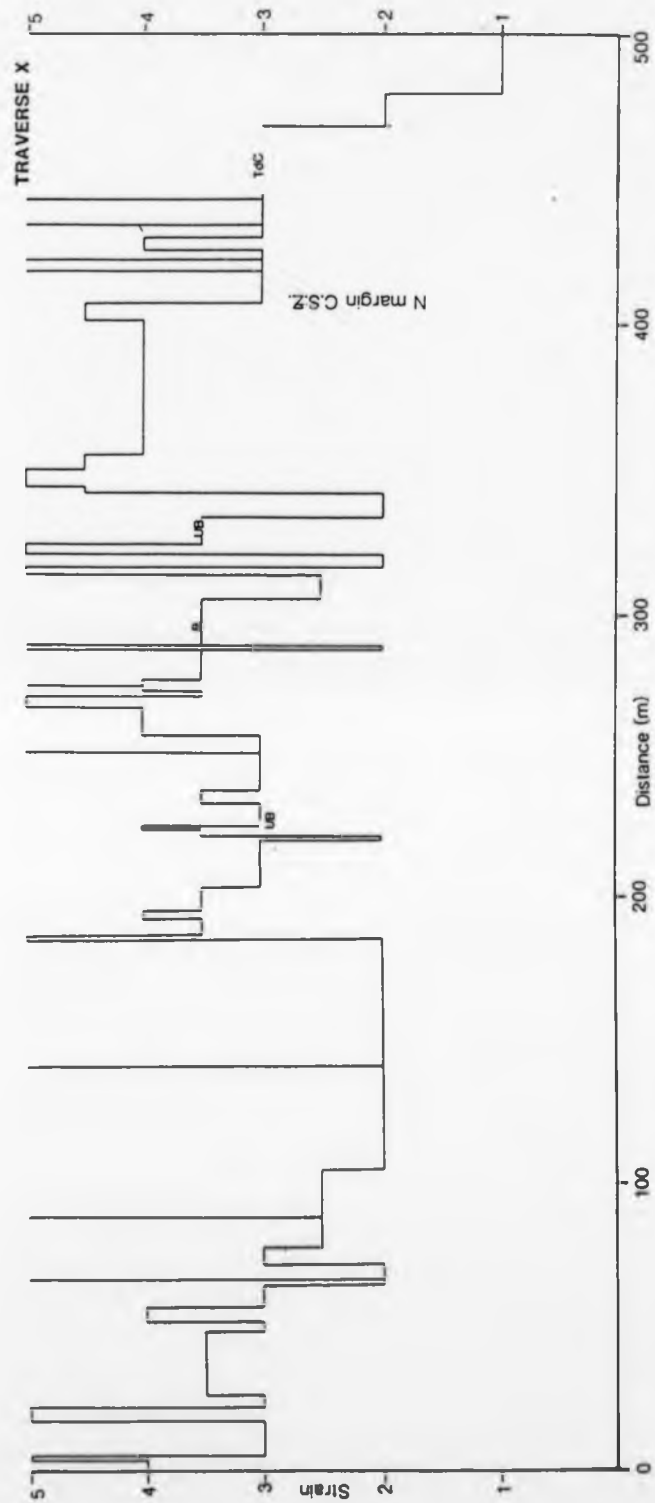


Fig 2.15

Fig 2.15 Qualitative strain profile along traverse X from GR 04222614,
to GR 04082672.

Fig 2.16

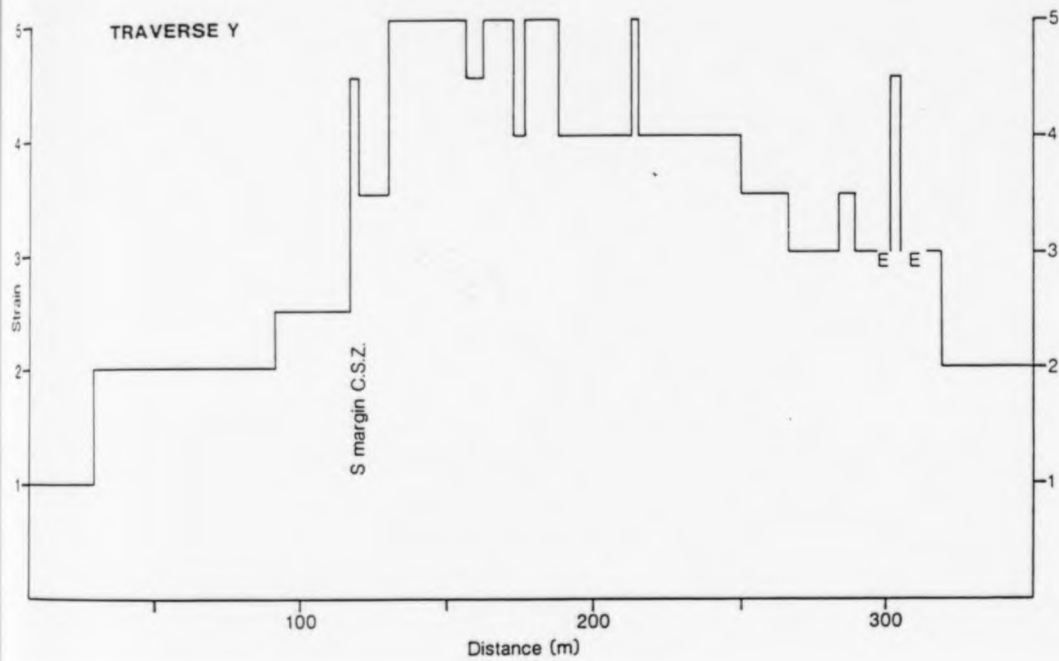


Fig 2.16 Qualitative strain profile along traverse Y from GR 05722537,
to GR 05292597.

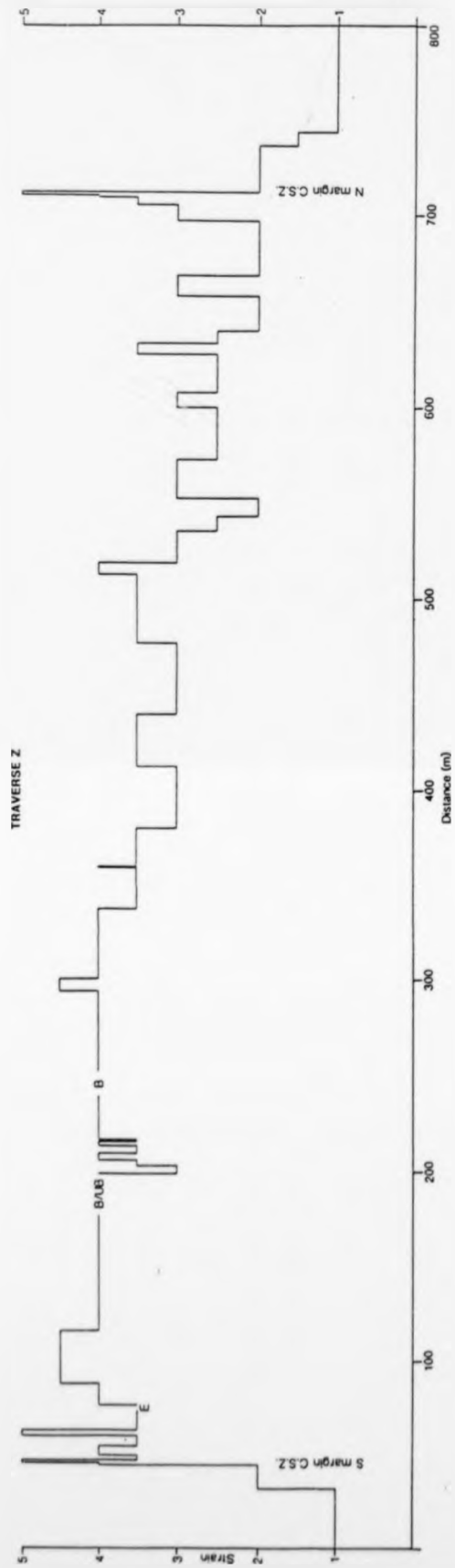


Fig 2.17

Fig 2.17 Qualitative strain profile along traverse Z from GR 09302370,
to GR 09732436.

Fig 2.18



Fig 2.18 Inverian folds that have been tightened and attenuated, with shearing along the limbs, during the Laxfordian deformation (GR 05372587).

Fig 2.19



Fig 2.19 Refolded folds Port Alltan na Bradhan (GR 05102610), the axes of both folds plunge shallowly to ESE parallel to the Laxfordian movement lineation.

but usually less within the host gneiss. Often the gneiss only displays a deflection of the foliation into the dyke margin and the majority of the deformation occurs within the dyke (Fig 2.20). Where the dyke margin is irregular the marginal shear zones form a network surrounding a block or blocks of less deformed material (Fig 2.21). Within the shear zone the deformation within the dykes is concentrated into discrete narrow shear zones that form an anastomosing pattern throughout the dyke (Fig 2.22). This network of zones surrounds blocks of undeformed dyke that have been shuffled in a process analogous to grain boundary sliding (Fig 2.23). Nearly all the shear zones within the network exhibit the same sense of displacement as those along the shear zone margins, some zones however have an opposite sense of movement due to the relative movement of the undeformed blocks. The sense of shear on the dykes both inside and outside the main shear zone is a dextral S-side-up movement. The lineation in the dyke shear zones plunges between 10° and 30° to ESE as does the penetrative lineation in the gneisses with high Laxfordian strain. Thus movement during the Laxfordian shearing was dominantly strike-slip but with the same dextral S-side-up sense as the Inverian shearing (Figs 2.24 & 2.25). This movement sense for the Laxfordian episode agrees with the conclusions of Jensen (1984) who used the symmetry of quartz c-axes to indicate the same sense of movement. The Laxfordian shearing took place at mid-amphibolite facies conditions and these continued after the main tectonic activity had ceased.

The history of the study area is neatly summarised in a small area to the E of Clachtoll (Fig 2.8). Here an area with Badcallian banding, displaying original ultramafic layers, early recumbent, isoclinal, intrafolial folds (Fig 2.26) and an undulating, flat-lying, weak foliation, is enclosed by two Inverian shear zones. These consist of broad belts, over 50 m in width, of moderately high-strain gneiss

Fig 2.20



Fig 2.20 Shear zone on the margin of a quartz-epidiorite dyke (GR 05652571).

Fig 2.21



Fig 2.21 Marginal shear zone on quartz-epidiorite dyke (top right) diverging from the margin due to a step in the contact (GR 05652506).

Fig 2.22

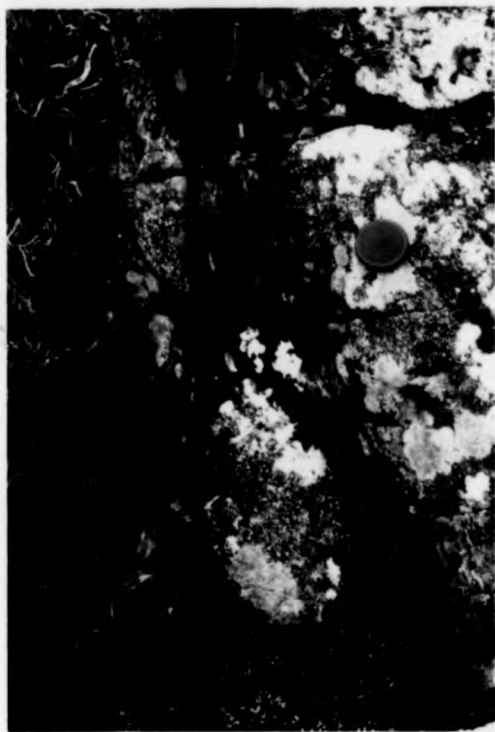


Fig 2.22 Shear zones forming an anastomosing network in a quartz-epidiorite dyke, surrounding pods of relatively undeformed dyke material (GR 05652571).

Fig 2.23

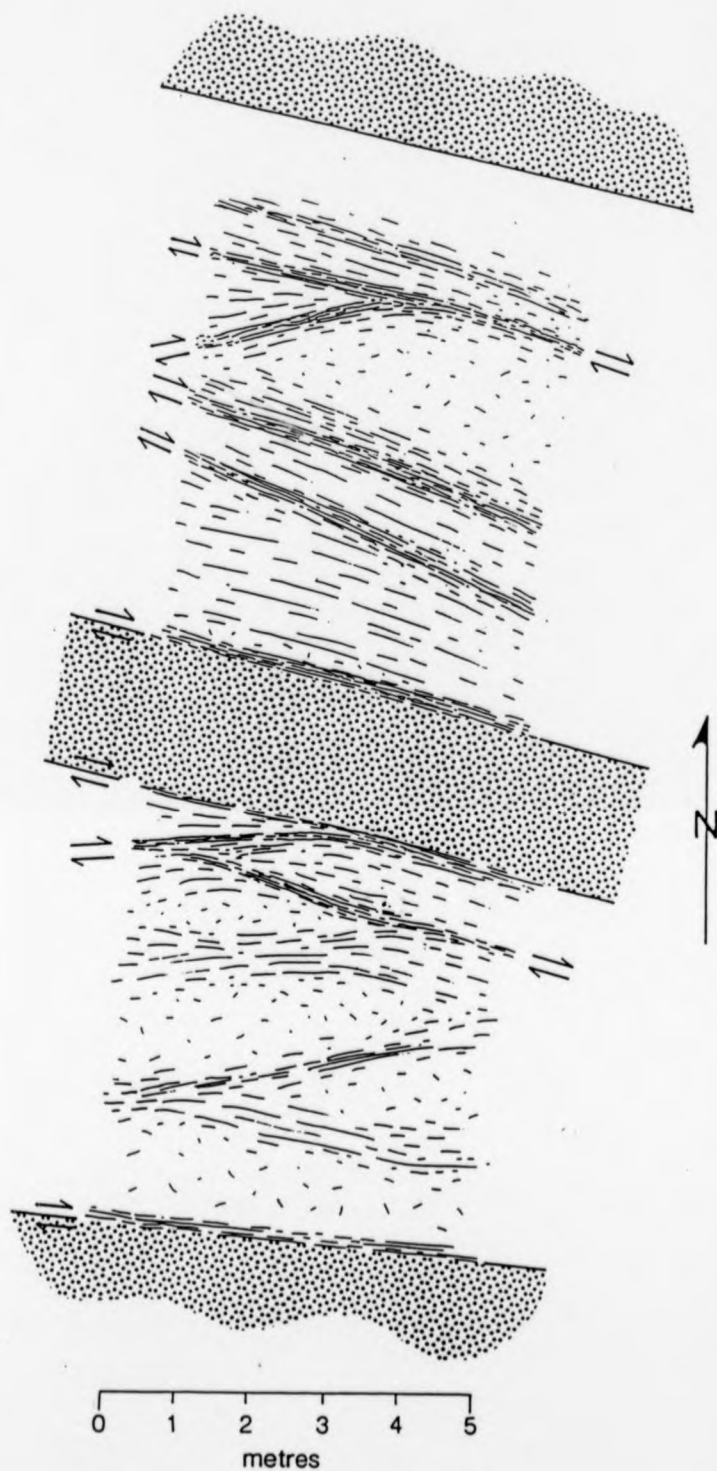


Fig 2.23 Log of dyke shown in Fig 2.22, shading = gneiss.

Fig 2.24

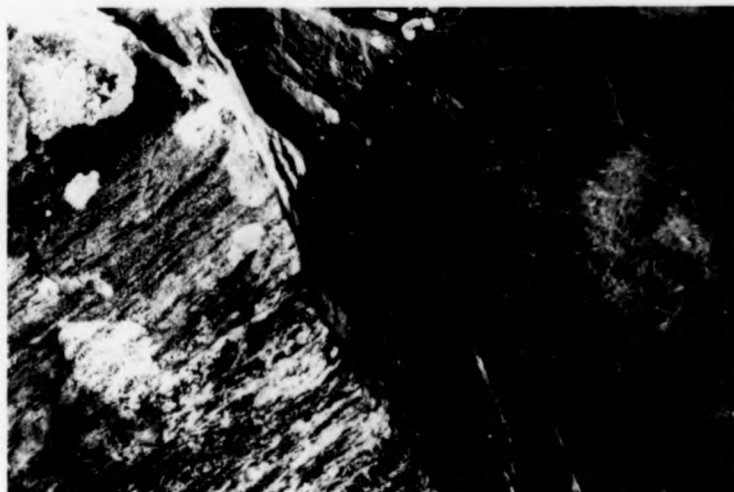


Fig 2.24 Vertical section through dyke margin at Achmelvich (GR 05922509) showing the absence of any deflection of the host gneiss fabric along the marginal shear zone, as this section is perpendicular to the movement direction.

Fig 2.25

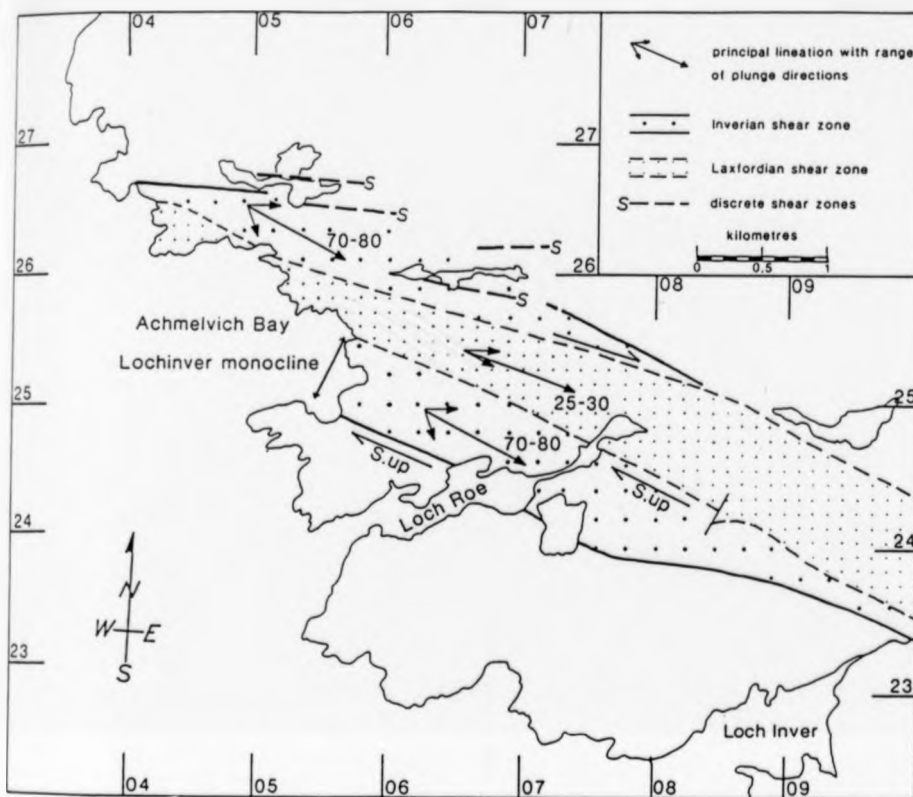


Fig 2.25 Movement direction summary diagram for the Inverian and Laxfordian movements on the Canisp Shear Zone.

Fig 2.26

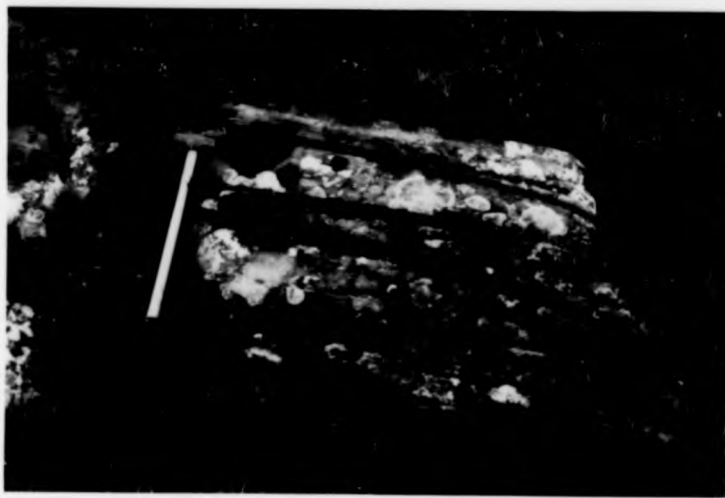


Fig 2.26 Recumbent folds of Badcallian age in ultrabasic gneiss (GR 05402714).

with a sub-vertical or steeply N-dipping foliation. They contain abundant folds, all with small interlimb angles, sub-vertical axial planes and axes plunging steeply ESE (Fig 2.27). These Inverian gneisses are intruded by three petrologically distinct dykes, all sub-parallel to the foliation. The area of Badcallian gneiss has no intrusions within it as the dykes were preferentially intruded along planes of weakness formed during the Inverian shearing. As already stated the emplacement of the quartz-epidiorite dykes was dilational, from the evidence of the ultramafic layer in the gneiss across the dyke. There is no direct evidence as to the mechanism of emplacement of the other dykes but these are also assumed to be dilational.

The Laxfordian deformation within this area is concentrated in discrete zones, both within the gneisses and in the dykes. The shearing in the dykes is confined mainly to the margins (Fig 2.28) but where dyke orientation is unfavourable for marginal shear the shear zones cut across the dyke sub-parallel to the Inverian foliation. The Laxfordian shear zones within the gneisses are generally sub-vertical or steeply S-dipping. They strike ESE-WNW and have a dextral strike-slip movement sense; thus they are analogous to the Laxfordian element of the Canisp Shear Zone.

Post-dating the Laxfordian deformation on the Canisp Shear Zone there was brittle reactivation along the margins of the shear zone and along the margins of some dykes. Brecciated mylonite on the S margin of the zone can be seen at several localities (Fig 2.29 & 2.30); this brecciation also affects the Inverian gneiss to the N of the main Laxfordian zone (Fig 2.31).

In a dyke on the S side of Achmelvich Bay the sheared margin has been brecciated and pods of pseudotachylite have formed within the breccia (Fig 2.32). Later pre-Torrionian NE-SW faulting has locally affected both the dykes and the main shear zone but the displacement

Fig 2.27



Fig 2.27 Inverian folding in gneisses (GR 05402705).

Fig 2.28

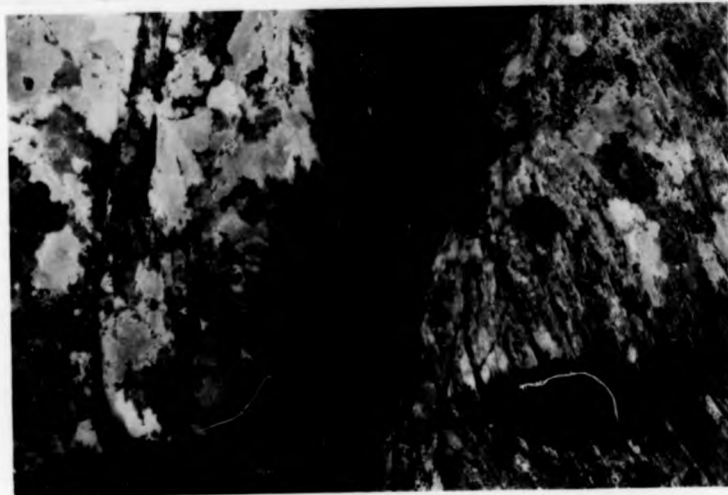


Fig 2.28 Laxfordian shear along the margin of a quartz-epidiorite dyke showing dextral movement sense from the deflection of the foliation in the gneiss (GR 05402717).

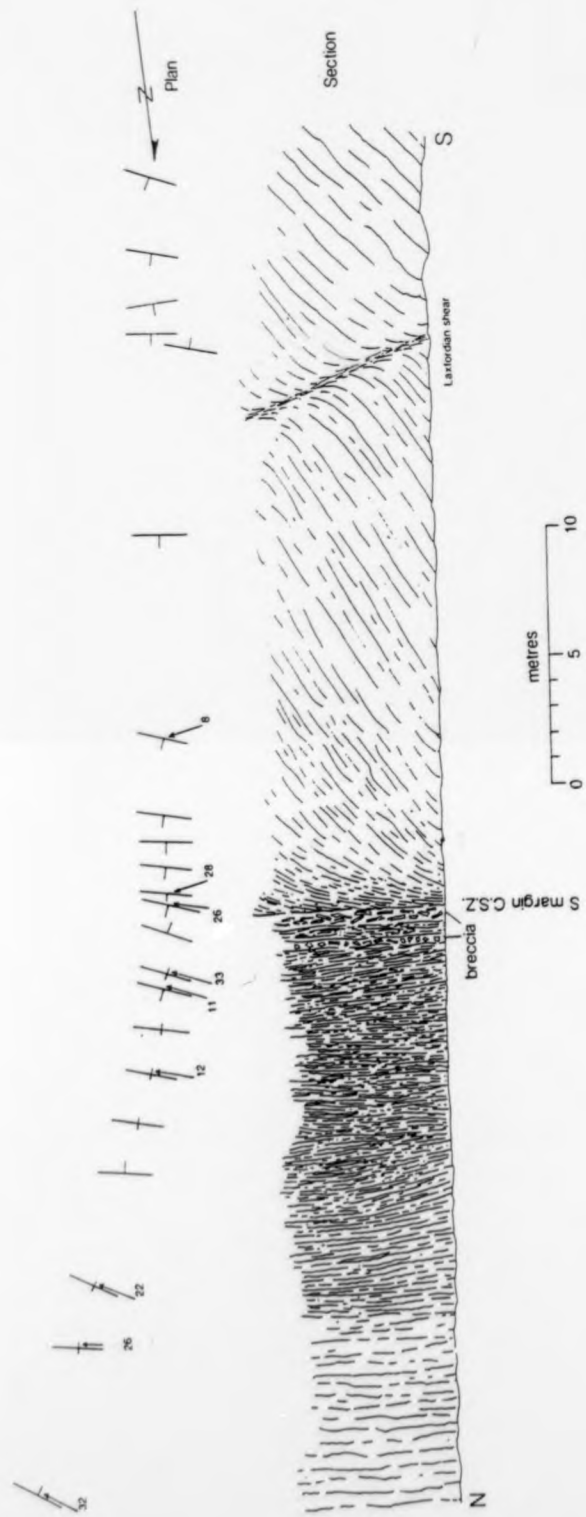


Fig 2.29 Log of the S margin of the Canisp Shear Zone (GR 083243).

Fig 2.30



Fig 2.30 Brecciated gneiss S margin Canisp Shear Zone (from Fig 2.29)
(GR 08282433).

Fig 2.31



Fig 2.31 Brecciated gneiss S of Clachtoll (GR 04102672).

Fig 2.32



Fig 2.32 Pseudotachylite within a brecciated, sheared dyke margin, S side Achmelvich Bay (GR 05482490).

on these faults is very small.

2.II.5 Discussion

Several workers have described pre-Laxfordian features in and around the Canisp Shear Zone. Sheraton *et al.* (1973 b), used the term "steep belt" to describe the zone of sub-vertical Inverian rocks from the Lochinver Monocline northwards and attributed the formation of this belt to the large scale monoclinal folding in the area. Also Evans & Lambert (1974) noted a zone of intensely deformed Inverian gneisses. However neither group of workers recognised that this represents a major Inverian shear zone, or discussed the movement on the zone, prior to the Laxfordian shearing. The intensity of the deformation to the N of the Laxfordian shear zone, and the attenuation of the fabric across the Lochinver Monocline, indicate that considerable movement has taken place, probably sub-parallel to the weak, steeply SE-plunging lineation. Certain other features within the zone, such as the refolded folds and the parallel emplacement of the dykes, are more easily explained by two separate phases of movement.

The change from dominantly dip-slip tectonics in the Inverian to dominantly strike-slip movement in the Laxfordian, but still with a dextral S-side-up sense, concurs with models for the structural history of the southern Lewisian (Coward & Park 1987).



2.III SMALL SCALE SHEAR ZONES

2.III.1 Introduction

2.III.1.a Aims and objectives

The principal objective of this part of the field work was to compile a data set based on observations from a large number of cm-scale shear zones from the Lewisian of the NW Highlands. This data could then be used to test and constrain a model for shear zone formation and development. The secondary objective was to investigate the factors influencing and controlling shear zone initiation and development and to assess the relative importance of localization and propagation in shear zone development.

2.III.1.b Methods of approach

The areas used for this part of the study were within the southern and central blocks of the mainland Lewisian outcrop. A traverse was taken beginning in the Torridon area and sampling at localities up to Tarbet just S of the Laxford Front (Fig 2.33). The choice of zones studied was governed to a large extent by the need to produce data that would be of use in testing and constraining a mathematical model. Most of the zones studied are in the quartz-epidiorite "Scourie" dykes. These were chosen for several reasons; firstly the shear zones within the dykes are of a suitable size, usually up to 5 cm in width, thus they can be analysed right across their width to provide a complete profile. Secondly the felsic aggregates within the dykes provide strain markers that can be used to construct strain profiles across the zone and hence provide estimates of displacement (Ramsay & Graham 1970). Thirdly the rheology of the dykes may be assumed to be relatively constant over the traverse, thus

Fig 2.33

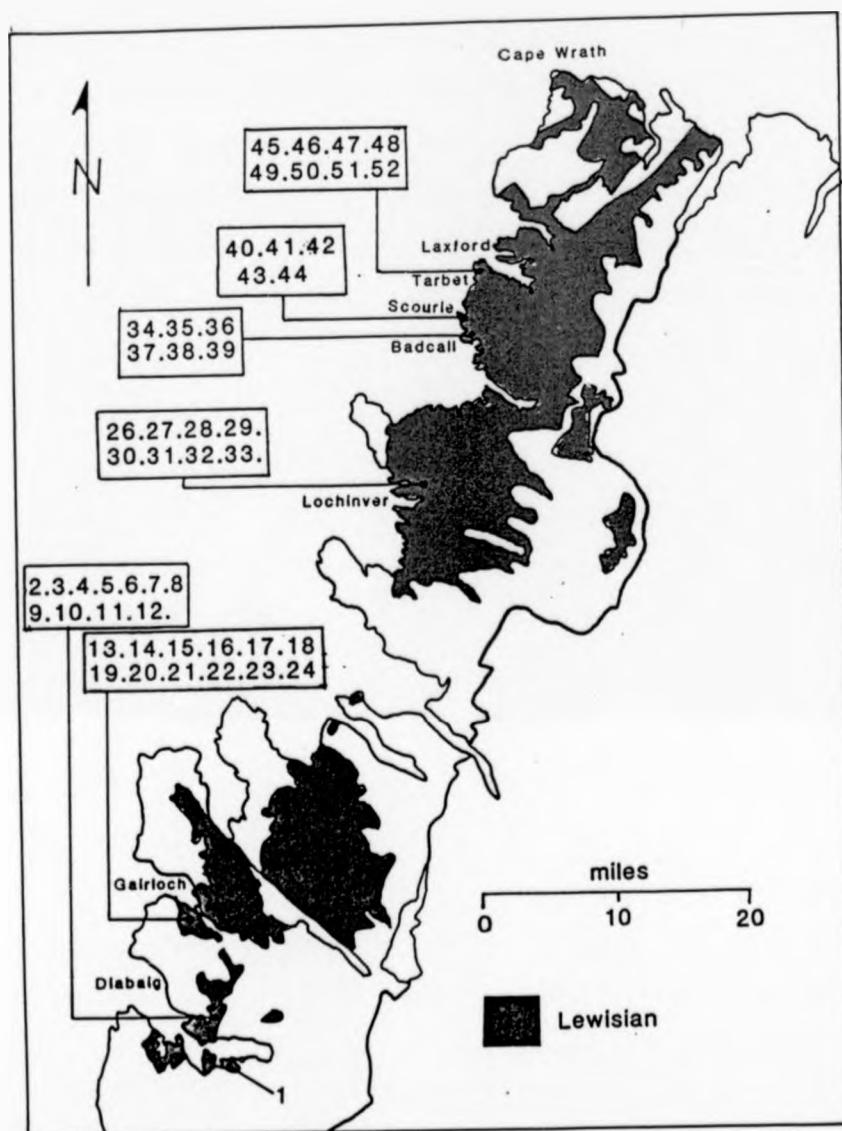


Fig 2.33 Location map for the 52 cm scale shear zones studied.

eliminating one variable that would influence the morphology of the shear zones. Fourthly the dykes are in general relatively undeformed prior to the formation of the shear zones during the Laxfordian (Fig 2.34) and hence pre-existing structures that could influence the development of the shear zones are rare. Thus, in summary, the dykes provide an excellent medium for the study of shear zones because they are 1) relatively homogeneous 2) have no pre-existing fabric or mineralogical banding 3) contain adequate strain markers and 4) are well exposed throughout the area.

Shear zones within the amphibolite facies gneisses in the area were also studied to provide data for the secondary objective of the work. These were usually of a slightly larger scale than those studied in the dykes.

As well as the study of individual zones in isolation, groups of zones that form networks were analysed in an attempt to understand more about the mechanisms that lead to the formation of anastomosing shear zone networks, often characteristic of the deformed dykes in the central region of the Lewisian. Shear zone tips were studied in particular detail as these represent the propagating edge of the zone and may provide particular insight into the way in which shear zones develop and the controls on their direction of propagation.

2.III.2 The data

2.III.2.a Methods

Fifty-two shear zones were examined in total along the traverse, but unfortunately a full analysis of each zone was not possible. In the field each zone was analysed in terms of orientation, displacement direction, lineation, width of deformation and, where possible, length. Photographs of the zone were taken in a plane

Fig 2.34

Fig 2.34 Undeformed quartz-epidiorite dyke (GR 82465956).

KEELE UNIVERSITY LIBRARY

containing the movement lineation and perpendicular to the plane of the zone, and also in the plane perpendicular to the movement direction where possible. Due to the nature of the outcrop of the epidiorite dykes it was nearly always possible to photograph the zones in the required planes as many of the movement directions are sub-horizontal.

2.III.2.b Description of selected zones.

Zone 2, Diabaig Inlier, Torridon. GR 82175901. (Fig 2.35a)

This shear zone was one of the widest zones studied being 3.1 m in width. The zone deforms Inverian gneiss and is Laxfordian in age (Cresswell 1972). The reason for studying this zone in particular is the presence of mafic bodies within the zone that have been deformed. These show a progressive increase in deformation across the zone, the bodies at the margins having a low axial ratio (<5), whereas those towards the centre are elongated along the plane of the foliation. Thus it can be assumed that these bodies will give an estimate of the strain across the zone. The results are shown in Fig 2.35b where the heterogeneous nature of the strain across the zone can be seen. This is analogous to the high and low-strain zones across the Canisp Shear Zone.

Zone 3, Diabaig Inlier, Torridon. GR 82465956. (Fig 2.36)

Shear zone 3 is a marginal shear zone within a quartz-epidiorite dyke. It contrasts with the shear zones seen within dykes in and around the Canisp Shear Zone in that the deformation is concentrated in one broad zone at the dyke margin. The deformation gradient between the dyke margin and the undeformed portion of the dyke is low. Estimates of the shear strain were obtained by measuring

Fig 2.35



Fig 2.35a Shear zone 2 (GR 82175901) showing the deformation of mafic bodies within the zone.

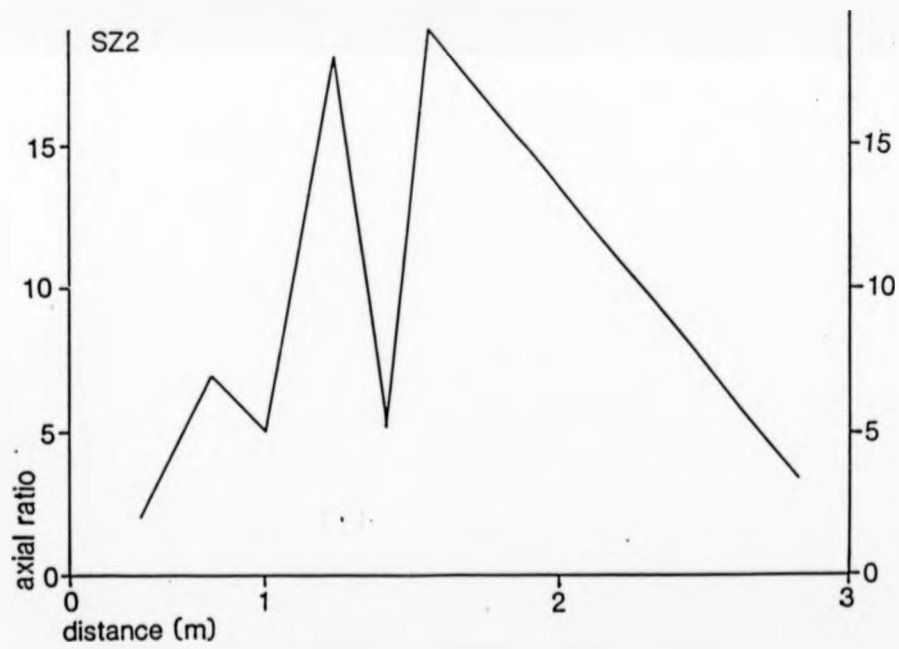


Fig 2.35b Strain profile of SZ2 constructed from the axial ratios of the deformed mafic bodies.

Fig 2.36



Fig 2.36 Shear zone 3 (GR 82465956) showing the deflection of veins into the zone.

the thickness of the vein that was progressively deformed by the zone. This gave a maximum γ of 7.5 close to the margin of the zone.

Zone 4, Diabaig Inlier, Torrison. GR 82465957. (Fig 2.37a)

This zone occurs in the same dyke as zone 3 and is parallel to the margin of the dyke. Unfortunately one side of the zone has been eroded away and therefore only one side of the strain profile could be obtained. Estimates of the maximum shear strain using the width of deformed veins gave a value of γ_{\max} of approximately 10, whereas later analysis using the Ramsay & Graham method gives a γ_{\max} of 7. The shape of the half-profile for this zone again shows a low strain gradient similar to shear zone 3 (Fig 2.37b).

Zones 7 & 8, Diabaig Inlier, Torrison, GR 83086089. (Figs 2.38a & b)

Shear zones 7 & 8 are very similar, and occur in a large quartz-epidiorite dyke just below An Ruadh Mheallan. They are 22 and 17 mm wide respectively and several metres in length. Both give good strain profiles (Figs 2.39), shear zone 7, despite being the larger of the two zones, shows considerably lower maximum shear strains (5.5γ) than shear zone 8 ($20+\gamma$) and also has a considerably smaller displacement of 11.6 cm compared with 23.2 cm for shear zone 8. At the point at which shear zone 8 was measured, the zone had split into two sub-parallel zones a few cm apart but the sum of these displacements will be of the same order as the displacement on the main zone. The strain profiles for zones 7 and 8 contrast with those of previous zones in having a much steeper deformation gradient on both sides of the zone; this may be connected with the decrease in width compared to previous examples.



Fig 2.37



Fig 2.37a Shear zone 4 (GR 82465957).

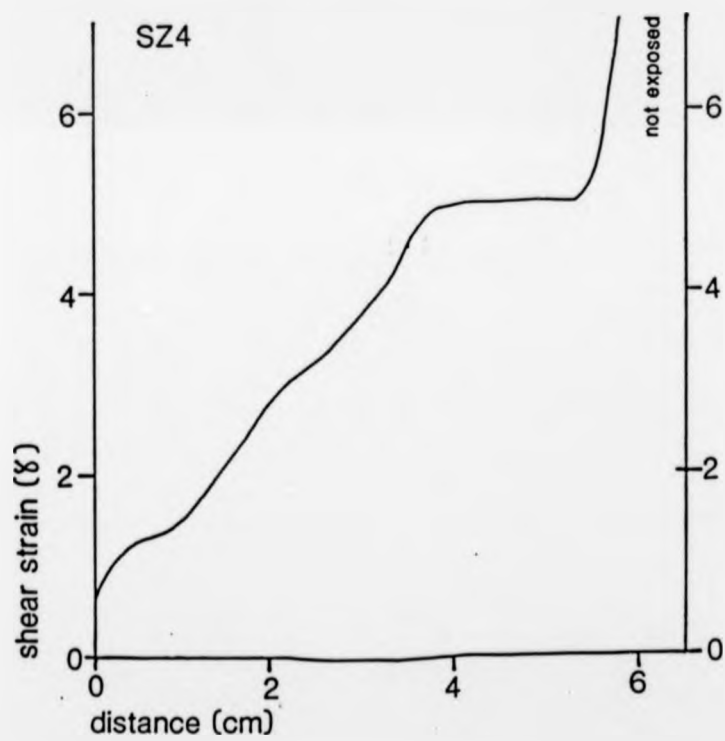


Fig 2.37b Strain profile for SZ4 showing the relatively low deformation gradient.

Fig 2.38

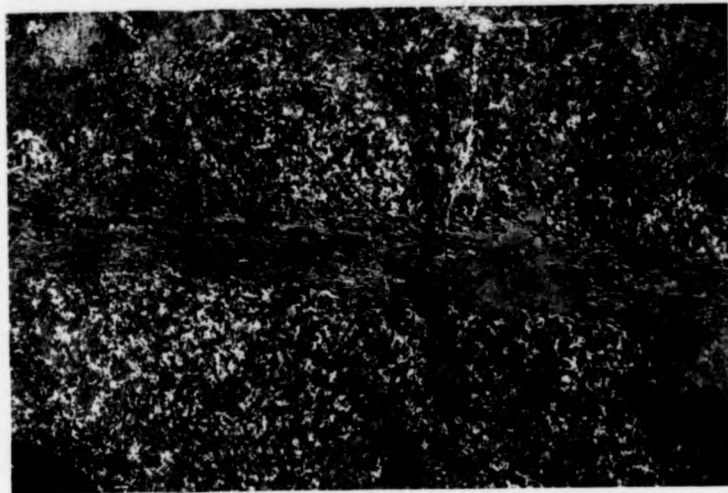


Fig 2.38a Shear zone 7 (GR 83086089).



Fig 2.38b Shear zone 8 (GR 83086089).

Fig 2.39

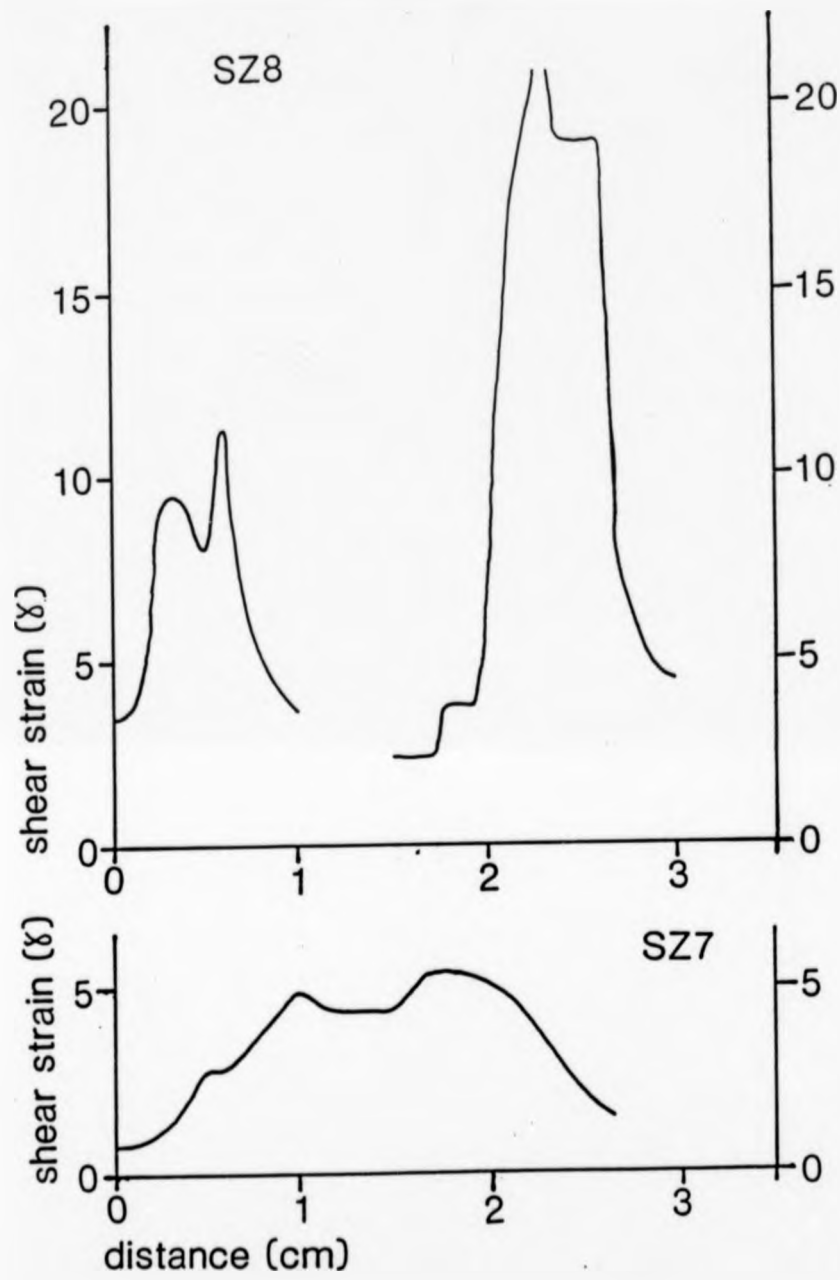


Fig 2.39 Strain profiles for SZ7 and SZ8.

Zone 9, Diabaig Inlier, Torridon, GR 83086089. (Fig 2.40a)

This shear zone is unique amongst all the zones studied in that it is exposed along its entire length and both tips can be seen. Unfortunately it is a very short section on a flat outcrop and therefore no lineation within the zone could be measured. The zone is sub-vertical and it is impossible to know the relation of the exposed part of the zone to the displacement vector or the propagation direction. Despite these limitations the zone was analysed and yielded a displacement of 3.5 cm at a point mid-way along the exposed 35 cm length. (Fig 2.40b) The tip zones were examined carefully and these show a fabric developing at 45° to the plane of the zone immediately in front of the tip (Figs 2.41), in agreement with the observations of Ramsay & Allison (1979). The strain profile for shear zone 9 is very similar to the zones shown in Ramsay & Graham (1970, Fig 16) being steep sided with a rounded tip.

Zone 11, Diabaig Inlier, Torridon, GR 83076088. (Fig 2.42)

This zone is another of particular interest, it appears to be a splay from a deformed vein within a quartz-epidiorite dyke and quickly dies out over 65 cm. The tip is well exposed and again displays a fabric developing at 45° to the plane of the zone (Fig 2.43). Strain profiles were constructed both across the zone and along the line of the zone from undeformed rock through the tip into the zone itself (Figs 2.44a & b). The profile across the zone is relatively flat compared with zones 7,8 and 9 with only a shallow strain gradient and a low peak strain ($3:5\bar{8}$). These low values are possibly due to the zone being a splay. Sections across the zone show a narrowing accompanied by an increase in peak strain, indicating that away from the tip a narrower zone accommodates a greater displacement. This zone also exhibits a broad area of fabric at 45° to the zone around the

Fig 2.40



Fig 2.40a Shear zone 9 (GR 83086089).

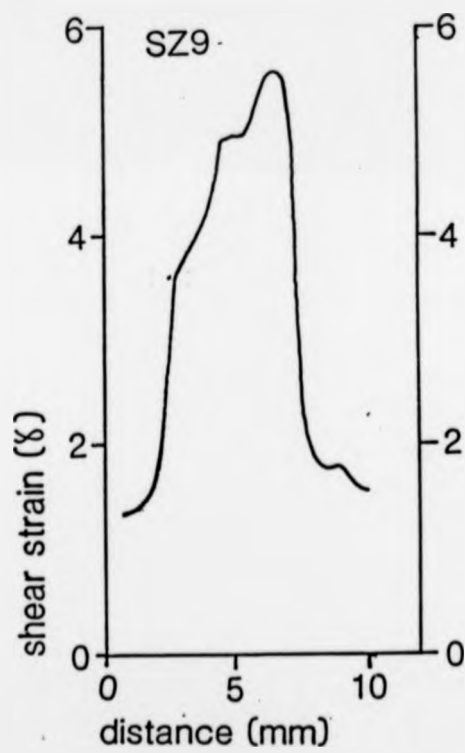


Fig 2.40b Strain profile SZ9.

Fig 2.41

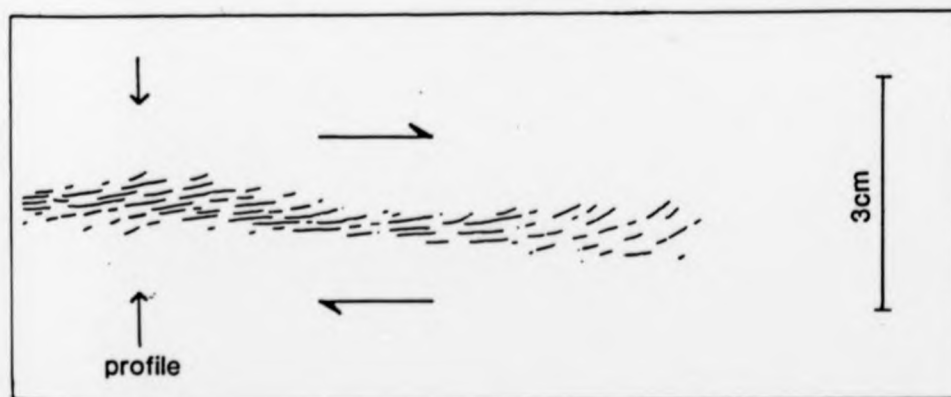
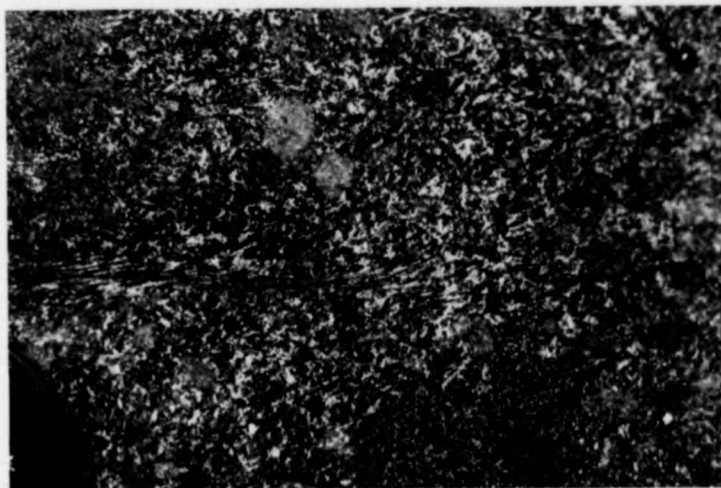


Fig 2.41 Close up view of the tip of SZ9 showing fabric developing at 45 to the plane of the zone in front of the tip.

Fig 2.42

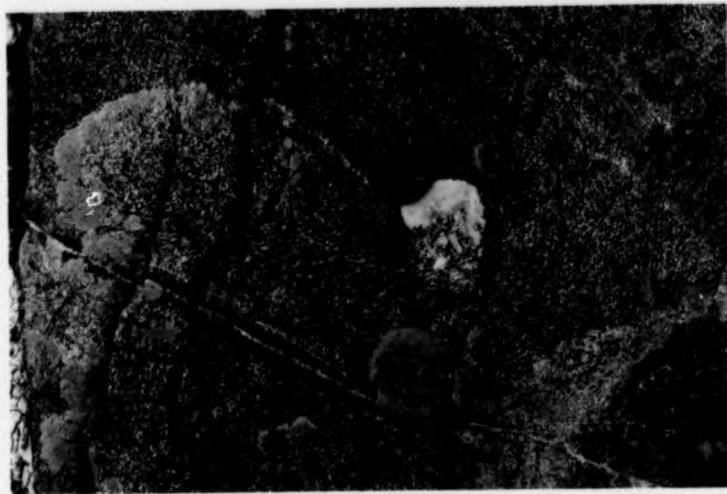


Fig 2.42 Shear zone 11 (GR 83076088).

Fig 2.43

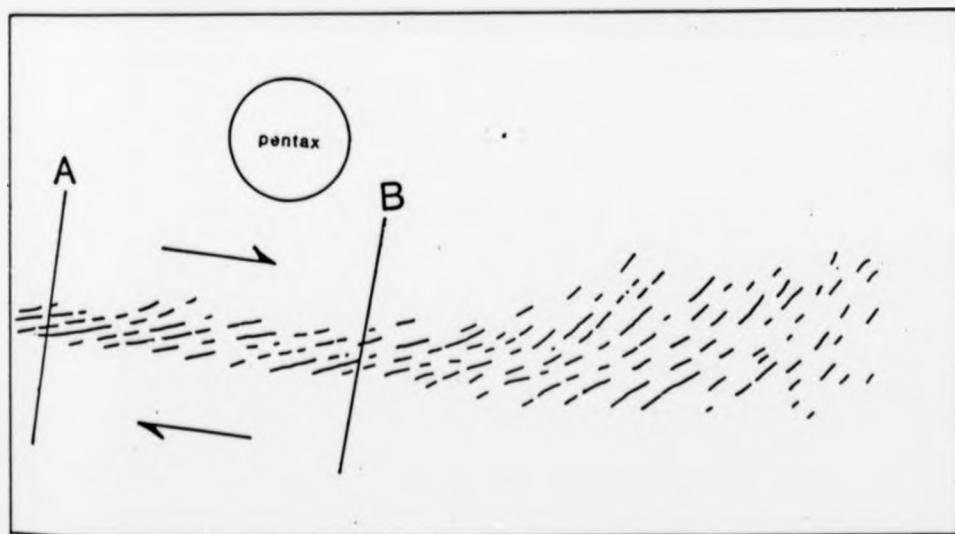


Fig 2.43 Close up of the tip of SZ11 showing the position of the profiles in Fig 2.44b and the widening of deformation around the shear zone tip.

Fig 2.44

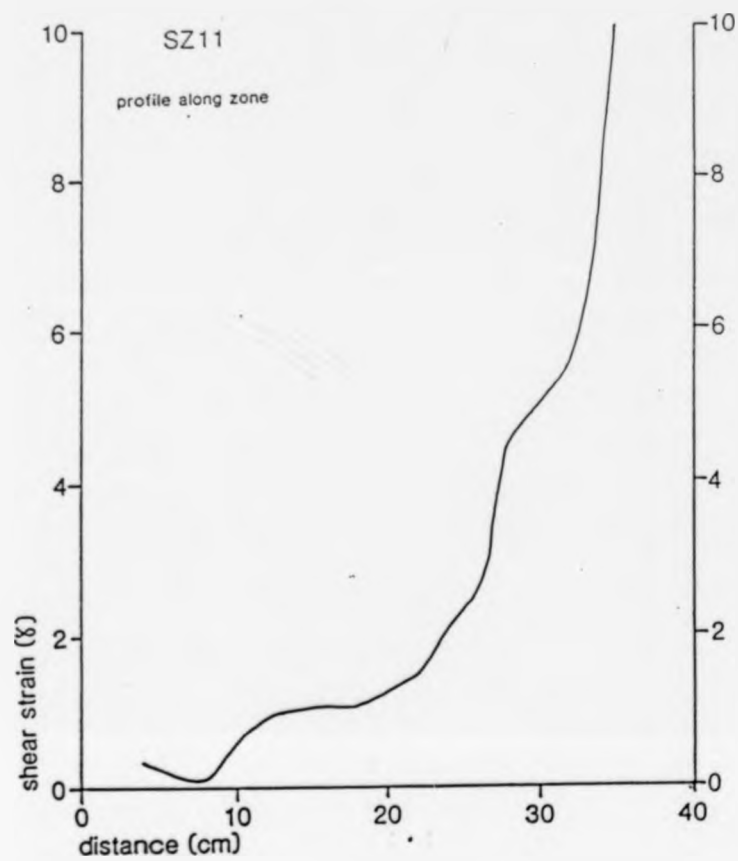


Fig 2.44a Profile of SZ11 along the line of the shear zone.

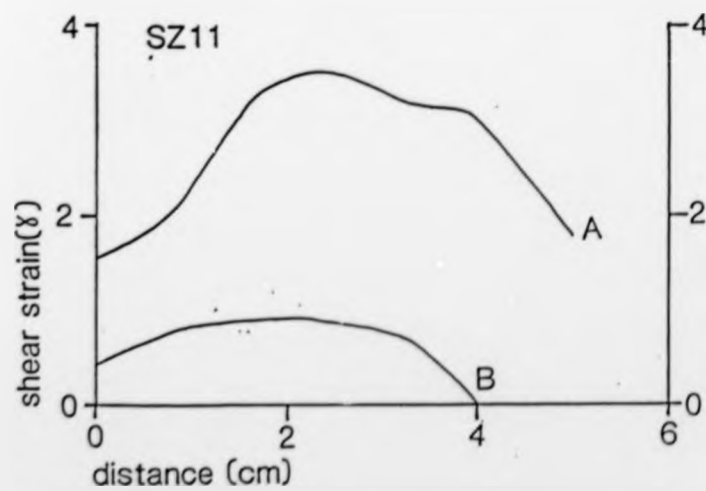


Fig 2.44b Strain profiles across SZ11 showing the increase in displacement away from the shear zone tip.

tip. If it were the case that this tip represented a "frozen" stage in the propagation of the zone, then the tip region should be no wider than the zone itself. Thus it can be inferred that at least part of the deformation in the area around the tip is due to accommodation of further displacement after the shear zone has ceased propagation. Therefore the widening at the tip represents the final stage of the deformation on the shear zone.

Zones 13 to 25 are taken from the South Sidhean Mhor area of the Lewisian outcrop near Gairloch. They outcrop on a ridge running NE from Loch Braigh Horrisdaile. Zones 13 and 16 deform the amphibolite facies gneisses whereas the rest are in the quartz-epidiorite dykes that trend NE - SW across the ridge.

Zone 13, South Sidhean Mor, Gairloch, GR 80337111. (Fig 2.45)

This zone is worthy of mention due to one particular feature. The displacement sense of the zone in the outcrop plane may be deduced from the offset of two leucocratic marker bands within the gneiss; however the curvature of these marker bands as they are deflected into the zone indicates the opposite sense of movement. This illustrates the problem that may arise when shear zones deform rocks with a good pre-existing foliation. The sense of curvature on the foliation as it enters the zone is a function of the relative orientation of the shear zone plane, the foliation plane in the host rock, and the displacement vector of the shear zone. Thus the sense of deflection of a pre-existing fabric cannot be used in isolation as an unequivocal indicator of the shear zone displacement sense (Wheeler 1987).

Fig 2.45



Fig 2.45 Shear zone 13 (GR 80337111) showing the apparent contradiction in movement sense.

Zones 23,24,25, South Sidhean Mor, Gairloch, GR 80197103. (Figs 2.46a & b)

These three zones all occur in one quartz-epidiorite dyke towards the SW end of the ridge. They are extremely planar zones, the outcrop pattern being a straight line for several m for each zone. The zones are sub-parallel (str. 090°), sub-vertical and are not parallel to the dyke margins. Another feature common to all three zones is the presence of a dark band along the centre of each zone consisting of extremely fine-grained material of indeterminate composition. These dark bands may represent the remains of a pre-existing "vein" developed along a fracture formed prior to the development of the shear zone, the zone then nucleated on this weaker feature in the subsequent deformation. It appears that the "veins" could have absorbed a considerable amount of deformation as the profiles for zones 23 & 25 (Figs 2.47) show markedly lower strains than those for similar sized zones in the same area. The presence of a pre-existing feature could also account for the planar nature of the zones. This explanation has been suggested by Segall & Simpson (1986) who describe shear zones nucleating on dilatant fractures in granitic rocks. An alternative explanation is that these zones propagated extremely quickly leading to the formation of a pseudotachylyte band along the centre of the zone, in this case the planar nature of the zones would be due to the speed of propagation (c.f. Coward 1976). Although it seems unlikely that only these three zones would show evidence of exceptionally quick propagation within such a small area, it is possible that they represent a different generation than the others in the area. On balance the localization explanation seems preferable.

Fig 2.46

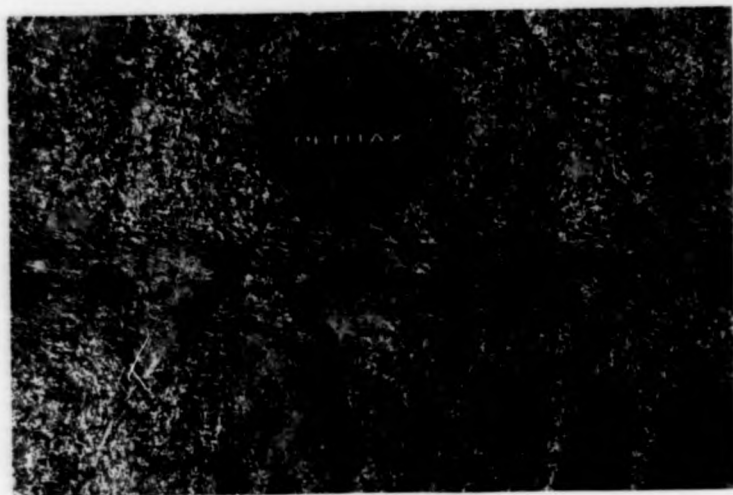


Fig 2.46a Shear zone 23 (GR 80197103).

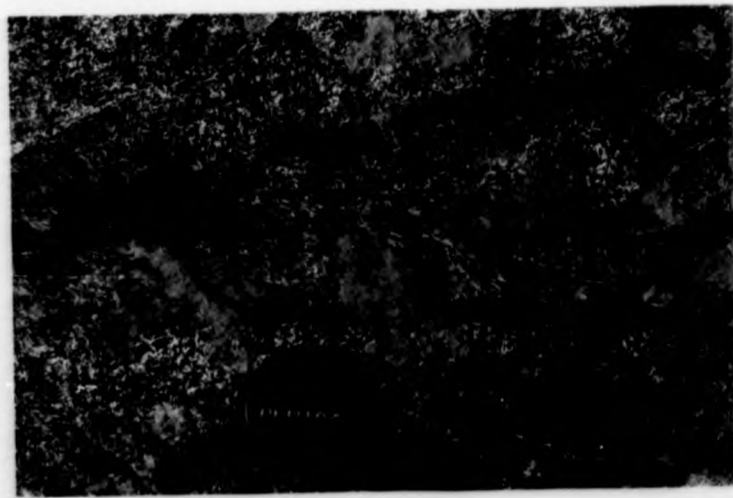


Fig 2.46b Shear zone 25 (GR 80197103).

Fig 2.47

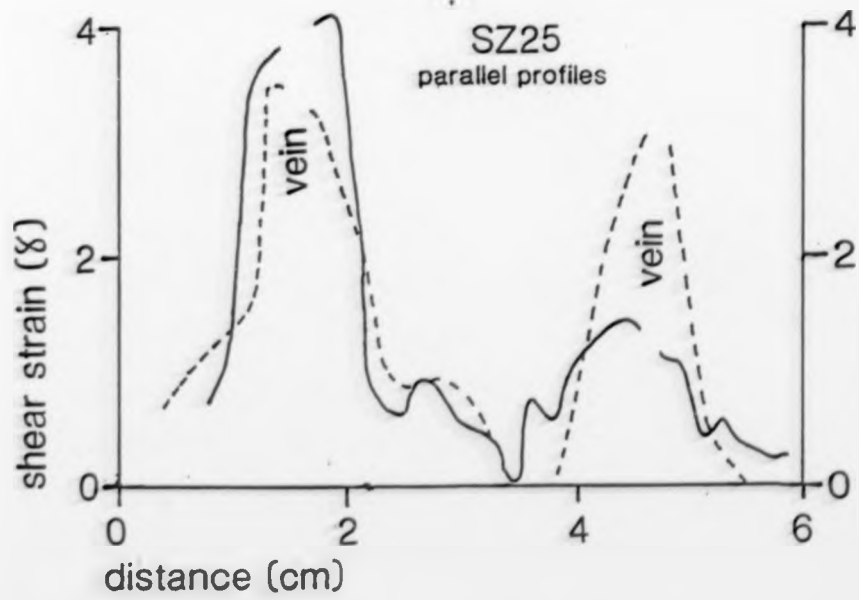
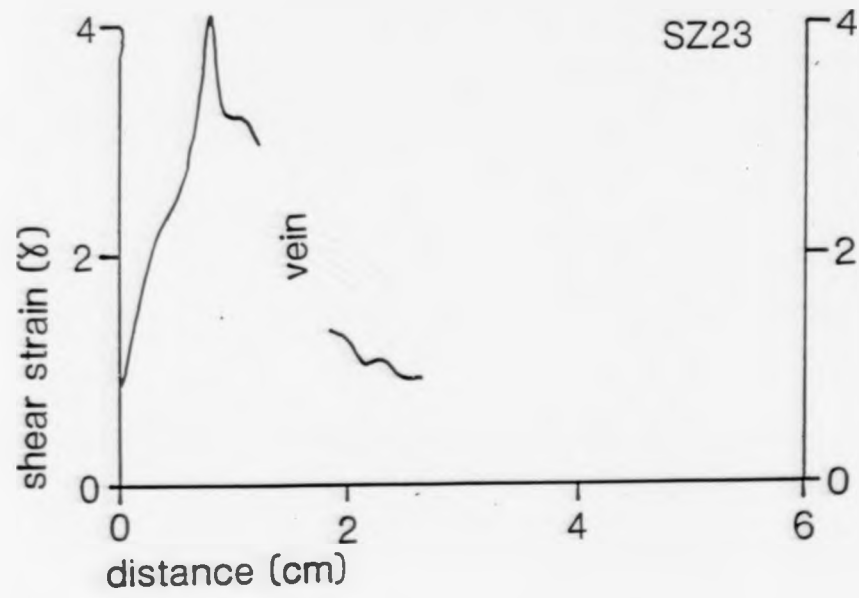


Fig 2.47 Strain profiles for SZ23 and SZ25.

Shear zones 26 to 33 were collected from the study area described in part 2.II of this chapter. Zones 26 to 30 deform the gneisses whereas zones 31 to 33 form part of an anastomosing network within one of the quartz-epidiorite dykes in the Canisp Shear Zone.

Zone 29, Clachtoll, Lochinver, GR 04232658. (Fig 2.48)

Shear zone 29 is typical of many of the shear zones seen within the gneisses of the Lochinver area. The zone has localized on the limb of an Inverian fold structure shearing the limb and tightening the fold inter-limb angle. An estimate of the maximum shear strain was made using the decrease in thickness of the mafic bands within the gneiss which gave a value of approximately 7.5%. This is another example of the way in which localization can be important in shear zone development.

Zones 31,32,33, Achmelvich, Lochinver, GR 05672570. (Fig 2.49a)

These three zones form part of an anastomosing network that deforms one of the quartz-epidiorite dykes within the Canisp Shear Zone (see also Fig 2.23). They are narrow, well defined zones and contrast markedly with the broad marginal shear zones seen in the Diabaig Inlier. Unfortunately the deformation within these narrow zones is often so intense that the felsic aggregates that define the foliation are often obliterated thus making analysis difficult. The strain profile for zone 32 is particularly peaked in the central region and gives a displacement of 10 cm across the 3.5 cm width (Fig 2.49b). Assuming that this is a representative figure for the zones within the dyke, then summing the total displacement of all the zones gives a figure of 8.75 m displacement between the walls of the dyke. This is probably a lower estimate as areas of low but finite deformation were not included. Within the dyke the shear zones show no

Fig 2.48



Fig 2.48 Shear zone 29 (GR 04232658).

Fig 2.49



Fig 2.49a Shear zone 32 (GR 05672570).

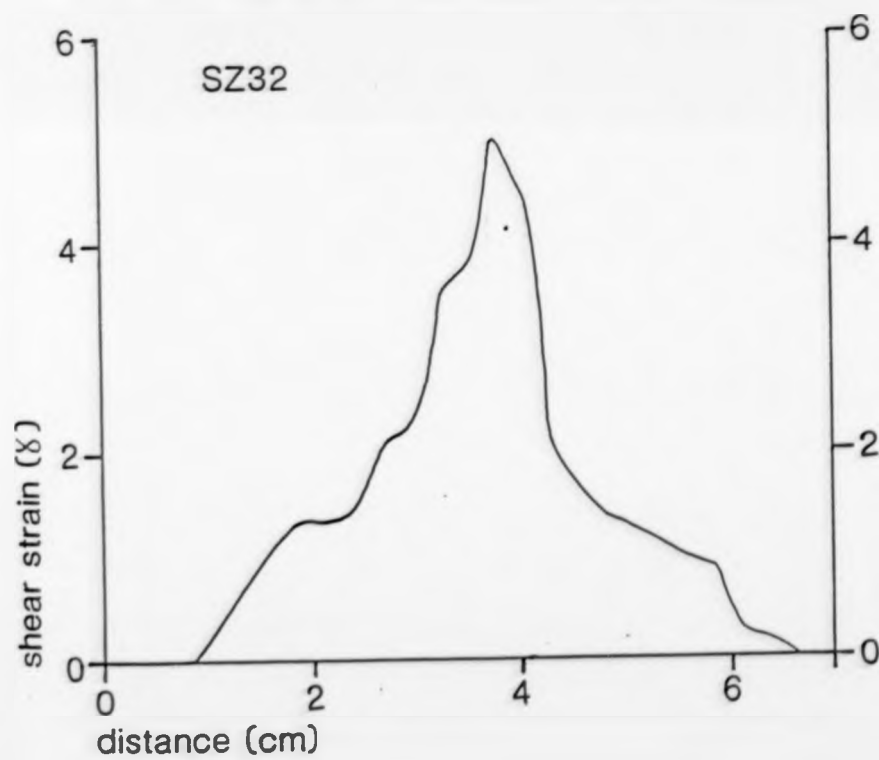


Fig 2.49b Strain profile for SZ32.

evidence for control on their morphology by pre-existing structures.

The group of zones studied on Badcall point near Scourie are in two groups; zones 34 to 37 are isolated zones within the large sheared quartz-epidiorite dyke on Badcall Point (Fig 2.50a) whereas zones 38 and 39 occur within a network developed in another part of the same dyke (Fig 2.50b). The zones at Badcall are more diffuse than those within the similar dyke at Lochinver.

Zones 38,39, Badcall Point, Scourie, GR 40214135. (Figs 2.51a & b)

The zones within the network are generally 10 to 20 cm in width and those studied gave displacements of 47.5 cm and 25.5 cm respectively (Figs 2.52). The zones within the network at Badcall are extremely curvilinear, some zones exhibiting geometries that would be impossible for movement (Fig 2.50b). Therefore the network must have been subsequently deformed either during or after its operation.

The shear zones studied at Creag a Mhail (40 to 44) are those described by Teall (1885). Here a shear zone striking WSW - ENE cuts and displaces a quartz-epidiorite dyke striking WNW - ESE. The displacement within the gneisses is transferred to a network of zones cross-cutting the dyke (Figs 2.53a & b) (c.f. Beach 1978 p17). The zones within the network are of similar size to those at Badcall but appear to be associated with much larger displacements; e.g. zone 40 (Fig 2.54a & b), 18 cm wide, shows 215 cm displacement and zone 43 (Fig 2.55a & b), 20 cm wide, shows 120 cm displacement. Shear zone 40 displays a classic flat-topped profile with high strain gradients on both sides. Shear zone 43 also shows high strain gradients but the profile is more irregular. Although the setting of the zones at Badcall and Creag a Mhail is very similar (i.e. both occur in dykes

Fig 2.50

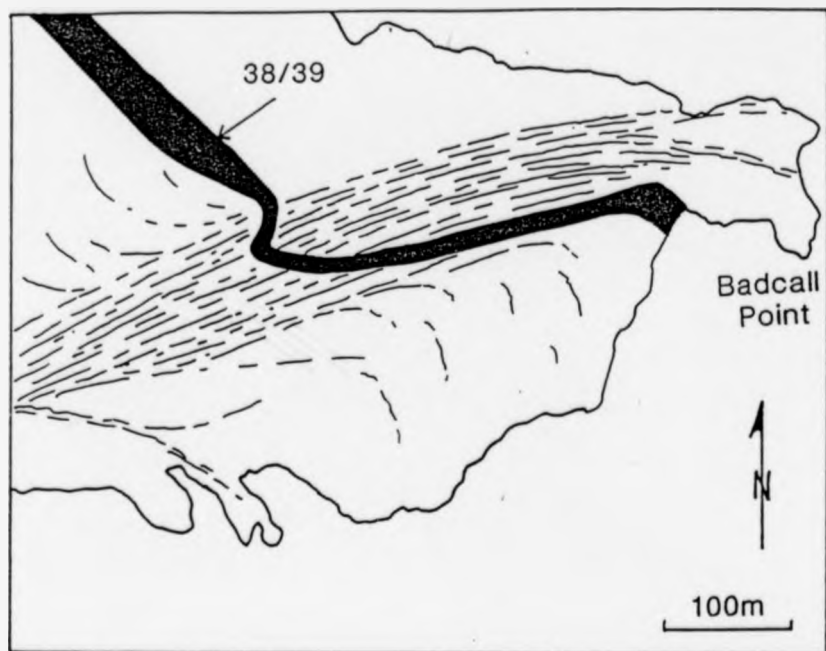


Fig 2.50a Geological map of the Badcall point area (from Beach 1978) showing the deflection of the quartz-epidiorite dyke through the shear zone.

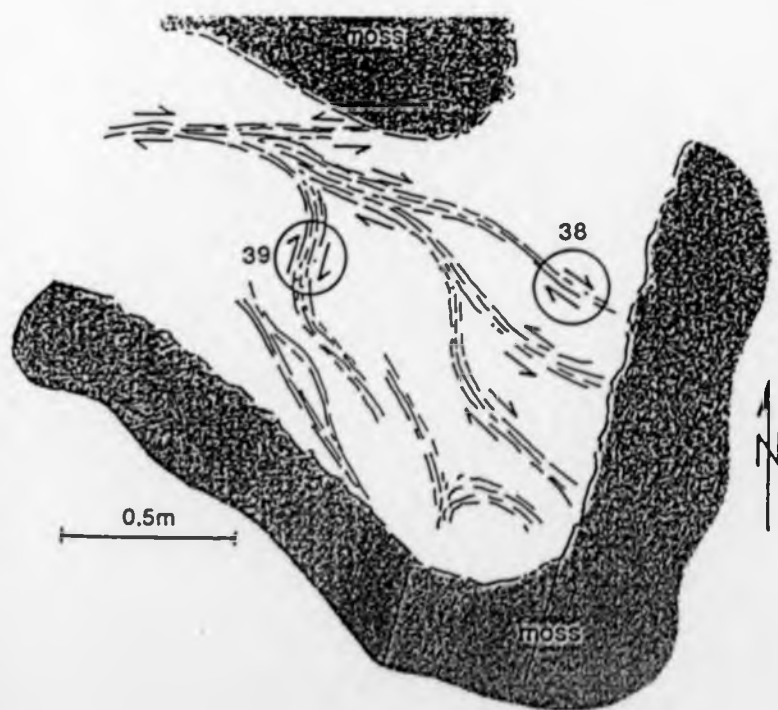


Fig 2.50b Sketch map of the shear zone network within the dyke as shown in Fig 2.50a.

Fig 2.51



Fig 2.51a Shear zone 38 (GR 40214135).

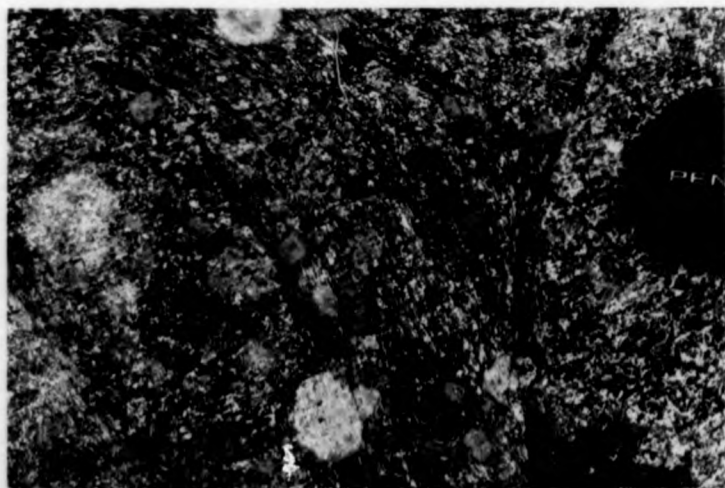


Fig 2.51b Shear zone 39 (GR 40214135).

Fig 2.52

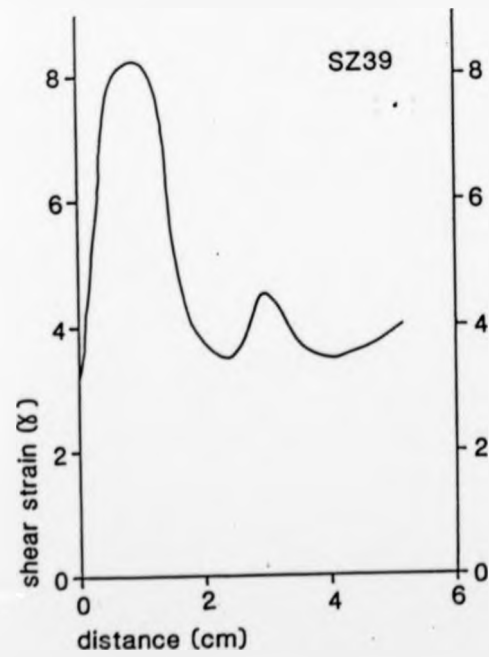
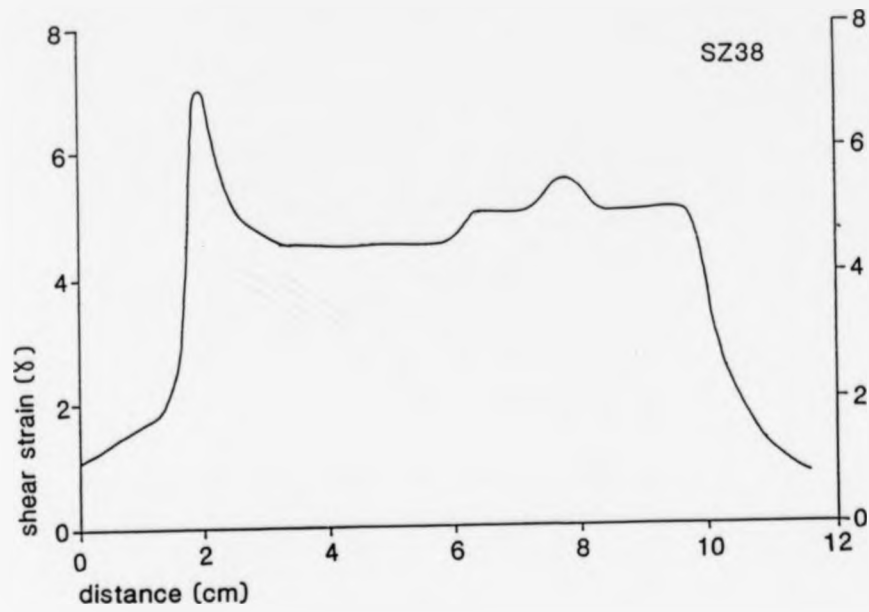


Fig 2.52 Strain profiles for SZ38 and SZ39.

Fig 2.53

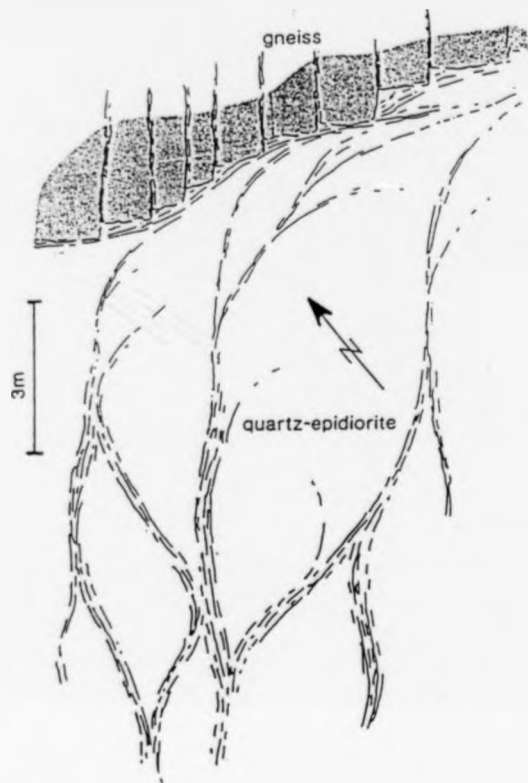


Fig 2.53a Field sketch of margin of the dyke at Creag a Mhail.

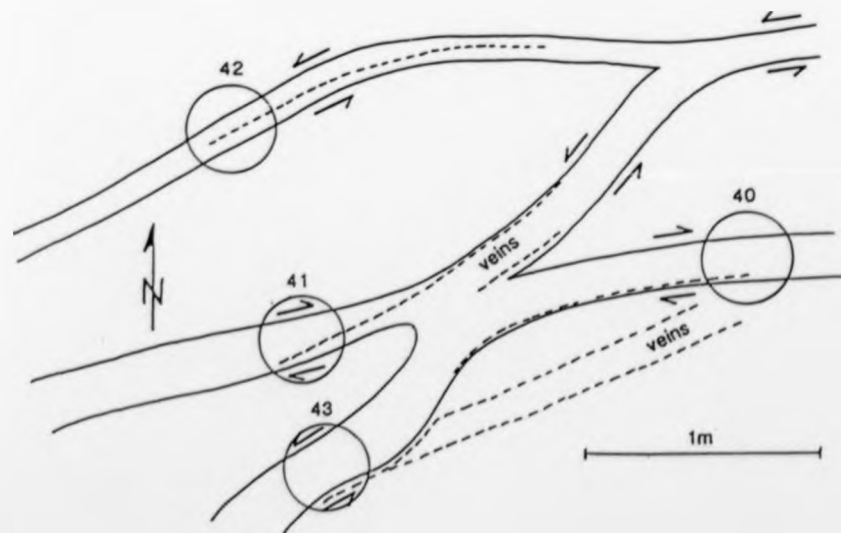


Fig 2.53b Map of the part of the shear zone network at Creag a Mhail used in the study showing the location of the sampled zones.

Fig 2.54

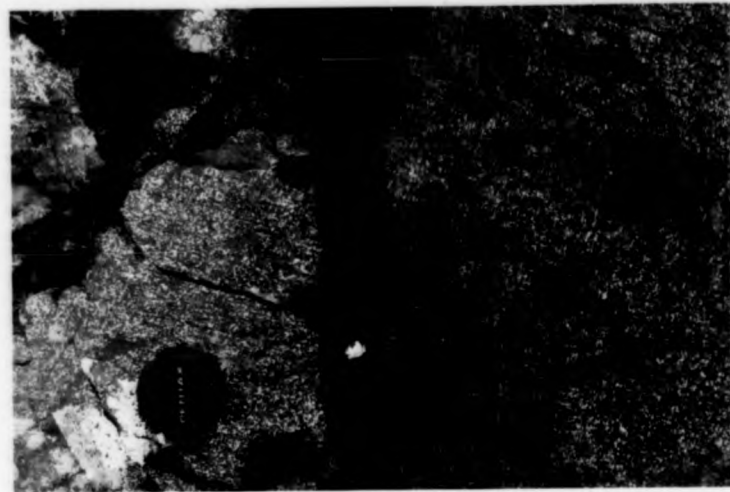


Fig 2.54a Shear zone 40 (GR 15414581).

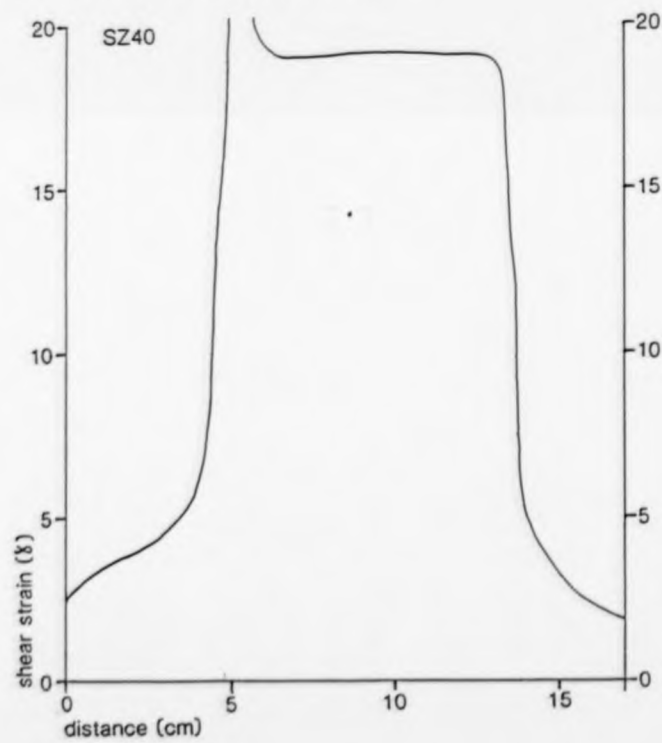


Fig 2.54b Strain profile SZ40.

Fig 2.55

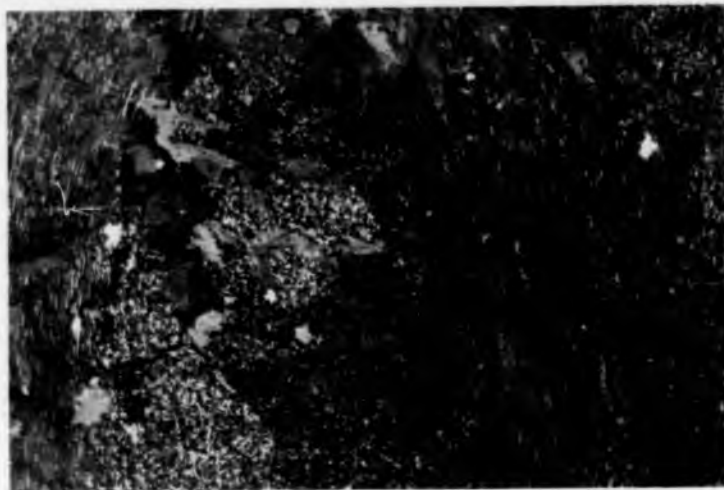


Fig 2.55a Shear zone 43 (GR 15414581).

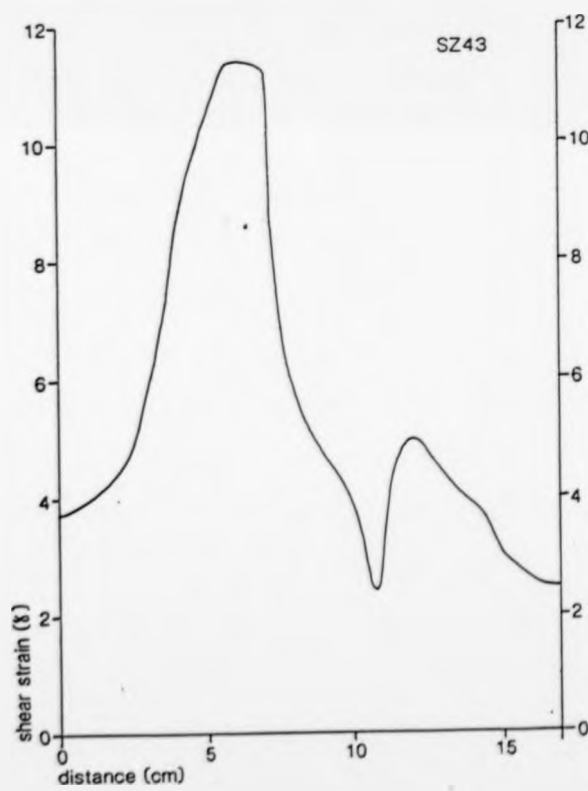


Fig 2.55b Strain profile SZ43.

that are being displaced by major shear zones) there appears to be a significant difference in morphology.

The most northerly group of zones studied occurs in a quartz-epidiorite dyke at Rudh an Tiompain, N of Tarbet, on the Rubha Ruadh peninsula (GR 16154954). The outcrop is a sub-horizontal wave-washed platform giving excellent clean exposure. The network trends at approximately 120° across the dyke and the zones all dip steeply to to the SW (Fig 2.56). The zones are very similar in character to those at Creag a Mhail and have well defined boundaries. Strain profiles plotted for these shear zones show extremely high shear strains, many as high as $\delta = 28$, and some give the theoretically impossible $\delta = \infty$ (Figs 2.57b & 2.58b). Thus estimates for displacement on these zones are a lower limit and the actual figure is probably much higher. One possible explanation for these extremely high strains is that there has been a significant degree of pure-shear during, or subsequent to, the deformation that is not accounted for by the Ramsay & Graham method for determining displacement. Alternatively the high strains could be due to the proximity of the Laxford Front Shear Zone. The density of zones and the size of the individual zones is not appreciably different from those at Badcall and Creag a Mhail; indeed on average they are slightly narrower than in these areas. Displacement estimates are in a fairly restricted range from 45.5 cm (47) to 62 cm (50), but it must be emphasised that the true figure is probably higher. The zones within this network are notably more planar than those in the networks at Lochinver, Badcall and Creag a Mhail possibly associated with the large displacements.

Fig 2.56

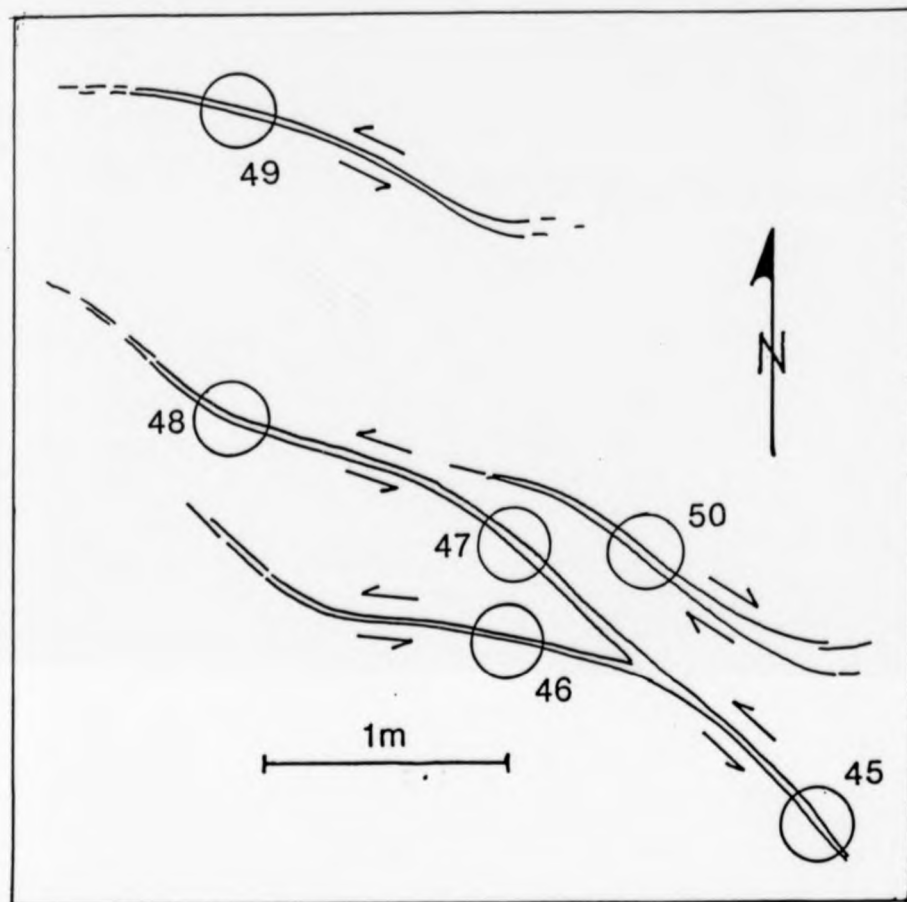


Fig 2.56 Map of part of the network within the quartz-epidiorite dyke at Rudh an Tiompain (GR 16154954) showing the location of sampled zones.

Fig 2.57



Fig 2.57a Shear zone 46 (GR 16154954).

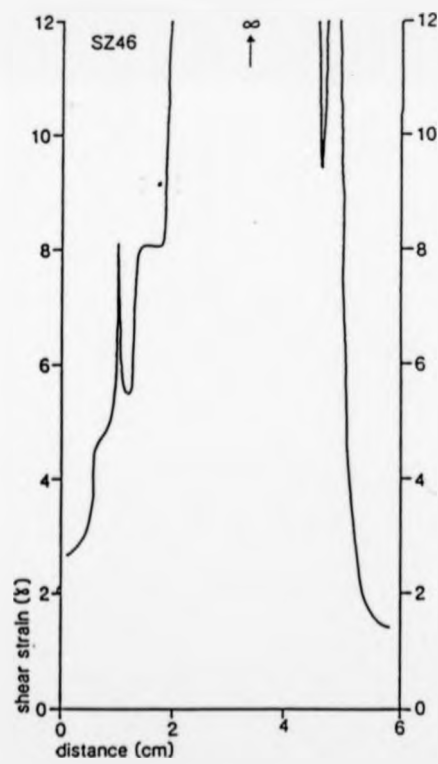


Fig 2.57b Strain profile for SZ46.

Fig 2.58

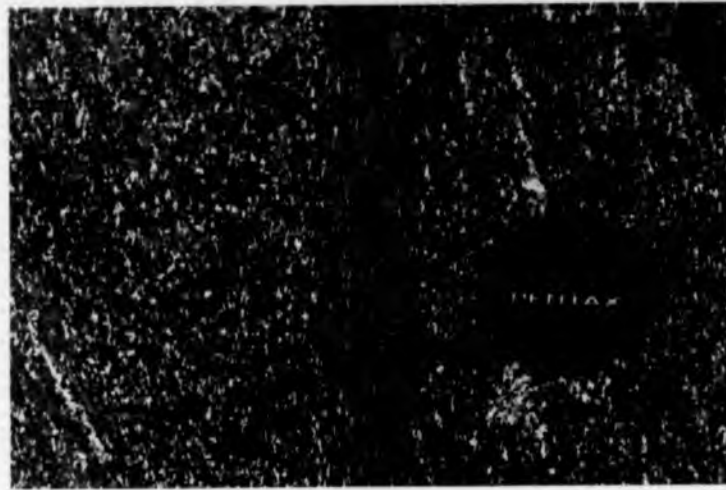


Fig 2.58a Shear zone 47 (GR 16154954).

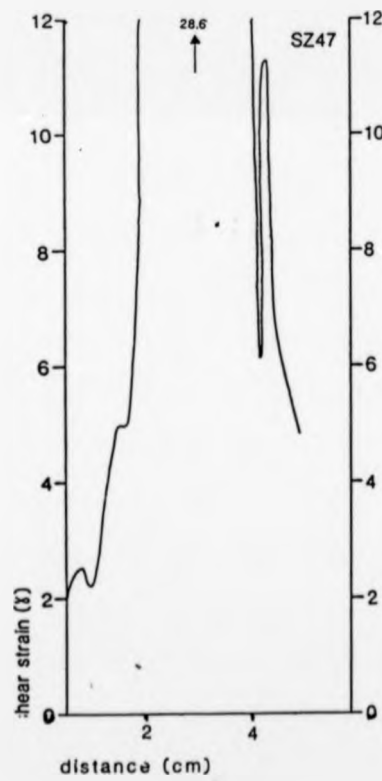


Fig 2.58b Strain profile for SZ47.

2.III.2.c Limitations of the data

All the data for strain profiles and displacements discussed thus far have been obtained using the method of Ramsay & Graham (1970). An alternative method using the axial ratios of the felsic aggregates within the quartz-epidiorite dykes has also been investigated. Zones suitable for this method are those in which the XZ plane; i.e. the plane that contains the movement lineation and is perpendicular to the shear plane, is exposed. This surface is then photographed in close up, the resulting picture enlarged, and the axial ratios of the felsic aggregates measured on traverses across the zone. This technique has been successfully applied by Coward (1976) and Niamatullah (1983) to measure strain in sheared rocks. However the initial analyses using this method produced extremely erratic results and it was therefore not considered worthwhile persevering with the technique (Fig 2.59). One problem with the method is that at high strains such as those in the centre of the zones at Lochinver, Creag a Mhail and Rudh an Tiompain, the felsic aggregates become so thin as to be unmeasurable and small inaccuracies of measurement for the width produce large variations in the axial ratio. This leads to extremely "peaky" and erratic profiles. A profile is illustrated for comparison with the shape of the Ramsay & Graham profile (Fig 2.60). The overall shape and width are broadly similar but considering that $\delta \approx \sqrt{X:Z}$ (for > 4) then it is apparent that these profiles represent considerably lower strains than those using the fabric orientation to determine δ . This conclusion must be regarded with caution due to the nature of the felsic aggregate data, but at least two explanations are possible. Firstly the felsic aggregates may undergo boudinage at high strains thus the long axis values for each individual section will be smaller than the true value for the original aggregate, thus the ratio will be lower. Secondly the Ramsay & Graham method may overestimate the true

Fig 2.59

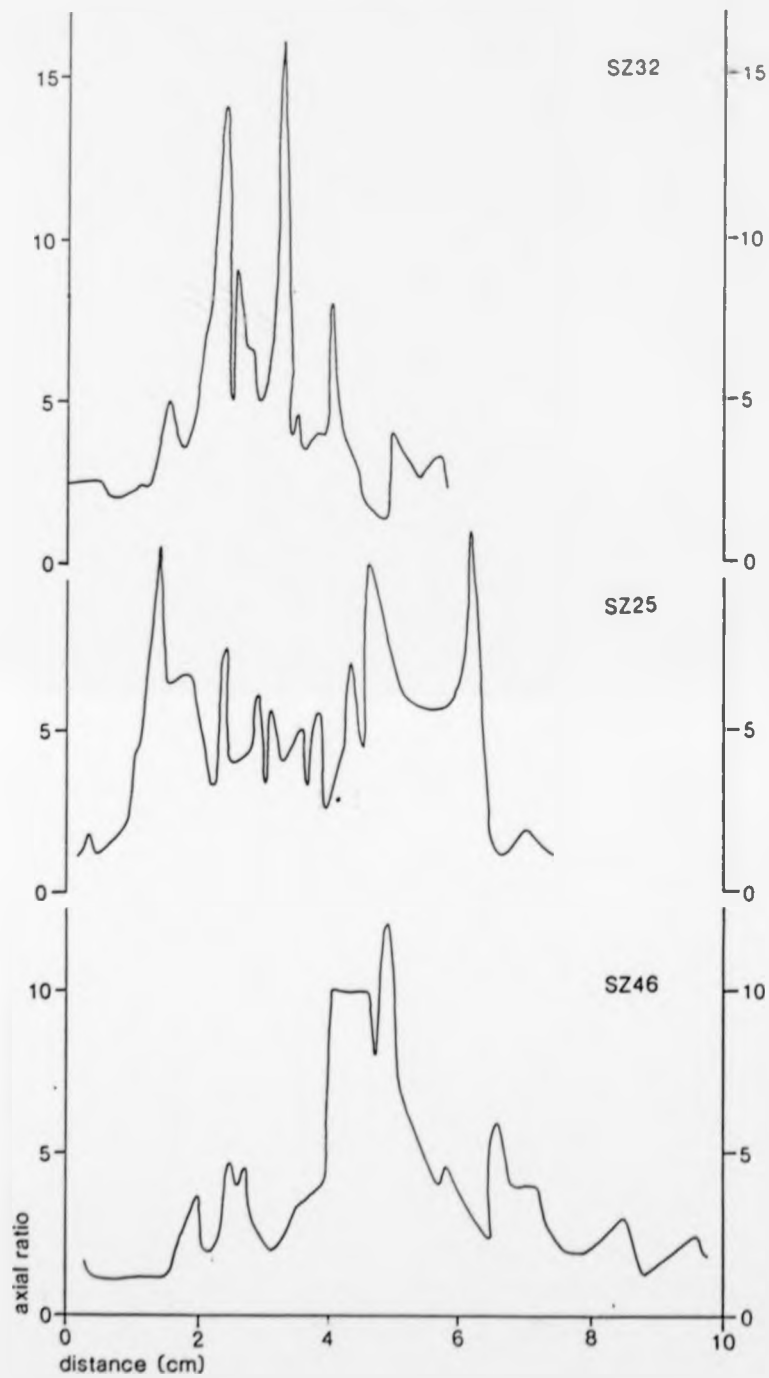


Fig 2.59 A selection of profiles constructed using the axial ratios of felsic aggregates within the quartz-epidiorite dykes, showing the extremely erratic nature of the data.

Fig 2.60

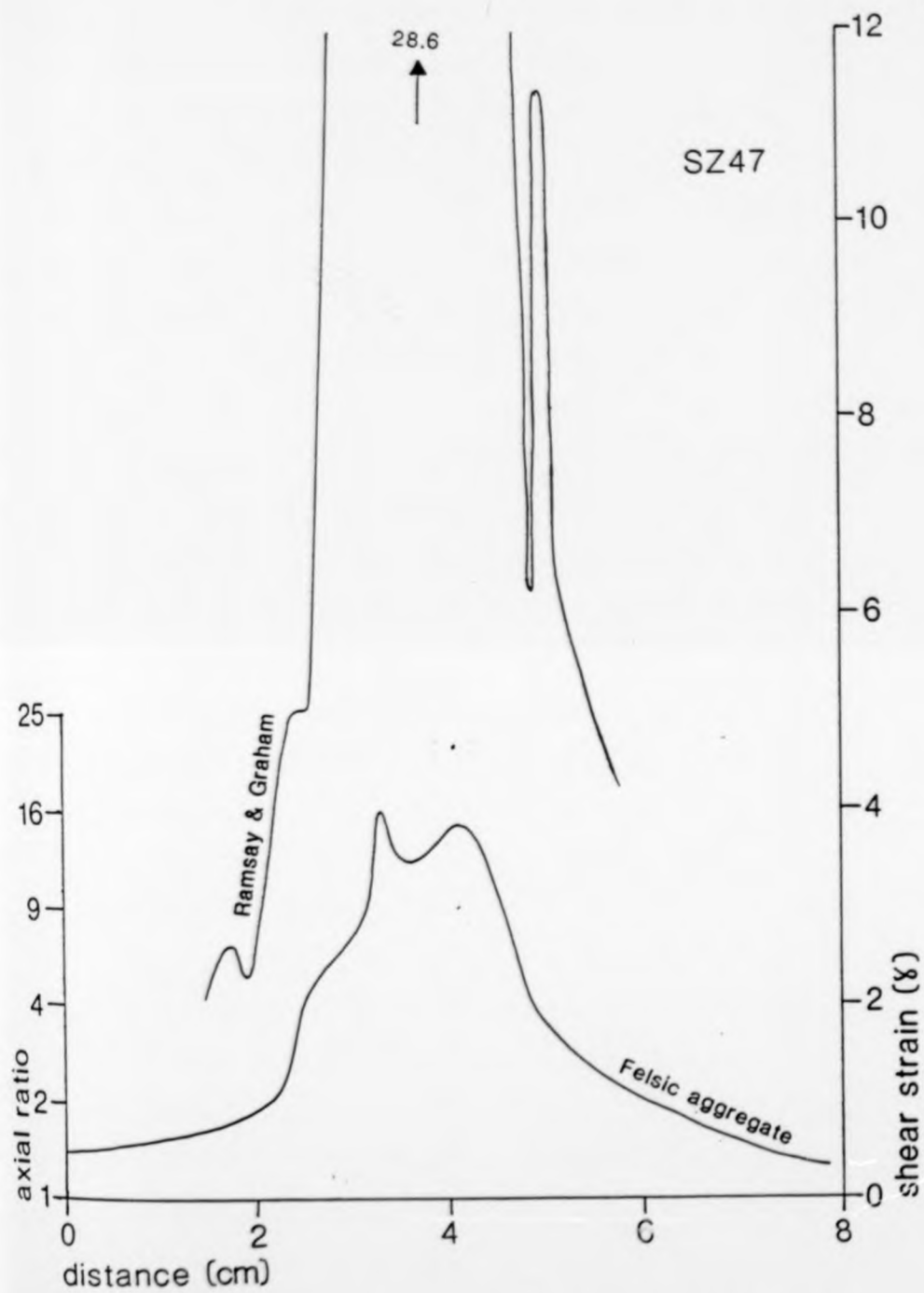


Fig 2.60 Comparison of the Ramsay & Graham (1970) type of strain profile with a profile constructed using felsic aggregate data. The felsic aggregate profile has been smoothed for clarity.

strain due to a component of pure shear during the deformation that is not accounted for by the method. Moreover volume change within the zones could affect both methods. It is not possible with the data available, within the scope of this study, to resolve this dilemma.

The limitations of the foliation orientation method of Ramsay & Graham must also be considered. The method assumes a simple shear mechanism for the formation of shear zones and no account is taken of any pure shear component perpendicular to the zone. Error of measurement is a crucial factor in the accuracy of results when using this technique (Fig 2.61). At low strains a 1° error of measurement only results in a small variation in γ ; i.e. $40^\circ - 39^\circ = 0.072 \gamma$, whereas at higher strains the variation is very large; i.e. $2^\circ - 1^\circ = 28.67 \gamma$. This means that the results are strongly dependant on the accurate determination of the position of the shear zone wall from which the angle θ is measured. As most shear zones vary in width slightly along their length and are often curvilinear, this is a considerable problem.

2.III.3 Summary of results and discussion

Data were collected from 52 shear zones, of which 43 occur in quartz-epidiorite dykes and the remaining 9 in tonalitic Lewisian gneiss. Of these 52 zones, 21 yielded strain profiles using the Ramsay & Graham method and from these, 19 estimates of displacement were obtained. A further 4 estimates of displacement were obtained from the offset of marker bands within the gneiss. Measurements were also made of the width of intense deformation in the centre of the shear zones and the total width of observable deformation as seen in the field. These measurements correspond to the width between the points of maximum gradient on a typical strain profile and the total width of the profile (Fig 2.62). The ratio between these two measurements is

Fig 2.61

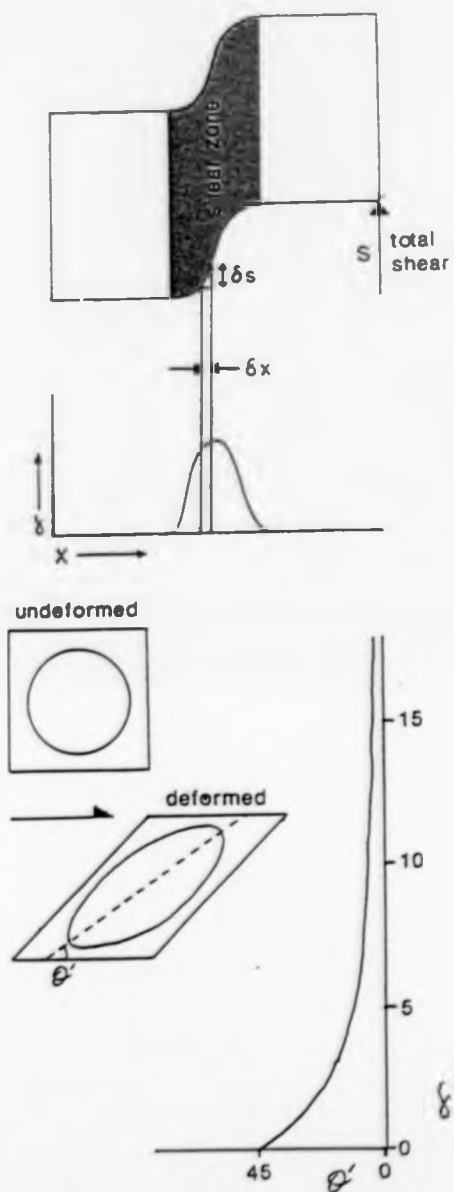


Fig 2.61 The method described by Ramsay & Graham (1970) for constructing strain profiles across shear zones, illustrating the large variations in δ with small changes in θ' at high strains.

Fig 2.62

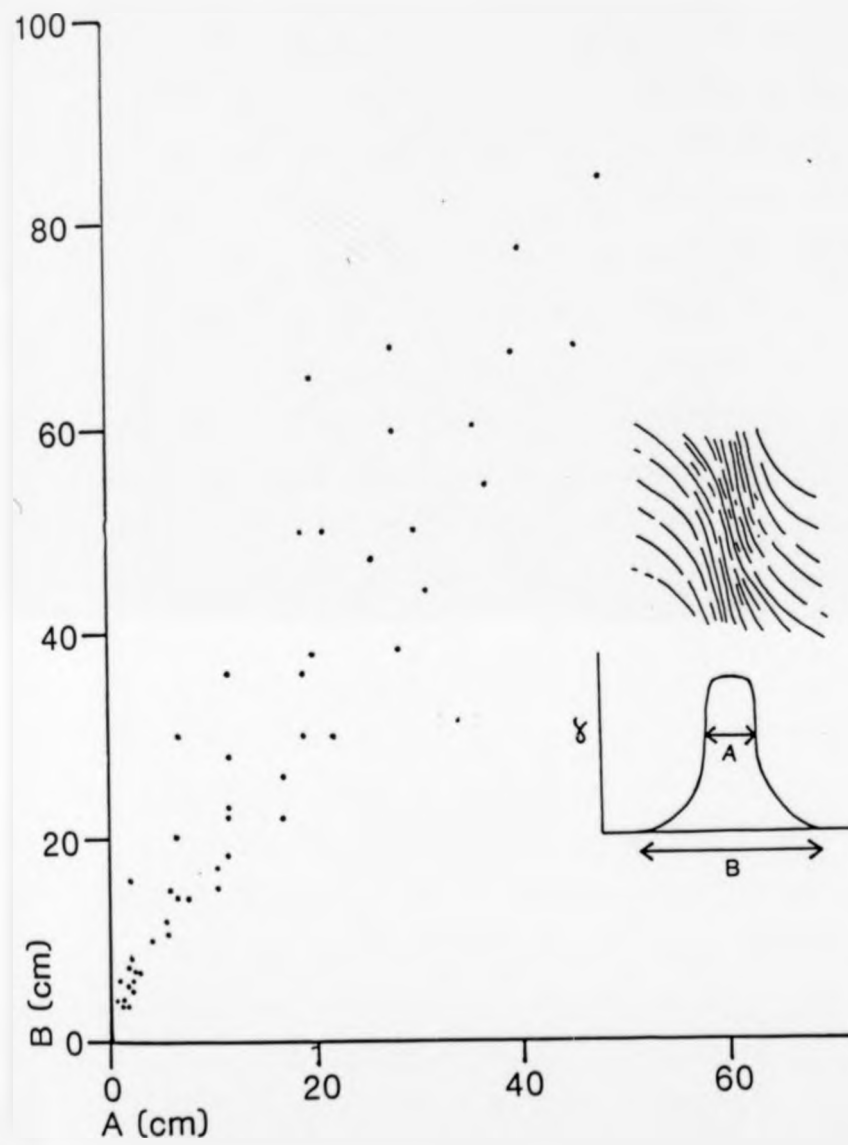


Fig 2.62 The relationship between the total width of a shear zone and the width of intense deformation at the centre of the zone.

approximately constant, but the significance of this relationship is not apparent. The relationship between displacement and width (Fig 2.63) for the sampled zones is not a constant ratio as might be expected; i.e. the wider the zone the greater the displacement. Other workers have related shear zone displacement to width by using a theoretical mean value for γ which would give the same displacement assuming that shear strain was constant across the zone. This value of mean γ is then plotted against shear zone width (Park 1981). Most of the work of this type carried out in the past has dealt with shear zones several km in width and these give an exponential relationship between mean shear strain and width. If the data of Park (1981) is replotted as displacement against width, the relationship is approximately a straight line, this however is not the case for the zones from this study. The dominant factor influencing the displacement/width plot appears to be the location of the zones, those from Torridon, Gairloch and Lochinver all clustering in an area close to the origin. Whereas those from Badcall, Scourie and Tarbet have undergone much larger displacements on similar sized zones. It is impossible to draw definite conclusions from a sample of only 17 data points but there does appear to be a location related change in the displacement/width relationship. This could be due to a number of factors, the most likely being a variation in the local ambient temperature at the time of deformation. An increase in temperature to the north of the area at the beginning of the Laxfodian has been reported by Dickinson & Watson (1976) who quote temperatures of 500° - 600° for the Assynt region near Lochinver and 600° - 700° for the Scourie area. Alternatively the proximity of a major shear zone (the Laxford Shear Zone) could alter the local stress field and lead to an increase in the displacement, but the shear zones studied at Gairloch and Lochinver are also close to major zones and so this seems unlikely.

Fig 2.63

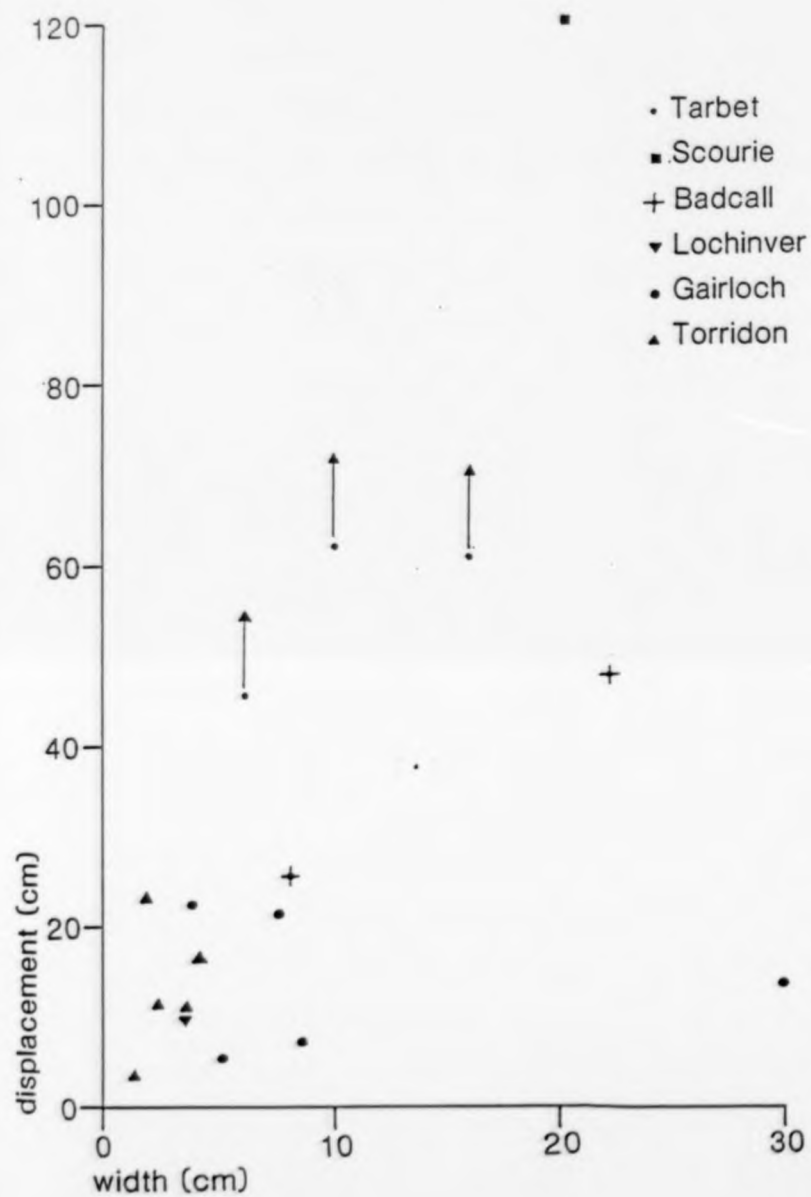


Fig 2.63 Plot of displacement versus width for shear zones from different areas. The data points for the Tarbet shear zones are shown with arrows as they are a minimum estimate and the true values are probably much higher.

There are no significant differences in the composition of the dykes between the N and the S of the area and so this may be ruled out. The timing of the deformation with relation to the peak metamorphic conditions could also affect the morphology of the zones but this explanation is effectively the same as a variation in ambient temperature during deformation. There is no change in the scale of the zones studied across the area and so the increase in displacement is accomodated solely by an increase in the peak shear strain.

2.IV CONCLUSIONS

2.IV.1 Fieldwork: Conclusions and relevance to modelling

The object of the fieldwork was to provide the basis for a model of shear zone initiation and development, both in terms of an understanding of the important factors that influence the morphology, location and orientation of shear zones and to provide data to test and constrain a model.

The Canisp Shear Zone (2.II) presents numerous problems for any attempt at a mathematical model of its development. Firstly the deformation is multiphase with significant changes in style of deformation and movement direction throughout the history of the zone. Secondly the deformation within the zone is extremely heterogeneous with extremes of high and low strain present in close proximity to each other. The lack of suitable pressure/temperature indicators means that the conditions prevailing at the time of deformation can only be established to within a large range of values. The zone is not exposed over its full length and there is only very equivocal evidence for the amount of displacement on the zone.

Despite these difficulties the information obtained from this part of the study can be used to a limited extent in the development of the model. The localization of the second phase of deformation on pre-existing planes of weakness emphasises the important influence of pre-existing structures on shear zone development in metamorphic terrains. East of Clachtoll (Fig 2.8) marginal shear zones on the quartz-epidiorite dyke diverge from the margin and propagate in a direction favourable for slip where the dyke margin is no longer orientated in a plane that will facilitate continued displacement.

The same effect was observed in some of the small shear zones, in which the morphology appears to be controlled by pre-existing structures. For example zones 23, 24 and 25 from the South Sidhean Mor area near Gairloch are located along pre-existing veins (Figs 2.46a & b); zone 29 from Lochinver on an attenuated fold limb (Fig 2.48); and zone 3 from the Diabaig Inlier near Torridon on a dyke margin (Fig 2.36). These however must be considered as special cases whereas in the general case the shear zone propagates through an homogeneous rock.

Where no structures are available for the shear zone to develop by localization the shear zone development must be controlled by the direction of propagation dictated by the local stress field. Thus tip regions are of prime importance as they represent the leading edge of the propagating zone. The tip zones observed in the field all exhibit a widening of the zone of deformation around the tip compared to the rest of the zone. This is interpreted as the accommodation of the final increments of displacement after the cessation of propagation. This means that tip zones observed in the field may not just be a "frozen" stage in the development of the zone.

The effect of regional variation in temperature/pressure conditions appears to have an influence on the amount of displacement that can be absorbed by a zone of given width. This is probably because of the effect of enhanced ductility due to strain softening; i.e. an increase in temperature would enhance dynamic recrystallization leading to accelerated structural and reaction softening.

The most difficult problem that arises from the interpretation of the data is that of rheology. The basis for any mathematical model of rock deformation is some type of flow law, this flow law is only significant if the parameters used for the rheological constants are reliable. All the shear zones studied are from metamorphic terrains, as are most ductile shear zones; whereas all the available rheological data is from either monomineralic samples (e.g. quartz, olivine and plagioclase) or from undeformed igneous rocks (e.g. granite, diabase). No data is available for rocks containing abundant prismatic minerals such as hornblende and biotite, and it is these minerals, because of their role in rotation and fabric softening, that exert an important influence on the deformation of the zones studied in this work. Because of this fundamental difficulty, there can be no precise quantitative correlation at present between the experimental rheology based model and the real shear zones of the study, although important qualitative conclusions can be drawn.

CHAPTER 3

3.1 THE CRACK TIP ANALOGY MODEL

3.1.1 Reasons for this approach

From the fieldwork it is apparent that localization plays an important role in the development of certain shear zones. However as already stated, these must be regarded as special cases where the pre-existing structures were present and had orientations that could be exploited by developing shear zones to accommodate remote displacements. As can be seen from the field data, shear zones do develop in rocks which have no pre-existing heterogeneities that would facilitate the localization of deformation. It is relatively simple to see how a shear zone could exploit an already weak region but the key to a complete understanding of shear zone deformation lies in an understanding of the processes that allow nucleation and propagation of a high-strain zone through previously homogeneous rock. Following this line of reasoning it was decided to develop a model for shear zone development based on the analogy of a propagating crack tip.

3.1.2 The crack tip analogy: fundamental theory and assumptions.

Previous workers have used brittle crack stress distribution theory in a variety of applications; Ball (1980) and Norton (1982) as the basis for models of shear zone development and Palmer & Rice (1973) for the growth of slip surfaces in overconsolidated clays. A similar approach was taken by Watterson (1979) who used the stress distribution around a lithospheric fault to model shear zone development (see 1.III.3).

The use of a brittle crack in an elastic medium to model a plastic shear zone requires some justification as there are obvious differences between the two types of discontinuity (Fig 3.1). The material properties of the medium and the weak zone within it have little effect on the geometry of the resulting stress field, thus any planar weak zone will have a similar stress distribution in a variety of materials, even in the extreme case of a viscous fluid. The crack analogy is used here only to derive the stress distributions around the tip of the shear zone. A ductile deformation flow law is then used to compute the strains and the resulting stress release.

The equations for the distribution of stress around a brittle fracture are derived by finding a suitable "stress function" which satisfies the "biharmonic equation" of linear elastic theory, in accordance with appropriate boundary conditions (Lawn & Wilshaw 1975). The surfaces of the crack, since they are stress-free boundaries of the body close to the crack tip, dominate the stress distribution in that area, whereas the remote boundary conditions and loading forces affect the intensity of the local stress field (Paris & Sih 1965).

Of the three principal modes of crack displacement, the ones most common in geological situations are Mode II and Mode III (Fig 3.2). The large confining pressures associated with geological fractures tend to suppress the tensile fractures of the opening mode, Mode I. Mode II and Mode III are analogous to pure-edge and pure-screw respectively in terms of crystal dislocations, and so, assuming a shear zone to be a disc-shaped area of deformation, both Mode II and Mode III will be operating (Fig 3.3). Of these Mode II will be the most important, as this will operate at the propagating tip where the displacement direction is parallel to the propagation direction.

Fig 3.1

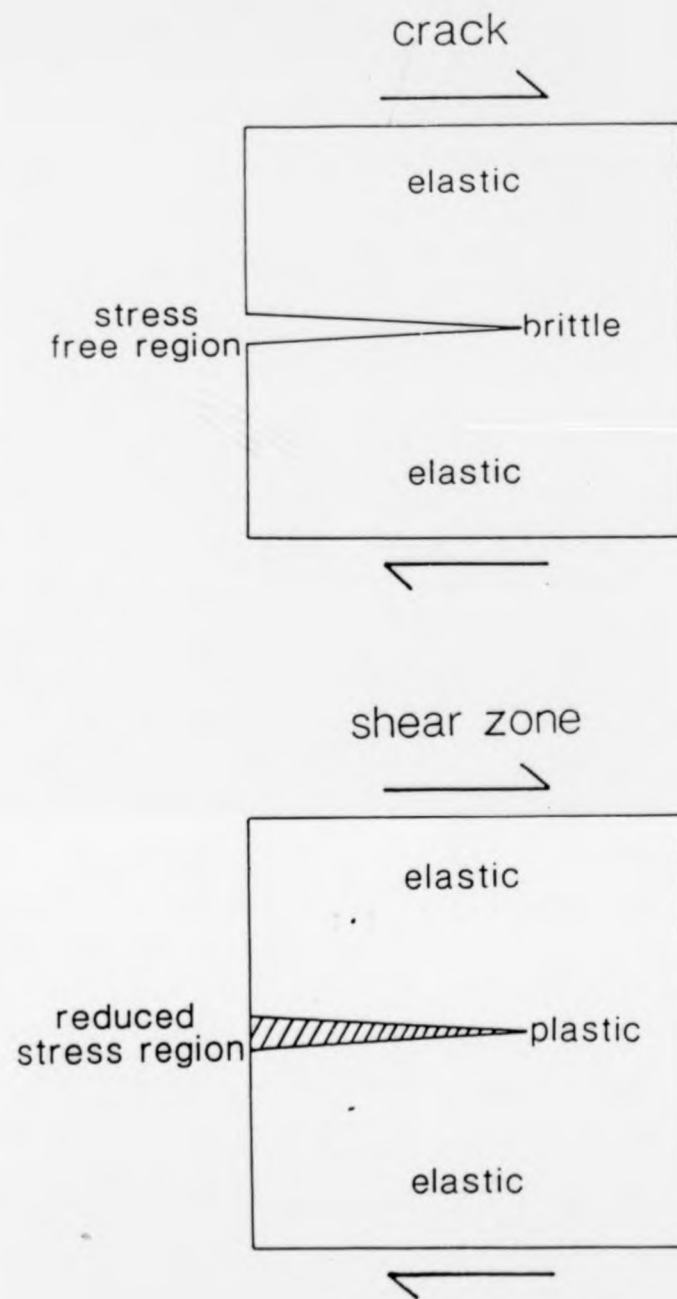


Fig 3.1 Comparison of the material properties of a brittle crack and a ductile shear zone.

Fig 3.2

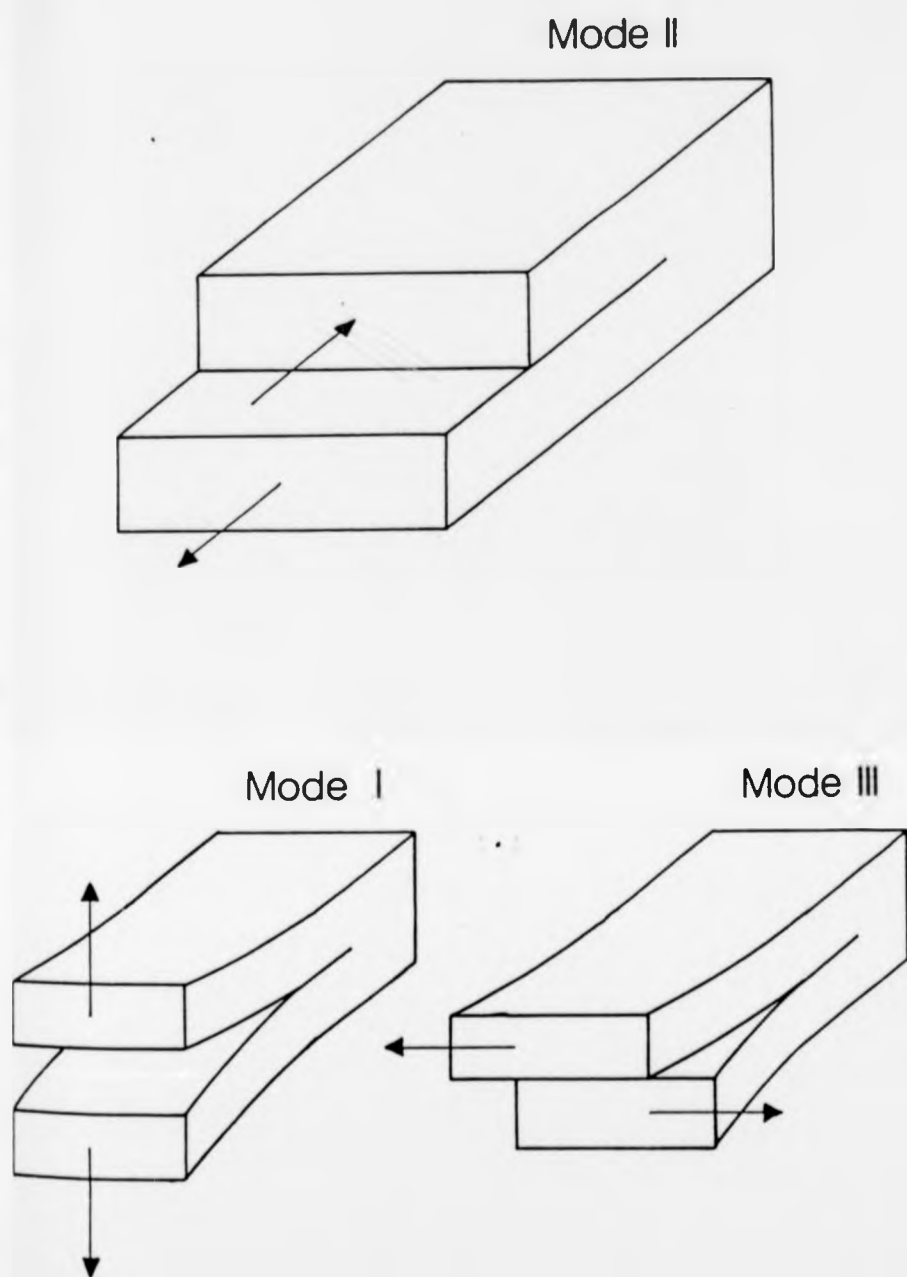


Fig 3.2 Principal modes of crack displacement (after Lawn & Wilshaw 1975).

Fig 3.3

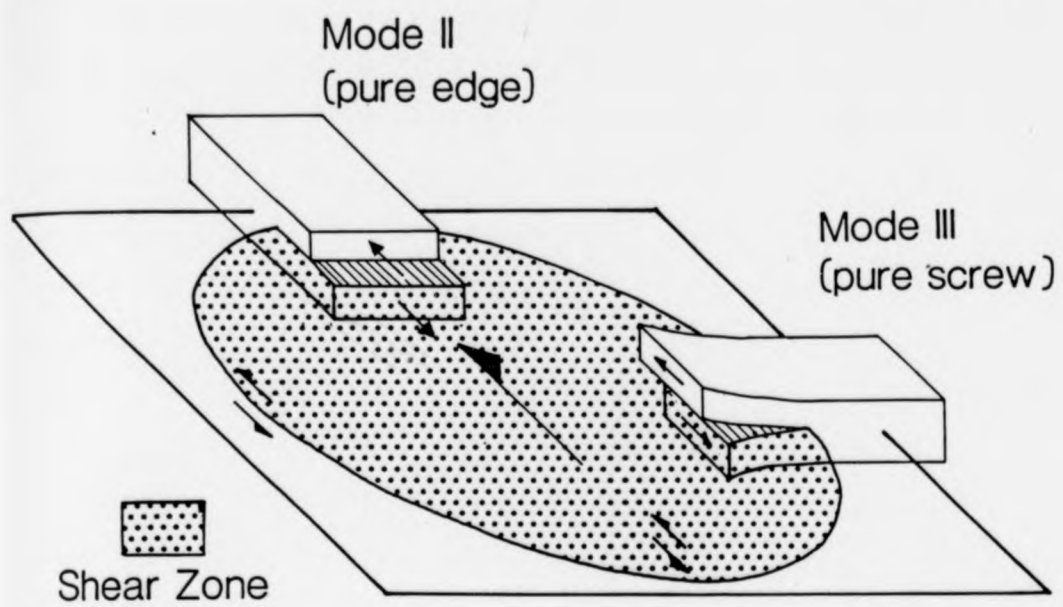


Fig 3.3 Modes of displacement operating in a deforming shear zone.

The equations for the Cartesian stress distributions around a Mode II plane crack can be divided into two parts, a stress intensity factor that depends on the boundary conditions of the system and determines the magnitude of the stresses, and a distribution term which depends on distance and direction from the tip (Fig 3.4). The distribution term may be further divided into a radial and an angular component.

$$\begin{Bmatrix} \sigma_{xx} \\ \sigma_{yy} \\ \sigma_{xy} \end{Bmatrix} = \frac{K_{II}}{(2\pi x)^{1/2}} \begin{Bmatrix} -\sin(\phi/2) [2 + \cos(\phi/2) \cos(3\phi/2)] \\ \sin(\phi/2) \cos(\phi/2) \cos(3\phi/2) \\ \cos(\phi/2) [1 - \sin(\phi/2) \sin(3\phi/2)] \end{Bmatrix} \quad (3.1)$$

where σ_{xx} , σ_{yy} , and σ_{xy} are the Cartesian stresses

K_{II} - is the stress intensity factor for Mode II fracture

x - is the radius from the crack tip

ϕ - is the angle to the plane of the crack (Fig 3.4)

$$K_{II} = \sigma_L (\pi C)^{1/2} \quad (3.2)$$

where C - is the crack half-length

σ_L - is the applied load stress

(Paris & Sih 1965)

Combining 3.1 and 3.2 and simplifying,

$$\begin{Bmatrix} \sigma_{xx} \\ \sigma_{yy} \\ \sigma_{xy} \end{Bmatrix} = \sigma_L (C/2x)^{1/2} \begin{Bmatrix} f_{xx}\phi \\ f_{yy}\phi \\ f_{xy}\phi \end{Bmatrix} \quad (3.3)$$

Fig 3.4

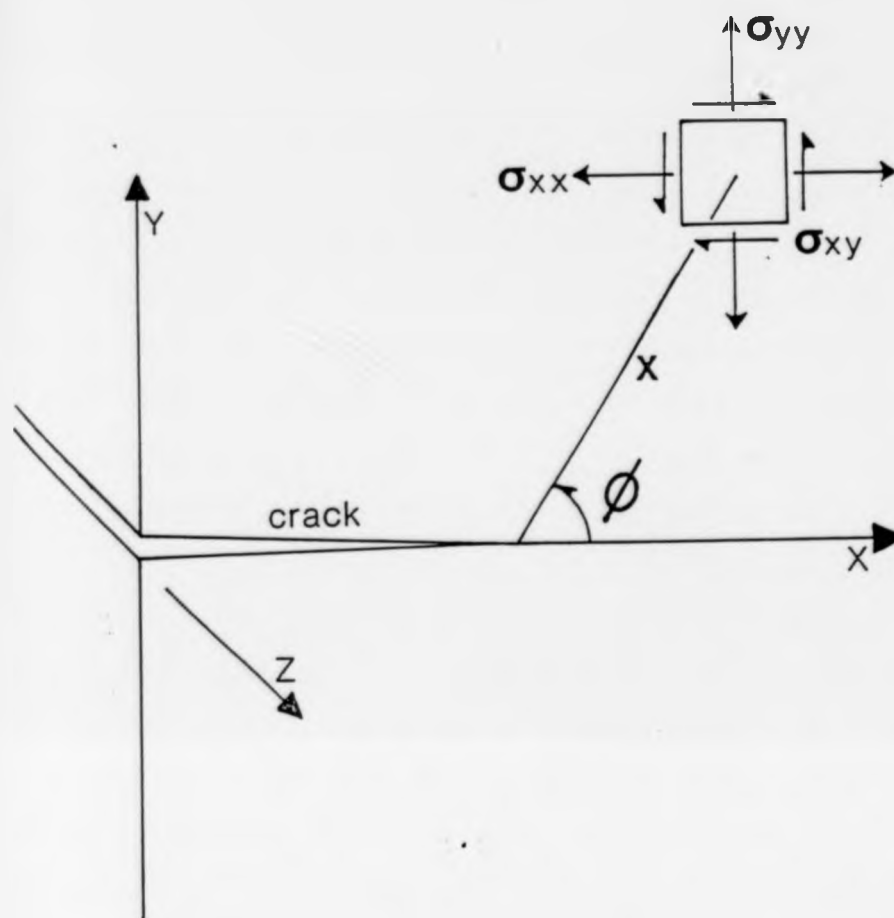


Fig 3.4 Co-ordinate frame used for calculating the stress field around a crack tip (after Lawn & Wilshaw 1975)(see also fig 3.8).

Several assumptions are made in the derivation of these equations, the key one being the "sharp slit" approximation, where the crack tip, in the unstressed state, is assumed to be perfectly sharp, this unavoidably introduces a mathematical singularity at the tip. The crack walls are taken to remain free of tractions at all stages of loading which introduces an obvious difference between the crack model and a deforming shear zone. The presence of finite plastic strain between the shear zone walls will re-scale the stress field but will not affect its geometry. The derivation of the equations neglects the higher order terms in the distribution function, and so the mathematics is only approximate for larger values of x . Hence the stress field cannot exactly match the outer boundary conditions. The assumption of plane strain in an ideal Hookean solid is also made.

The Cartesian stress distributions have been calculated using these equations and are shown in figs 3.5 - 3.7. In calculating the values for these maps the boundary conditions were set to unity thus giving dimensionless maps which show the pattern of the stress distributions. The co-ordinate scheme used for the calculations is shown in fig 3.8. The peak values shown at the crack tip itself are artificial due to the singularity at the tip, and have been introduced to allow completion of the diagrams. The stress fields for σ_{xx} and σ_{yy} both give a value of zero for the line immediately in front of the crack tip ($Y = 0, X < 0$. see fig 3.8) whereas σ_{xy} is a maximum along this line; the significance of this is dealt with later in this chapter.

In order to calculate the differential stress available to drive the system the principal stresses σ_1 and σ_2 must be calculated. These are given by the principal stress equations (Jaeger & Cook 1979)

Fig 3.5

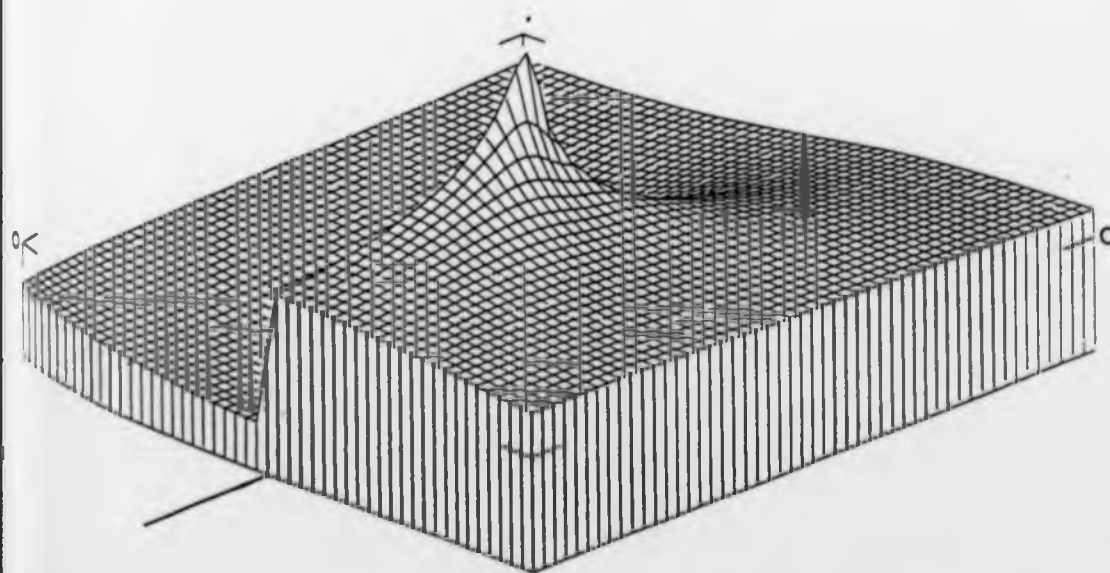
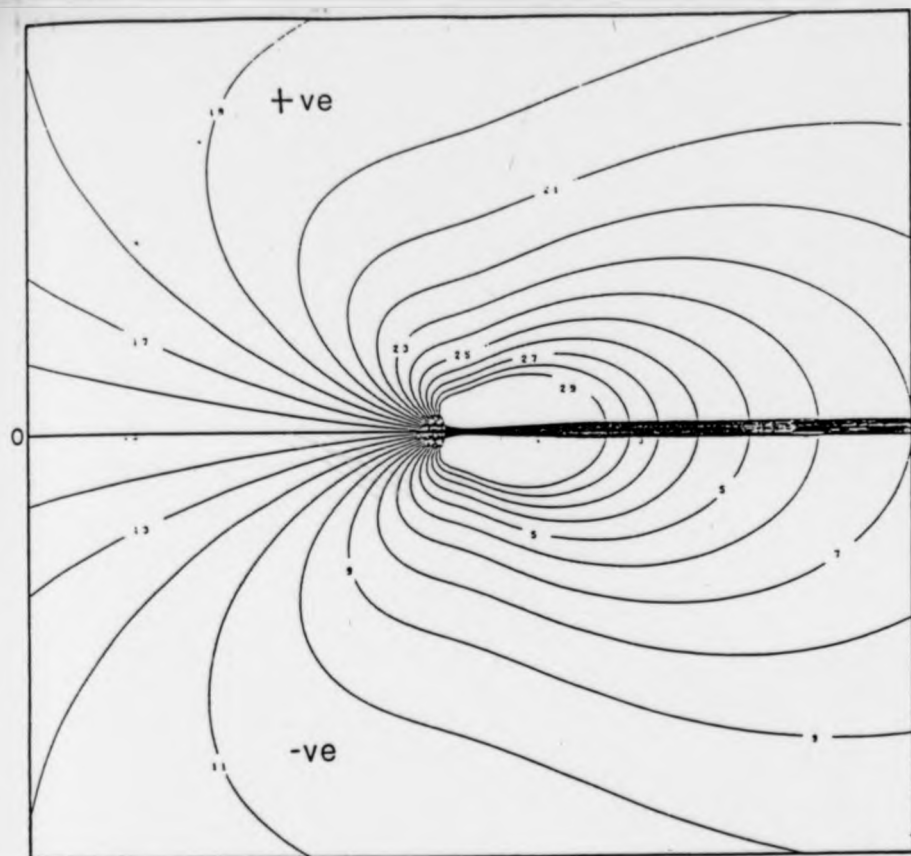


Fig 3.5 Dimensionless distribution map of σ_{xx} for Mode II fracture, all boundary conditions are set to unity. The peak value is artificial due to the singularity at the crack tip. (See fig 3.8 for orientation and co-ordinate frame used.)

Fig 3.6

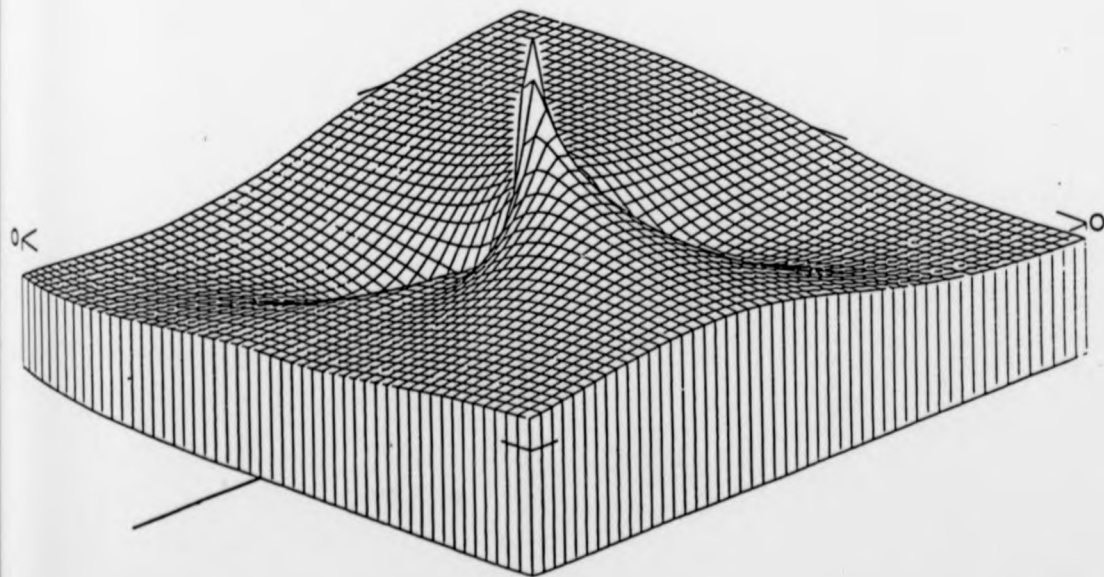
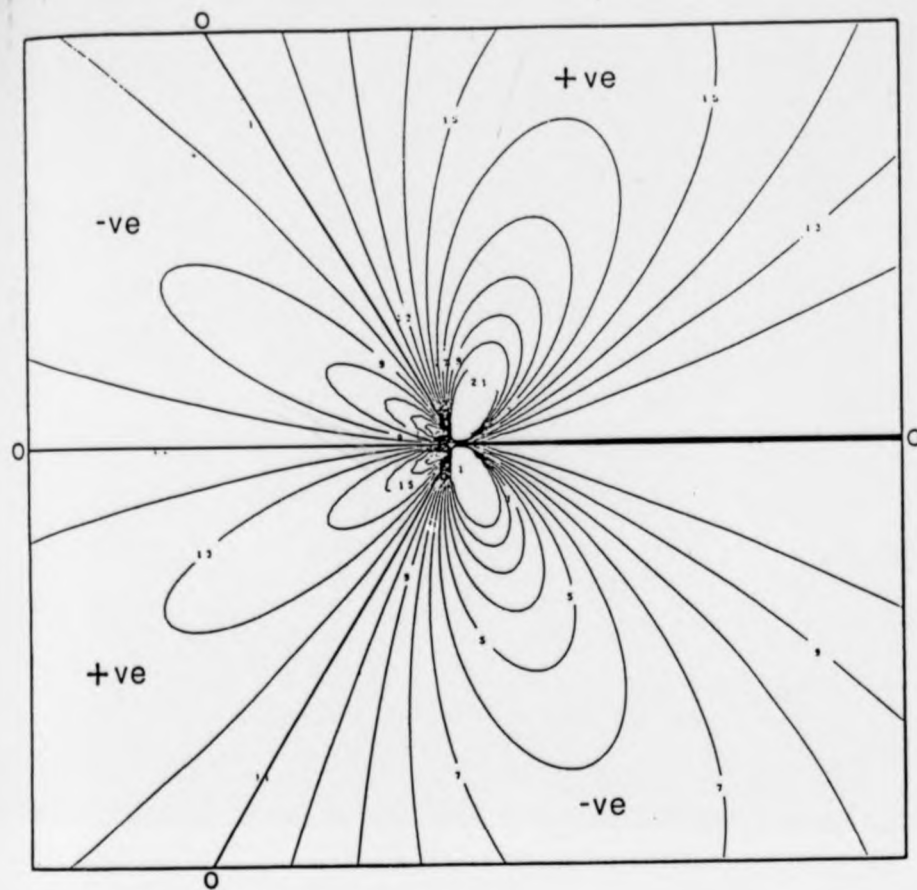


Fig 3.6 Dimensionless distribution map of σ_{yy} for Mode II fracture, all boundary conditions set to unity. The peak value is artificial due to the singularity at the crack tip.

Fig 3.7

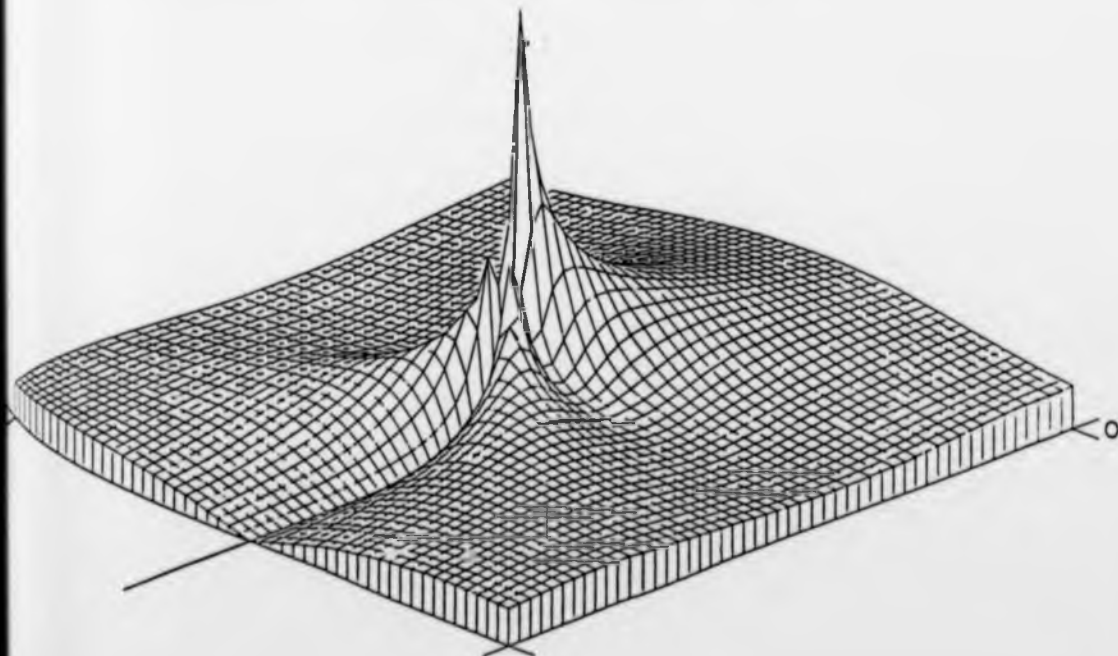
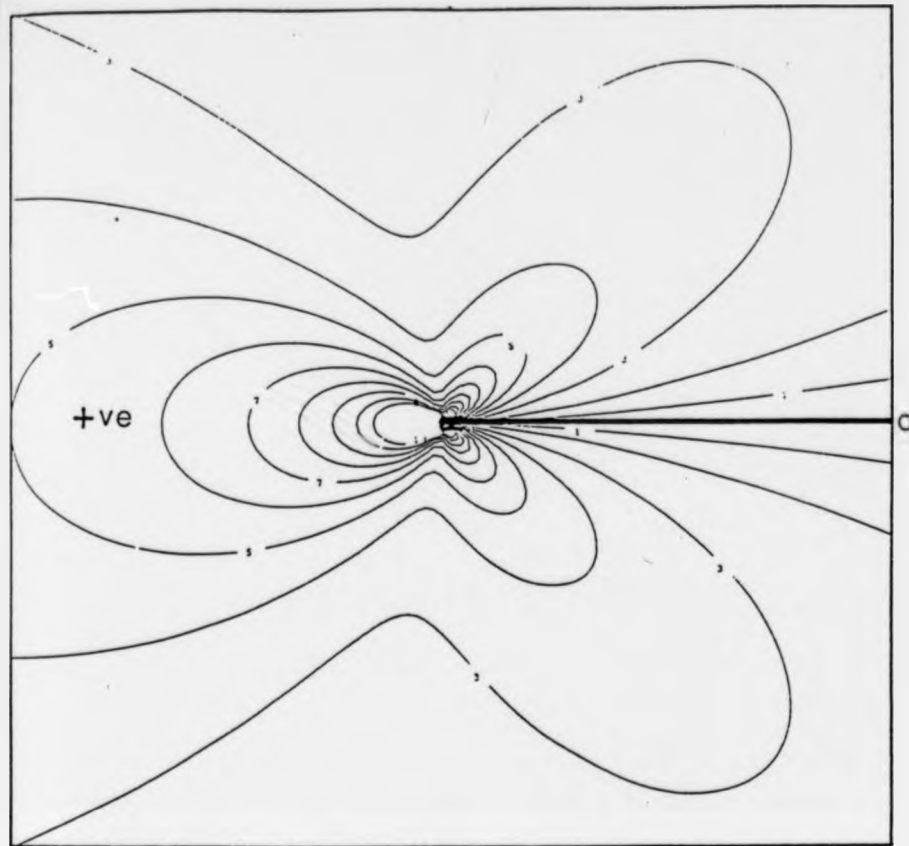


Fig 3.7 Dimensionless distribution map of σ_{xy} for Mode II fracture, all boundary conditions are set to unity. The peak value is artificial due to the singularity at the crack tip.

Fig 3.8

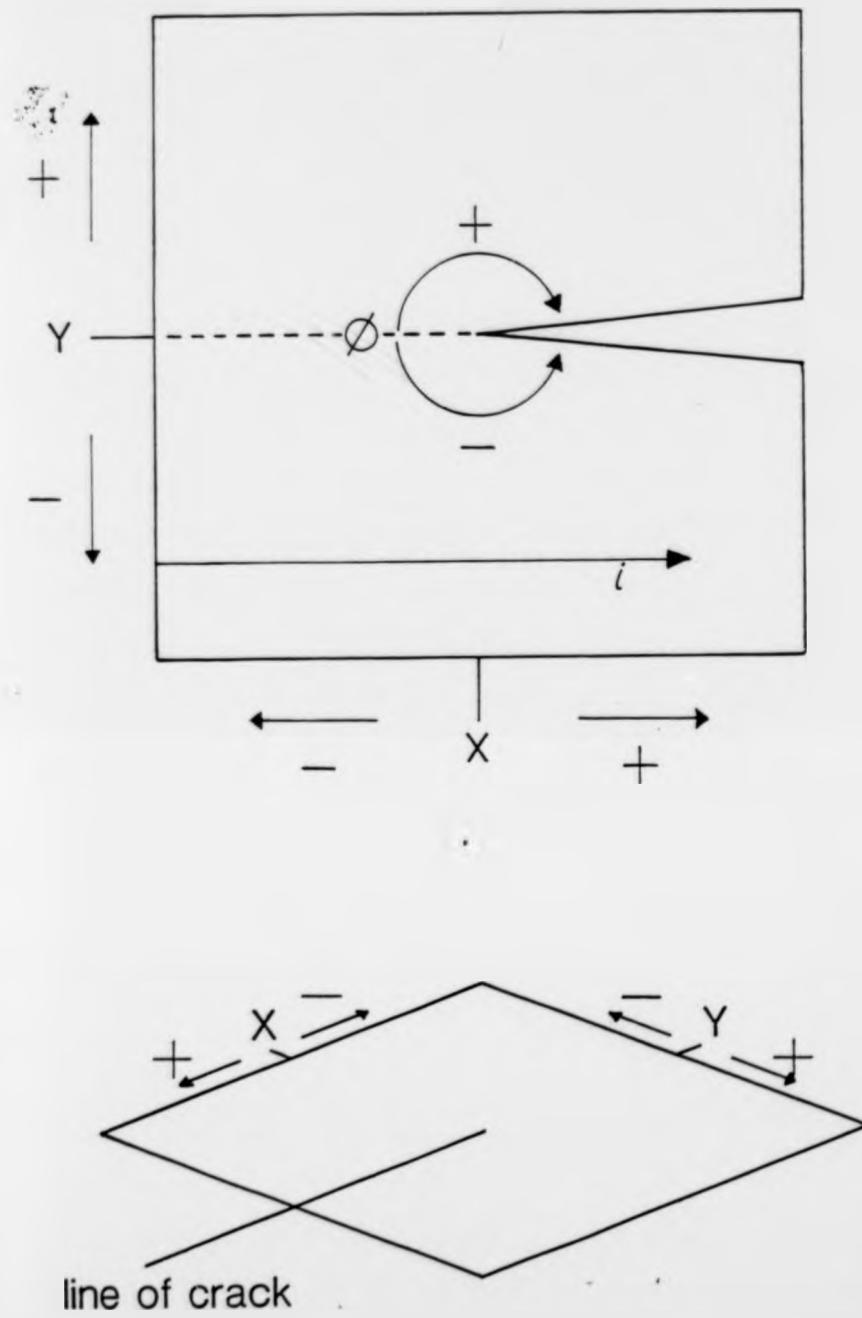


Fig 3.8 Co-ordinate frame used for maps and surface view block diagrams. *i* is a general integration path as used when calculating strain.

$$\sigma_1 = 1/2 (\sigma_{xx} + \sigma_{yy}) + [\sigma_{xy}^2 + 1/4 (\sigma_{xx} - \sigma_{yy})^2]^{1/2} \quad (3.4)$$

$$\sigma_2 = 1/2 (\sigma_{xx} + \sigma_{yy}) - [\sigma_{xy}^2 + 1/4 (\sigma_{xx} - \sigma_{yy})^2]^{1/2} \quad (3.5)$$

The distributions of σ_1 and σ_2 calculated from these equations are shown in figs 3.9 and 3.10 respectively and differential stress ($\sigma_1 - \sigma_2$) is shown in fig 3.11. These maps are again dimensionless in that the boundary conditions are set to unity to enable a comparison of the distributions to be made. Figures 3.9 and 3.10 show the relationship between σ_1 and σ_2 . σ_1 is positive over a large area around the tip with only a small negative region of low magnitude, whereas σ_2 has a reversed distribution in terms of both pattern and magnitude. As can be seen from fig 3.11 differential stress is a maximum along the $Y = 0, X < 0$ line enabling the crack to propagate forwards in the same plane.

The orientation of the principal stress axes relative to the plane of the crack can be calculated from

$$\tan(2\theta) = \frac{2 \sigma_{xy}}{\sigma_{xx} - \sigma_{yy}} \quad (3.6)$$

The calculated orientations are shown in fig 3.12 and the position of the axes in front of the crack can be seen to be at 45° to the plane of the crack. From the equation

Fig 3.9

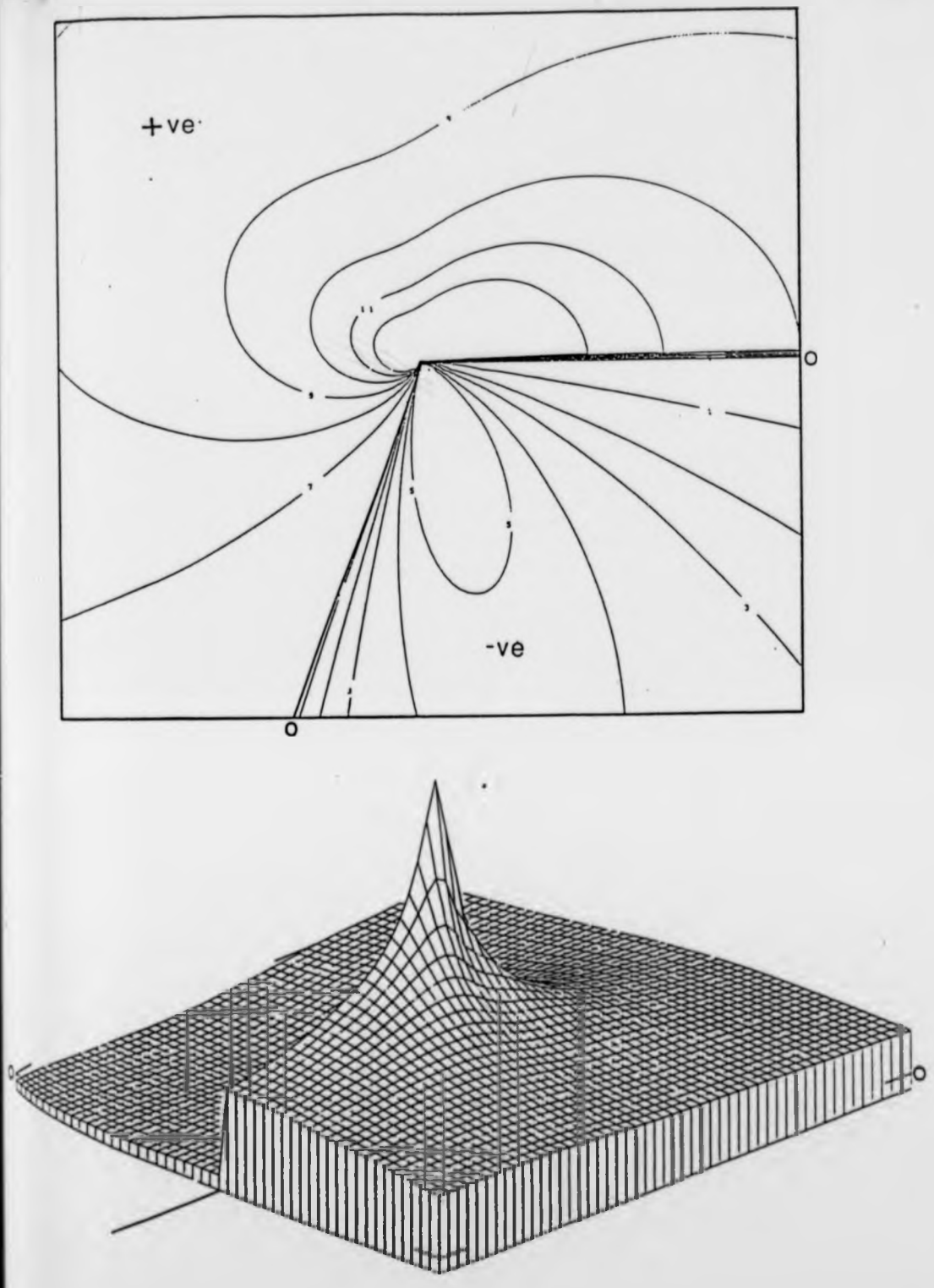


Fig 3.9 Dimensionless distribution map of σ_1 for Mode II fracture, all boundary conditions set to unity. The peak value is artificial due to the singularity at the crack tip.

Fig 3.10

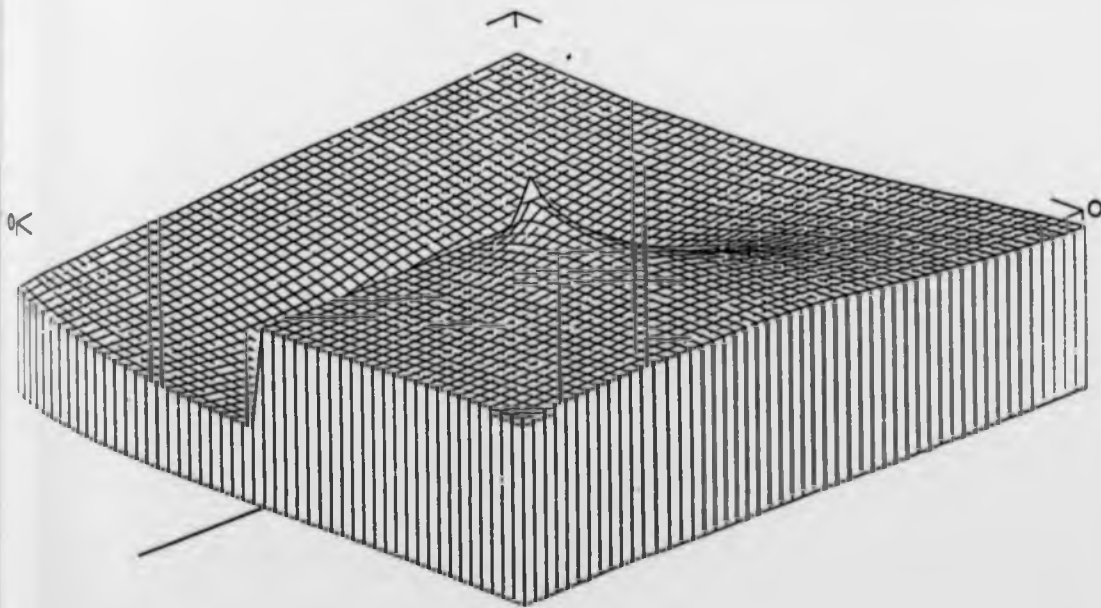
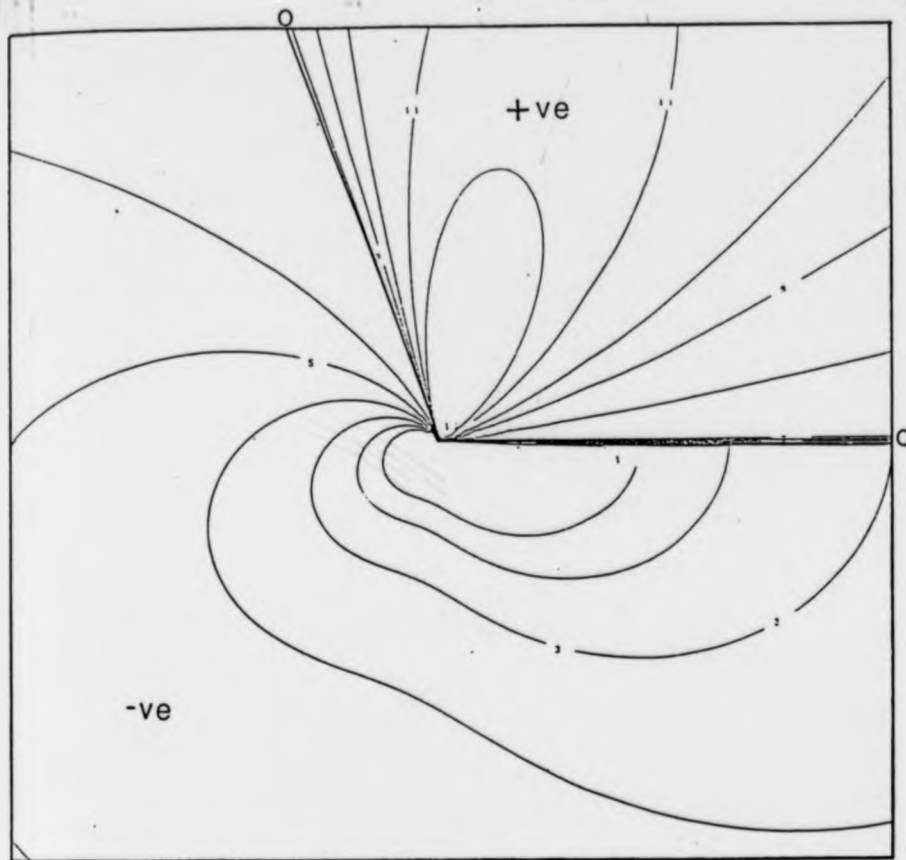


Fig 3.10 Dimensionless distribution map of σ_2 for Mode II fracture, all boundary conditions set to unity. The peak value is artificial due to the singularity at the crack tip.

Fig 3.11

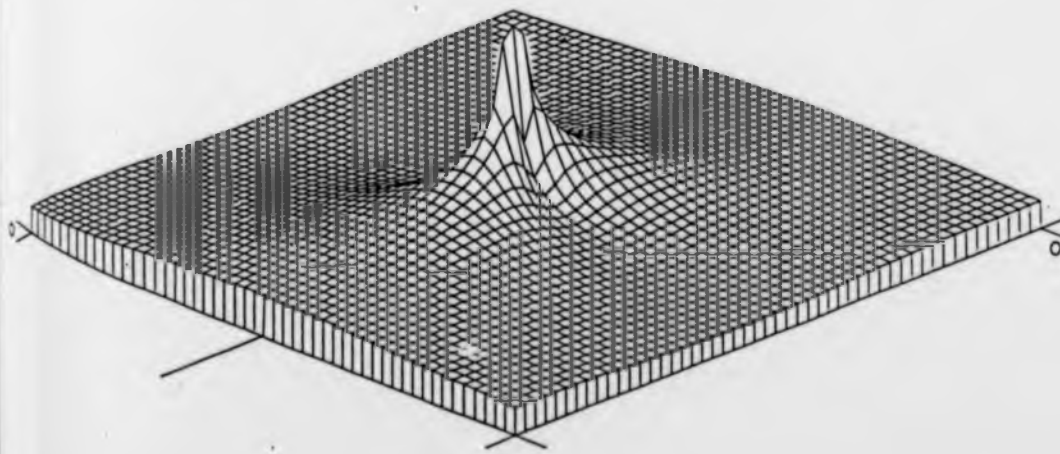
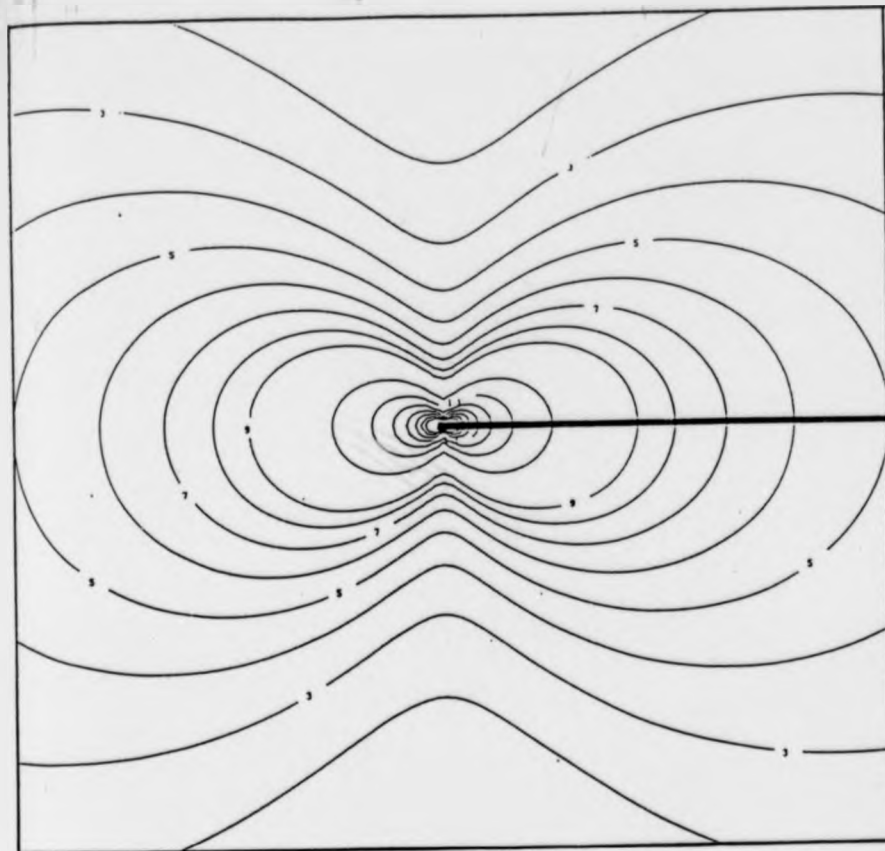


Fig 3.11 Dimensionless distribution map of differential stress for Mode II fracture, all boundary conditions set to unity. The peak value is artificial due to the singularity at the crack tip.

Fig 3.12

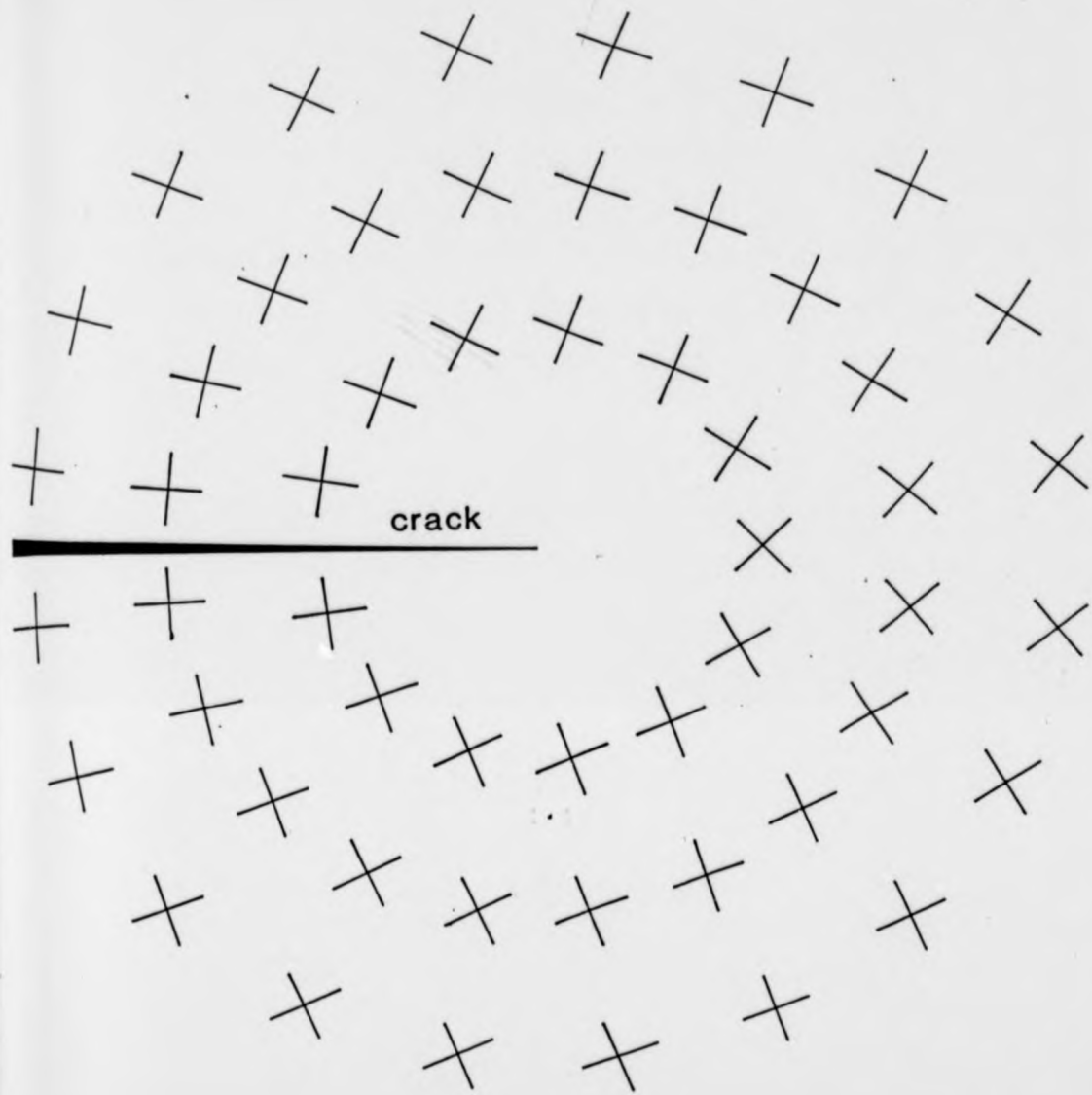


Fig 3.12 Orientation of principal stress axes around a Mode II crack tip.

$$\tau = 1/2 (\sigma_1 - \sigma_2) \sin(2\theta) \quad (3.7)$$

it can be seen that τ is a maximum when $\theta = 45^\circ$ ($\tau = 1/2(\sigma_1 - \sigma_2)$) so τ is a maximum in front of the crack along the $Y = 0, X < 0$ line.

Combining equations 3.3, 3.4 and 3.5 an expression can be obtained for differential stress in terms of the boundary conditions of load stress (σ_L) and crack half-length (C) and the distribution function.

$$\begin{aligned} (\sigma_1 - \sigma_2) = & \left[1/2(\sigma_{xx} + \sigma_{yy}) + [\sigma_{xy}^2 + 1/4(\sigma_{xx} - \sigma_{yy})^2]^{1/2} \right] \\ & - \left[1/2(\sigma_{xx} + \sigma_{yy}) - [\sigma_{xy}^2 + 1/4(\sigma_{xx} - \sigma_{yy})^2]^{1/2} \right] \end{aligned} \quad (3.8)$$

$$(\sigma_1 - \sigma_2) = [4\sigma_{xy}^2 + 1/4(\sigma_{xx} - \sigma_{yy})^2]^{1/2} \quad (3.9)$$

substituting from equation 3.3

$$= \left[4 \left[\sigma_L (C/2x)^{1/2} f_{xy}\theta \right]^2 + 1/4 \left[\sigma_L (C/2x)^{1/2} (f_{xx}\theta - f_{yy}\theta) \right]^2 \right]^{1/2} \quad (3.10)$$

$$= \left[4 \sigma_L^2 (C/2x) (f_{xy}\theta)^2 + 1/4 \sigma_L^2 (C/2x) (f_{xx}\theta - f_{yy}\theta)^2 \right]^{1/2} \quad (3.11)$$

$$= \sigma_L (C/2x)^{1/2} \left[4(f_{xy}\theta)^2 + 1/4(f_{xx}\theta - f_{yy}\theta)^2 \right]^{1/2} \quad (3.12)$$

simplifying

$$(\sigma_1 - \sigma_2) = \sigma_L (C/2x)^{1/2} f(\phi) \quad (3.13)$$

Thus giving an expression for differential stress in terms of the boundary conditions.

3.1.3 Strain distribution.

In order for the model to be applicable, the transition must now be made from a crack to a shear zone. The preceding stress distributions calculated using the brittle crack theory may now be used to calculate the ductile strains around a propagating shear zone tip. The strain (ϵ) at any point is a function of the strain rate ($\dot{\epsilon}$) and time. The strain rate is a function of the stress at that point, the ambient temperature and the rheological constants for the particular rock type. To obtain the strain at any point the strain rate is integrated with respect to time,

$$\epsilon = \int_t^{\infty} \dot{\epsilon} dt' \quad (3.14)$$

dt' may be written as

$$dt' = \frac{dt}{dx} dx \quad (3.15)$$

as dx/dt is velocity 3.15 may be re-written as

$$dt' = 1/V dx \quad (3.16)$$

where V - is the propagation velocity of the shear zone.

Thus by integrating in a reference frame fixed to the propagating shear zone tip it is possible to integrate with respect to distance (x) as opposed to time, which is geologically more convenient.

Combining 3.14 and 3.16

$$\epsilon = \int_x^{\infty} \dot{\epsilon} 1/V dx \quad (3.17)$$

A dislocation creep flow law is used to obtain the strain rate ($\dot{\epsilon}$) (see 1.II.3.c)

$$\dot{\epsilon} = A \exp(-Q/RT) (\sigma_1 - \sigma_2)^n \quad (3.18)$$

simplifying

$$\dot{\epsilon} = A_1 (\sigma_1 - \sigma_2)^n \quad (3.19)$$

substituting into 3.17

$$\epsilon = \int_x^{\infty} A_1 (\sigma_1 - \sigma_2)^n 1/V dx \quad (3.20)$$

substituting for $(\sigma_1 - \sigma_2)$ from 3.13

$$\epsilon = \int_x^{\infty} A_1 \sigma_L^n (C/2x)^{n/2} f^n(\phi) 1/V dx \quad (3.21)$$

the constants are then removed from the integral to give

$$\mathcal{E} = 1/V \cdot A_1 \cdot \sigma_L^n (C/2)^{n/2} \int_x^\infty x^{-(n/2)} f^n(\phi) dx \quad (3.22)$$

This equation can be usefully divided into a pre-multiplier containing the constants (velocity, the rheological parameters, load stress, temperature and shear zone half-length), and a shape function which is dependent on distance (x) and the angular function ($f \phi$).

This equation enables maps of the distribution of strain to be calculated for different values of the rheological constant n (Figs 3.13 - 3.15). These maps have been normalized by setting the pre-multiplier to unity in order to show the distribution of strain which is dependent on the shape function. The terms in the pre-multiplier will just have a re-scaling effect on these basic strain distributions. The values shown along the crack itself are again artificial as the actual value is a singularity.

The importance of the factor n is evident from the accentuation of the shape of the normalized strain maps (Figs 3.13 - 3.15) with increasing n . For low values of n the normalized strain profile across the shear zone, as seen in the surface view block diagram (Fig 3.13), has a broad region in which the strain increases gradually towards the centre of the shear zone. As n is increased (Figs 3.14 and 3.15) the region of high normalized strain becomes more localized around the zone. This is also shown in the contour maps (Figs 3.13 - 3.15), for low values of n the normalized strain contours are at a high angle to the line of the shear zone, but with increasing n they become sub-parallel to the zone. The profile of normalized strain perpendicular to the shear zone, for $n = 3$, shows a marked similarity to the shapes of published strain profiles from natural examples of shear zones (see Chpt 2), this is particularly apparent in the shape

Fig 3.13

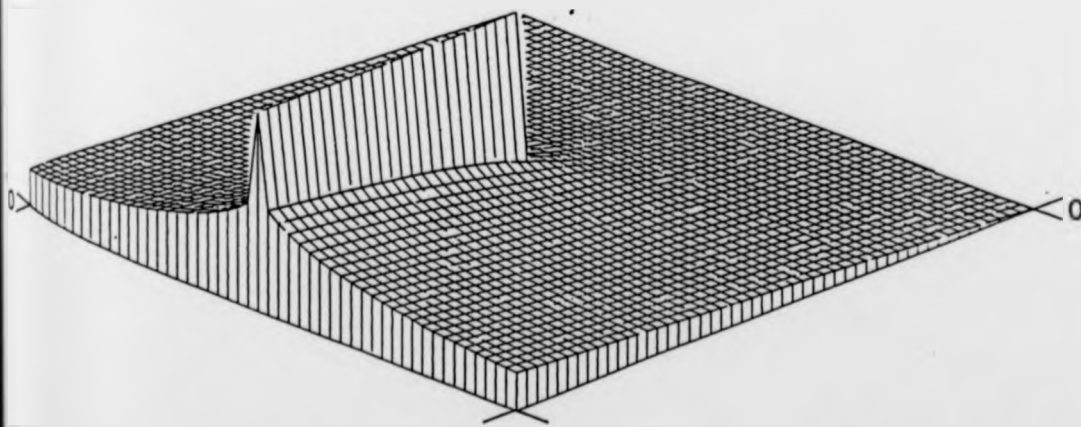
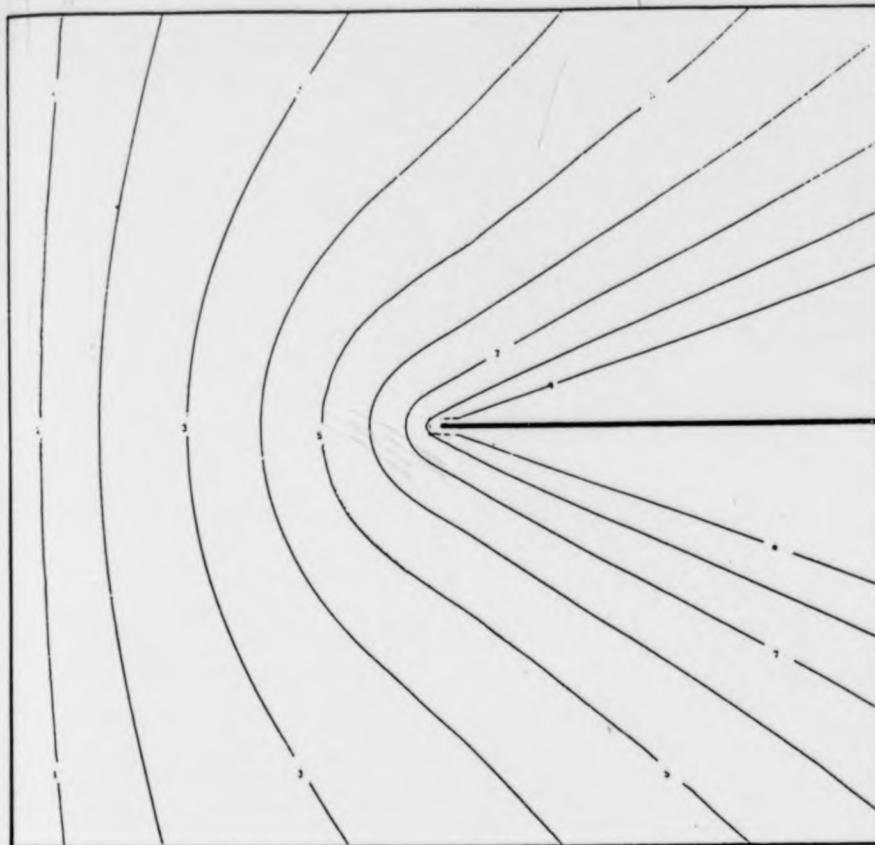


Fig 3.13 Distribution of normalized strain around a shear zone tip for $n = 1$ in equation 3.22.

Fig 3.14

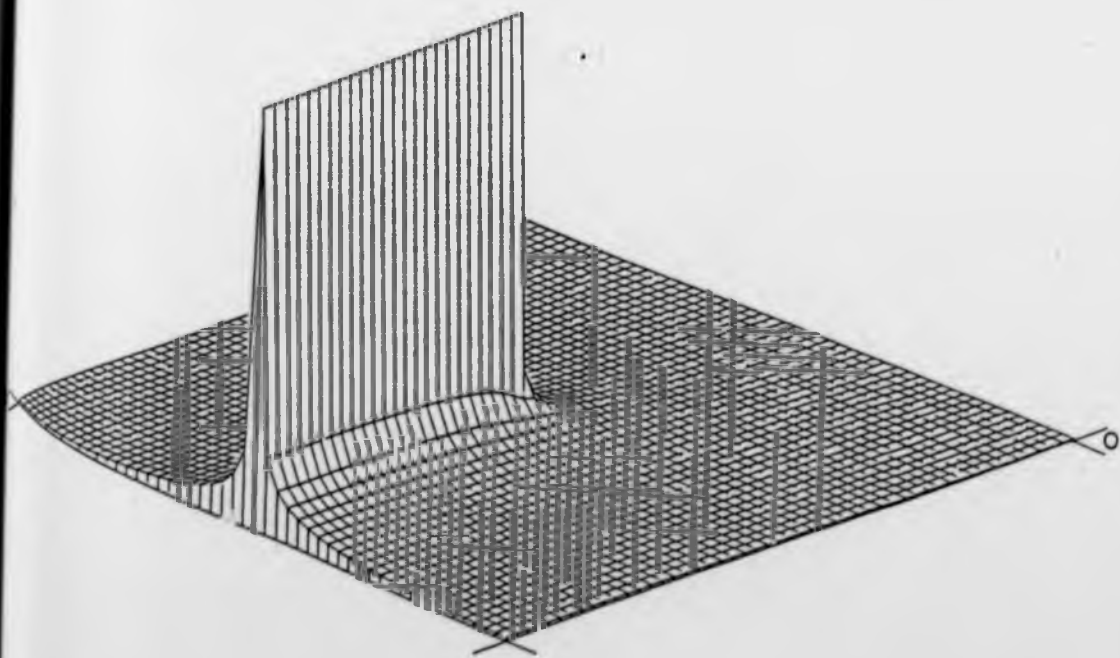
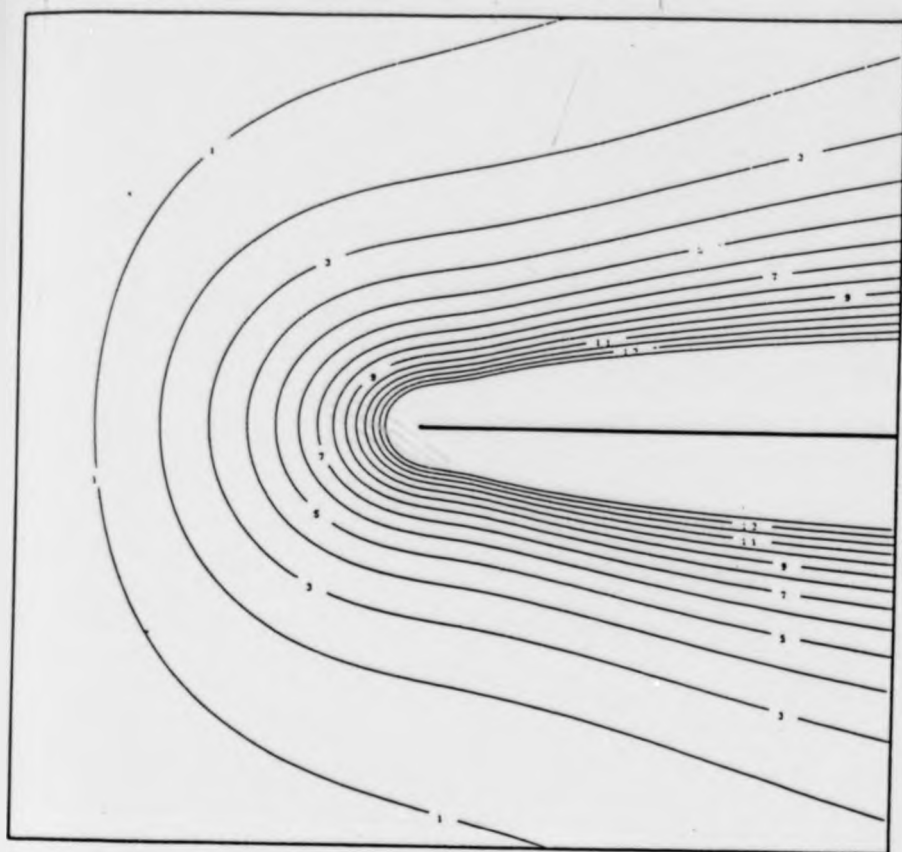


Fig 3.14 Distribution of normalized strain around a shear zone tip for $n = 3$ in equation 3.22.

Fig 3.15

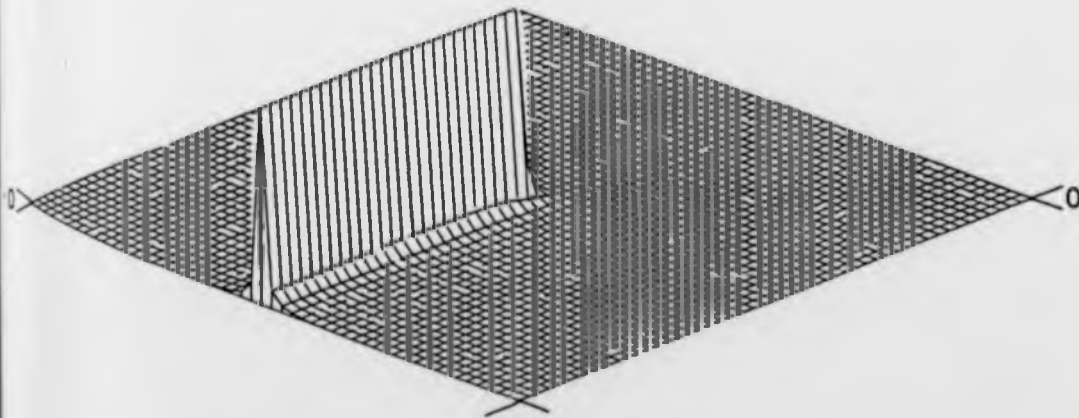
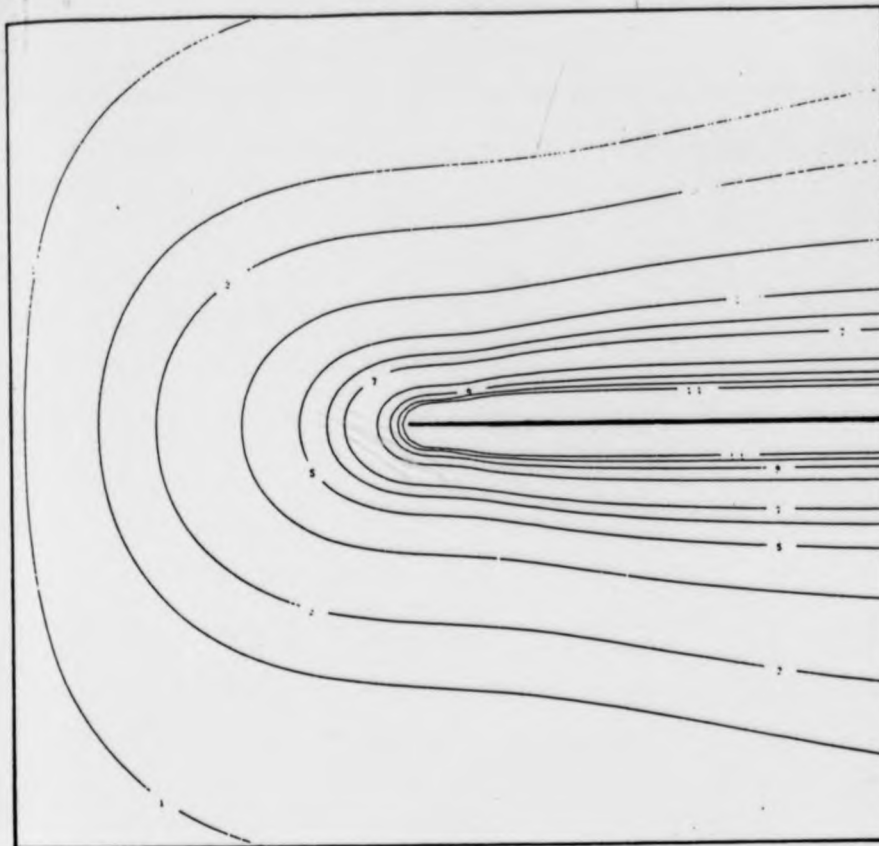


Fig 3.15 Distribution of normalized strain around a shear zone tip for $n = 5$ in equation 3.22.

of the sides of the profiles. The absence of a flat or rounded top, as seen from natural examples, is due to the initial theory for the model.

3.1.4 Self-consistency test of the model.

For the proposed model to be self-consistent the driving stress must be relieved at the shear zone tip. The stress release is given by

$$\text{stress release} = K \cdot \epsilon \quad (3.23)$$

where K - is a function of the elastic modulus and Poissons ratio

For the shear zone to propagate, the driving stress/stress release ratio (R) must be small (~ 1) at the shear zone tip

$$\frac{\text{driving stress}}{\text{stress release}} = R \sim 1 \quad (\text{at the tip}) \quad (3.24)$$

so R may be calculated by combining equations 3.13, 3.22 and 3.23 to give

$$R = \frac{\sigma_L (C/2x)^{1/2} f(\phi)}{K \cdot 1/V \cdot A_1 \cdot \sigma_L^n (C/2)^{n/2} \int_x^\infty x^{-(n/2)} f^n(\phi) dx} \quad (3.25)$$

A typical driving stress/stress release ratio map is shown in fig 3.16.

Fig 3.16

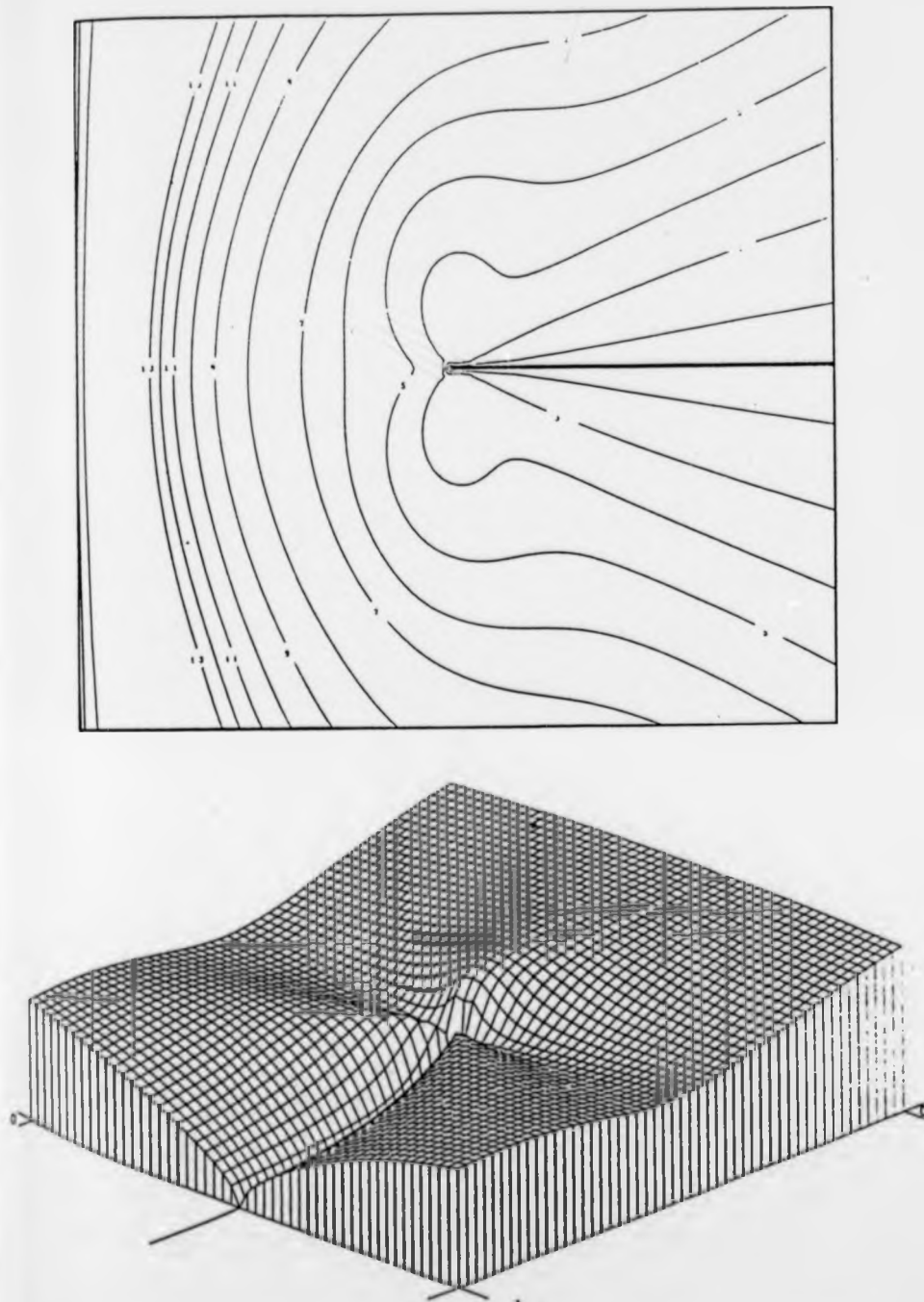


Fig 3.16 Driving stress/stress release ratio (R) map for dry quartz. Using the standard parameters given in table 3.1 and the rheological constants of Koch *et al.* (1980). The increase in R to the left of the contour map is due to the method of integration used, and the problem of being unable to integrate from infinity numerically.

3.1.5 The importance of the factor n

It is useful at this point to introduce a term related to the driving stress/stress release ratio (R); this is the dimensionless driving stress/stress release ratio (R_d). This is calculated in the same way as R but with the boundary conditions set to unity to clarify the effect of the shape function. The dimensionless driving stress/stress release ratio (R_d) is now calculated along the $Y = 0, X < 0$ line (Fig 3.8) and the influence of the factor n can be clearly demonstrated. Figures 3.17 - 3.20 show the effect of increasing n from 2 to 5. These graphs show the variation of R_d with distance from the shear zone tip which is at the origin. For values of n less than 3, R_d increases towards the shear zone tip, and hence for these values the requirement that $R \sim 1$ at the shear zone tip cannot be satisfied and the model breaks down. For values of n greater than 3, R_d decreases into the tip region and so the model remains valid. For the special case of $n = 3$ R_d is a constant independent of distance (x). The model therefore predicts that materials with an n value of less than 3 will not enable shear zones to form or propagate. The critical effect of the factor n forms the basis of the second phase of the model development as it enables a single value to be obtained for the dimensionless driving stress/stress release ratio (R_d) of 0.5 (Fig 3.18). Also for a given set of boundary conditions the driving stress/stress release ratio (R) will be a constant with respect to distance from the shear zone tip, along the $Y = 0, X < 0$ line.

The importance of the factor n has been recorded from studies of polycrystalline metals, where values of n of 4.5 and 5.5 are common. Such materials localize deformation more easily than materials with lower n values (Weertman & Weertman 1975).

Fig 3.17

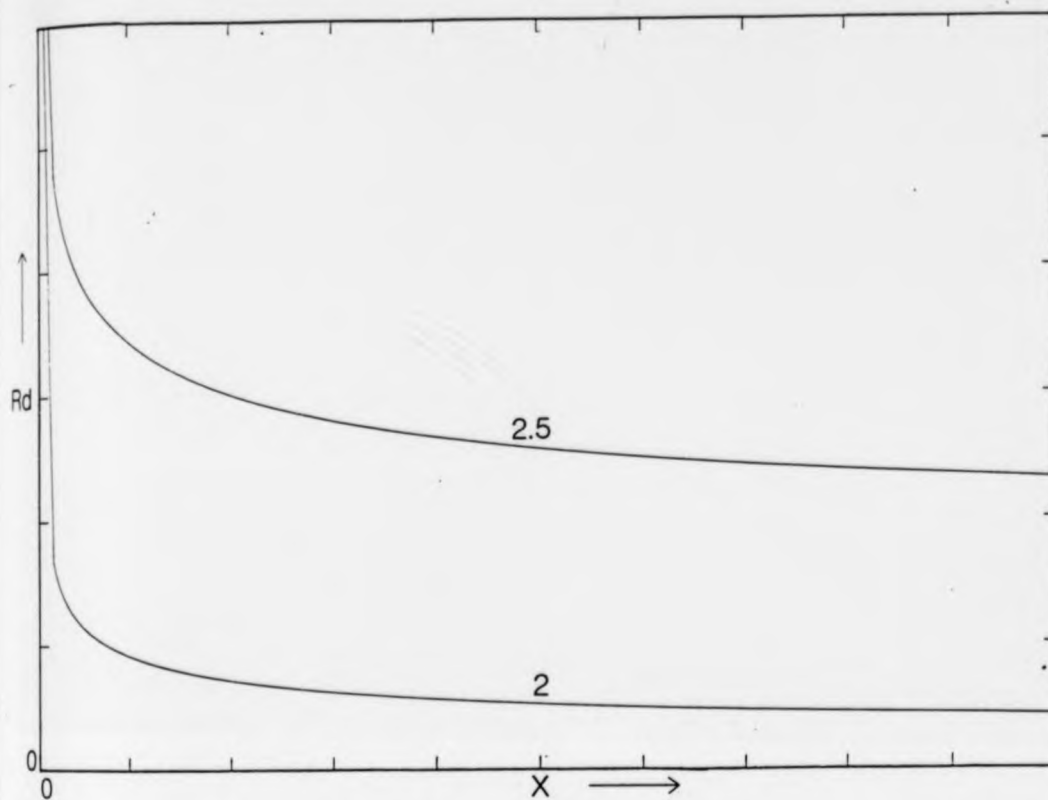


Fig 3.17 Dimensionless driving stress/stress release ratio (R_d) plotted against distance on the $Y = 0, X > 0$ line for $n = 2$ and 2.5 .

Fig 3.18

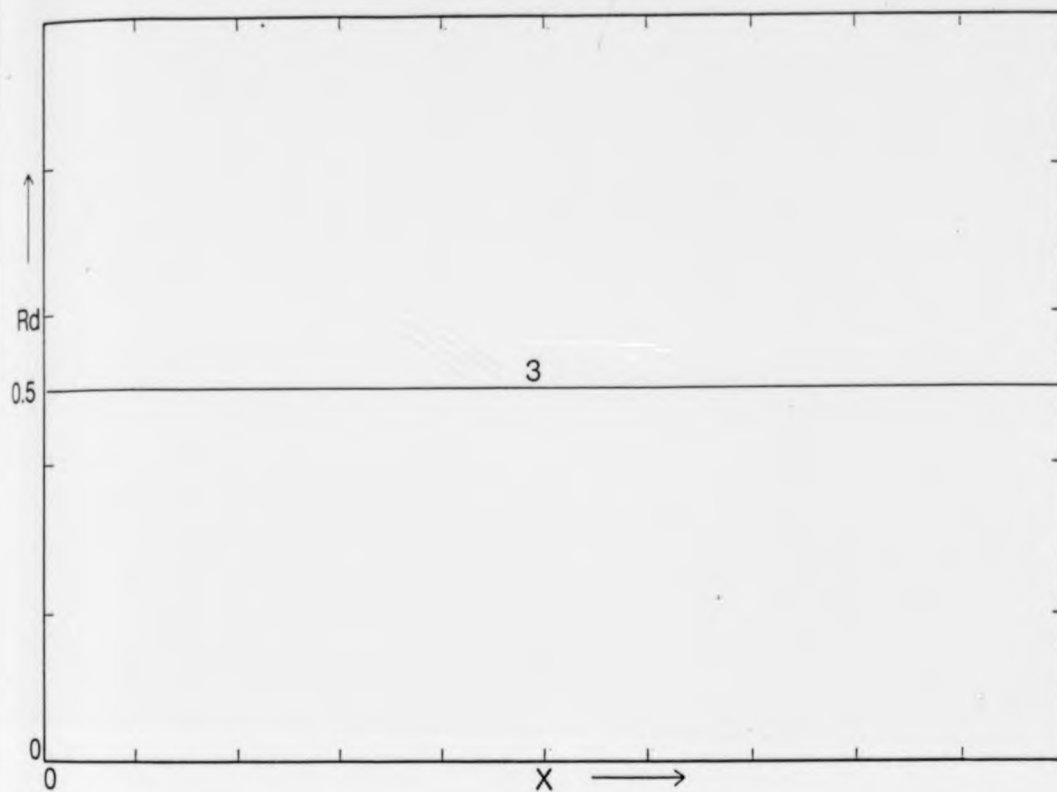


Fig 3.18 Dimensionless driving stress/stress release ratio (R_d) plotted against distance on the $Y = 0, X > 0$ line for $n = 3$.

Fig 3.19

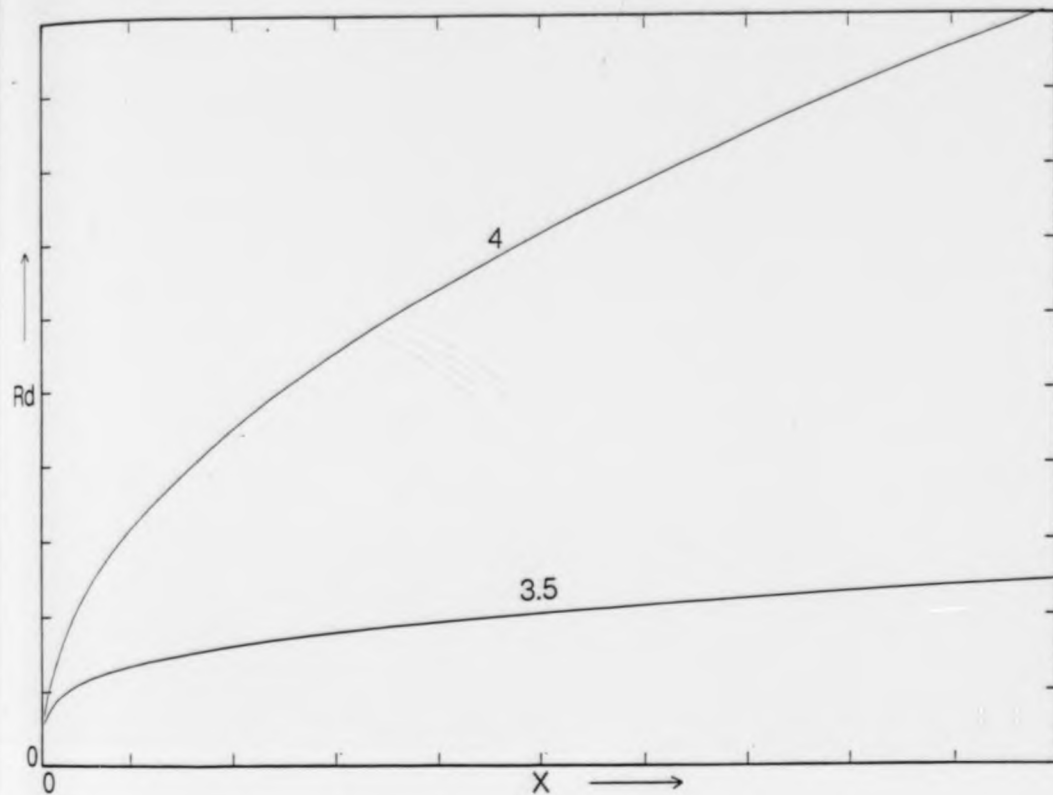


Fig 3.19 Dimensionless driving stress/stress release ratio (R_d) plotted against distance on the $Y = 0, X > 0$ line for $n = 3.5$ and 4 .

Fig 3.20

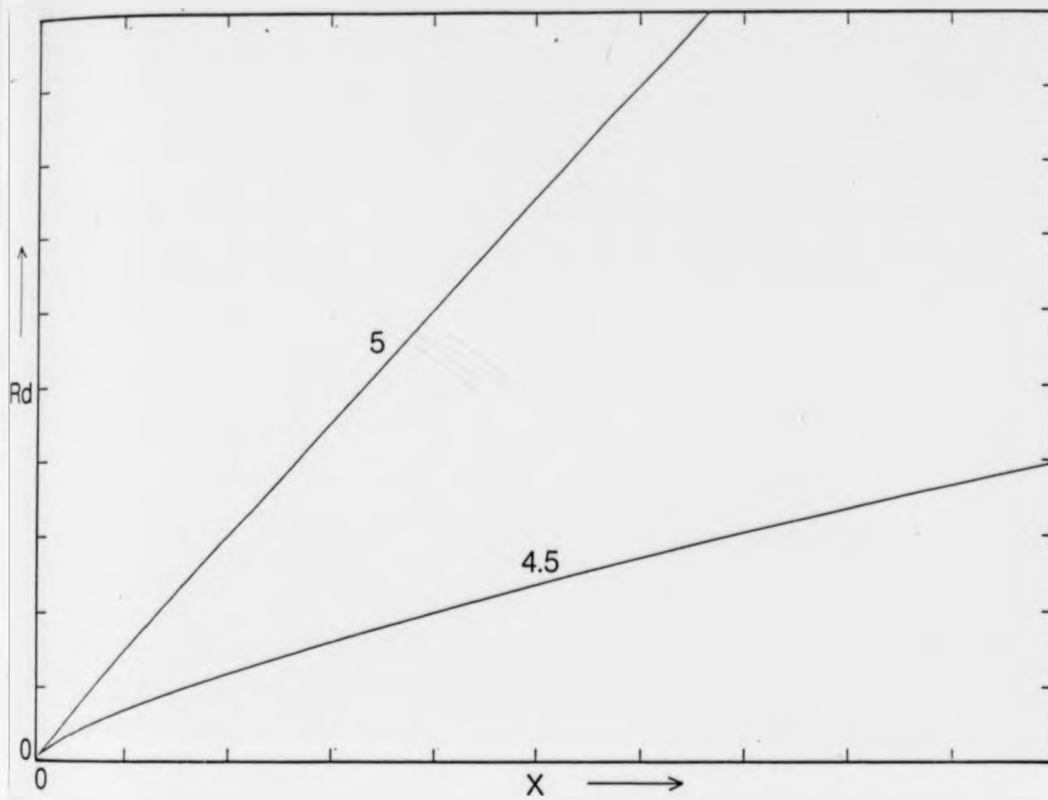


Fig 3.20 dimensionless driving stress/stress release ratio (R_d) plotted against distance on the $Y = 0, X > 0$ line for $n = 4.5$ and 5 .

3.II THE PRE-MULTIPLIER RELATIONSHIPS.

3.II.1 Derivation of the pre-multiplier relationships.

For the line $Y = 0$, $X < 0$ in front of the shear zone tip, ϕ in equation 3.1 is zero. This means that σ_{xx} and σ_{yy} are also zero (Figs 3.5 & 3.6) and that $f_{xy}(\phi) = 1$. Therefore for this section ($Y = 0$, $X < 0$) from 3.1

$$\sigma_{xy} = \sigma_L (C/2x)^{1/2} \quad (3.26)$$

The terms σ_{xx} and σ_{yy} disappear from the principal stress equations 3.4 and 3.5 giving

$$\sigma_1 = (\sigma_{xy}^2)^{1/2} \quad (3.27)$$

$$\sigma_2 = - (\sigma_{xy}^2)^{1/2} \quad (3.28)$$

Therefore

$$(\sigma_1 - \sigma_2) = 2\sigma_{xy} = 2\sigma_L (C/2x)^{1/2} \quad (3.29)$$

for the $Y = 0$, $X < 0$ line.

The stress release along this section is given by

$$= K.A. \exp(-Q/RT) 2\sigma_L^n (C/2)^{n/2} 1/V \int_x^{\infty} x^{-(n/2)} dx \quad (3.30)$$

re-writing 3.29 as

$$(\sigma_1 - \sigma_2) = 2\sigma_L (C/2)^{1/2} x^{-1/2} \quad (3.31)$$

The driving stress/stress release ratio (R) along the $Y = 0$, $X < 0$ line is given by combining 3.30 and 3.31

$$R = \frac{2\sigma_L (C/2)^{1/2}}{K A \exp(-Q/RT) (2\sigma_L)^n (C/2)^{n/2} 1/V} \times \frac{x^{-1/2}}{\int_x^\infty x^{-(n/2)} dx} \quad (3.32)$$

Again this equation may be divided into a pre-multiplier (B) containing the boundary conditions and the material constants, and the dimensionless ratio (R_d) dependent on distance (x) and the factor n.

Re-writing 3.32 as

$$R = B \cdot \frac{x^{-1/2}}{\int_x^\infty x^{-(n/2)} dx} \quad (3.33)$$

$$R = B \cdot x^{1/2} (n-3) (1-n/2) \quad (3.34)$$

Therefore for $n = 3$

$$R = B \cdot (-1/2) \quad (3.35)$$

The driving stress/stress release ratio is therefore independent of x as has been shown numerically in fig 3.18. The algebraic solution gives a negative value for R_d due to the limits being set in the conventional manner to integrate from x to infinity. If the limits are reversed to allow integration from infinity towards the shear zone tip, as required by the model, the sign of the integral changes and R_d becomes positive.

Therefore

$$R = B \cdot 1/2 \quad (3.36)$$

3.II.2 The interrelationship equations.

As the driving stress/stress release ratio is a constant for $n = 3$ it is possible to derive a series of equations that can be used to quantify the interrelationships between the various boundary conditions i.e. temperature, load stress, shear zone half-length, propagation velocity and the rheological parameters.

From 3.32 and 3.36

$$R = \frac{V}{K \cdot A \cdot \exp(-Q/RT) \cdot (2\sigma_L)^2 \cdot (C/2)} \cdot 1/2 \quad (3.37)$$

Using equation 3.37 it is possible to draw up a series of graphs showing the effect of temperature, load stress, shear zone half-length and propagation velocity on the driving stress/stress release ratio (R) (Figs 3.21 - 3.24). These graphs were calculated for a dry quartz rheology (Koch *et al.* 1980) (see table 1.1 this study) and using the standard parameters given in table 3.1 for temperature, stress, half-length and propagation velocity. In order for the model to be self consistent R must be approximately equal to 1 at the shear zone tip (see 3.I.4 and 3.I.5). Using this constraint it is possible to predict from figures 3.21 - 3.24 that shear zones will propagate more easily for higher temperatures, higher load stresses, larger half-lengths and lower propagation velocities. Following on from this it is possible to rearrange equation 3.37 to give an expression in terms of any of the boundary conditions:

Fig 3.21

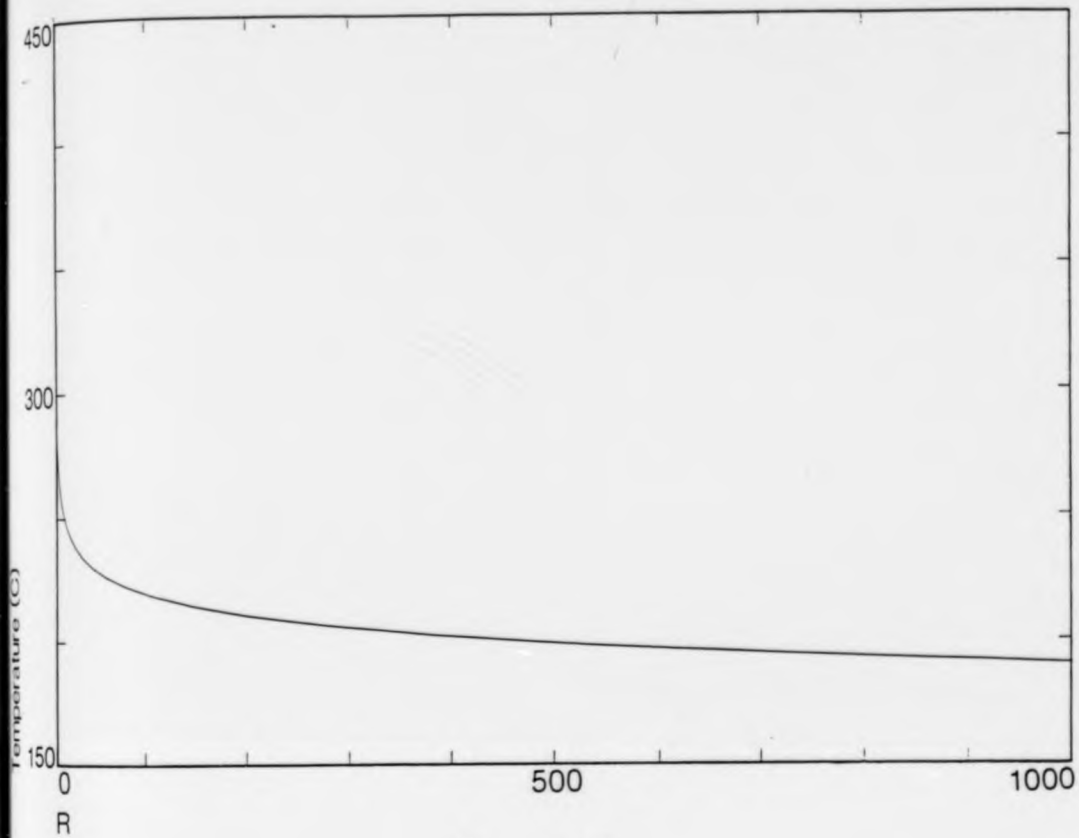


Fig 3.21 Driving stress/stress release ratio (R) plotted against temperature for dry quartz.

Fig 3.22

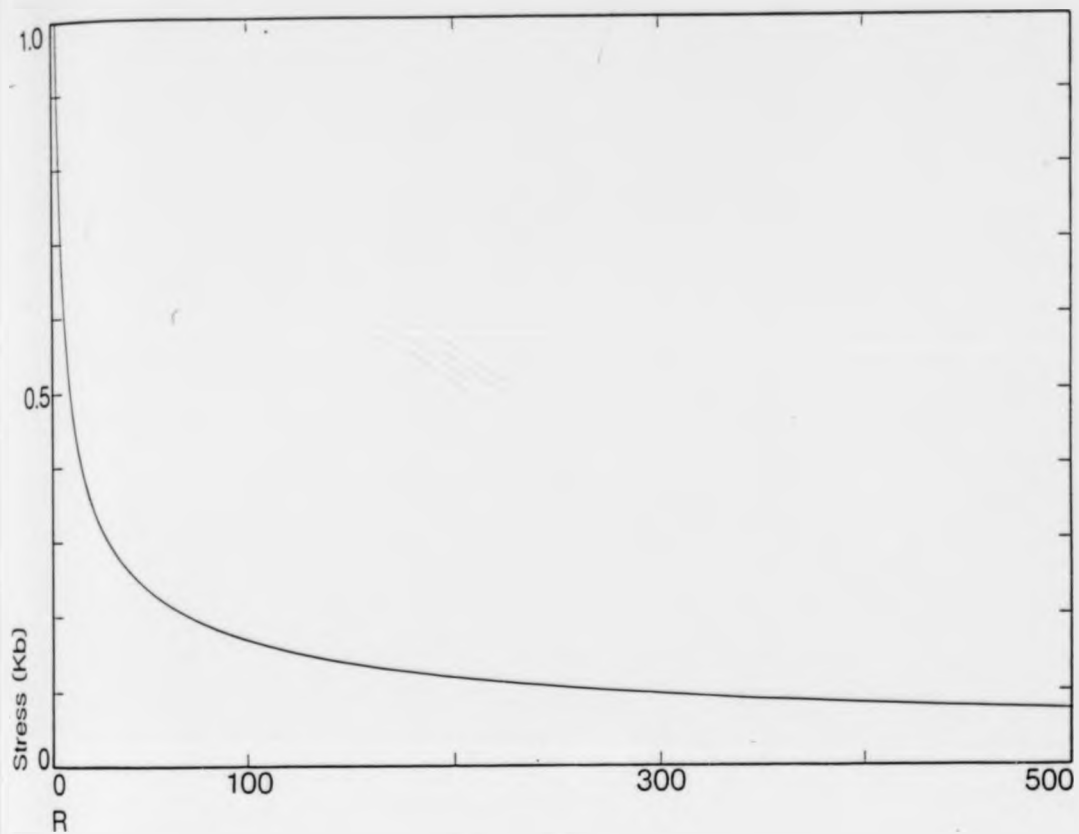


Fig 3.22 Driving stress/stress release ratio (R) plotted against applied load stress for dry quartz.

Fig 3.23

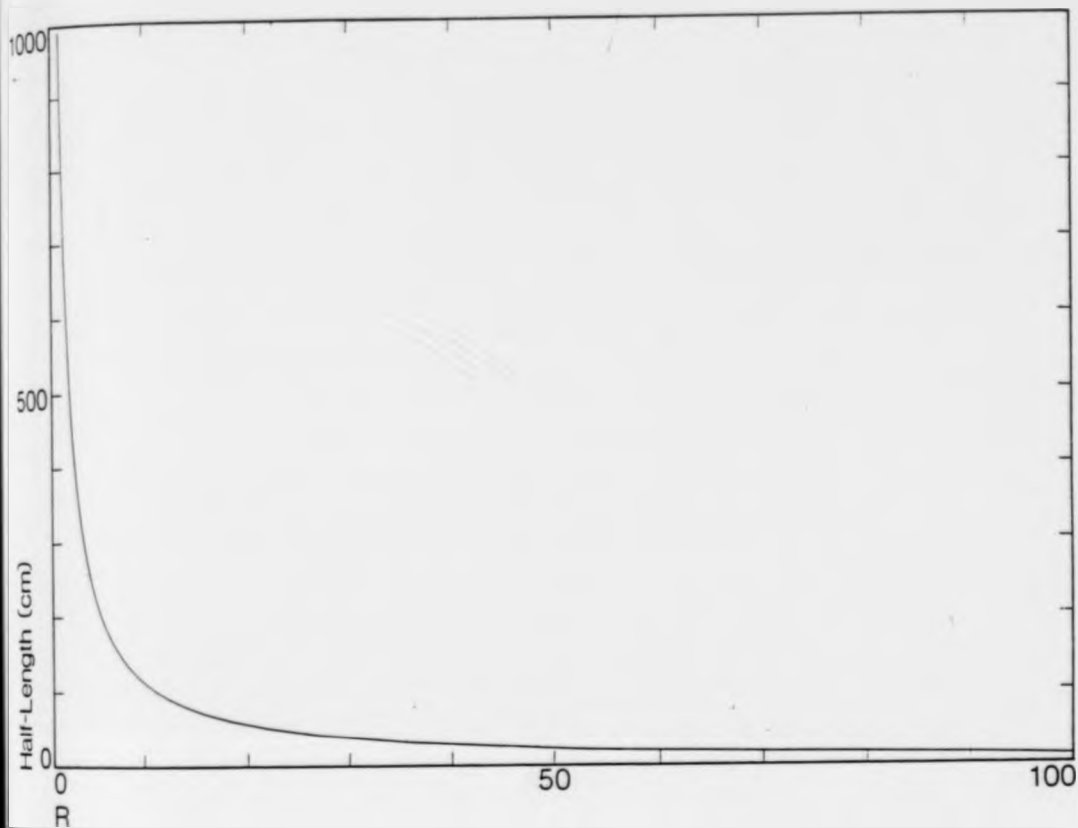


Fig 3.23 Driving stress/stress release ratio (R) plotted against shear zone half-length for dry quartz.

Fig 3.24

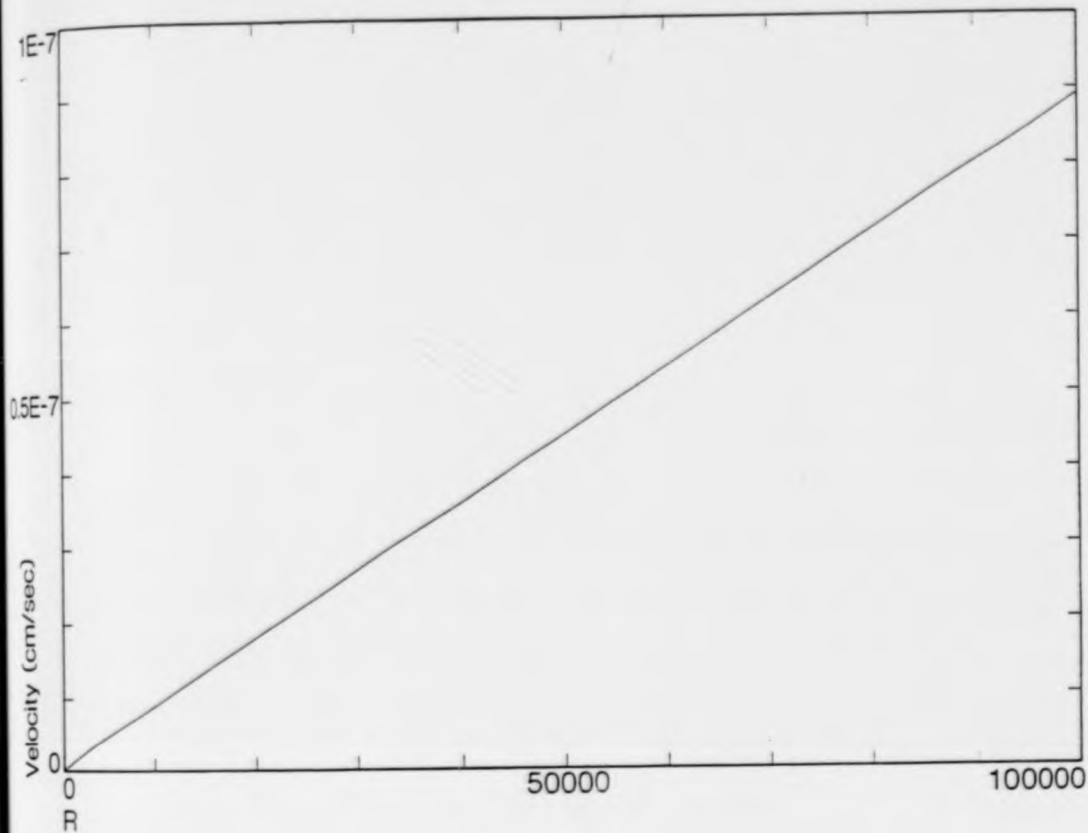


Fig 3.24 Driving stress/stress release ratio (R) plotted against propagation velocity for dry quartz. ($1E-7 = 1 \times 10^{-7}$)

$$2.R.K.A.\exp(-Q/RT) (2\sigma_L)^2 (C/2) = V \quad (3.38)$$

$$\left[\frac{V}{8.R.K.A.\exp(-Q/RT) (C/2)} \right]^{1/2} = \sigma_L \quad (3.39)$$

$$\frac{V}{R.K.A.\exp(-Q/RT) (2\sigma_L)^2} = C \quad (3.40)$$

It is not necessary to derive a fourth equation for temperature as all combinations of the four principal boundary conditions can be investigated using equations 3.38 - 3.40. It is also possible using these equations to examine the effect of the rheology of the host material on the conditions required for shear zone development and propagation.

3.III RESULTS AND CONCLUSIONS

3.III.1 Results from the interrelationship equations.

The results from equations 3.38 - 3.40 are shown in figures 3.25 - 3.48. The graphs have been drawn for values of R of 1, 10 and 100 to show the conditions under which shear zone propagation is most likely. The lines for the various values of R are in effect contours of "ease of propagation", with R = 1 representing the conditions of most likely propagation. The rheological parameters used are given in table 1.1, and are those of Koch *et al.* (1980) for dry quartz, Bodine *et al.* (1981) for dry olivine, Shelton and Tullis (1981) for plagioclase (anorthosite), and Carter *et al.* (1981) for granite. In order to draw the graphs where a variation between two out of four parameters are shown, the remaining two parameters must be set at a fixed value. The set of standard values used for this purpose is shown

Fig 3.25

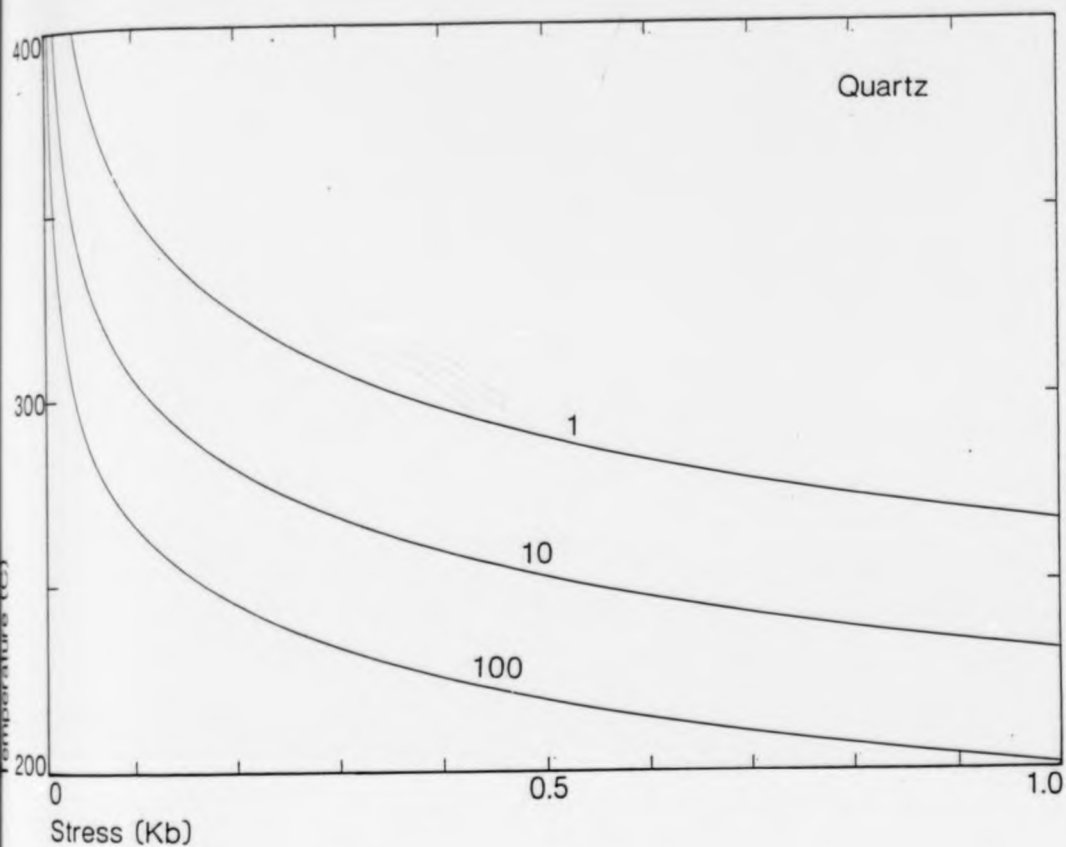


Fig 3.25 Temperature plotted against applied load stress for dry quartz, for $R = 1, 10, 100$.

Fig 3.26

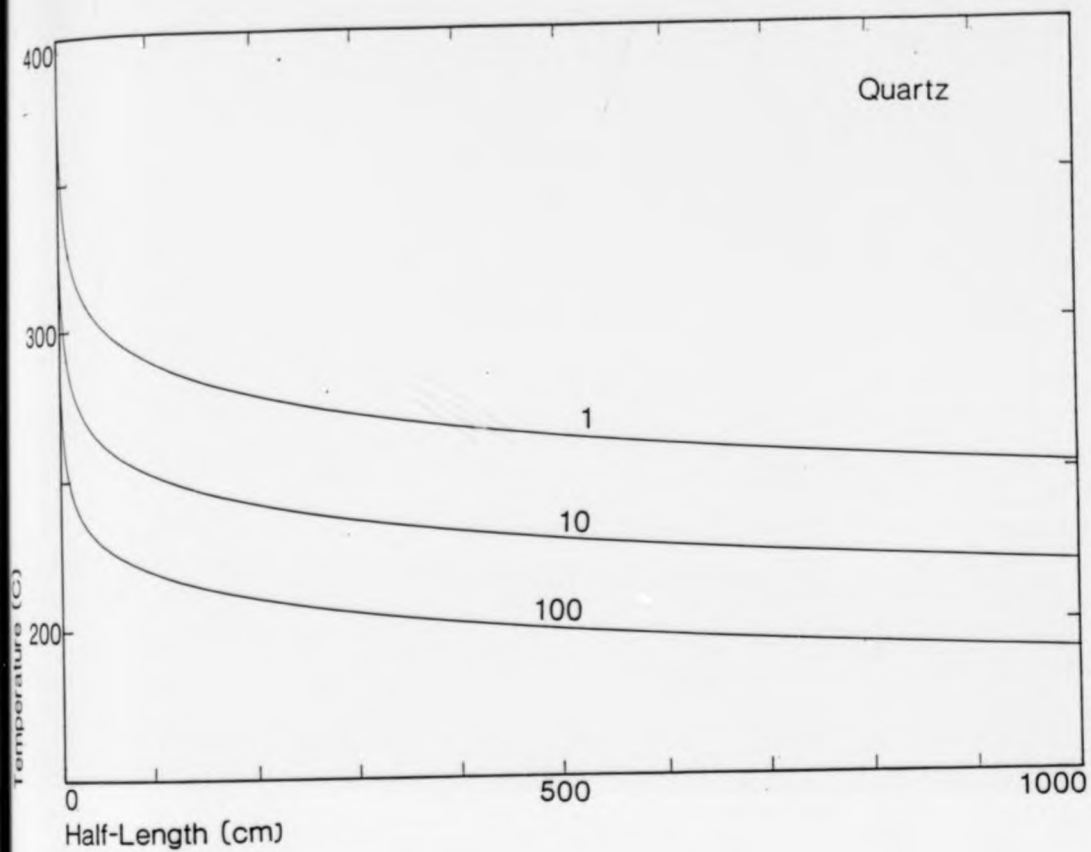


Fig 3.26 Temperature plotted against shear zone half-length for dry quartz, for $R = 1, 10, 100$.

Fig 3.27

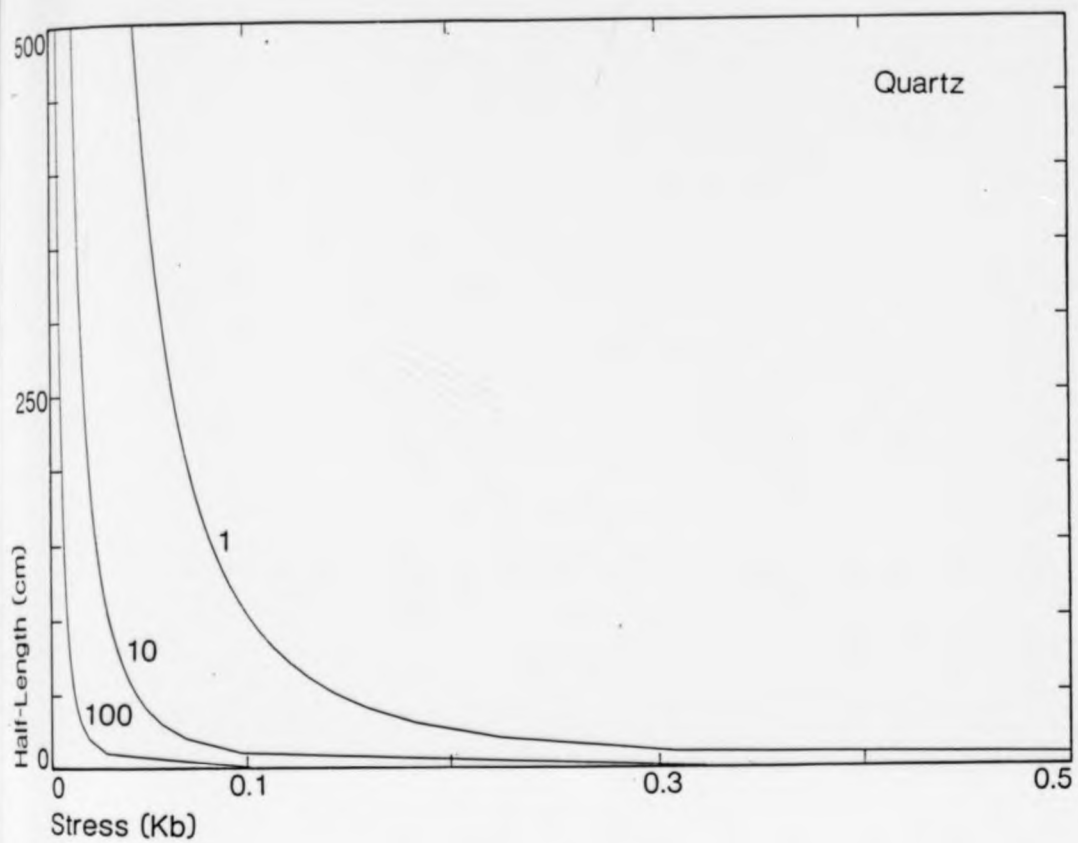


Fig 3.27 Shear zone half-length plotted against applied load stress for dry quartz, for $R = 1, 10, 100$.

Fig 3.28

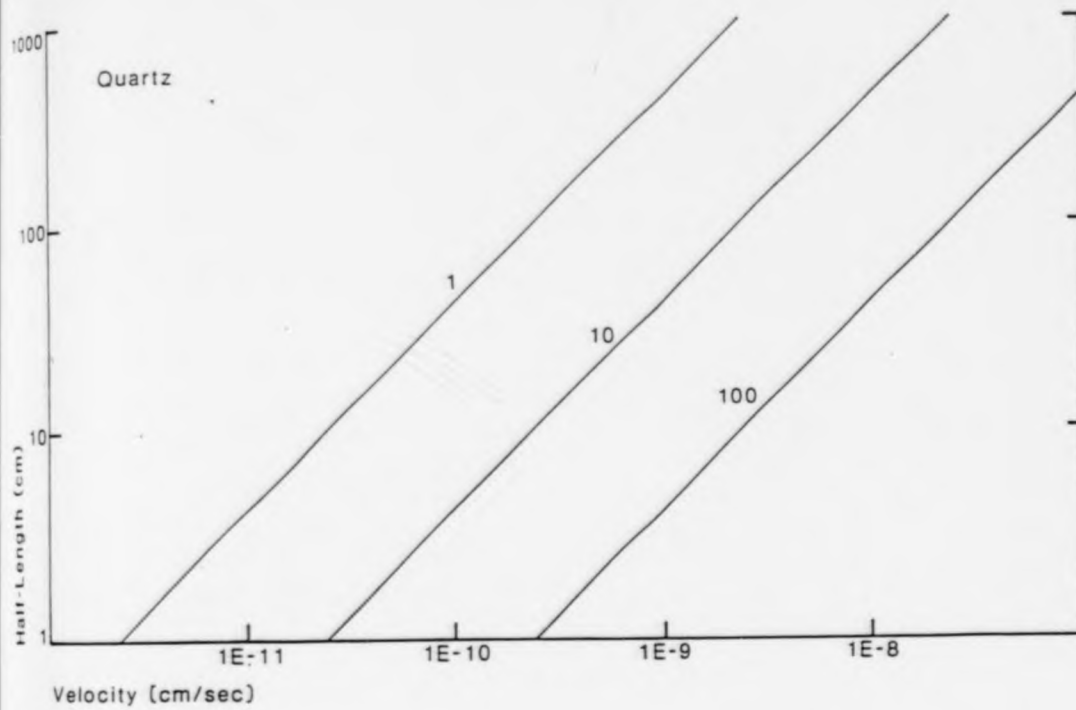


Fig 3.28 Shear zone half-length plotted against propagation velocity for dry quartz, for $R = 1, 10, 100$. ($1E-11 = 1 \times 10^{-11}$)

Fig 3.29

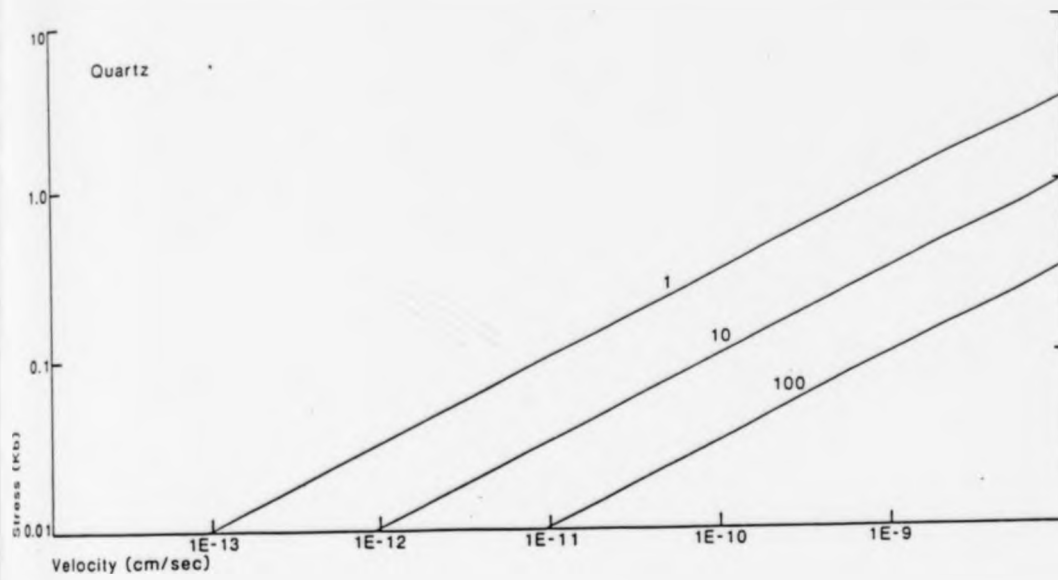


Fig 3.29 Applied load stress plotted against propagation velocity for dry quartz, for R = 1, 10, 100. (1E-11 = 1×10^{-11})

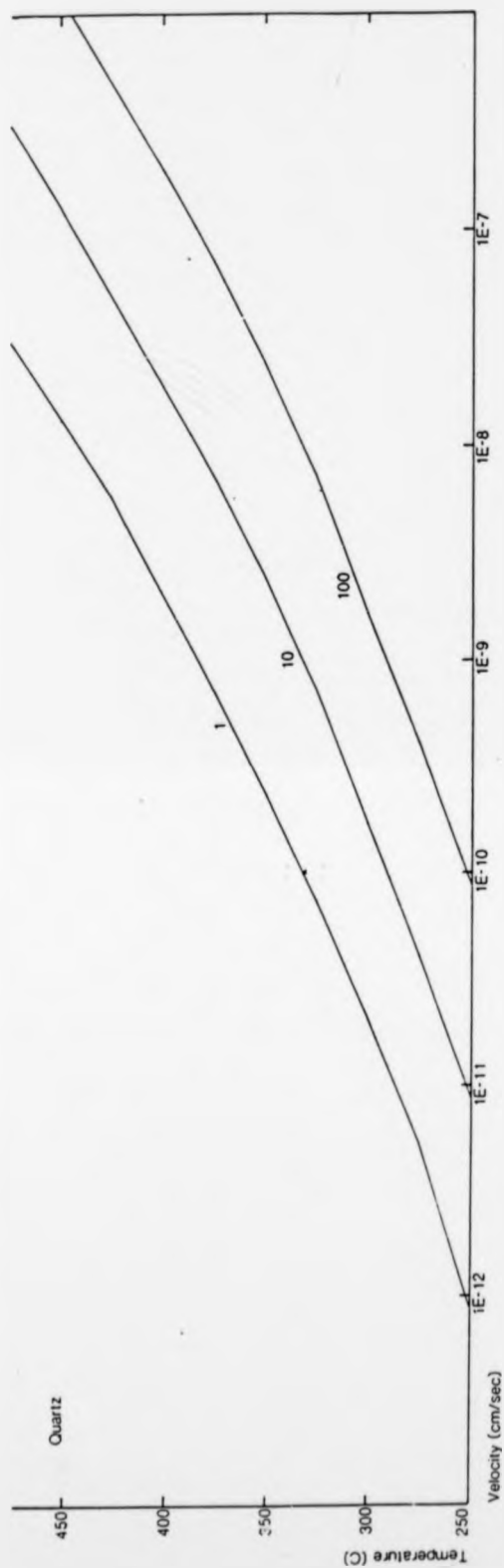


Fig 3.30 Temperature plotted against propagation velocity for dry quartz, for $R = 1, 10, 100$. ($1E-11 = 1 \times 10^{-11}$)

Fig 3.31

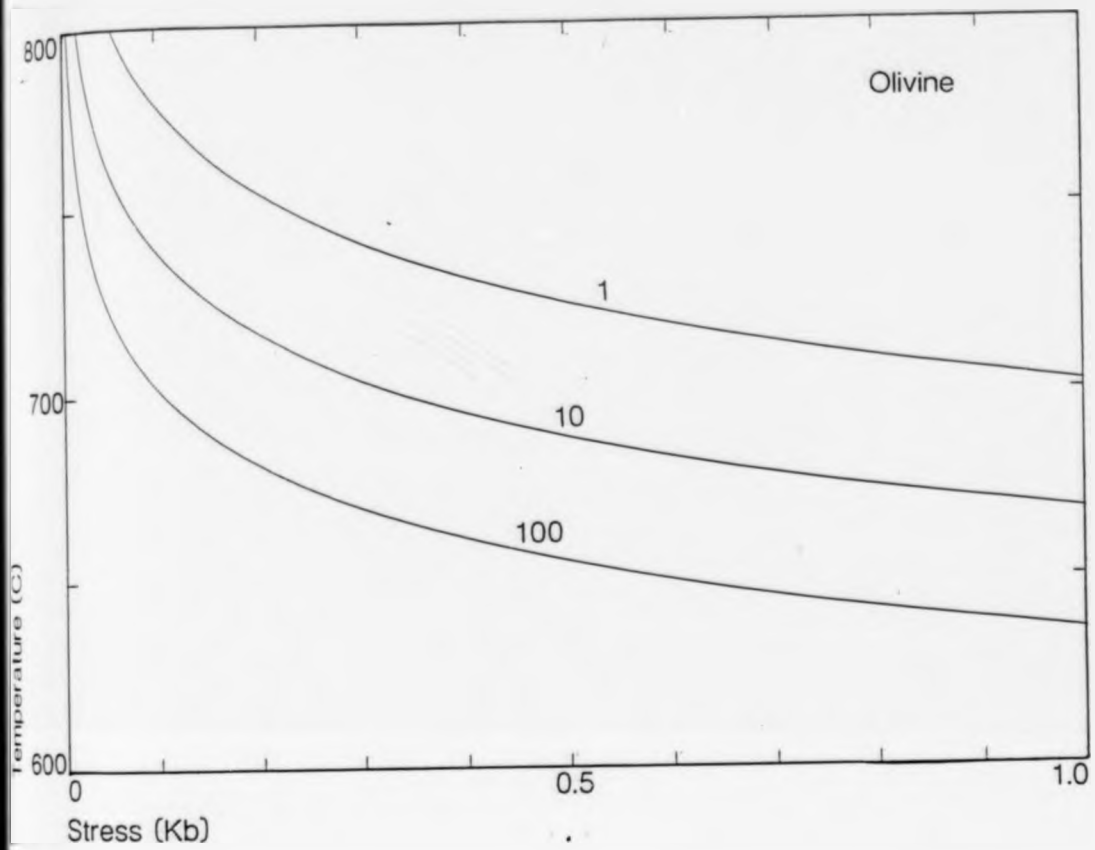


Fig 3.31 Temperature plotted against applied load stress for dry olivine, for $R = 1, 10, 100$.

Fig 3.32

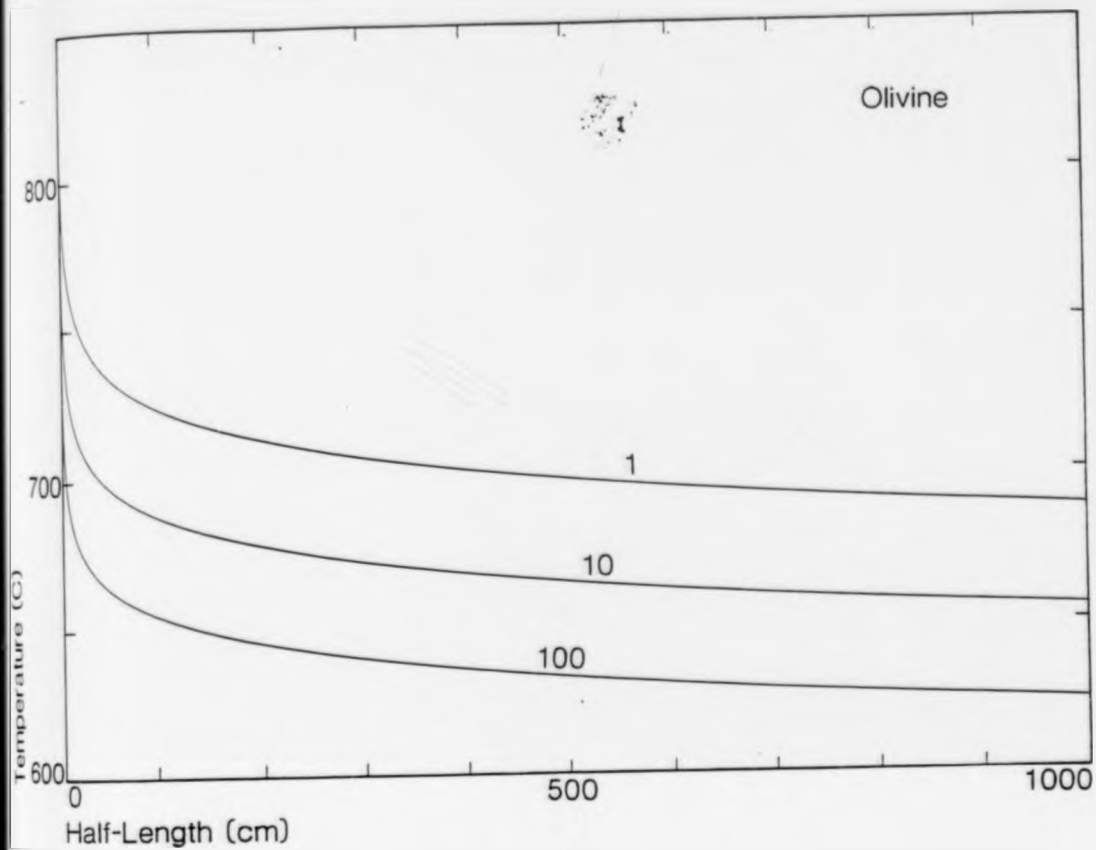


Fig 3.32 Temperature plotted against shear zone half-length for dry olivine, for $R = 1, 10, 100$.

Fig 3.33

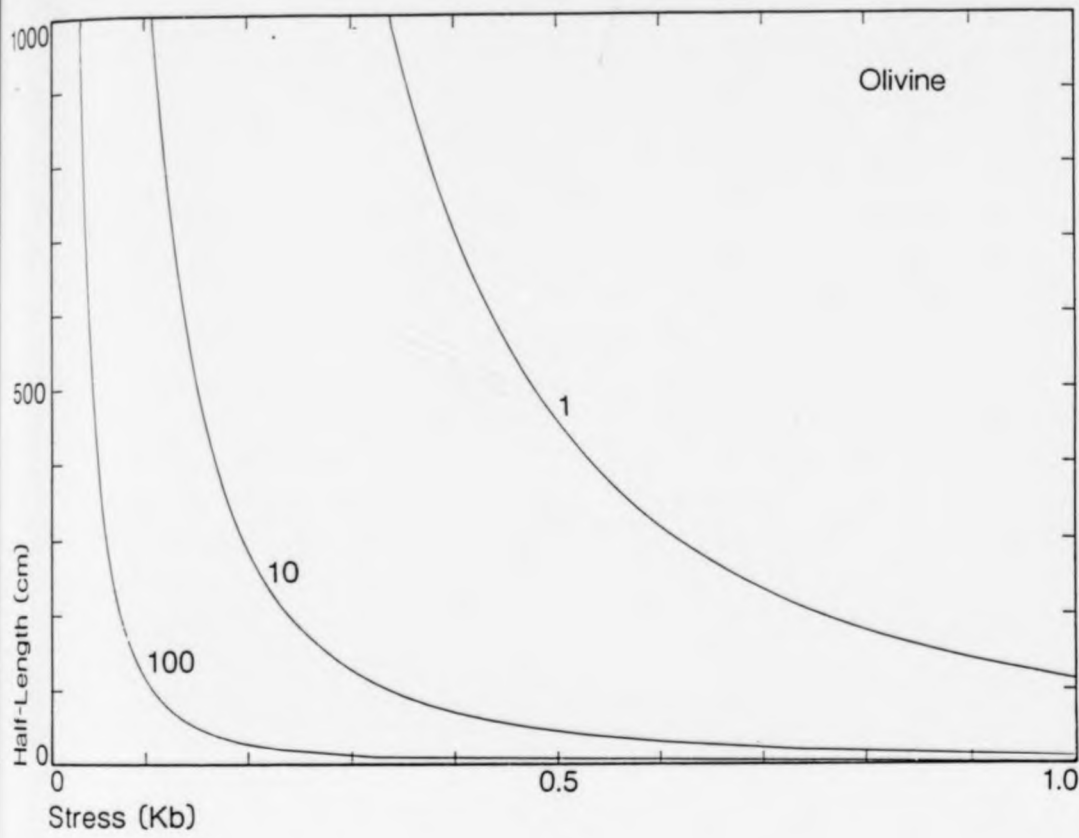


Fig 3.33 Shear zone half-length plotted against applied load stress for dry olivine, for R = 1, 10, 100.

Fig 3.34

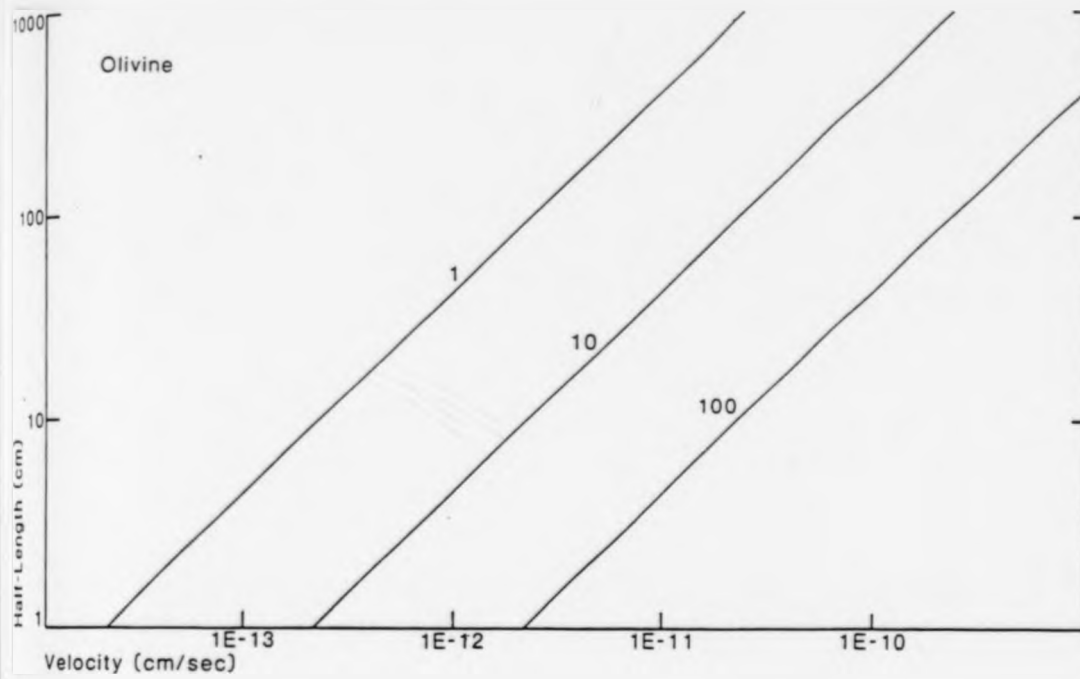


Fig 3.34 Shear zone half-length plotted against propagation velocity for dry olivine, for $R = 1, 10, 100$. ($1E-11 = 1 \times 10^{-11}$)

Fig 3.35

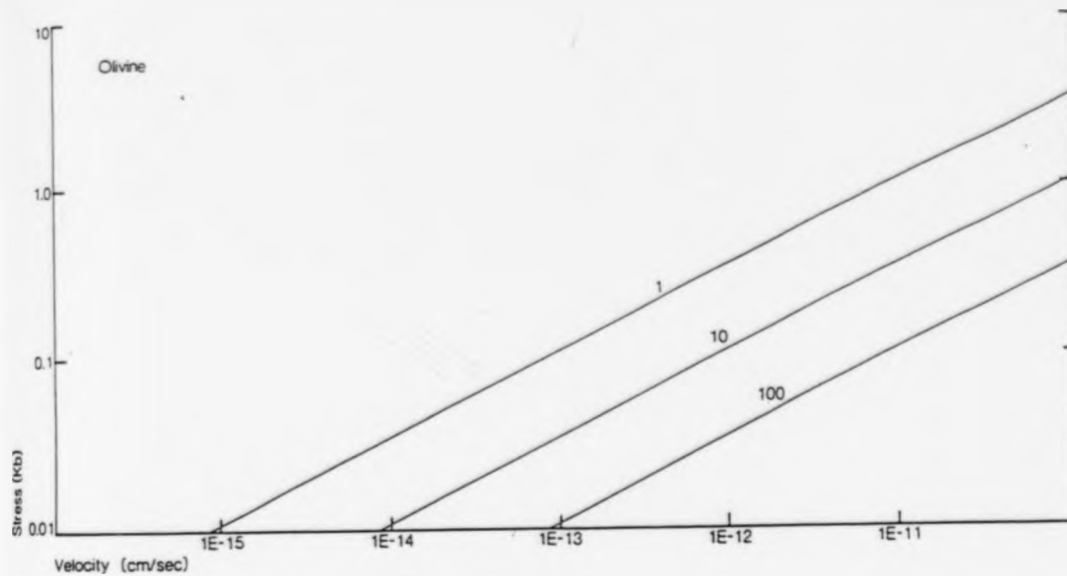


Fig 3.35 Applied load stress plotted against propagation velocity for dry olivine, for R = 1, 10, 100. (1E-11 = 1×10^{-11})

Fig 3.36

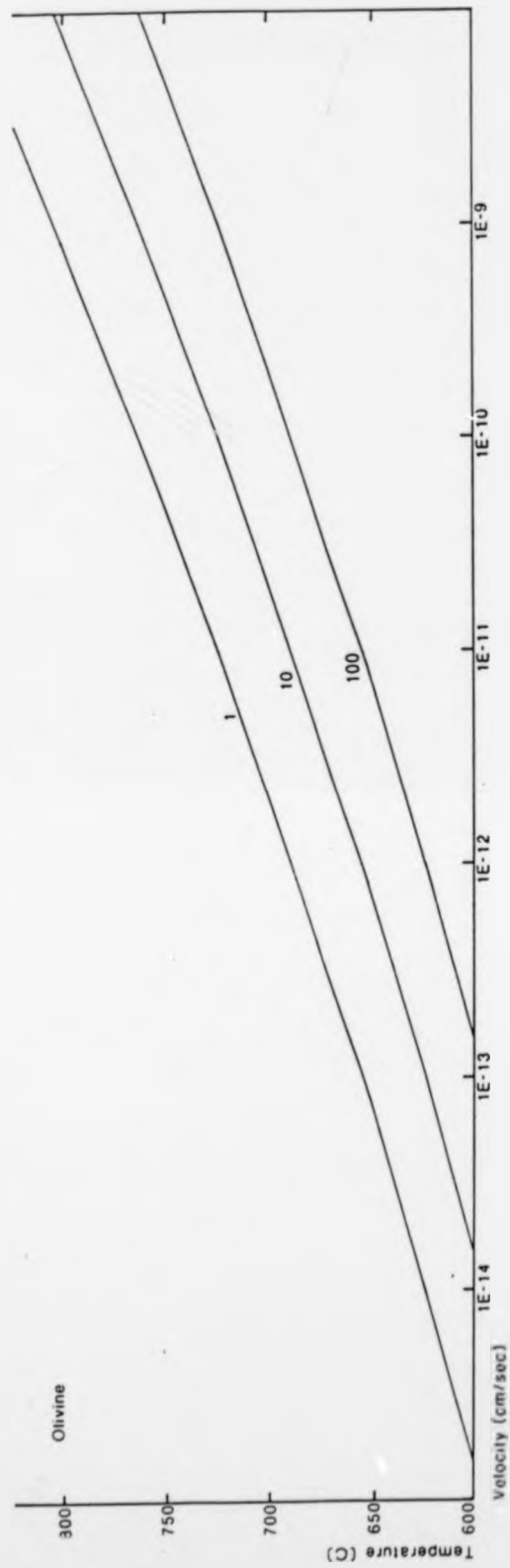


Fig 3.36 Temperature plotted against propagation velocity for dry olivine, for $R = 1, 10, 100$. ($1E-11 = 1 \times 10^{-11}$)

Fig 3.37

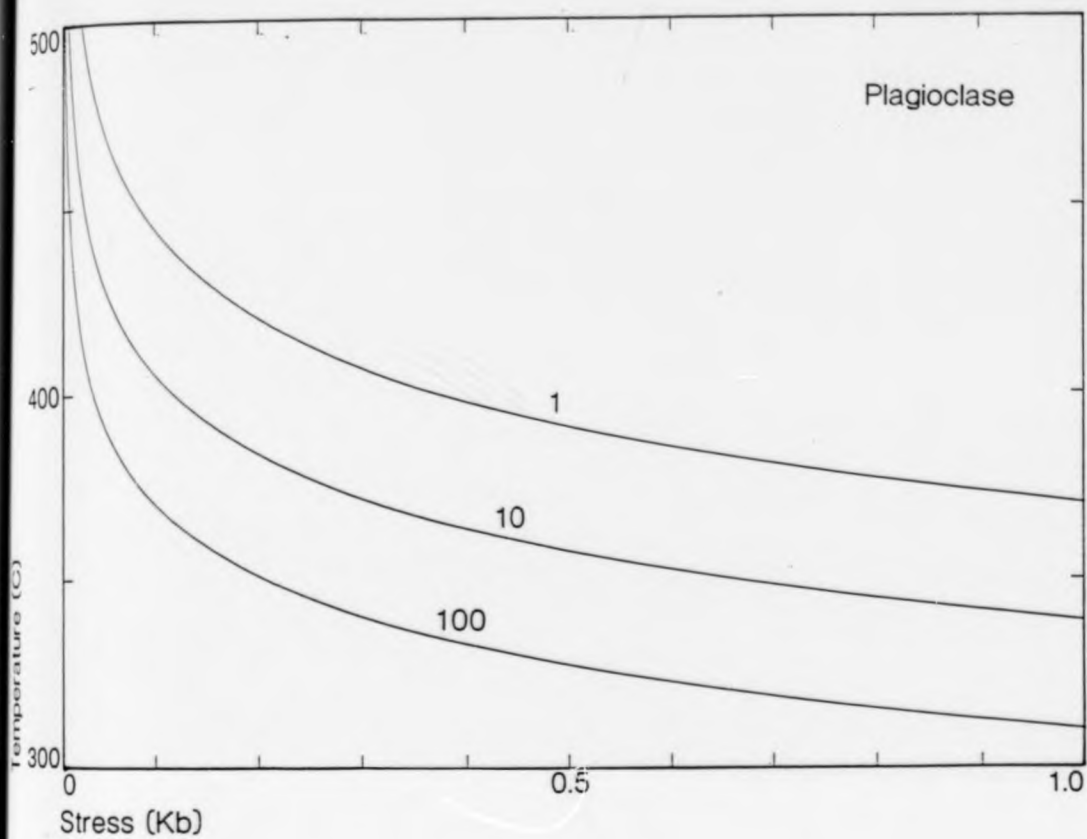


Fig 3.37 Temperature plotted against applied load stress for plagioclase, for $R = 1, 10, 100$.

Fig 3.38

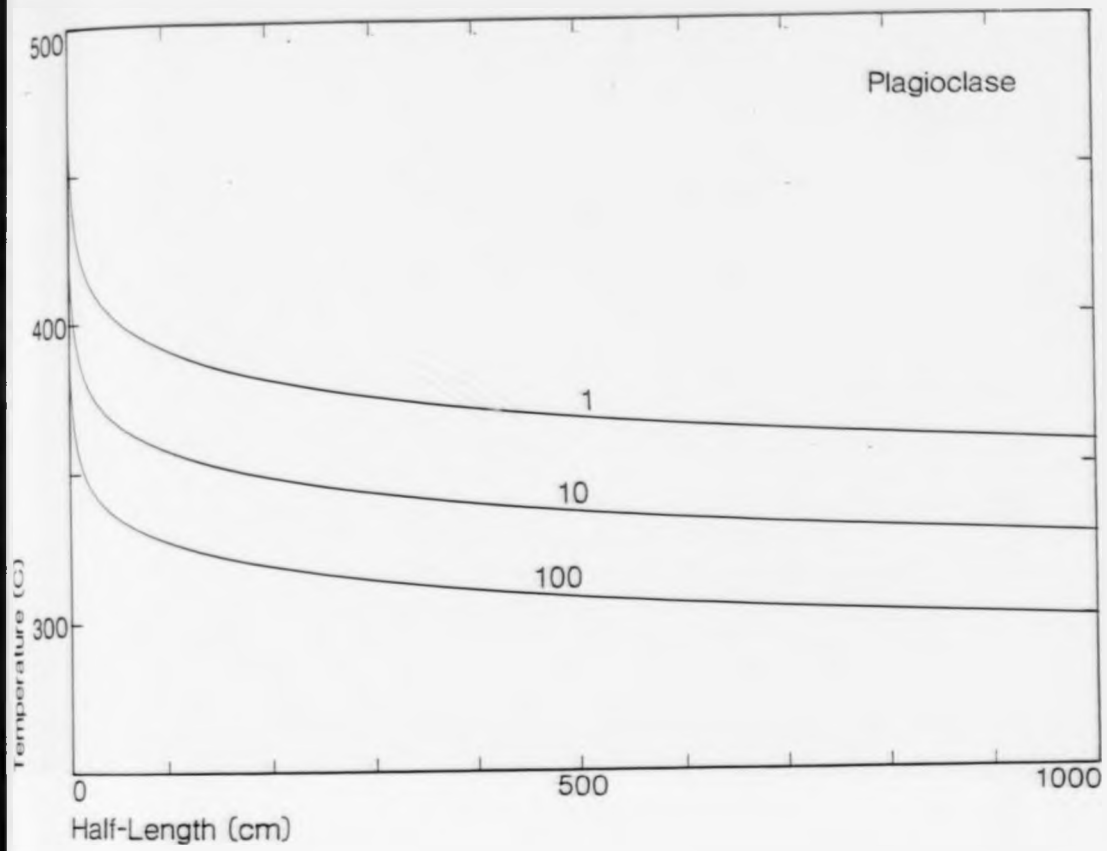


Fig 3.38 Temperature plotted against shear zone half-length for plagioclase, for $R = 1, 10, 100$.

Fig 3.39

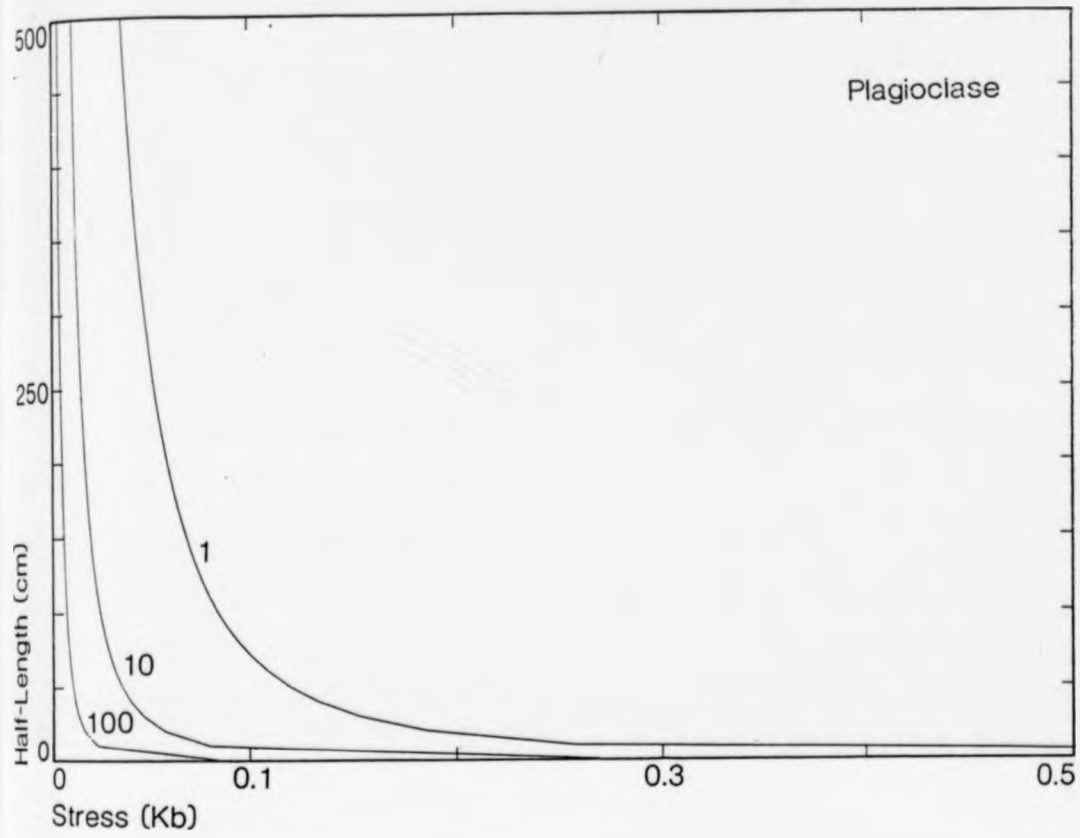


Fig 3.39 Shear zone half-length plotted against applied load stress for plagioclase, R = 1, 10, 100.

Fig 3.40

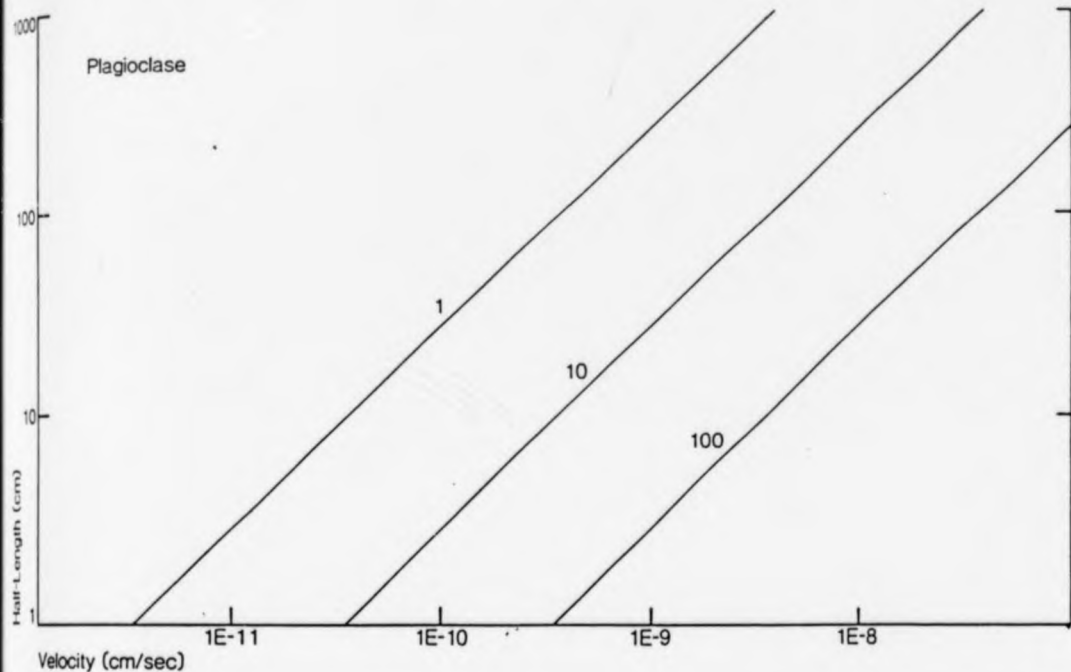


Fig 3.40 Shear zone half-length plotted against propagation velocity for plagioclase, for R = 1, 10, 100. (1E-11 = 1×10^{-11})

Fig 3.41

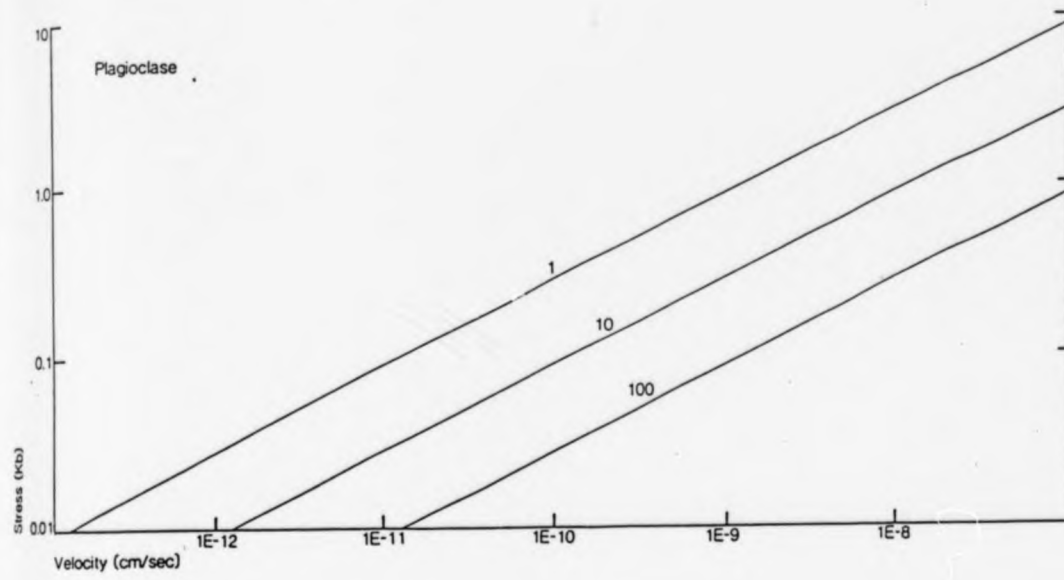


Fig 3.41 Applied load stress plotted against propagation velocity for plagioclase, for $R = 1, 10, 100$. ($1E-11 = 1 \times 10^{-11}$)

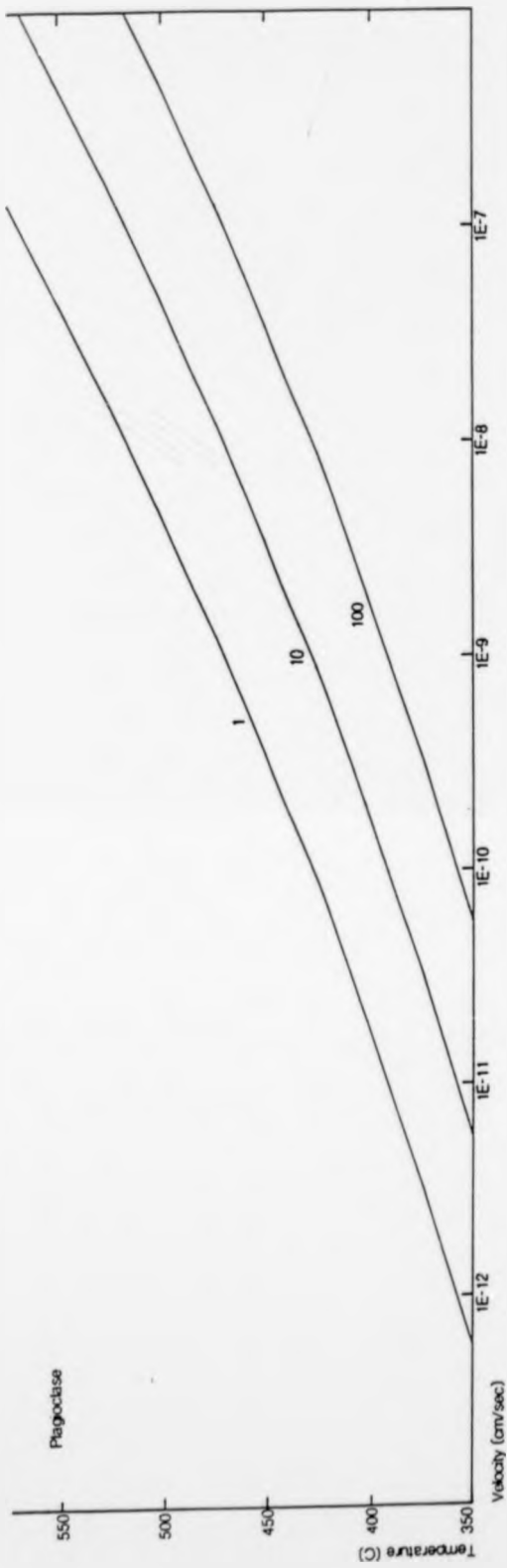


Fig 3.42

Fig 3.42 Temperature plotted against propagation velocity for plagioclase, for $R = 1, 10, 100$. ($1E-11 = 1 \times 10^{-11}$)

Fig 3.43

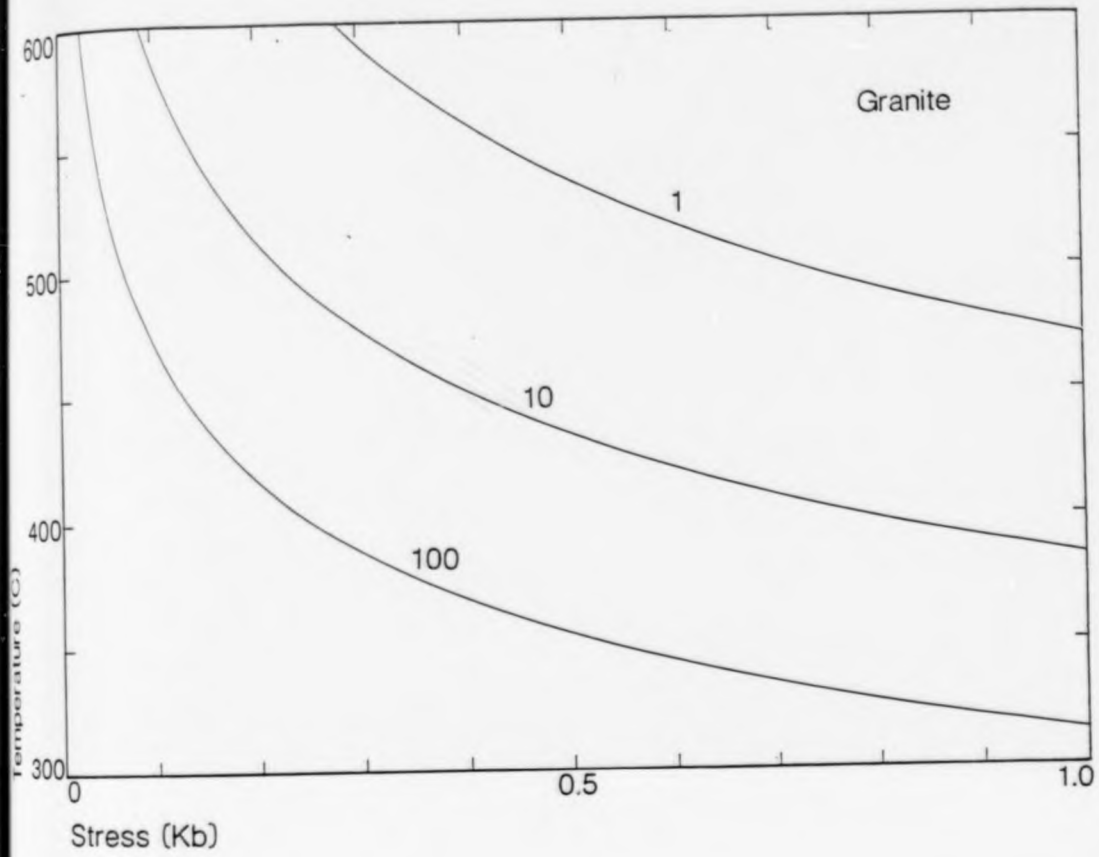


Fig 3.43 Temperature plotted against applied load stress for dry granite, for $R = 1, 10, 100$.

Fig 3.44

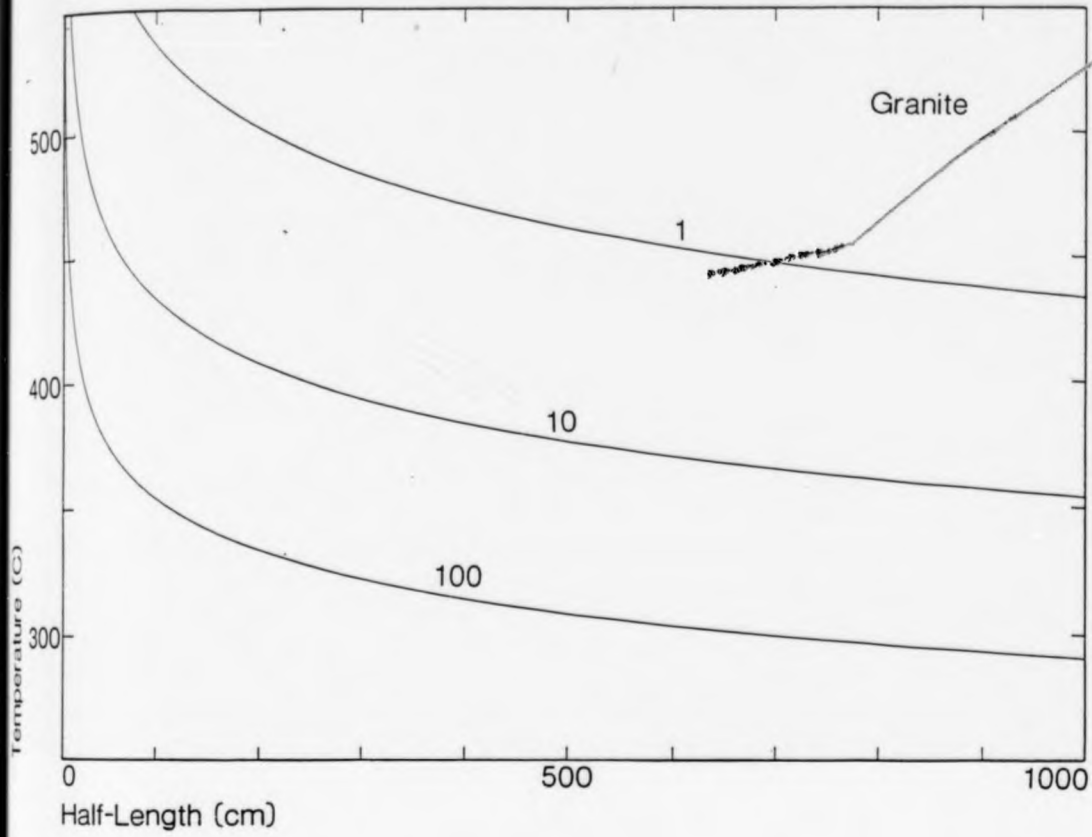


Fig 3.44 Temperature plotted against shear zone-half length for dry granite, for $R = 1, 10, 100$.

Fig 3.45

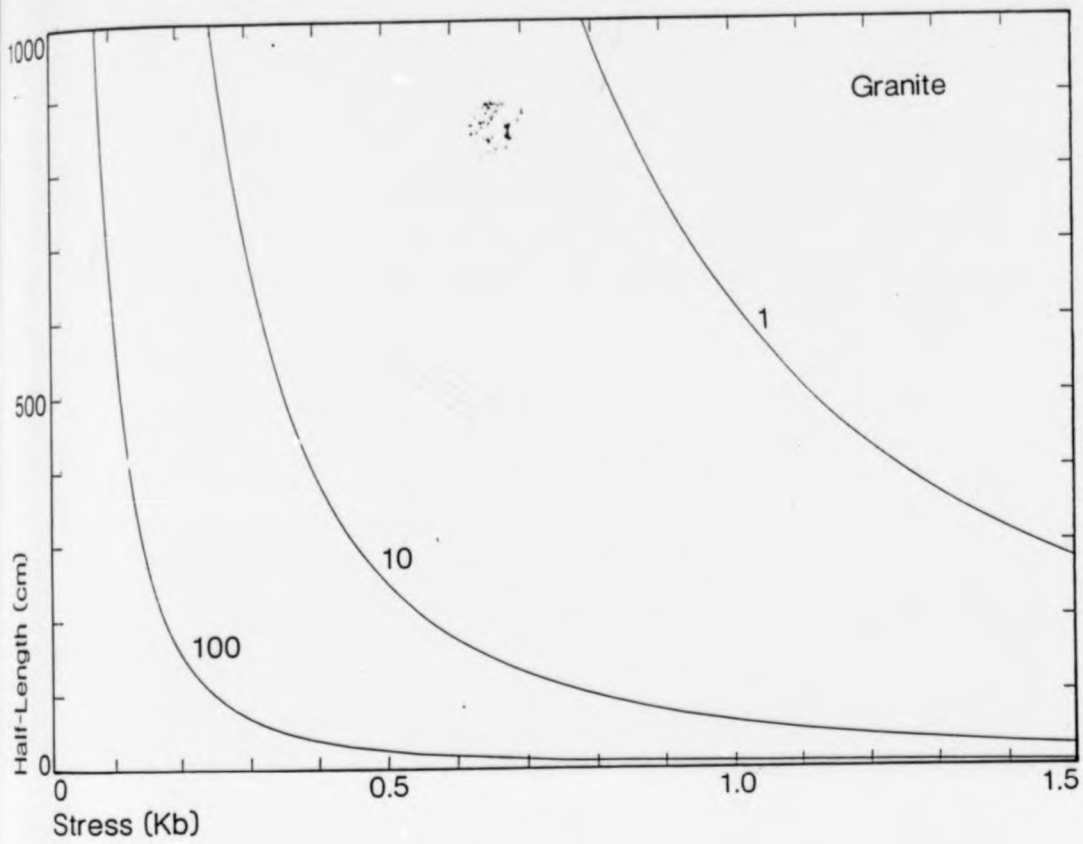


Fig 3.45 Shear zone half-length plotted against applied load stress for dry granite, for $R = 1, 10, 100$.

Fig 3.46

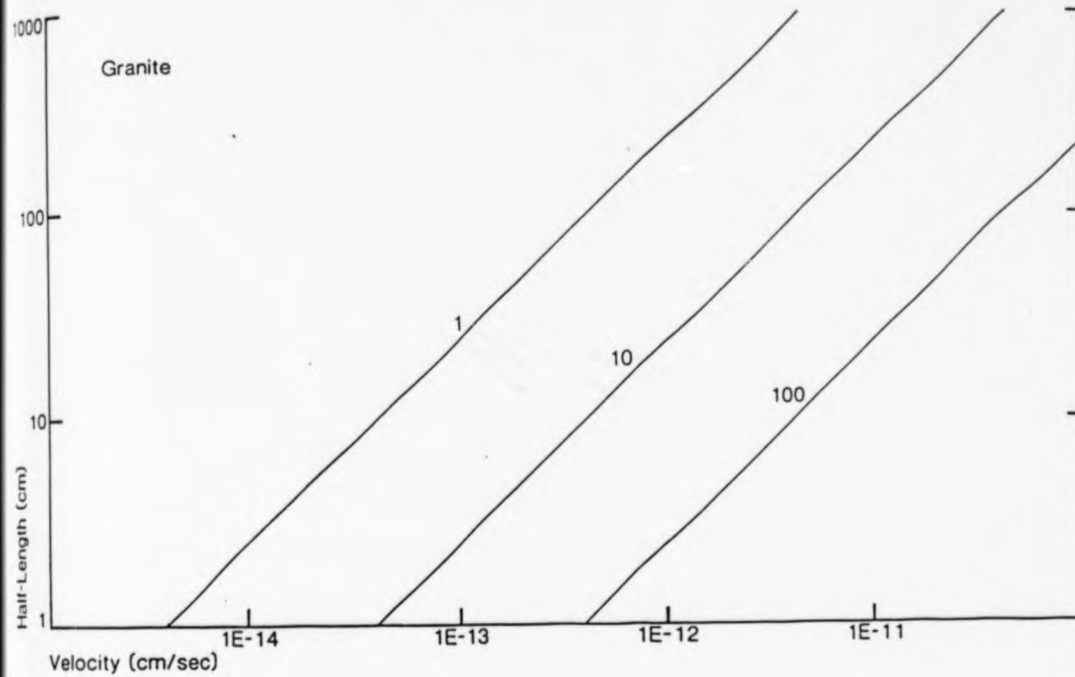


Fig 3.46 Shear zone half-length plotted against propagation velocity for dry granite, for $R = 1, 10, 100$. ($1E-11 = 1 \times 10^{-11}$)

Fig 3.47

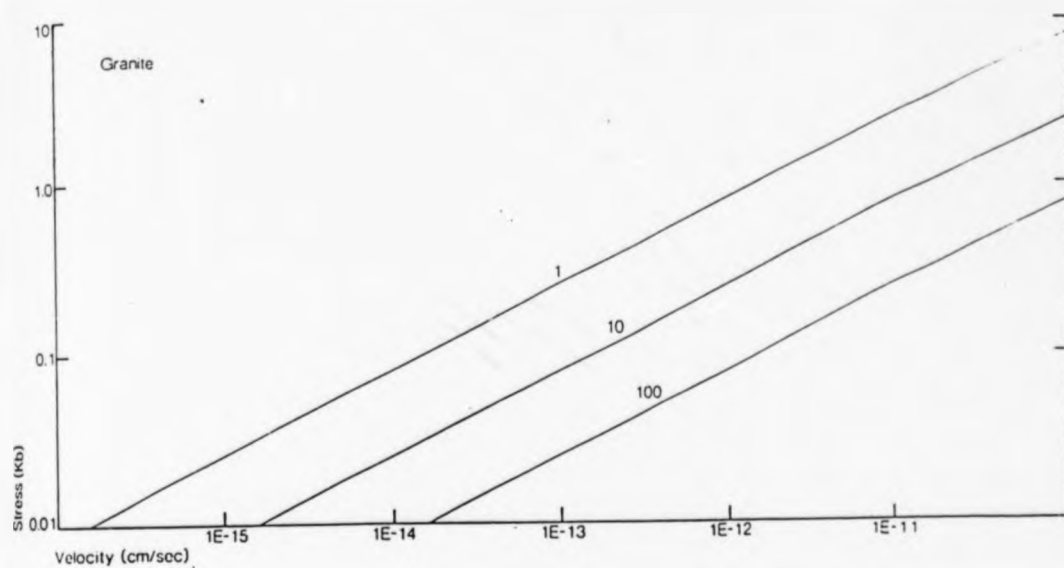


Fig 3.47 Applied load stress plotted against propagation velocity for dry granite, for R = 1, 10, 100. (1E-11 = 1×10^{-11})

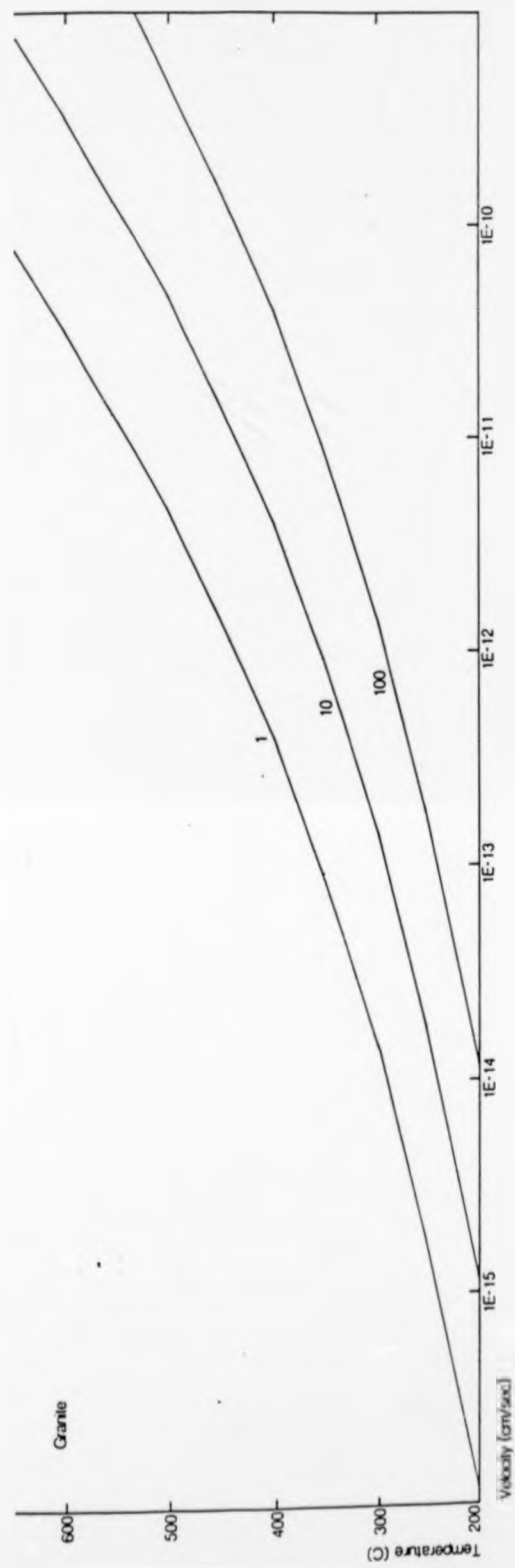


Fig 3.48 Temperature plotted against propagation velocity for dry granite, for $R = 1, 10, 100$. ($1E-11 = 1 \times 10^{-11}$)

TABLE 3.1

STANDARD PARAMETERS USED IN THE INTERRELATIONSHIP EQUATIONS.

Rheology	Temperature C°	Applied load Stress Kb	Shear zone Half-Length cm	Propagation Velocity cm/sec
Dry Quartz <u>Koch et al.</u> (1980)	350	0.5	100	1×10^{-11}
Dry Olivine <u>Bodine et al.</u> (1981)	700	0.5	100	1×10^{-11}
Plagioclase (anorthosite) <u>Shelton &</u> <u>Tullis (1980)</u>	450	0.5	100	1×10^{-11}
Dry Granite <u>Carter et al.</u> (1981)	400	0.5	100	1×10^{-11}

in table 3.1. These values were chosen for a number of reasons, partly through experiment (to find a suitable value for propagation velocity), and partly from previous work and field related studies. The value of 0.5 Kb used for the applied load stress was obtained from Norton (1982) and represents a probable upper limit for geologically available differential stress. The value of 100 cm used for the shear zone half-length was chosen with a view to the fact that the stress field theory requires an infinitely thin "sharp-tipped" crack, and as longer shear zones would have an appreciable width, a low value for half-length was used. The temperature values were based on data from the available literature, and consideration of the melting temperatures of the minerals/rocks. The precise values of these standards are not critical to the argument as the effect of changing them can be seen from the graphs.

The way in which these graphs can be used may be demonstrated by taking fig 3.25 as an example. In this figure the relationship between temperature and load stress for dry quartz is shown. Firstly from the "contoured" values of R it can be seen that shear zone propagation is favoured by higher temperatures. For a given value of stress, R decreases with increasing temperature. Likewise higher stresses will favour shear zone propagation, as has been demonstrated earlier (Figs 3.21 & 3.22). Secondly the general form of the $R = 1$ curve shows that as the stress tends to zero, temperature tends to infinity, so that for very small applied stresses very high temperatures are required for shear zone propagation. With increasing stress however the temperature necessary for propagation has a very limited range for geologically realistic stress values. As the temperature tends to zero the stress tends to infinity reaching a value of 103.5 Kb at 105°C. Under favourable circumstances temperature, half-length and local applied stress at naturally

occurring shear zones can be measured. The real value of this model is its ability to predict the propagation velocity of a shear zone, given the half-length, load stress and temperature conditions, using figures 3.28 - 3.30 etc. For example figure 3.28 shows that a shear zone of 10 cm half-length can propagate at up to 2.65×10^{-11} cm/sec whereas a zone of 100 cm half-length can propagate at 2.45×10^{-10} cm/sec, for an applied stress of 0.5 Kb and at a temperature of 350°C . So in general smaller shear zones cannot propagate as fast as large shear zones. The effect of temperature on the propagation velocity is particularly marked. Raising the temperature by only 50°C can result in an increase in the possible propagation velocity of several orders of magnitude.

The effect of the rheological constants used in equations 3.38 - 3.40 is shown in figures 3.49 - 3.51. These show the temperature, load stress and half-length values necessary for shear zone propagation in dry quartz, plagioclase and granite. The lines drawn are all for $R = 1$ to clarify the relationship between the various rheologies. Figure 3.51 illustrates the type of relationship that can be obtained. Here the combinations of shear zone half-length and applied load stress necessary for continued shear zone propagation are shown for quartz, plagioclase and granite. A standard temperature of 400°C is used and a propagation velocity of 1×10^{-11} cm/sec. Assuming an available load stress of 0.5 Kb shear zones in quartz are able to propagate even for very low half-lengths, whereas in a plagioclase rheology, shear zones of less than 57 cm long will be unable to propagate. Continued propagation of shear zones in granite will only be possible for very large zones under these conditions. From figures 3.49 - 3.51 granite appears to resist shear zone propagation to a greater degree than two of its main constituent minerals, quartz and plagioclase. This may be due to different

Fig 3.49

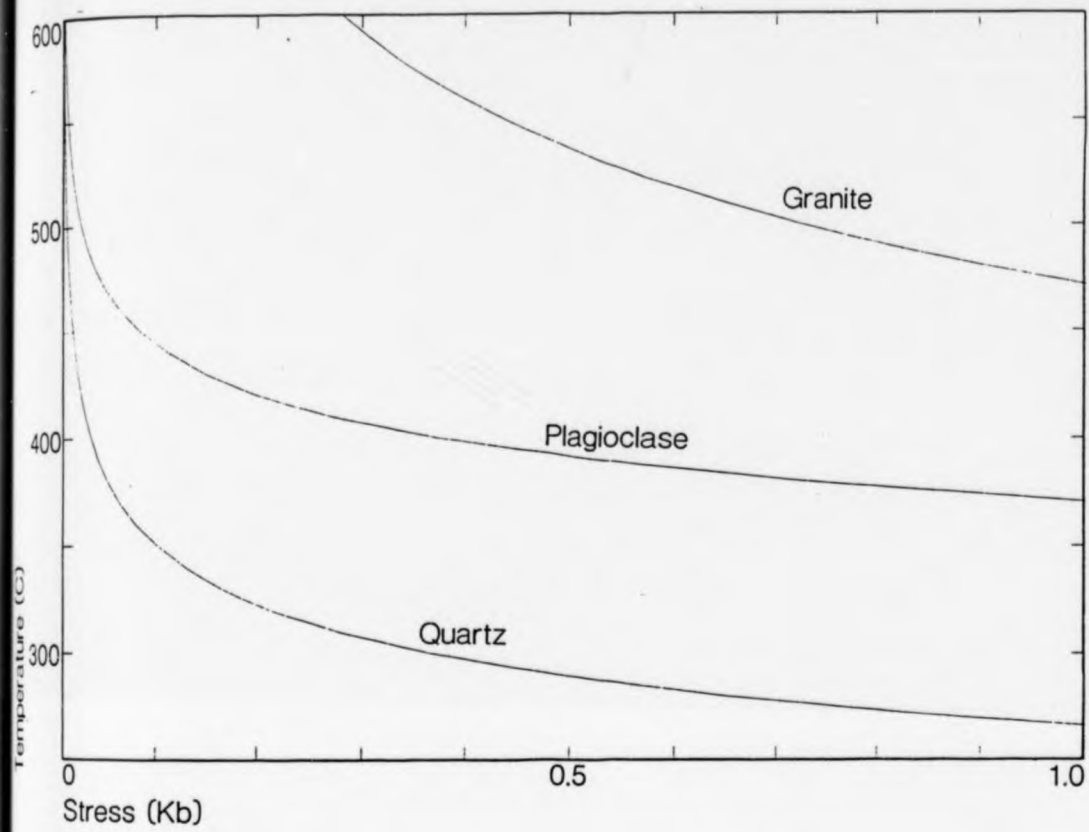


Fig 3.49 Temperature plotted against applied load stress for dry quartz, plagioclase and dry granite, $R = 1$ for each rheology.

Fig 3.50

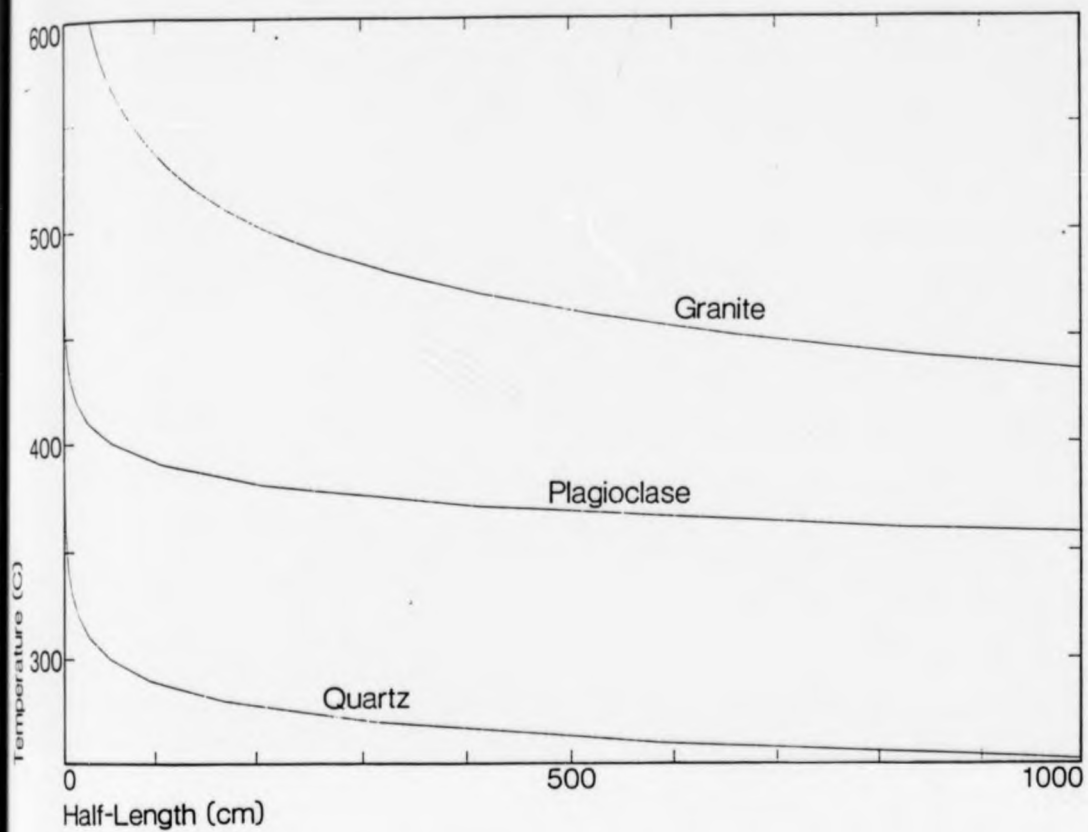


Fig 3.50 Temperature plotted against shear zone half-length for dry quartz, plagioclase and dry granite, $R = 1$ for each rheology.

Fig 3.51

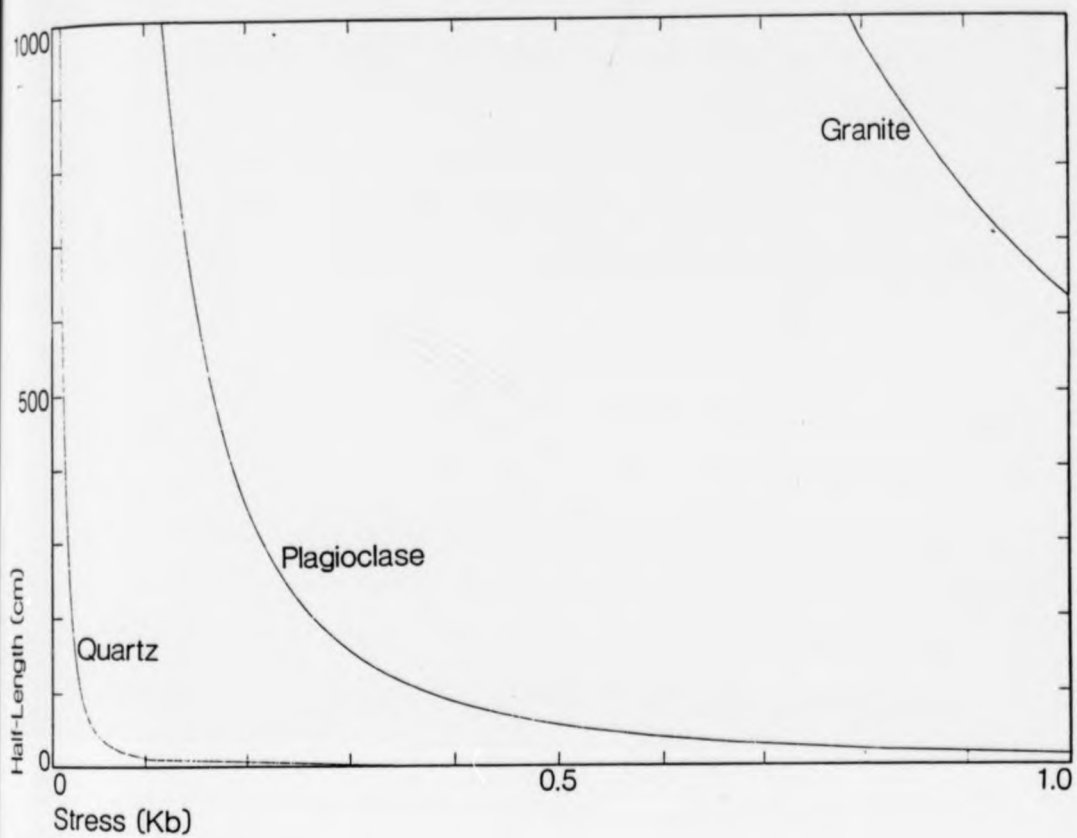


Fig 3.51 Shear zone half-length plotted against applied load stress for dry quartz, plagioclase and dry granite, $R = 1$ for each rheology and a standard temperature of 400°C .

experimental techniques used to obtain the values for the flow law , as the apparent relative strength of granite is surprising.

3.III.2 Discussion and conclusions.

The results obtained using equations 3.38 - 3.40 as represented in figures 3.25 - 3.51 are geologically realistic and hence support the approach used in the model. The ability to quantify the relationships between temperature, load stress, half-length and propagation velocity is a necessary step in the understanding of shear zone processes. The range of conditions that will favour shear zone development can now be identified and, most significantly, estimates of the propagation velocity may be obtained. The prediction that shear zones will not develop or propagate in materials with an n value of less than 3 is supported by observations from the study of polycrystalline metals, where materials with a higher n value will localize deformation more easily. The fact that several common geological materials do have an n value of less than 3 e.g. wet quartz ($n = 2.44$ Koch et al. 1980) and yet contain shear zones, does not invalidate the model. In such cases the deformation may have been accommodated by means other than dislocation creep, and strain softening effects may also have aided localization of the deformation.

The use of the interrelationship equations 3.38 - 3.40 is necessarily confined to materials with an n value of approximately 3, due to the need to obtain a single value for the dimensionless ratio (R_d). Although most geological materials do fit this criterion (see table 1.1) the restriction must be remembered when using the model.

The model is necessarily dependent for its accuracy on the published experimental data for the rheological constants, and as can be seen from table 1.1 there are considerable differences between authors, probably due to different experimental conditions. For

geological materials however it is almost impossible to define accurately a single number for any of the material constants, especially for polymineralic samples.

CHAPTER 4

4.1 DEVELOPMENT OF THE MODEL

4.1.1 Introduction.

In Chapter 3 the crack tip analogy model is used to predict the possible sets of conditions that will favour shear zone development and propagation. The interrelationships between the boundary conditions to the system have been quantified and estimates of propagation velocity may be obtained. To apply the results from Chapter 3 to naturally occurring shear zones, reliable estimates of ambient temperature and applied load stress are required, and these are difficult to establish in the majority of cases. In order to make the model more applicable to natural examples, parameters that can be measured in the field such as strain distribution and displacement must be incorporated into the model. These will provide further control on the range of acceptable values for the less well constrained boundary conditions such as temperature and load stress.

4.1.2 Strain distribution.

4.1.2.a Initial theory.

For the majority of real shear zones an estimate of the maximum shear strain (γ) may be obtained by a variety of methods, and strain profiles across the zone may be calculated.

From equation 3.3

$$\sigma_{xy} = \sigma_L (C/2x)^{1/2} f_{xy}(\phi) \quad (4.1)$$

This expression for σ_{xy} may then be substituted into equation 3.20 to give an expression for the shear strain γ (ϵ_{xy}).

$$\gamma = \int_x^\infty A \exp(-Q/RT) \sigma_L^n (C/2x)^{n/2} f_{xy}^n(\phi) 1/V dx \quad (4.2)$$

rearranging

$$\gamma = 1/V A \exp(-Q/RT) \sigma_L^n (C/2)^{n/2} \int_x^\infty x^{-n/2} f_{xy}^n(\phi) dx \quad (4.3)$$

Thus the shear strain at any point may be calculated. This enables a map of the distribution of γ around a shear zone tip to be constructed (Fig 4.1). In this figure, and all following figures drawn from the model, the flat top to the strain profile is artificial and has been constructed to eliminate the effect of the mathematical singularity at the shear zone tip, as this would lead to strains of $\gamma = \infty$ along the shear zone.

4.1.2.b The effect of the boundary conditions.

To demonstrate the changes in strain that result from changes in the boundary conditions, a series of profiles have been constructed (Figs 4.2 - 4.5). These profiles are drawn at a point one quarter of the total shear zone length away from the tip, so that the effect of changing the shear zone length may be examined. The standards used for the boundary conditions are $T = 350^\circ\text{C}$, $\sigma_L = 0.5 \text{ Kb}$, $C = 100 \text{ cm}$ and $V = 1 \times 10^{-11} \text{ cm/sec}$. The profiles shown in figures 4.2 - 4.5 show that the strain profile will increase in amplitude and broaden with increasing

Fig 4.1

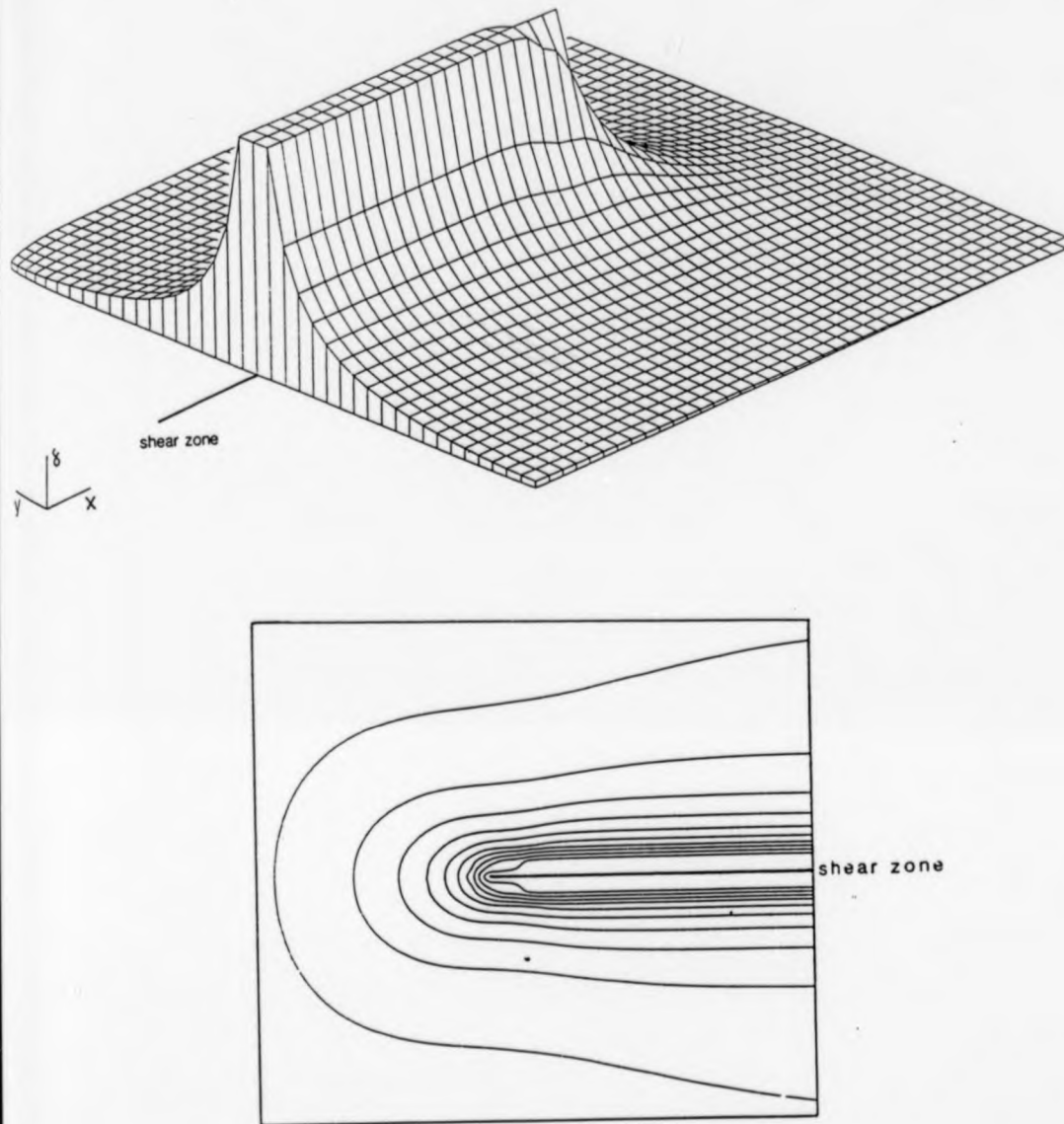


Fig 4.1 Generalized surface view and contour map for the distribution of γ around a propagating shear zone tip.

Fig 4.2

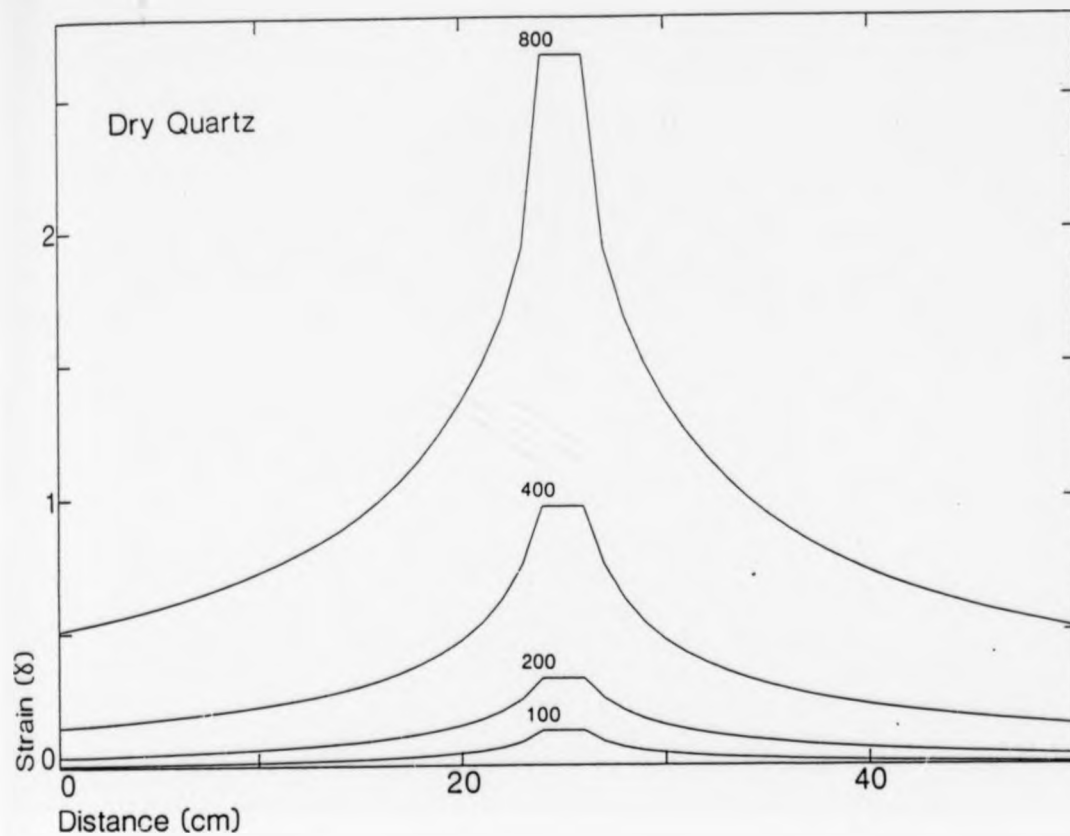


Fig 4.2 Strain profiles for a shear zone in dry quartz for shear zone half-lengths of 100 cm, 200 cm, 400 cm and 800 cm.

Fig 4.3

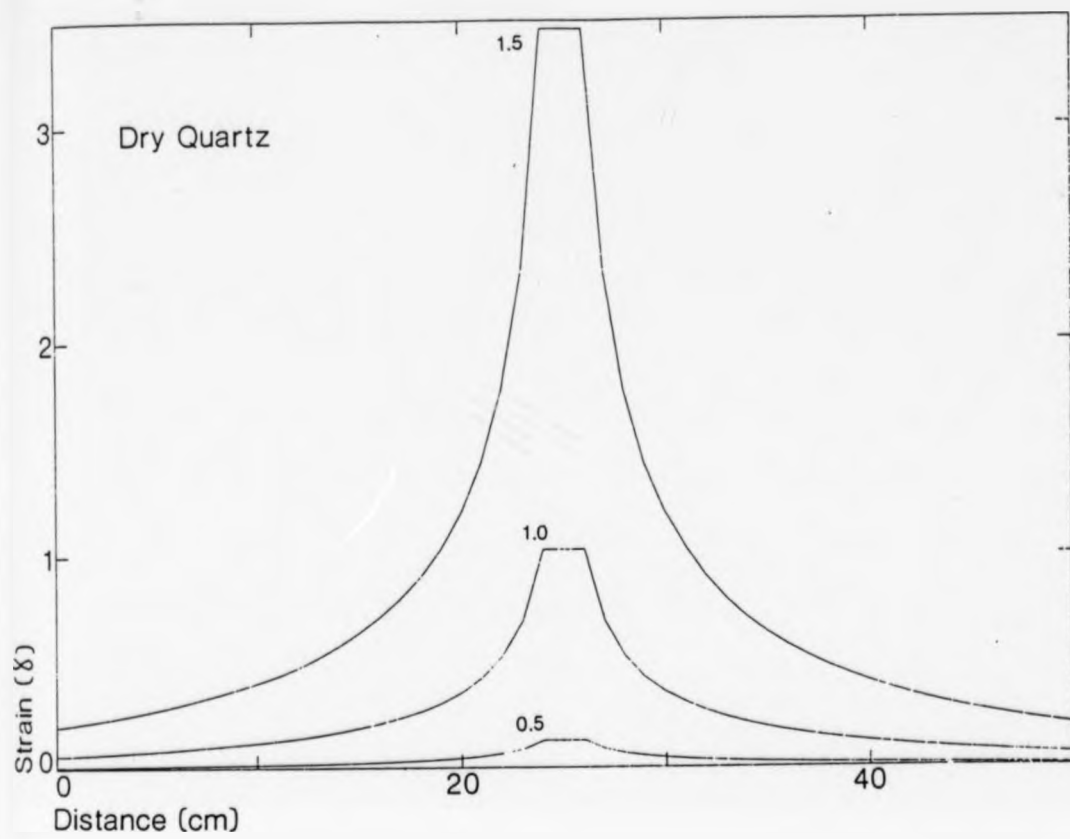


Fig 4.3 Strain profiles for a shear zone in dry quartz for applied load stresses of 0.5 Kb, 1.0 Kb and 1.5 Kb.

Fig 4.4

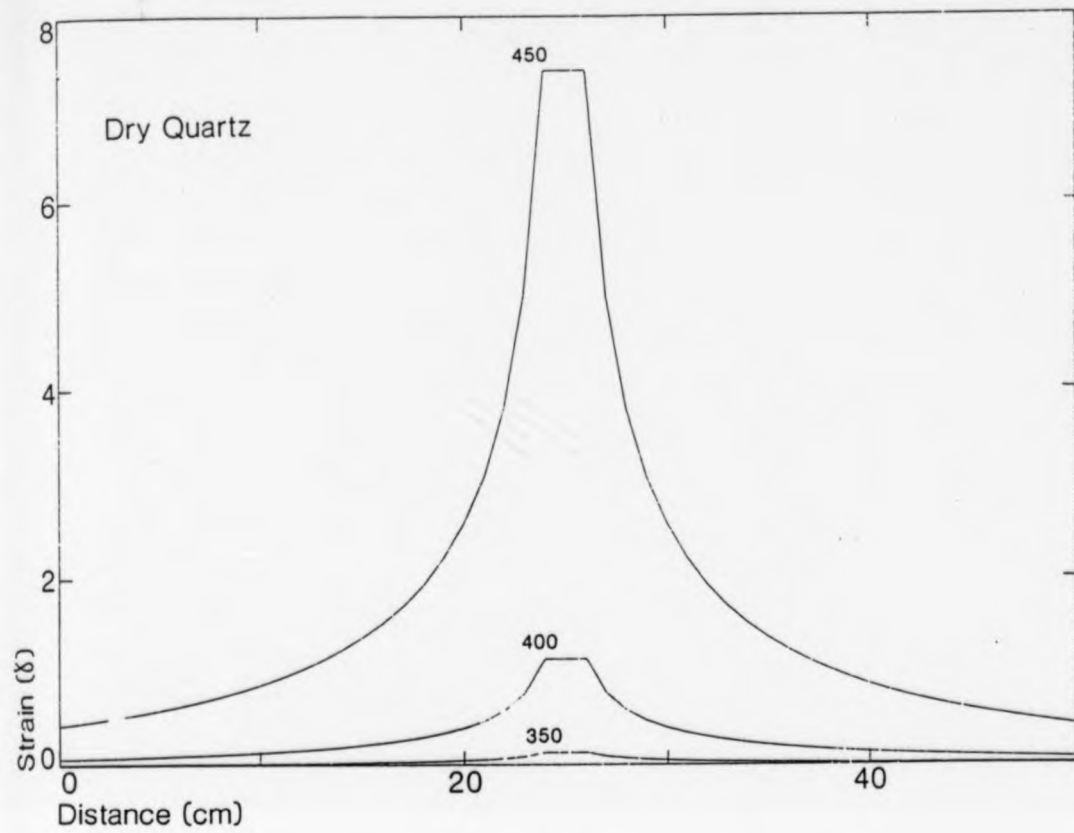


Fig 4.4 Strain profiles for a shear zone in dry quartz at temperatures of 350°C, 400°C and 450°C.

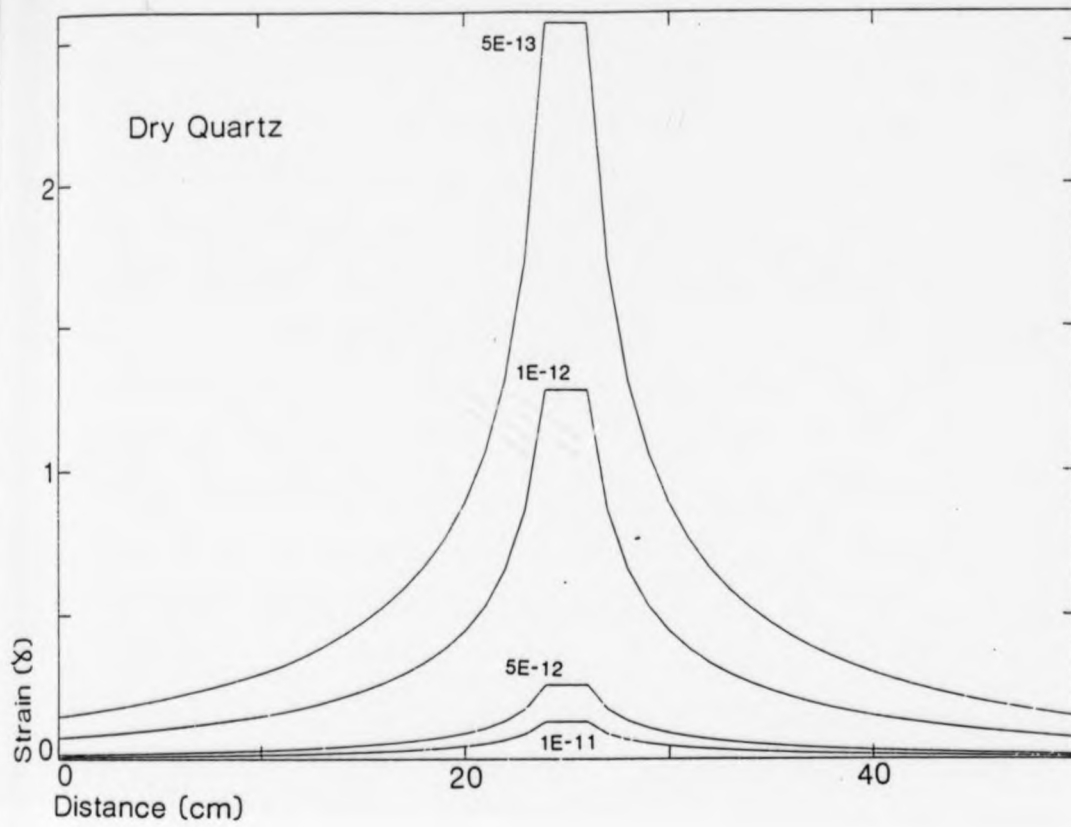


Fig 4.5 Strain profiles for a shear zone in dry quartz for propagation velocities of 1×10^{-11} cm/sec, 5×10^{-12} cm/sec, 1×10^{-12} cm/sec and 5×10^{-13} cm/sec.

half-length, load stress and temperature, and with decreasing propagation velocity. As shown in Chapter 3, temperature has a particularly strong influence on the shear zone, an increase of only 50°C giving an increase in peak strain of 7% (Fig 4.2). The inverse relationship between peak strain and propagation velocity may be explained by the energy balance of the system. Since only a finite amount of energy is available, a balance must be maintained between the energy used to propagate the shear zone and that used to deform the surrounding rock. An increase in applied load stress increases the amount of energy available to the system and hence if the propagation rate remains constant the peak strain may increase. An increase in temperature will allow the rock to deform more easily and so the strain may increase without any change in applied stress. The stress available to produce strain at any point is a function of the shear zone half-length, and so an increase in half-length will increase the strain at any given point. The prediction that strain at a point will increase as the shear zone lengthens, leads to the conclusion that as the shear zone grows the strain profile should change, and this would result in an evolution of the strain profile along the length of the shear zone. As natural examples of shear zones have a relatively constant strain profile along their length, then the possible increase in total strain with increasing length must be balanced by an increase in the propagation velocity. Therefore the model predicts that as shear zones grow their propagation rate increases. This relationship may be quantified by using a reference point fixed relative to the shear zone tip, with a calculated shear strain that remains constant as the half-length is changed.

From equation 4.3

$$\gamma = 1/V (C/2)^{n/2} F \quad (4.4)$$

Where F is a constant for a fixed point with constant γ .

Incorporating γ into the constant which becomes F1

$$V = F1 (C/2)^{n/2} \quad (4.5)$$

The constant F1 can be evaluated if all other parameters remain fixed.

The effect on the propagation velocity of varying the half-length may now be calculated. The results are shown in figure 4.6 which is constructed for a range of values of shear strain; this shows the amount by which the propagation velocity must increase in order to maintain a constant strain profile as the shear zone length increases.

4.1.2.c The effect of rheological change.

Figure 4.7 shows the effect of changing the rheology of the deforming material. In order to produce a strain profile of similar dimensions plagioclase requires a higher temperature than quartz, or alternatively a longer shear zone, higher applied stress or a lower propagation velocity. Thus, if the boundary conditions remain fixed, the model predicts that a shear zone crossing a lithological boundary from a quartzite to a dunite, for example, would narrow markedly and show a considerable decrease in total strain. As the displacement on a shear zone may be calculated from the area under the strain profile graph (Ramsay & Graham 1970), the model then predicts that as a shear zone crosses a lithological boundary, the amount of displacement on that zone will change, assuming all the other boundary conditions

Fig 4.6

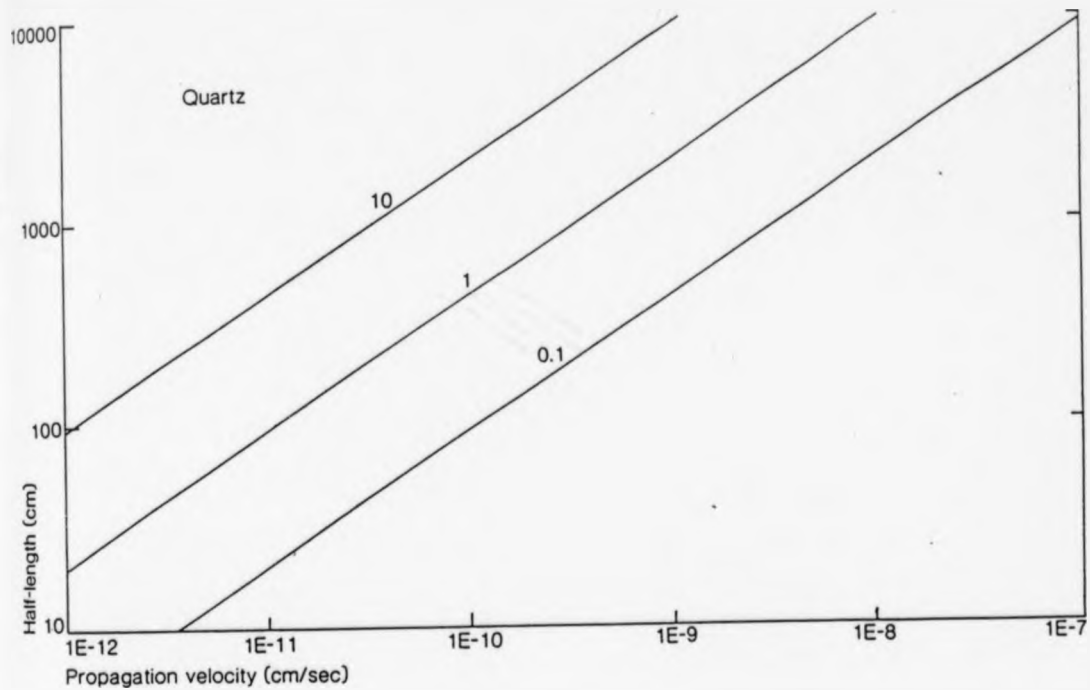


fig 4.6 The variation of propagation velocity with increasing shear zone length for a shear zone in dry quartz, contoured for values of γ ($T = 400^{\circ}\text{C}$, $\sigma_L = 0.5 \text{ Kb}$).

Fig 4.7

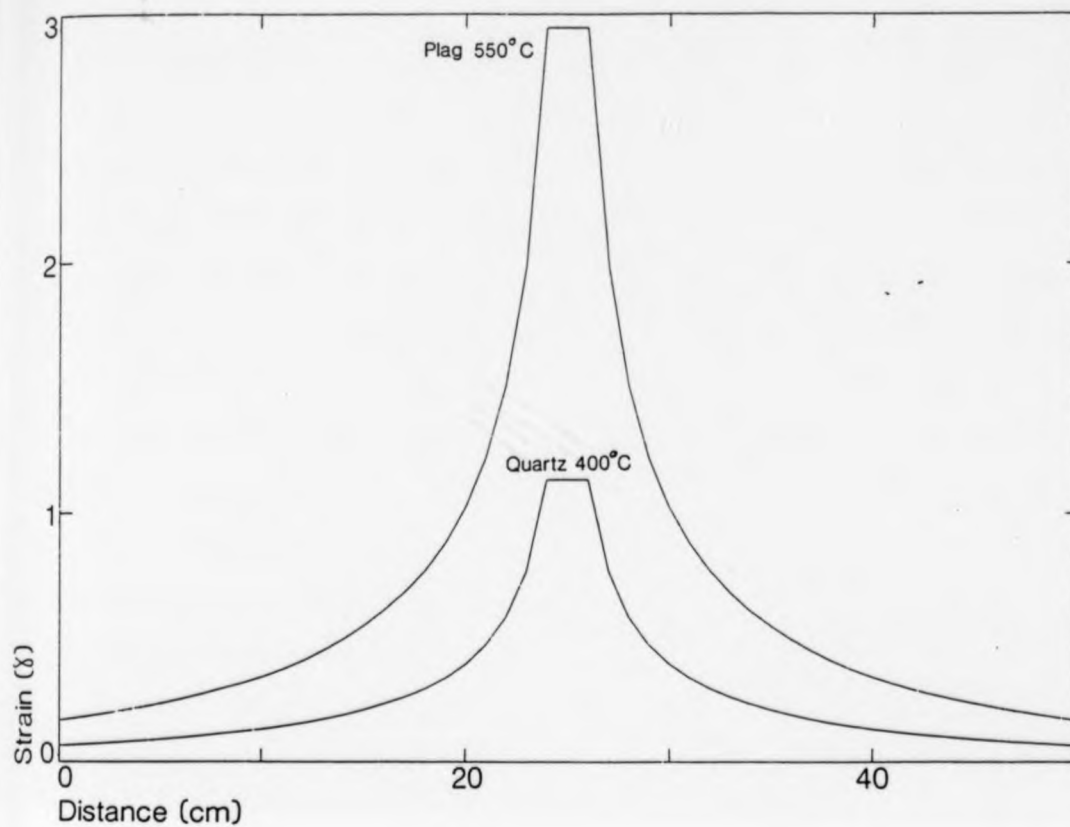


Fig 4.7 Comparison of profiles for shear zones in plagioclase and quartz showing the higher temperature required for a shear zone in plagioclase to produce a profile of similar magnitude to that in quartz, all other parameters remaining constant.

remain constant. It is possible that the displacement could change across a boundary, but this change would be accommodated over a considerable length of the shear zone. It is also possible that the style and mechanism of deformation may change across such a boundary in a way not accounted for by the model. In the extreme case of a zone crossing from a quartzite to a dunite there could be a change from a wide ductile shear zone in the quartzite to a narrow brittle or brittle-ductile shear zone in the dunite. Such a change in deformation mechanism is outside the scope of this model.

Both the above explanations require that all the boundary conditions are kept constant across the lithological boundary; a more physically realistic solution is that the propagation velocity of the shear zone changes allowing continuity of displacement across the boundary. Thus the propagation velocity of a shear zone crossing from quartzite to dunite would need to decrease from 1×10^{-11} cm/sec in the quartzite to 0.225×10^{-19} cm/sec in the dunite in order to maintain the same displacement ($T = 650^\circ\text{C}$, $\sigma_L = 0.5 \text{ Kb}$, $C = 20 \text{ cm}$).

4.1.2.d Theoretical foliation orientations.

Once the shear strain distribution around the shear zone tip has been calculated, the theoretical foliation orientations can be plotted.

$$\tan 2\theta' = 2/\delta \quad (4.6)$$

Where θ' is the angle of the foliation relative to the shear zone (Ramsay & Graham 1970).

Figures 4.8 & 4.9 show plots of the theoretical foliation orientations for shear zones in quartz at 350°C and 400°C ($\sigma_L = 0.5$, $V = 1 \times 10^{-11}$ cm/sec, $C = 20$ cm). This again demonstrates the widening of the shear zone with increasing temperature, although the same effect could be obtained by increasing the shear zone length, increasing the load stress or decreasing the propagation velocity.

4.1.3 Displacement fields.

4.1.3.a Initial theory and assumptions.

The displacement field around a shear zone can be calculated by integrating the shear strains along a path perpendicular to the shear zone at any point along its length, thus calculating the area under the strain profile curve.

$$S = \int_0^y \gamma \, dy' \quad (4.7)$$

Where S is the displacement (Ramsay & Graham 1970).

Substituting from equation 4.3 for γ ;

$$S = \int_0^y \left[1/V A \exp(-Q/RT) \sigma_L^n (C/2)^{n/2} \int_x^\infty x^{-n/2} f_{xy}^n(\phi) \, dx \right] dy' \quad (4.8)$$

Taking the constants out of the integral;

$$S = 1/V A \exp(-Q/RT) \sigma_L^n (C/2)^{n/2} \int_0^y \int_x^\infty x^{-n/2} f_{xy}^n(\phi) \, dx \, dy' \quad (4.9)$$

Fig 4.8

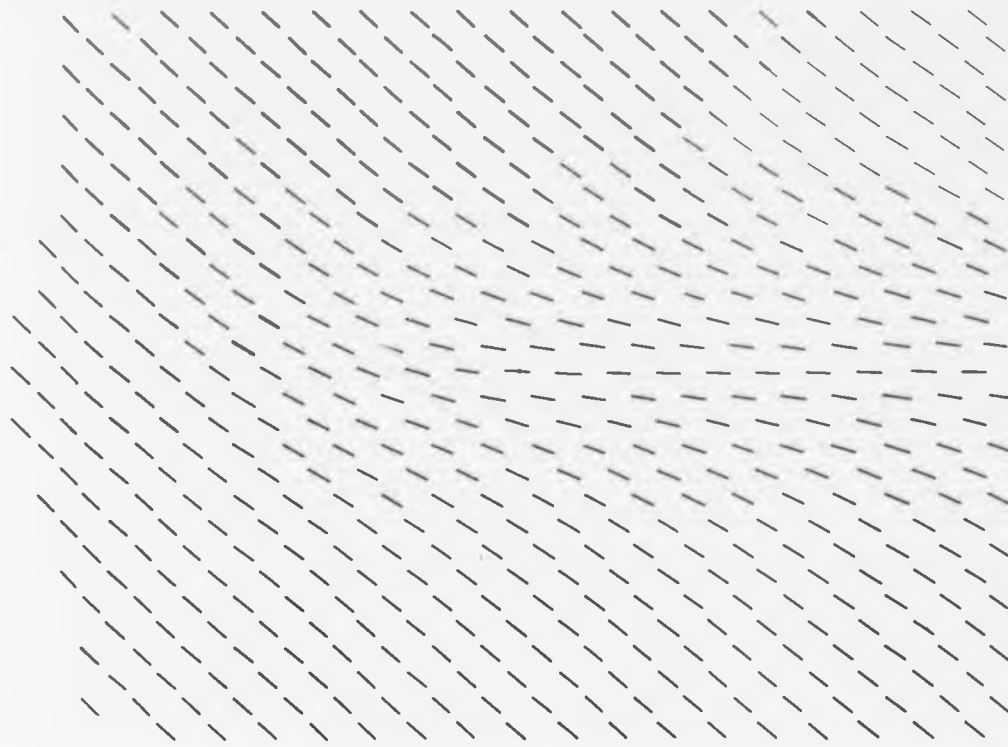


Fig 4.8 Theoretical foliation orientations around a propagating shear zone tip in quartz at 350°C ($C = 100$ cm, $\sigma_L = 0.5$ Kb and $V = 1 \times 10^{-11}$ cm/sec).

Fig 4.9

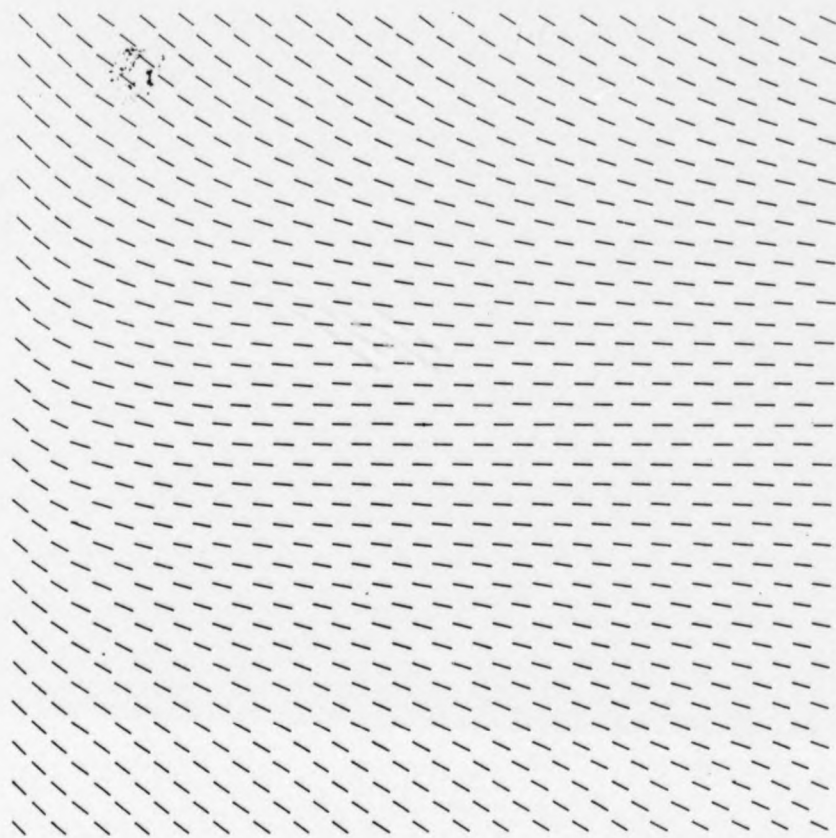


Fig 4.9 Theoretical foliation orientations around a propagating shear zone tip in quartz at 400°C, drawn to the same scale as figure 4.8 ($C = 100$ cm, $\sigma_L = 0.5$ Kb and $V = 1 \times 10^{-11}$ cm/sec).

For the purposes of this model, zero displacement is assumed to take place on an infinitely thin line along the centre of the shear zone. Thus one side of the zone will have a positive displacement and the other an equal, but negative, displacement. The integration is done along paths going outwards from the centre of the zone towards the margins thus avoiding the problem of integrating across the line behind the mathematical singularity at the tip.

Figures 4.10 - 4.12 show the displacement field in both contour and surface views highlighting the symmetry of the field. This approach to the integration predicts that the displacement increases away from the shear zone to infinity; this is acceptable if the deformation along the shear zone is controlled by the need to accommodate a remote displacement, as is usual in nature. If the deformation on the shear zone is purely stress controlled and there is no net displacement of the walls at a finite distance from the zone, then the displacement must decay to zero away from a peak close to the zone. This would be accommodated by small strains in the host rock and is necessary to maintain continuity around the isolated shear zone. Figure 4.13 is a hypothetical model of the displacement field around such an isolated stress-controlled shear zone.

4.1.3.b The effect of the boundary conditions.

The effect on the displacement field of changing the boundary conditions is shown in figures 4.14 - 4.29. In order to construct these graphs a standard reference point fixed relative to the shear zone dimensions is used. The change in displacement at this point is plotted with respect to each of the boundary conditions for the four rheologies. The fixed reference point used is a point half the shear zone length perpendicularly away from the zone at the mid point of the zone. The standard parameters used for calculating these relationships

Fig 4.10

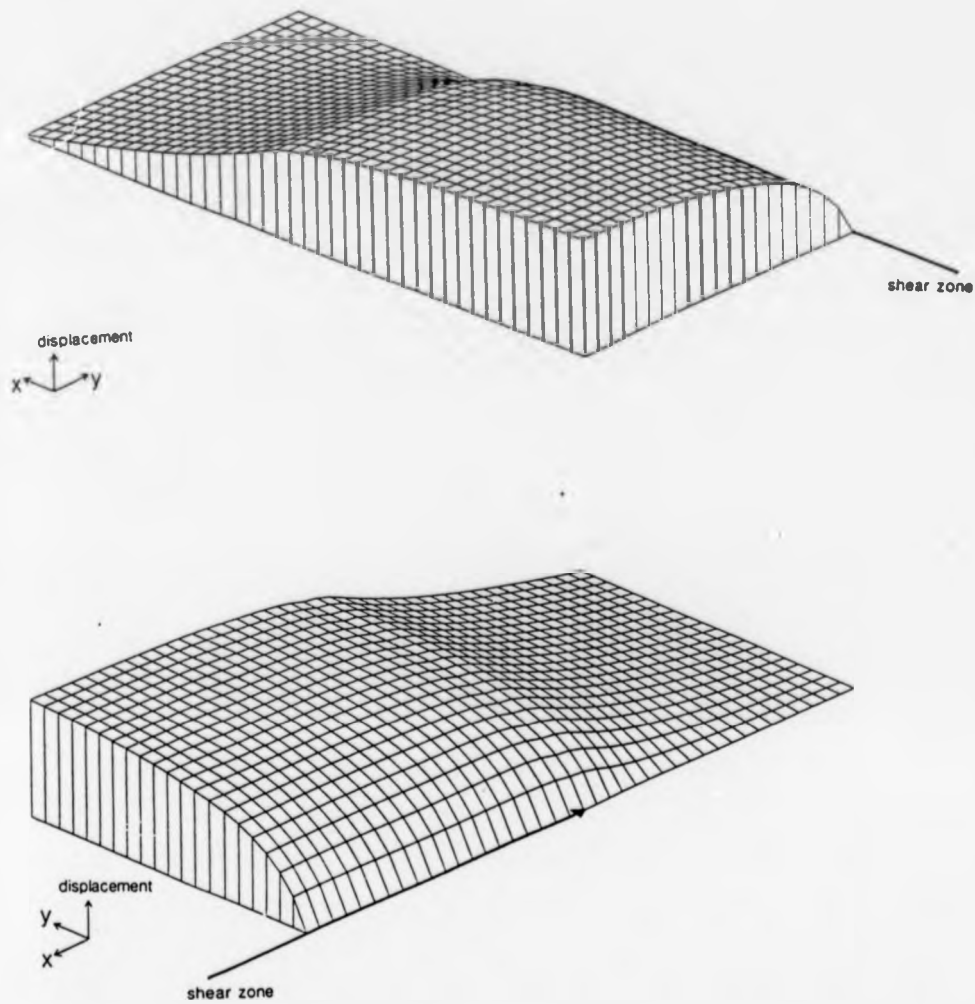


Fig 4.10 Generalized surface views of a portion of the displacement field around a propagating shear zone tip.

Fig 4.11

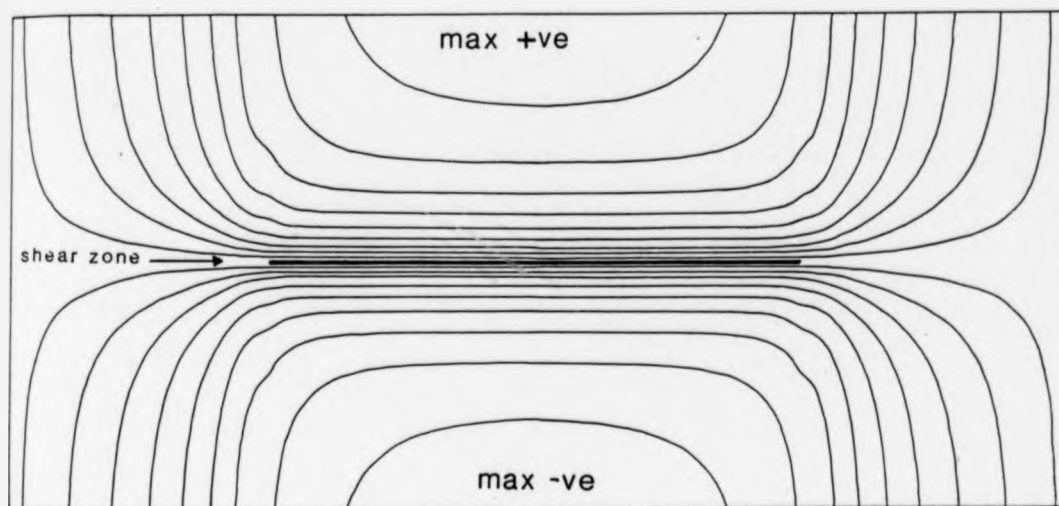


Fig 4.11 Generalized contour map of the displacement field around a propagating shear zone tip.

Fig 4.12

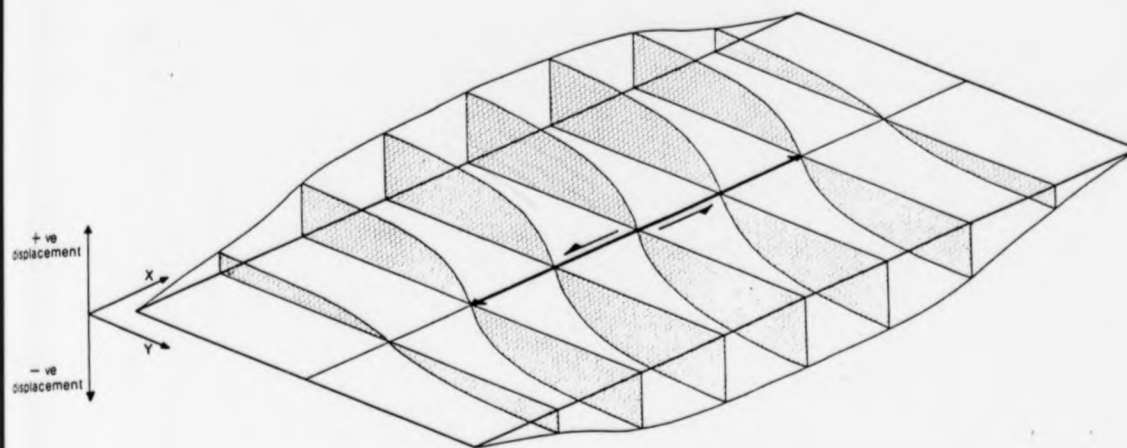


Fig 4.12 Generalized fence diagram of the displacement field around a propagating shear zone tip showing the symmetry of the field across the zone.

Fig 4.13

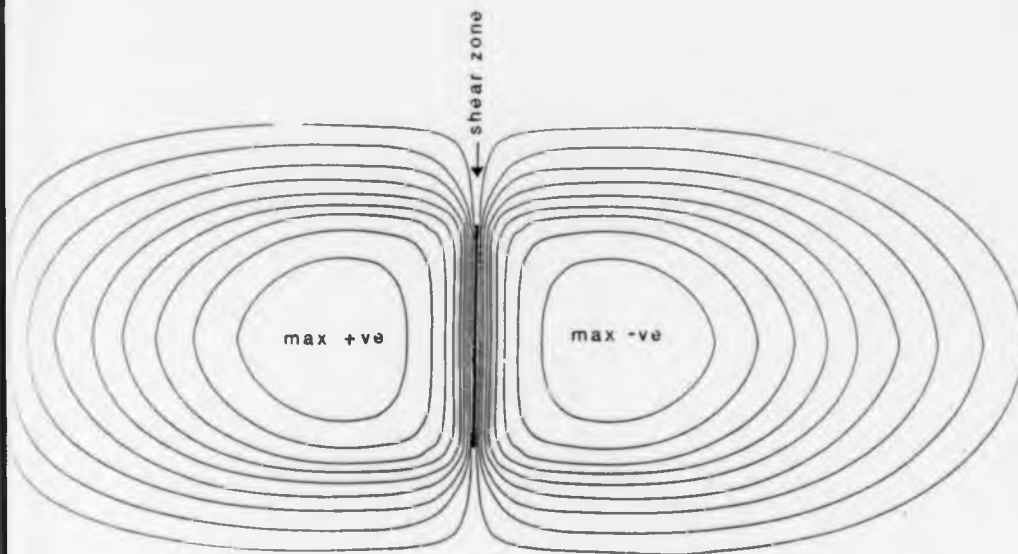


Fig 4.13 Hypothetical contour map of the displacement field around an isolated stress controlled shear zone allowing for the continuity of zero displacement around the zone.

Fig 4.14

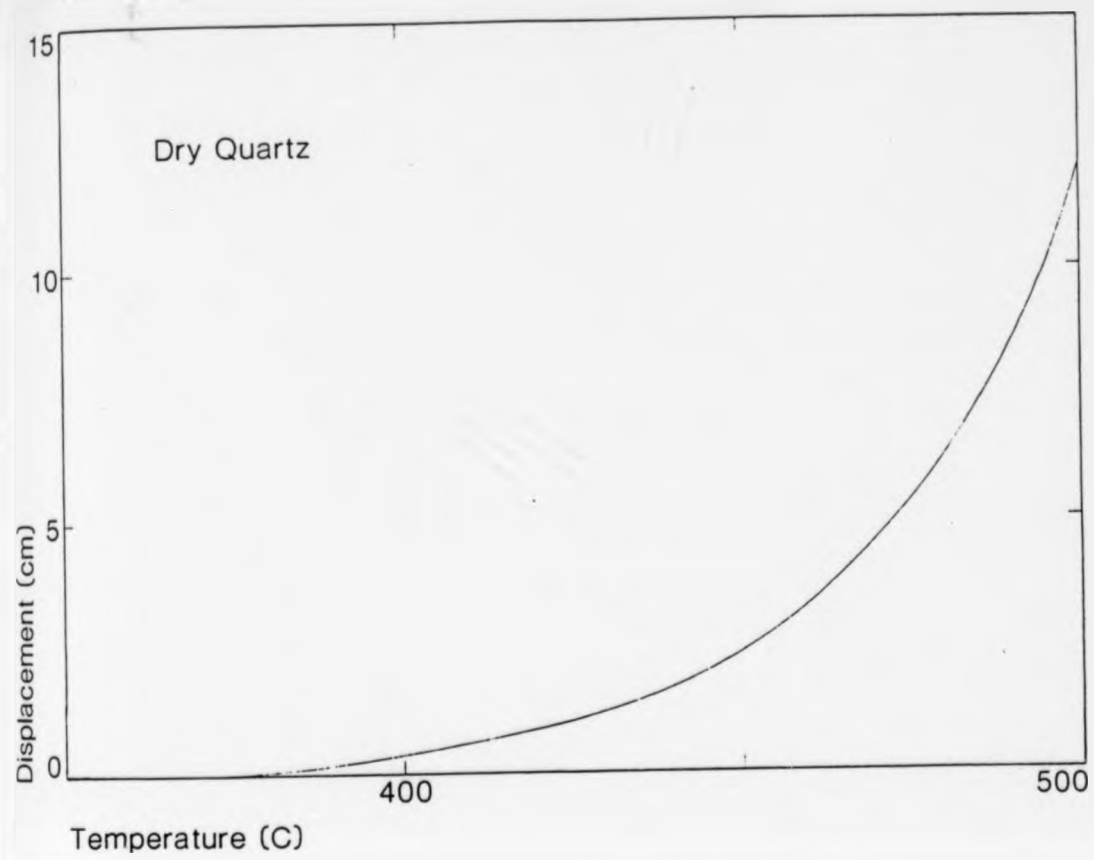


Fig 4.14 Displacement plotted against temperature for dry quartz.

Fig 4.15

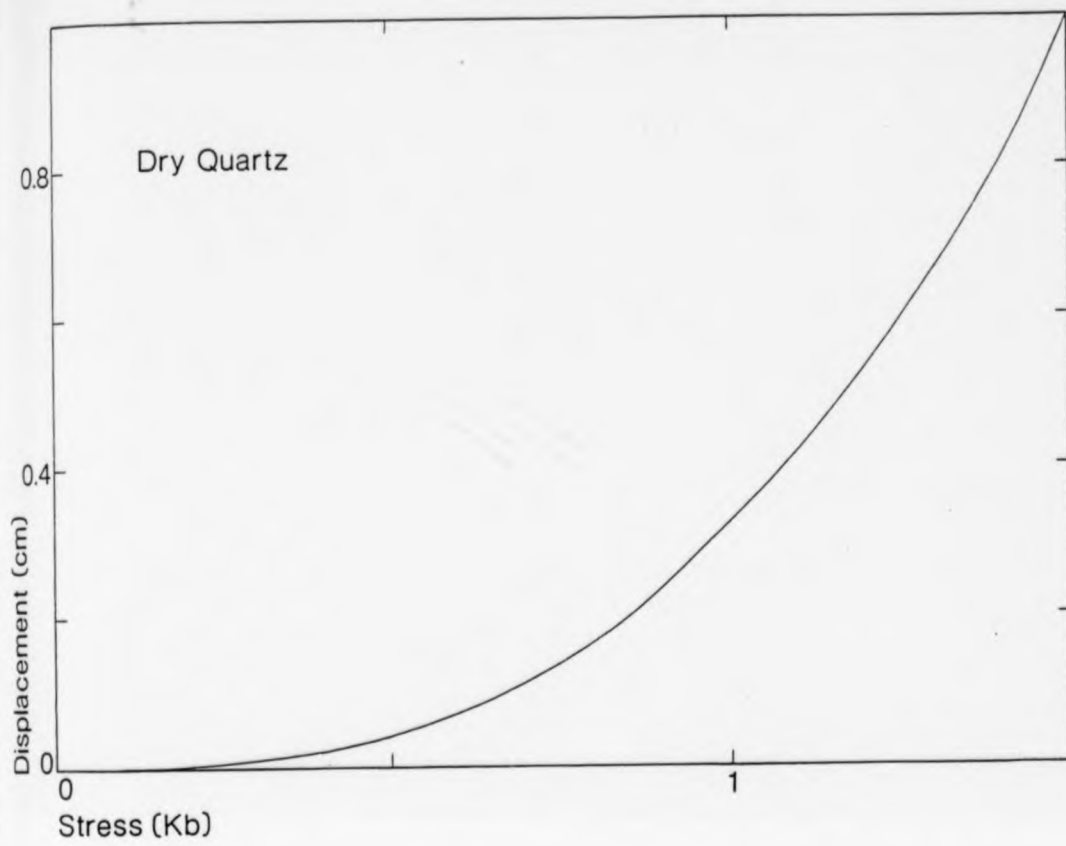


Fig 4.15 Displacement plotted against applied load stress for dry quartz.

Fig 4.16

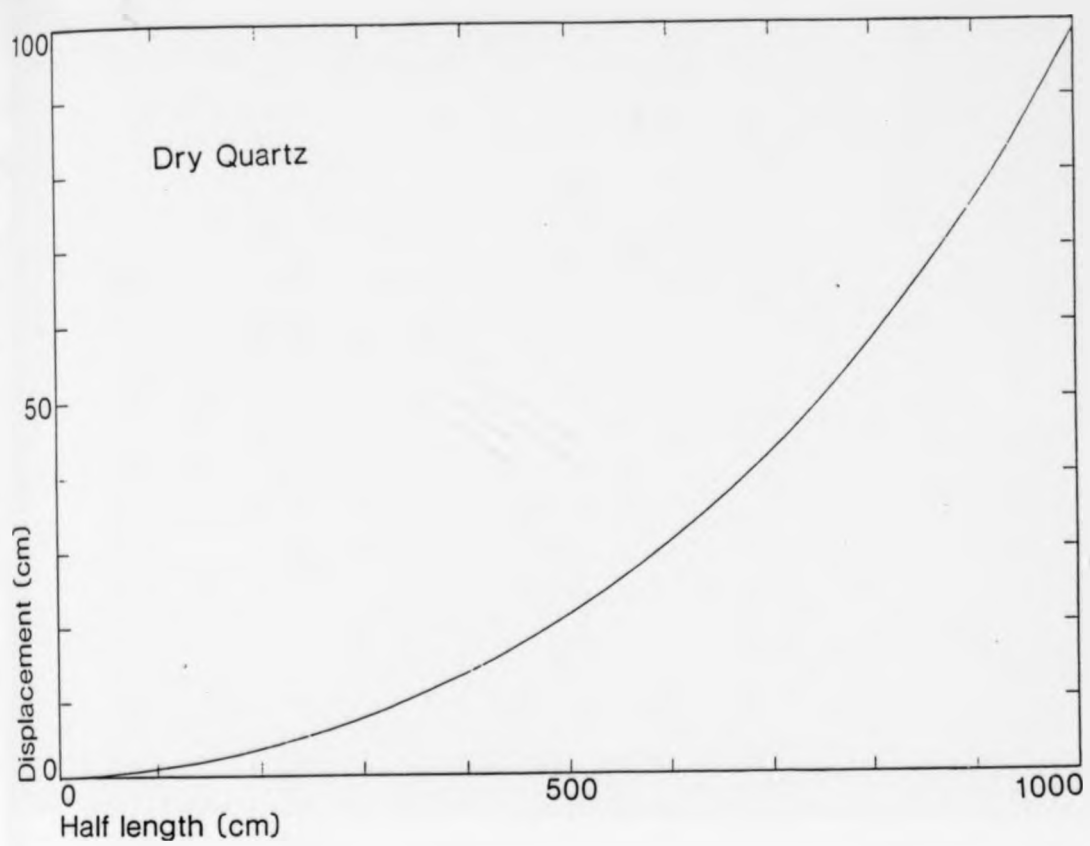


Fig 4.16 Displacement plotted against half-length for dry quartz.

Fig 4.17

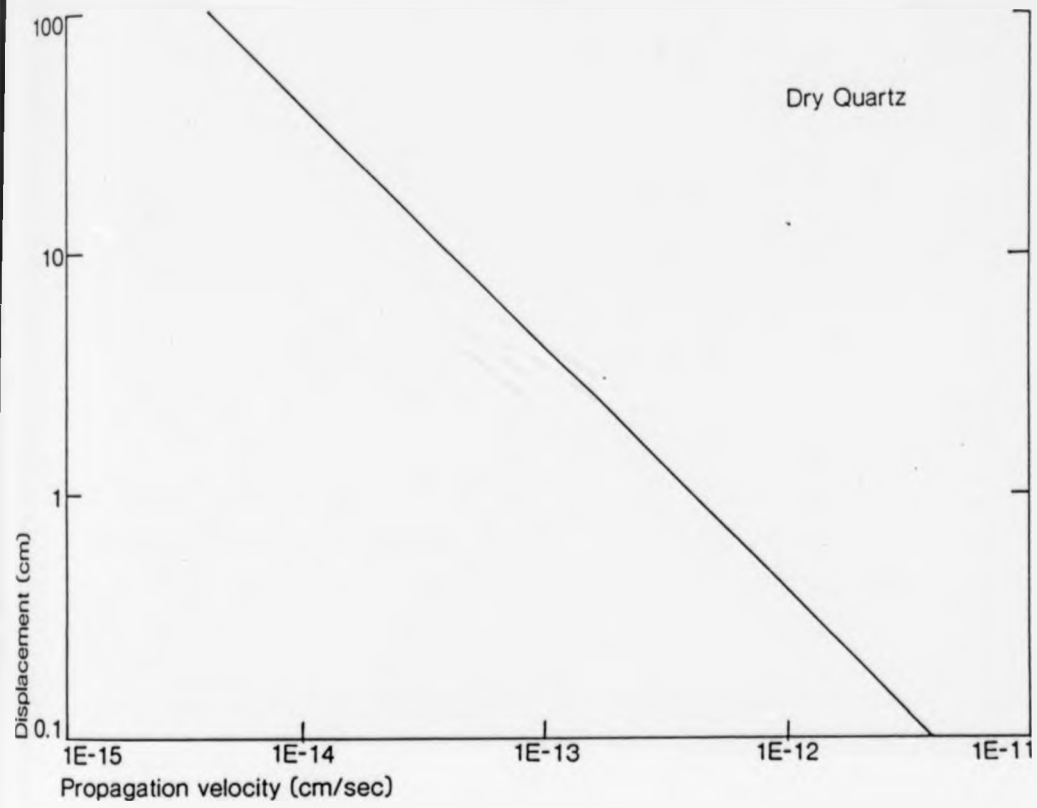


Fig 4.17 Displacement plotted against propagation velocity for dry quartz.

Fig 4.18

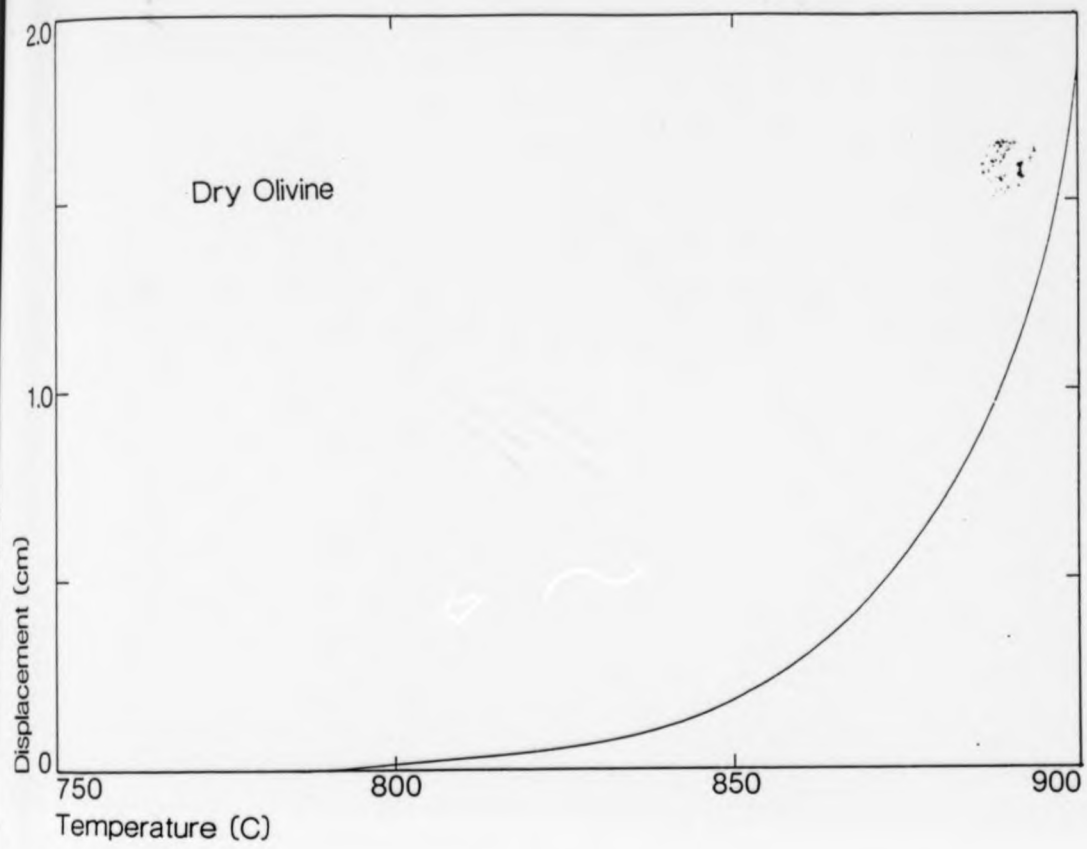


Fig 4.18 Displacement plotted against temperature for dry olivine.

Fig 4.19

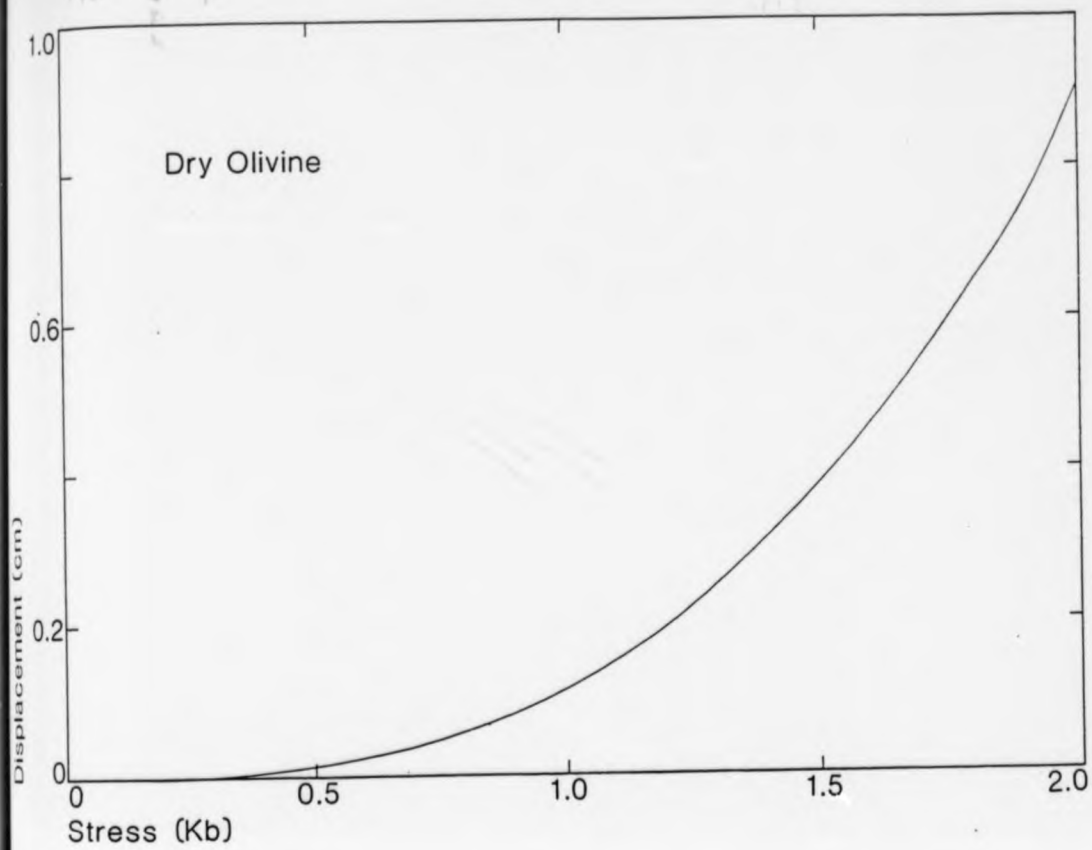


Fig 4.19 Displacement plotted against applied load stress for dry olivine.

Fig 4.20

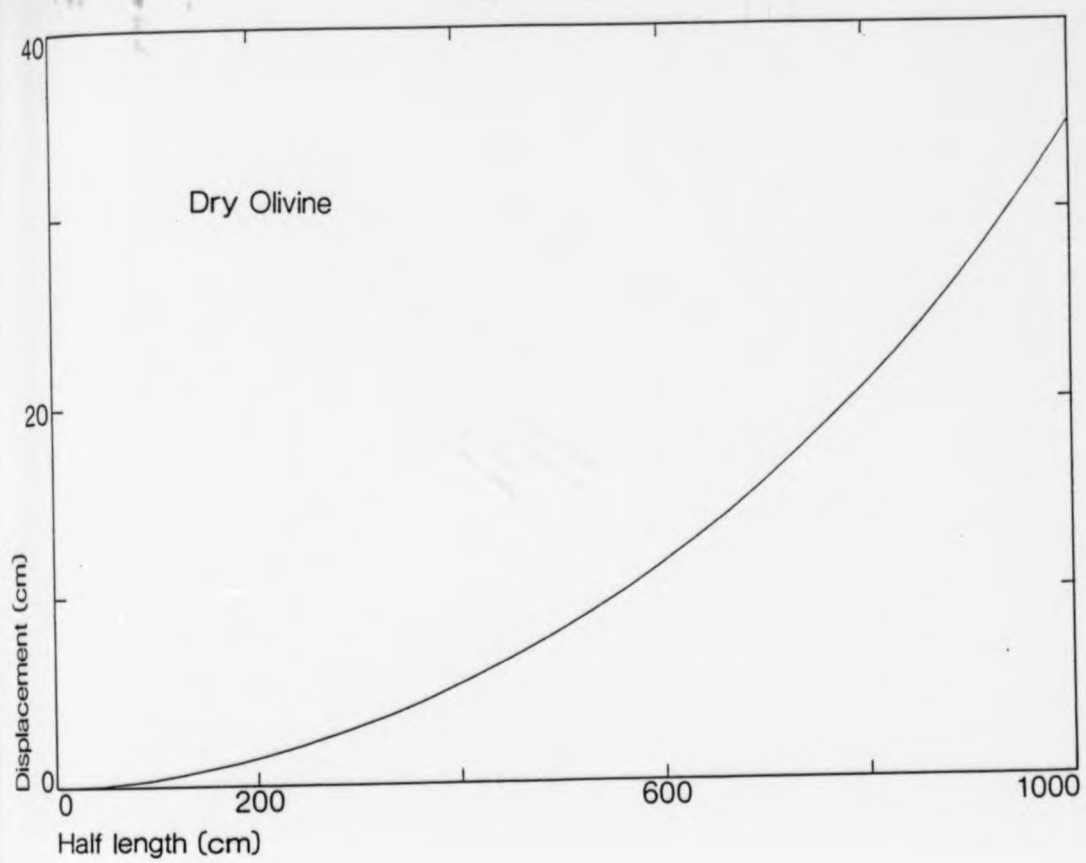


Fig 4.20 Displacement plotted against half-length for dry olivine.

Fig 4.21

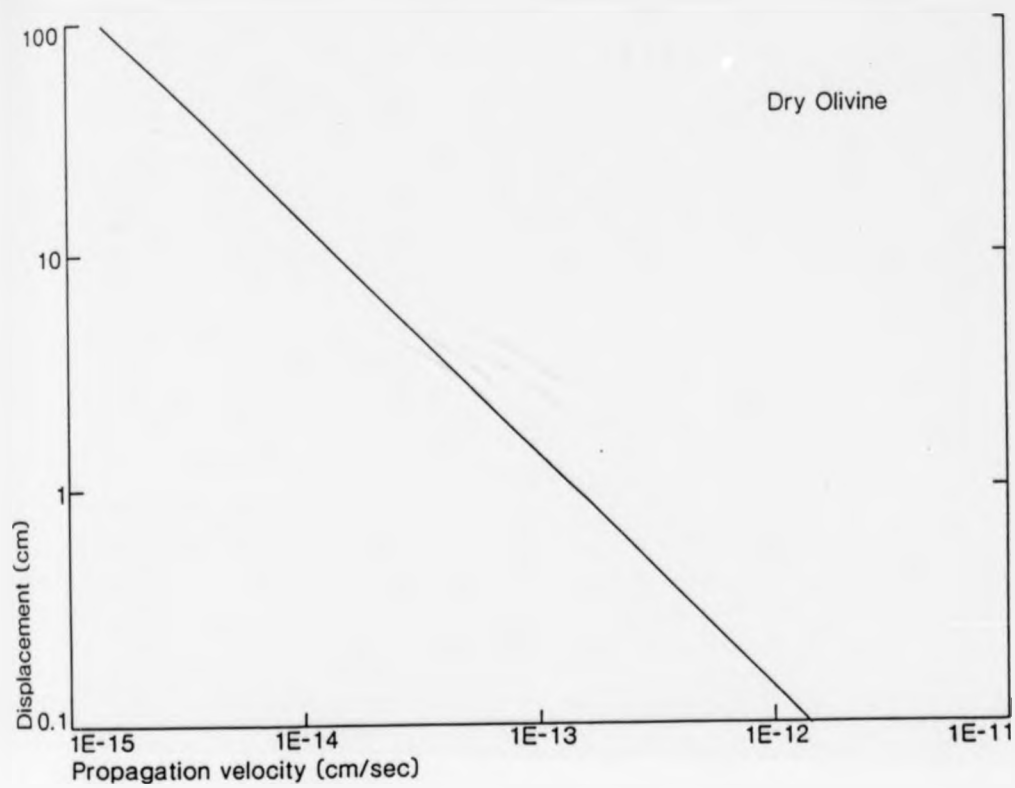


Fig 4.21 Displacement plotted against propagation velocity for dry olivine.

Fig 4.22

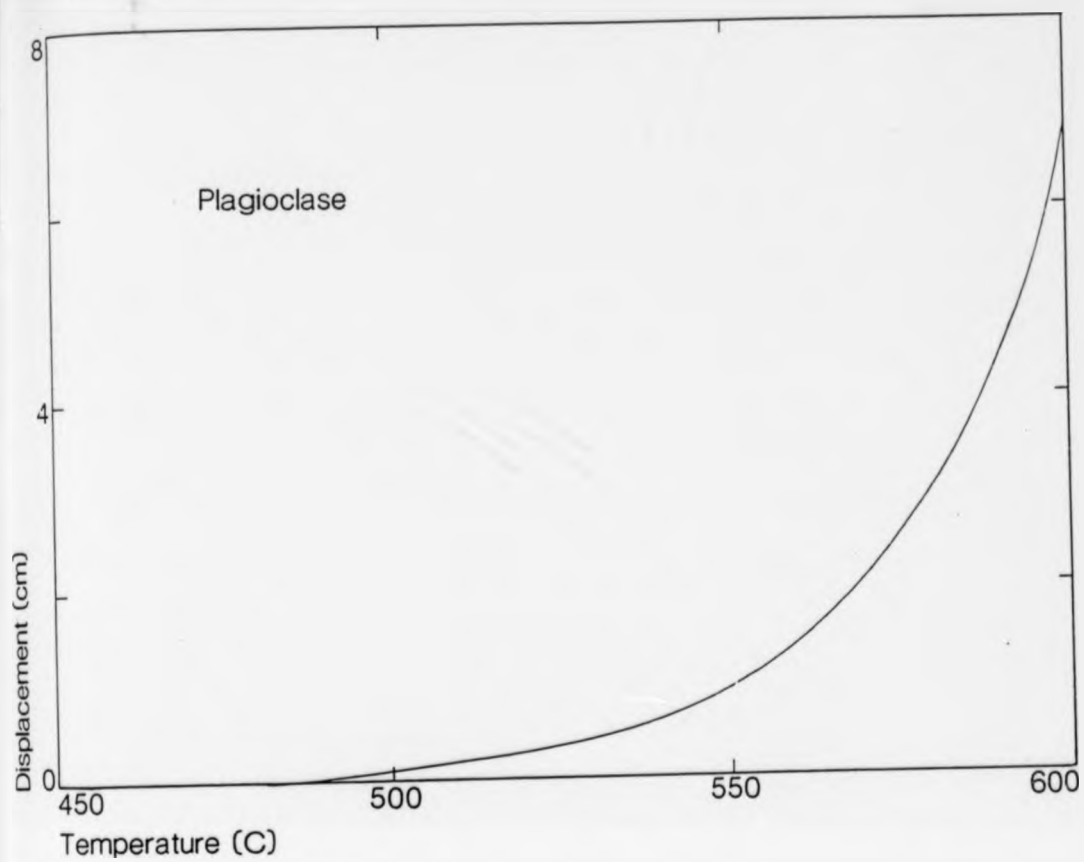


Fig 4.22 Displacement plotted against temperature for plagioclase.

Fig 4.23

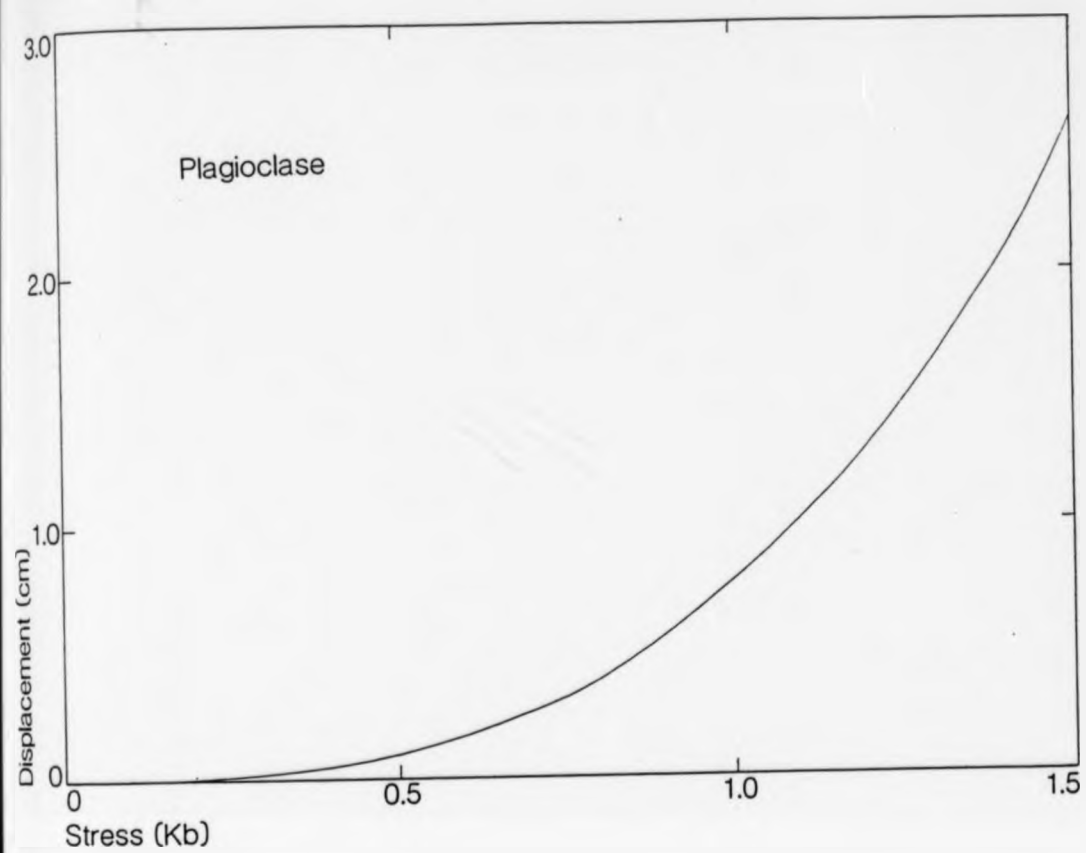


Fig 4.23 Displacement plotted against applied load stress for plagioclase.

Fig 4.24

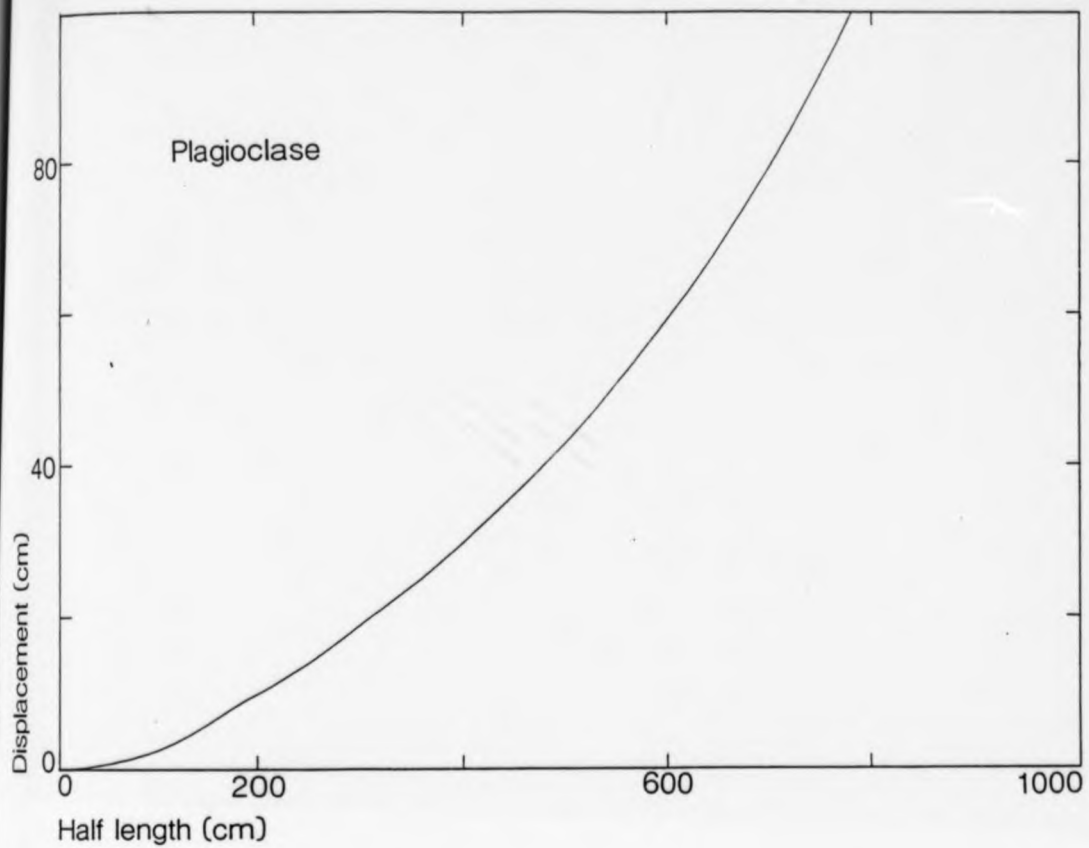


Fig 4.24 Displacement plotted against half-length for plagioclase.

Fig 4.25

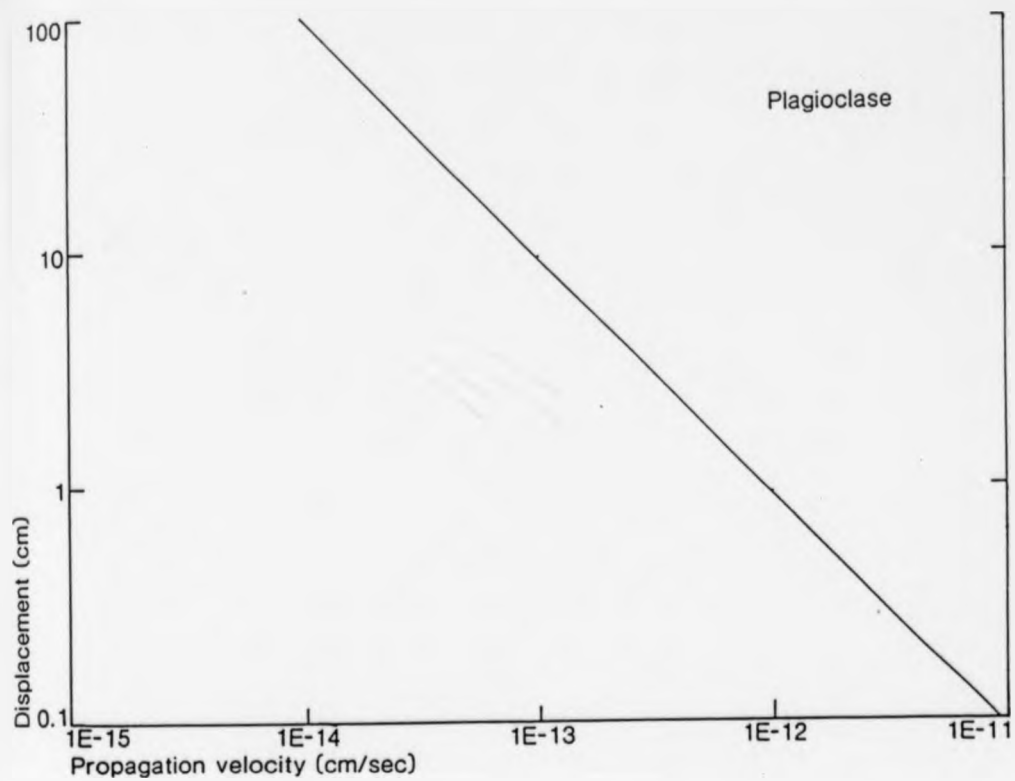


Fig 4.25 Displacement plotted against propagation velocity for plagioclase.

Fig 4.26

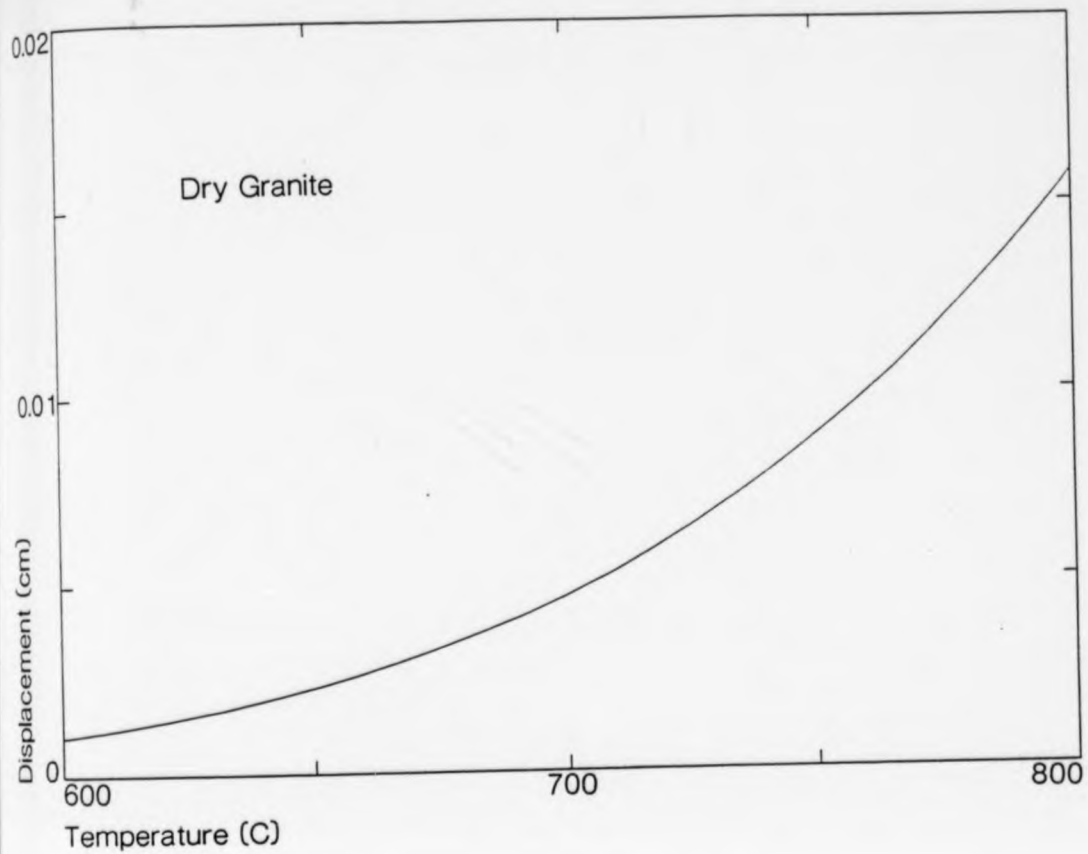


Fig 4.26 Displacement plotted against temperature for dry granite.

Fig 4.27

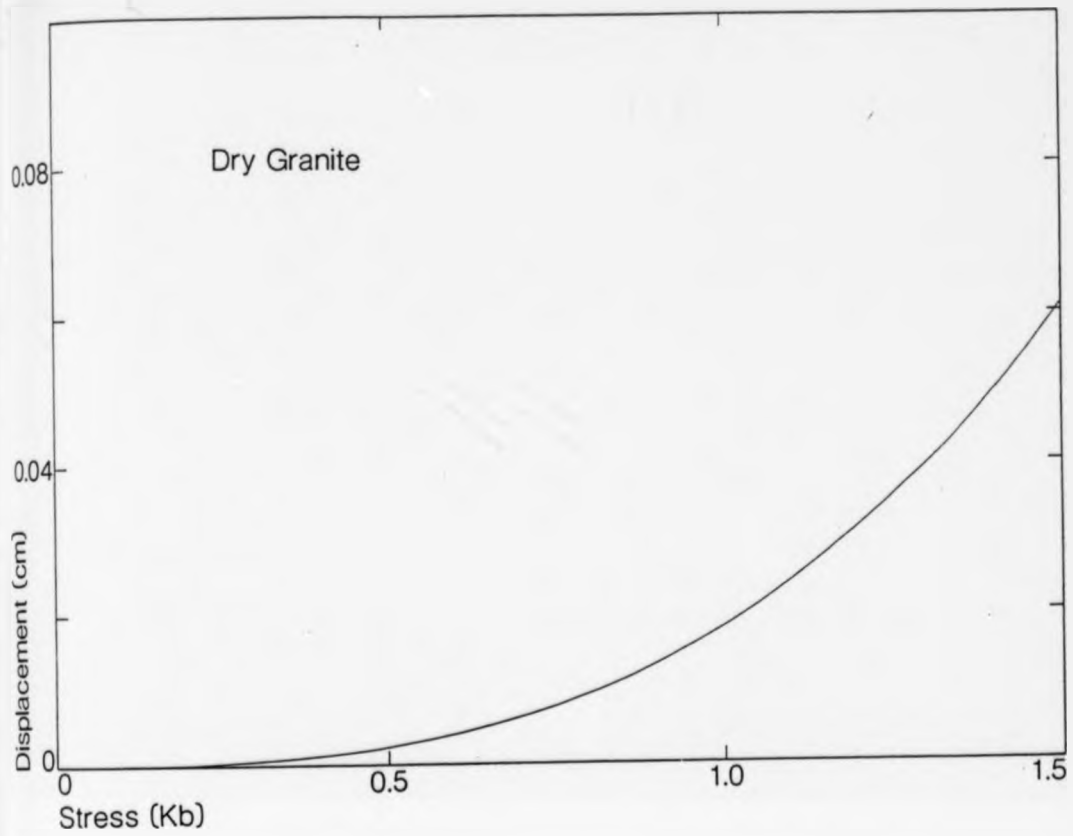


Fig 4.27 Displacement plotted against applied load stress for dry granite.

Fig 4.28

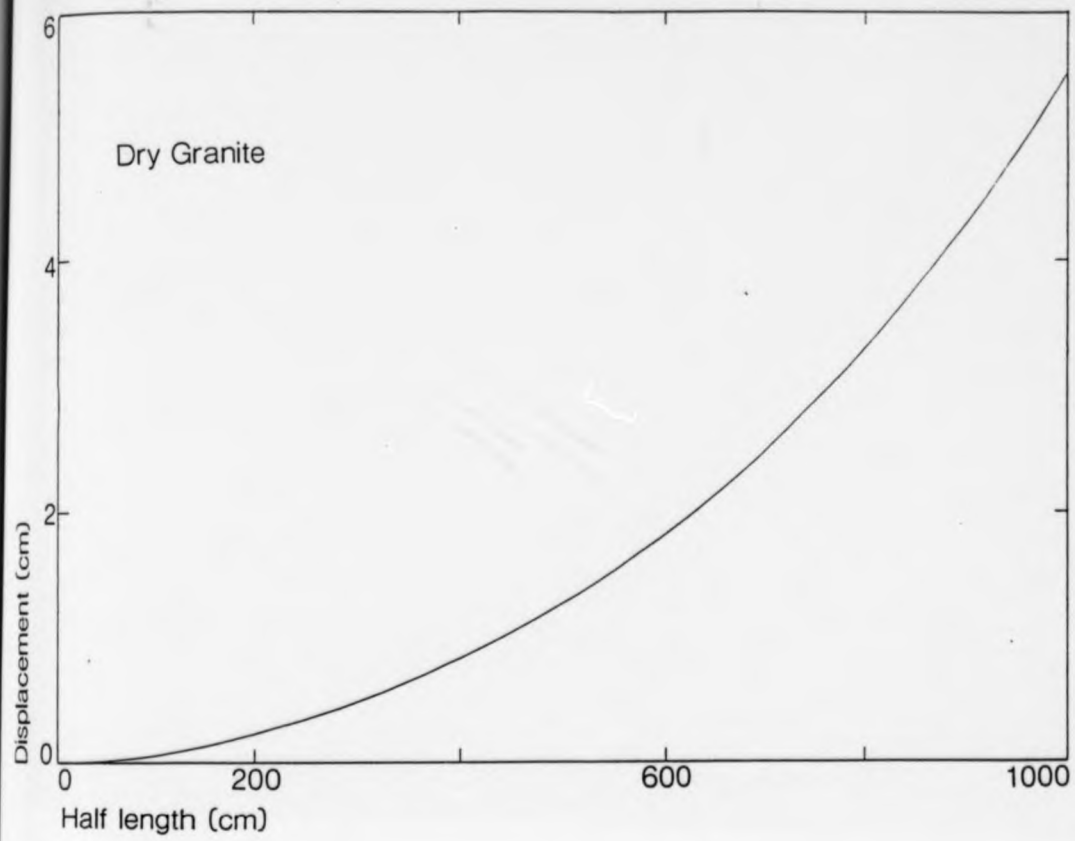


Fig 4.28 Displacement plotted against half-length for dry granite.

Fig 4.29

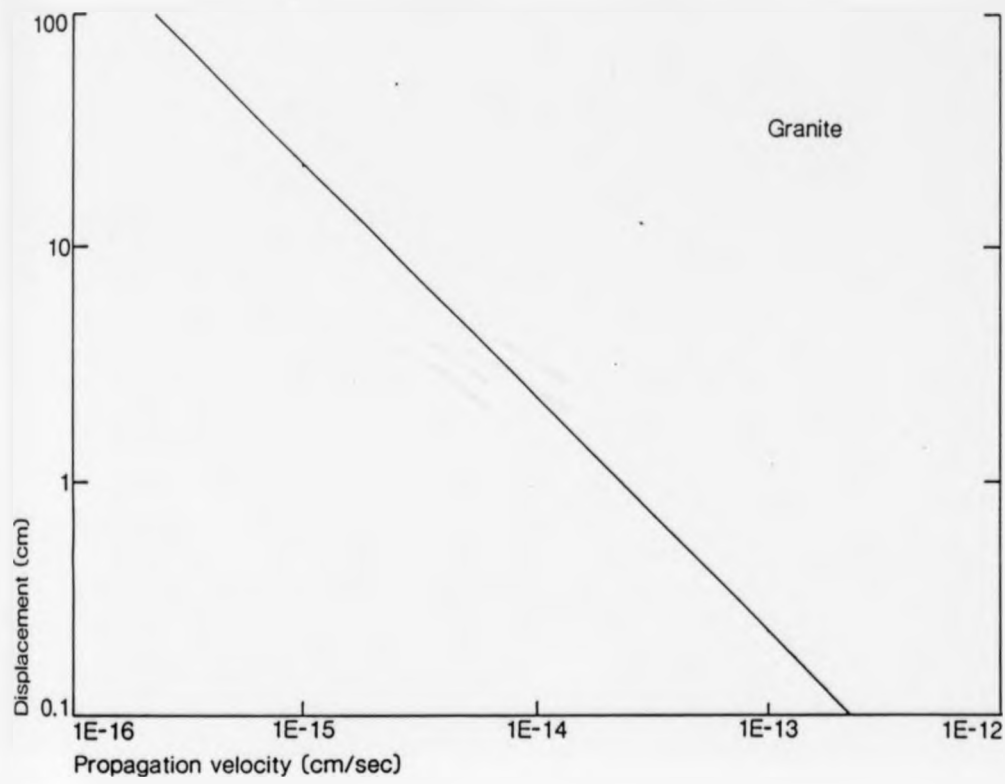


Fig 4.29 Displacement plotted against propagation velocity for dry granite.

TABLE 4.1

STANDARD PARAMETERS USED IN THE DISPLACEMENT RELATIONSHIP GRAPHS.

Rheology	Temperature C°	Applied load Stress Kb	Shear zone Half-Length cm	Propagation Velocity cm/sec
Dry Quartz Koch et al. (1980)	350	0.5	20	1×10^{-11}
Dry Olivine Bodine et al. (1981)	800	0.5	20	1×10^{-11}
Plagioclase (anorthosite) Shelton & Tullis (1980)	500	0.5	20	1×10^{-11}
Dry Granite Carter et al. (1981)	650	0.5	20	1×10^{-11}

are given in table 4.1.

Again the strong effect of temperature on the deforming shear zone is shown in these graphs. For quartz, a 50°C increase in temperature from 450° - 500°C gives a five-fold increase in displacement (Fig 4.14). This effect is less strong for the granite rheology due to the very low value of the A parameter in the flow law. Increasing the half-length by one order of magnitude increases the displacement by two orders of magnitude. Since the propagation velocity has an inverse relationship with the displacement, decreasing the velocity by a factor of 10 will increase the displacement by the same factor.

4.II APPLICATION OF THE MODEL

4.II.1 Theory and methods.

4.II.1.a Problems of application.

In order to apply the model to a naturally occurring shear zone values must be obtained for as many of the critical parameters as possible. Some are relatively easy to measure if the zone is well exposed, ie: shear zone half-length, strain profile and displacement. Other parameters are more difficult to obtain but under favourable conditions a reasonable estimate may be possible, ie: temperature and applied load stress. The one parameter that cannot be measured is the propagation velocity, and this is what the model may be used to predict. The most serious difficulty in applying the model is that the rheology of the rocks containing the shear zones is uncertain, as most ductile shear zones occur in medium to high grade metamorphic rocks where the deformation may well be controlled by mechanisms that have

not been examined experimentally and the appropriate flow laws are consequently unknown. These problems do not prohibit the application of the model since comparison of predicted and observed phenomena is a useful method of testing the model and may elucidate the different mechanisms involved.

4.II.1.b Theory of application.

Equation 4.9 may be divided into two parts, the integral, depending on the distance x and the angular function, and a premultiplier containing the boundary conditions. For a given point, fixed with respect to the shear zone tip, the integral will be a constant. By taking the fixed reference point as the point at which maximum displacement occurs then equation 4.9 can be rewritten as:

$$S_{\max} = 1/V A \exp(-Q/RT) \sigma_L^n (C/2)^{n/2} J \quad (4.10)$$

Where J is a constant.

This equation can be used to examine the relationships between the boundary conditions for the point of maximum displacement. For a 'normal' example of a natural shear zone the displacement and half-length will be known, temperature and load stress will be known to within a range of values and propagation velocity will be unknown. It is therefore possible to construct graphs in temperature/stress/propagation velocity space that will show a field within which the propagating shear zone may have operated. It may then be possible to further constrain the area of the field to give a more limited range of conditions, i.e. the geologically probable as opposed to the possible.

Once the above technique has been applied to a particular shear zone, a set of values for the boundary conditions may be selected and used to construct a synthetic strain profile for the zone to assess the validity of the values chosen

4.II.2 Application to shear zones from the North West Highlands.

4.II.2.a The stress/temperature/propagation velocity diagrams.

Using equation 4.10 stress/temperature/propagation velocity diagrams have been drawn for selected shear zones from the North West Highlands (see chapter 2)(Figs 4.30 - 4.32). The main constraint when selecting these zones to test the model is that the shear zone half-length must be known consequently only isolated zones may be used, as those that occur in networks cannot meet this criterion. In order to apply the model to the Canisp Shear Zone, an estimate of the length of the zone must be made. This is done using the aspect ratio of the shear zone (Norton 1982). Most shear zones have an aspect ratio (length : width) of approximately 500 : 1, thus the Canisp Shear Zone, which has an average width of 0.75 Km, should be in the order of 380 Km long. This is a major assumption and is used in order to enable comparison of the results between a large crustal scale shear zone and the smaller outcrop scale zones. The absence of reliable temperature estimates for the time of shear zone formation in the southern outcrop of the mainland Lewisian is a problem. A temperature of 550°C has been used as this is a representative value for the mid-amphibolite facies conditions under which these zones were operating.

Figures 4.30 - 4.32 have been drawn for shear zones 9, 22 and 24 (see chapter 2) as these give the best control on displacement and half-length, so displacement can be used to constrain the other variables. The three diagrams show that for the smaller shear zone (9)

Fig 4.30

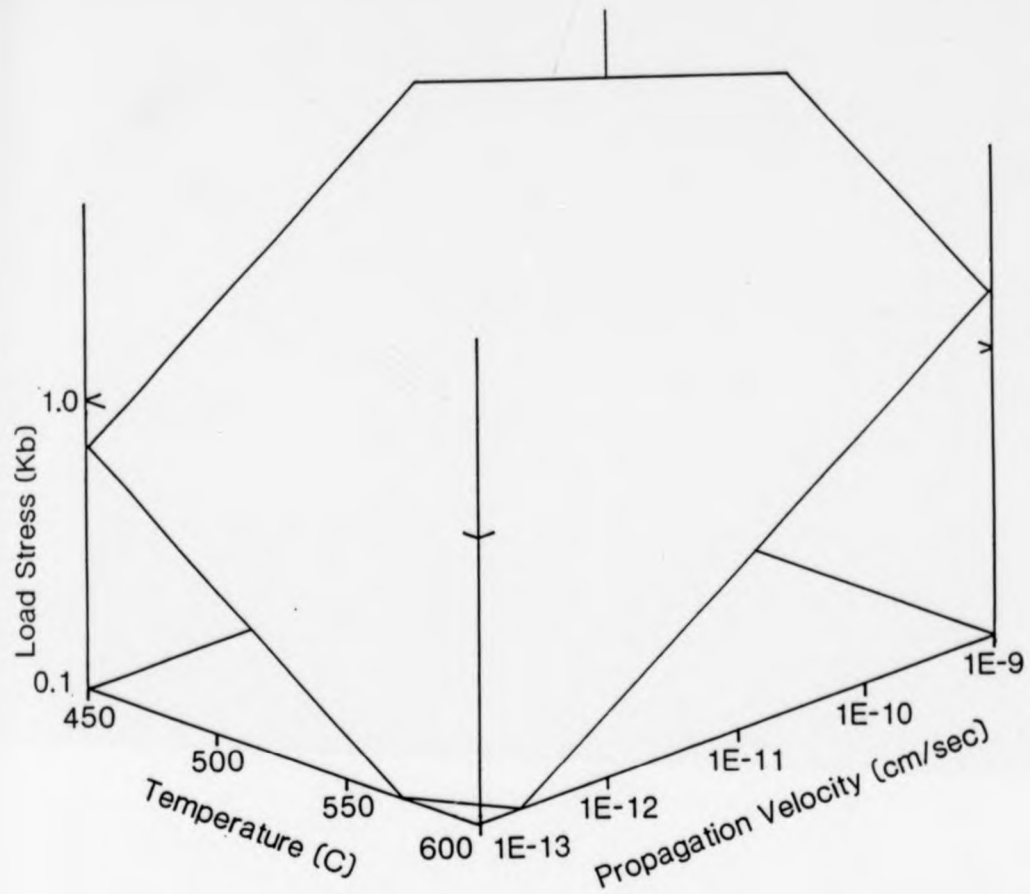


Fig 4.30 Stress/temperature/propagation velocity diagram for shear zone 9.

Fig 4.31

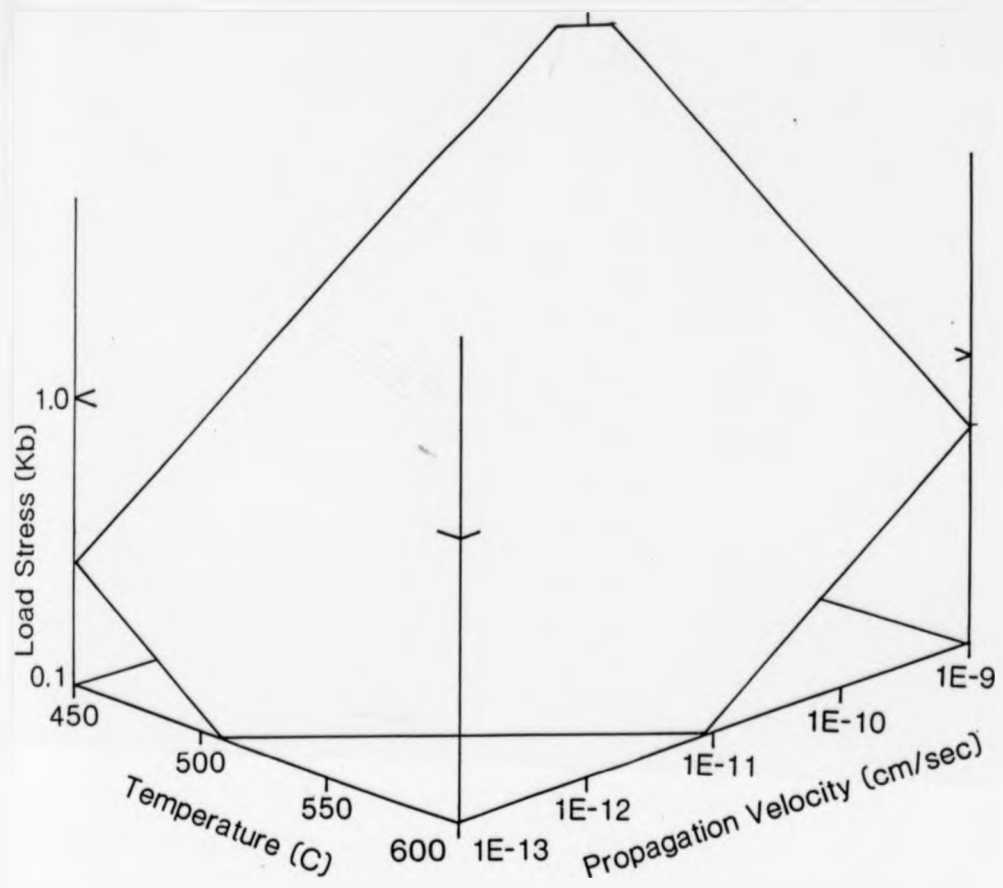


Fig 4.31 Stress/temperature/propagation velocity diagram for shear zone 22.

Fig 4.32

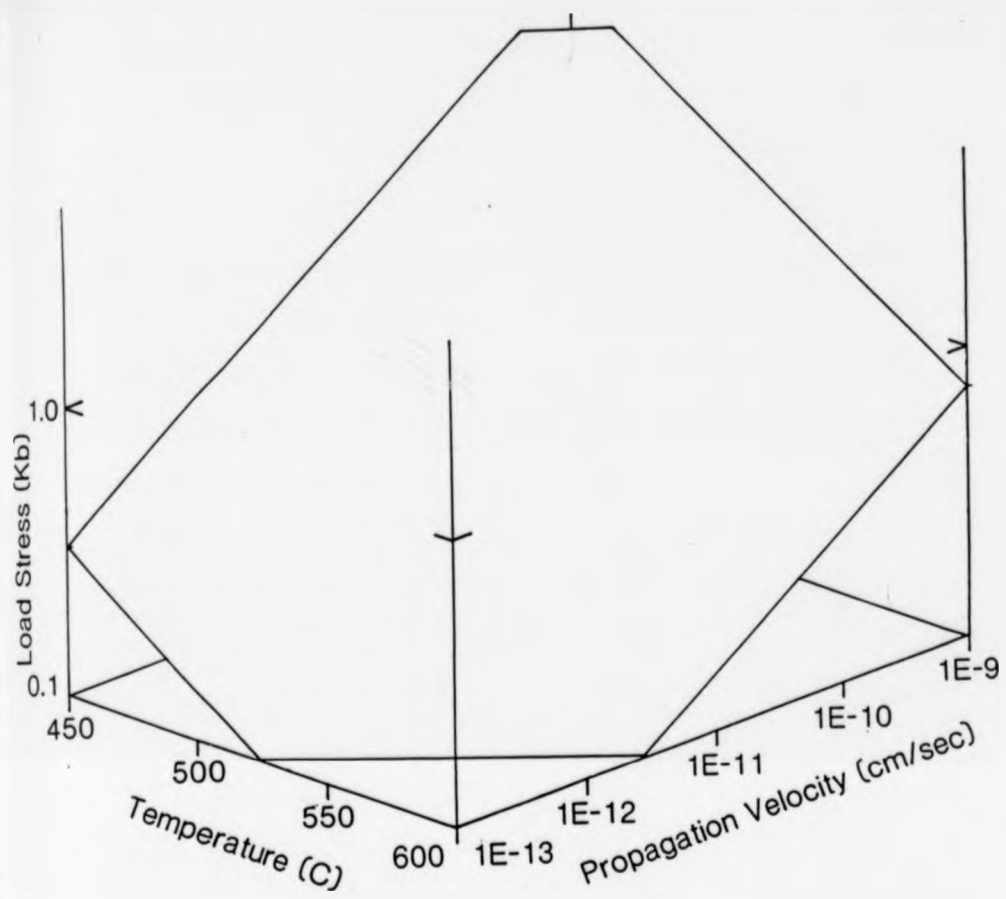


Fig 4.32 Stress/temperature/propagation velocity diagram for shear zone 24.

the stresses required to produce the observed displacement are greater than for larger zones, as predicted earlier, assuming the other boundary conditions remain constant. Taking as an example the point of 500°C at 1×10^{-11} cm/sec propagation velocity, shear zone 9 requires an applied stress of 0.667 Kb, shear zone 24 - 0.31 Kb and shear zone 22 - 0.25 Kb. Applying the model to the Canisp Shear Zone for the same conditions, a stress of only 0.0035 Kb is required. Taking the North West Highlands as a region the temperature at the time of shear zone formation can be assumed to be relatively constant for the purposes of the model, and so only two variables remain; stress and propagation velocity. Some variation in applied stress must occur over the area in question but large scale variations of several orders of magnitude are unlikely, hence the propagation velocity of the shear zones will be the principal variable. One way in which the propagation velocity can be constrained is by estimating the length of time taken for the shear zones to reach the observed lengths. If the Canisp Shear Zone propagated at 1×10^{-11} cm/sec, a value which fits the smaller shear zones well, then to reach its estimated length of 380 Km would have taken approximately 120,000 Ma which is clearly impossible. A value of 1×10^{-5} cm/sec gives a time of propagation of 120,500 years, which is more reasonable, and the stress required to propagate at this rate would be 0.43 Kb which is more realistic than the value of 0.0035 Kb required at a velocity of 1×10^{-11} cm/sec.

Applying the same argument to the smaller shear zones gives similar results to the large zone. Assuming shear zone 9 to have been propagating at 1×10^{-11} cm/sec then it would have taken 127,000 years to reach 40 cm. shear zones 22 and 24 would have taken 158,500 years and 95,000 years respectively at the same velocity to reach their present lengths. These calculations are made assuming that the applied stress levels are approximately 0.5 Kb. These results suggest that all

the shear zones were propagating over the same time span regardless of size, and that the larger shear zones have propagated more quickly. This is in close agreement with the conclusions of Norton (1982). One problem with this approach is that differences in the present length of shear zones cannot result solely from variations in propagation velocity as these two boundary conditions are linked by the model in that, assuming all other conditions remain constant, there is only one propagation velocity for a given length of zone. There must be an initial variation in the size of the shear zones, or in the local stress/temperature conditions at the time of initial propagation, that will lead to certain zones becoming dominant. Once these zones have become dominant their rate of growth will continue to exceed that of other zones as long as there are no changes in the local conditions. The explanation for the initial variation in shear zone size is likely to be linked to the localization mechanism of initiation. Some shear zones may localize on larger pre-existing structures or heterogeneities; or alternatively locally higher temperatures and/or load stresses may result in a higher initial propagation velocity which will give the zone a 'head start'. The estimates of length of time of operation are, of course, only approximate and intended for comparison only, as the propagation rate will change with increasing length through the lifetime of the zone.

Figures 4.30 - 4.32 are constructed using the values for a plagioclase rheology (Shelton & Tullis 1982). Changing the rheology to diabase (Caristan 1982) has the effect of increasing the stress necessary to maintain propagation at a fixed rate at constant temperature for a given zone (Fig 4.33). It is not possible from the data available to tell which rheology gives the 'correct' values.

Fig 4.33

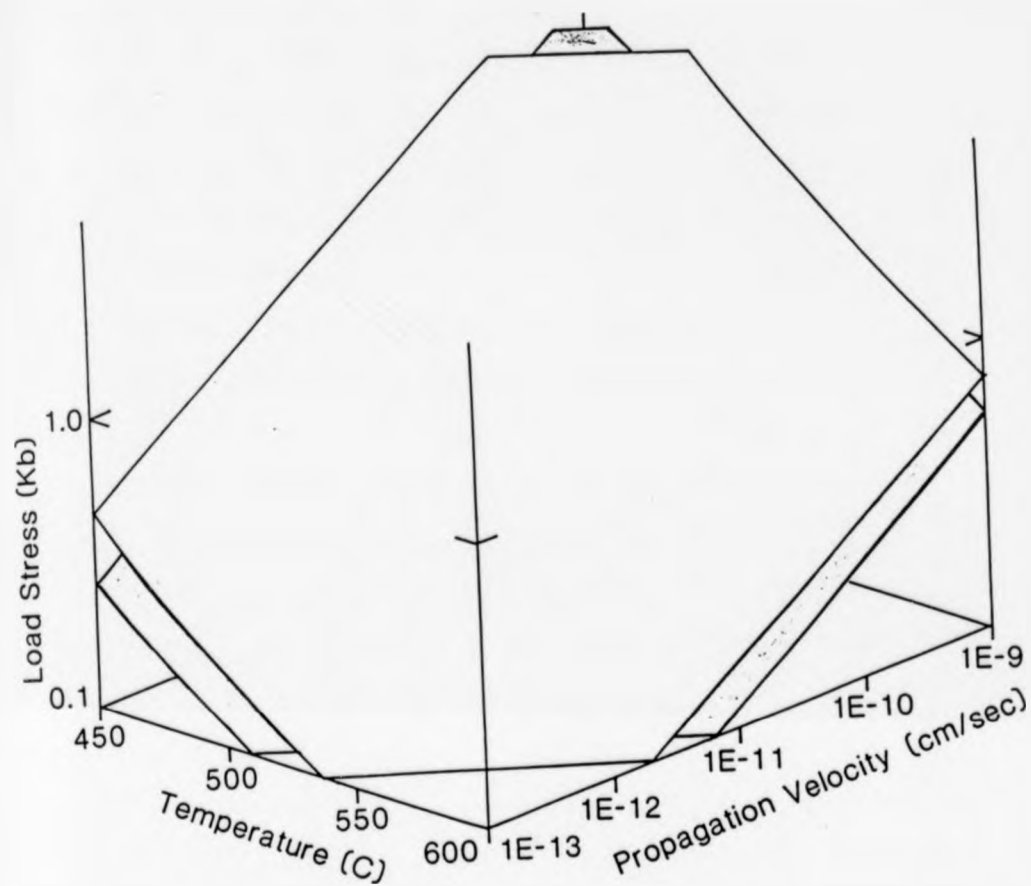


Fig 4.33 Comparison of stress/temperature/propagation velocity diagrams for shear zone 22 using plagioclase rheology (shaded) and diabase rheology.

4.II.2.b Comparison of strain profiles.

Once a set of probable conditions for a particular zone have been established, as outlined above, a synthetic strain profile may be constructed for the zone and compared to the profile measured in the field. This has been done for shear zones 9, 22 and 24 (Figs 4.34 - 4.36). These figures have been constructed using an artificial peak value for the synthetic profiles as the model cannot predict a true value for this point due to the mathematical singularity at the shear zone tip. The profiles are constrained by the displacement ie: the area below the profile. This leads to the most obvious difference between the calculated and observed profiles - the low strain part of the profile. Measured profiles are often restricted in their accuracy of measurement for very low strains; strains of less than 1% are often difficult to detect. The model can calculate very low strains and takes account of these when constructing the profile for a fixed displacement. This results in the calculated profiles being much wider for the low strain part of the curve. Conversely for the high strain area the calculated profile is narrower than the observed. This is due to the initial theory for the model which uses the brittle crack analogy, hence the shear zone cannot have an appreciable width of constant high strain which would give a flat-topped strain profile.

Outside of these extremes the synthetic strain profiles show a very good fit to the observed profiles, particularly for the simple type of profile (shear zones 9 & 22). The predicted width at moderate strains is very similar and the predicted strain gradient of the profile between the moderate and high strains is also very close to the observed profiles. Most of the difference between the profiles is due to the method of calculation of the area below the curve; the observed profiles use only the area below the profile truncated at the lowest value of strain, whereas the calculated profiles use a broader

Fig 4.34

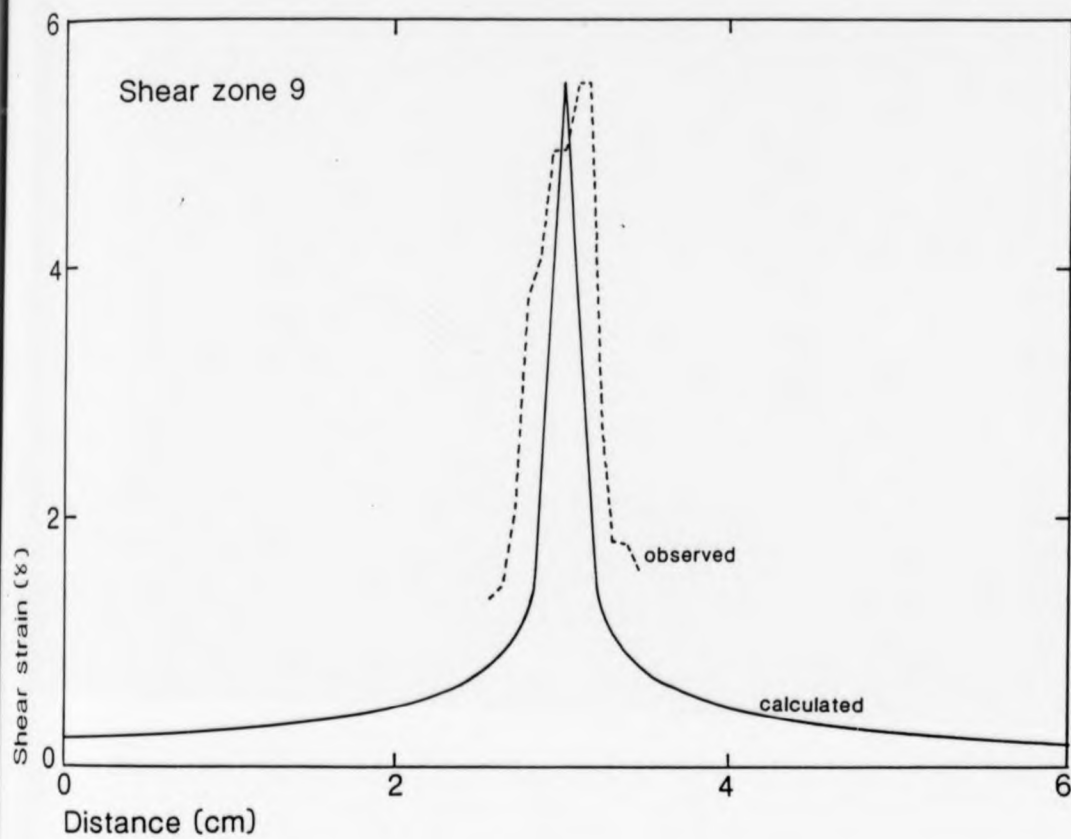


Fig 4.34 Comparison of calculated and observed strain profiles for shear zone 9.

Fig 4.35

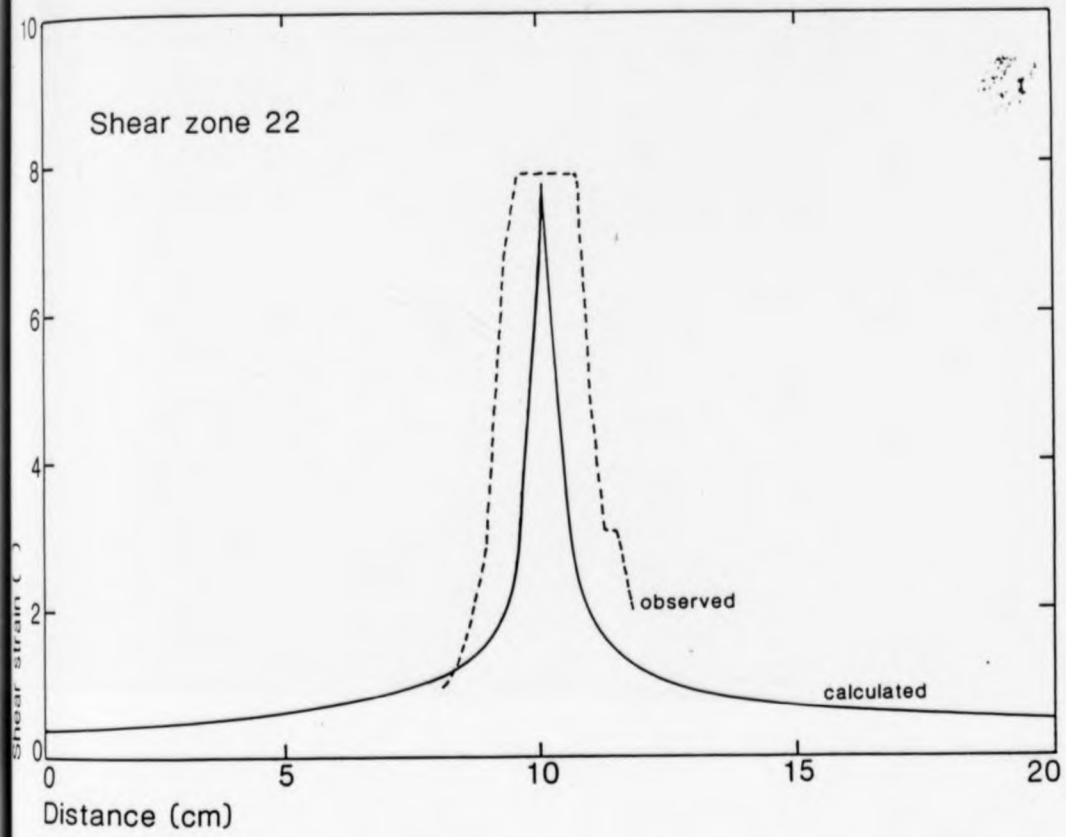


Fig 4.35 Comparison of calculated and observed strain profiles for shear zone 22.

Fig 4.36

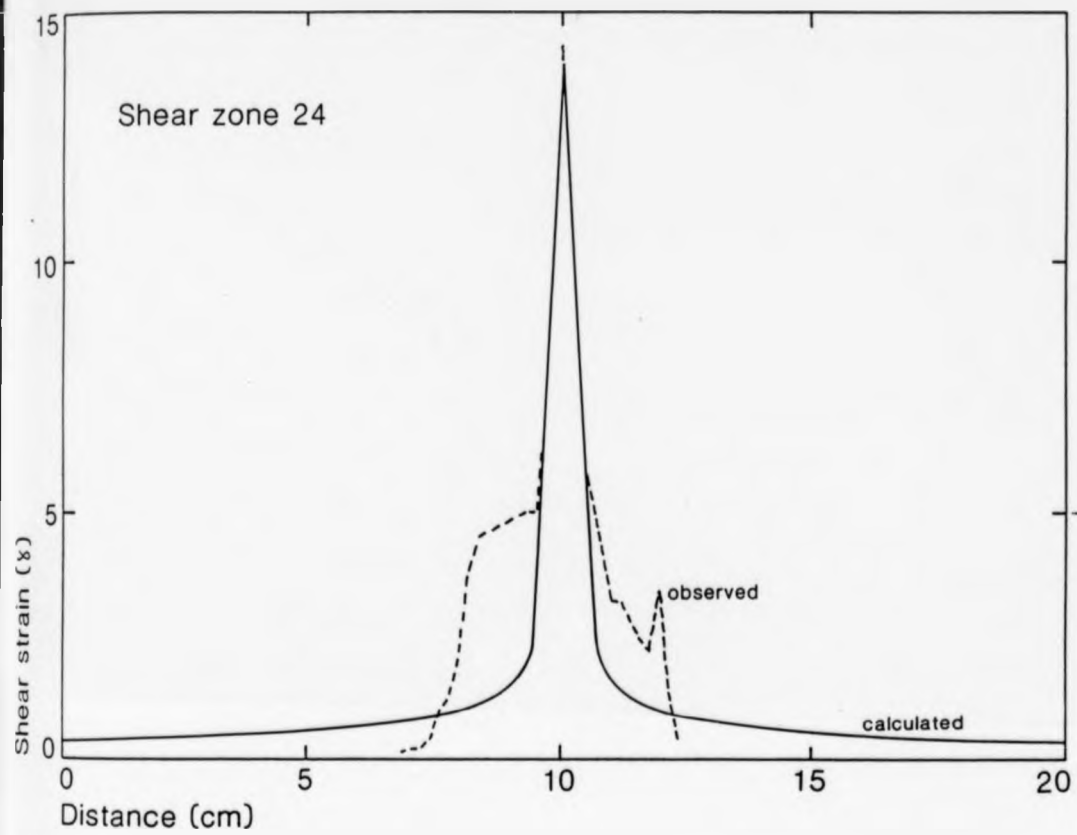


Fig 4.36 Comparison of calculated and observed strain profiles for shear zone 24.

profile at lower strains (Fig 4.37). Figure 4.38 has been constructed by extrapolating the strain profile for shear zone 22 at lower strains, recalculating the displacement and using this to draw a revised calculated profile. This takes account of the low strains that are impossible to measure in the field and consequently improves the match of the profiles.

Changing the rheology used to calculate the strain profile does not alter the shape of the profile as this is dictated by the displacement, which is used to constrain the temperature, stress and propagation velocity.

4.II.2.c Foliation orientations.

Comparing the theoretical foliation orientation patterns with observed field examples shows a close agreement between the calculated and the measured orientations around shear zone tip zones. Figure 4.39 shows the measured foliation orientations at the tip of shear zone 11 which is very similar to the calculated pattern for a shear zone in plagioclase at 550 C, 0.5 Kb and 1×10^{-11} cm/sec propagation velocity, the foliation in front of the zone being at approximately 45° to the shear zone walls. Figure 4.39 also shows a shear zone tip from an alpinised Hercynian granite from the Pennine Zone of the Central Alps (Ramsay & Allison 1979), which is also very similar to the calculated pattern. The model predicts that at very low strains there will still be a foliation at 45° to the shear zone, whereas in natural examples the foliation will disappear at low strains, thus the model has a foliation at 45° to the zone even at some distance from the zone as it cannot predict 'undeformed' rock.

Fig 4.37

Shear zone 22

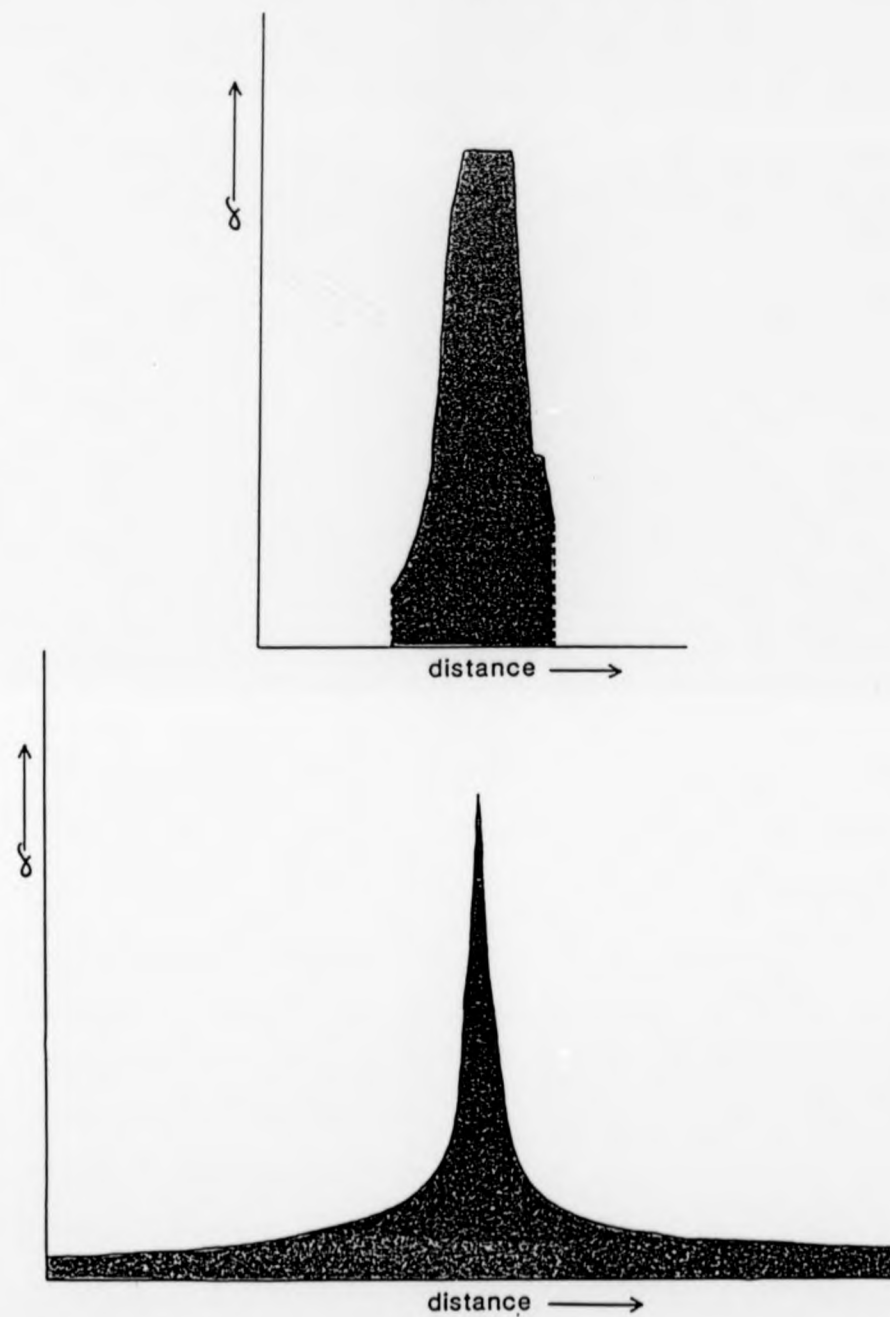


Fig 4.37 Comparison of the method of calculating the displacement between the observed profiles (top) and the calculated profiles (below) for shear zone 22.

Fig 4.38

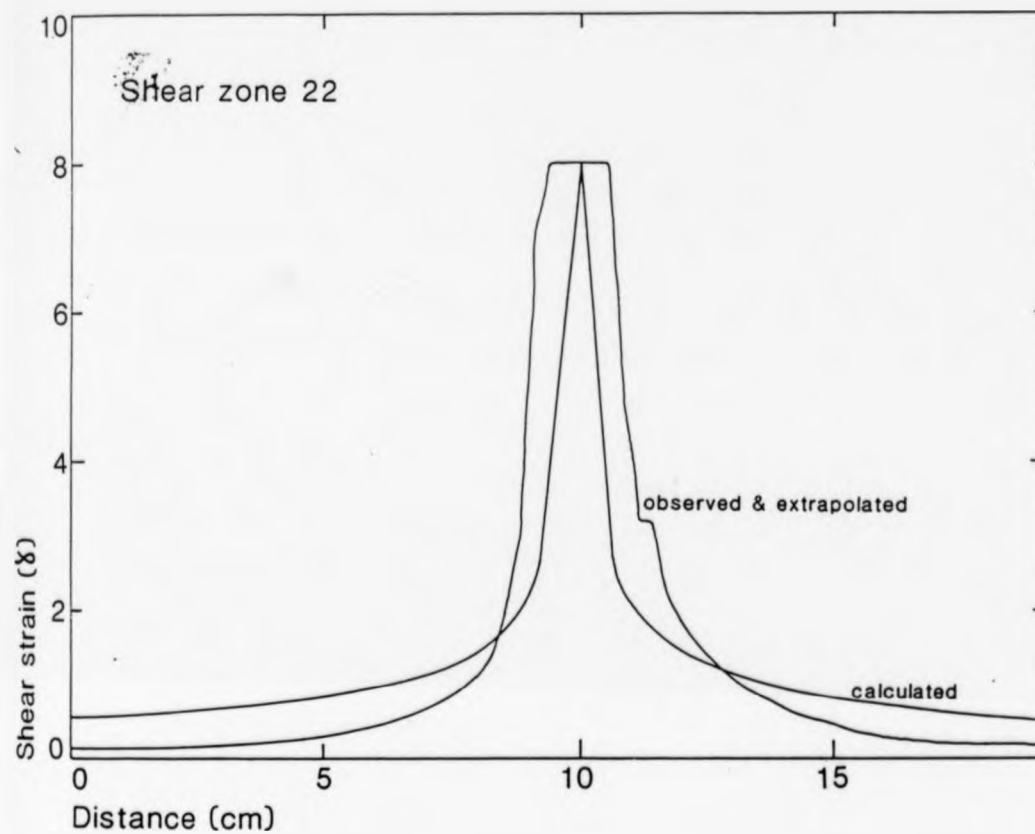


Fig 4.38 Comparison of the calculated strain profile constructed using the higher estimate of displacement obtained from the extrapolated observed strain profile, showing increased similarity due to the incorporation of the very low strain part of the observed profile.

Fig 4.39

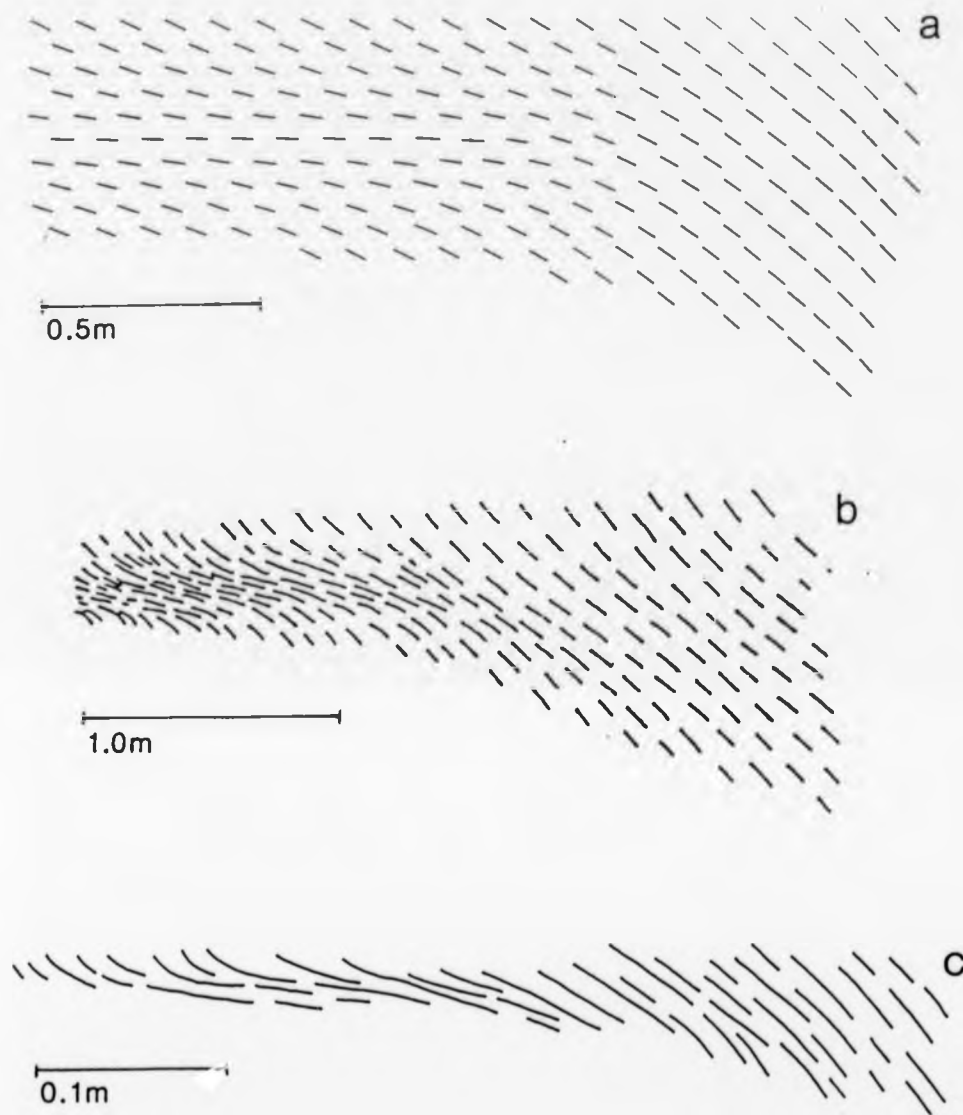


Fig 4.39 Comparison of foliation orientations at the tip of shear zones;

a/ Calculated using the model ($T = 550^{\circ}\text{C}$, $\sigma_L = 0.5 \text{ Kb}$, $C = 100 \text{ cm}$ $V = 1 \times 10^{-11} \text{ cm/sec}$).

b/ Shear zone in alpinised Hercynian granite (Ramsay & Allison 1979).

c/ Shear zone 11, Lewisian epidiorite (this study).

4.III CONCLUSIONS

The development of the model to include shear strain and displacement leads to several important conclusions;

1/ Propagation velocity must change with increasing shear zone length, assuming all other boundary conditions remain constant. This is necessary to maintain a constant strain profile along the length of the zone, as observed from natural examples. The results in chapter 3 support this conclusion.

2/ Propagation velocity will change as the shear zone crosses a lithological boundary, again assuming all other boundary conditions remain constant. Displacement on the shear zone cannot change significantly across boundaries and so the change is accommodated by the propagation velocity.

3/ The relationship between displacement and the boundary conditions may be calculated and quantified.

To apply the model to naturally occurring shear zones a variety of techniques may be used, the stress/temperature/propagation velocity diagrams, strain profile comparison and foliation orientation comparison. Estimates of the time taken to propagate to the observed lengths may be used to further constrain the values obtained. The results from all these techniques support the model and are in agreement with the conclusions of chapter 3. There is a particularly strong agreement using the strain profile and foliation orientation comparison techniques. The results of the calculations for the time span of operation of the shear zones indicate that all zones were

active for approximately the same length of time, which agrees closely with the conclusions of Norton (1982). Possibly the most significant conclusion from the application of the model is that the mechanisms of initiation and the local conditions at the time of initiation may be the dominant factors influencing the final length of the shear zone and the amount of displacement that it can accommodate.

CHAPTER 5

5.1 CONCLUSIONS

The aim of this study was to present a model for the development of shear zones. The following conclusions are presented in a sequence commencing with the initiation of a shear zone, through its development, to the cessation of deformation on the zone

5.1.1 Initiation

It is impossible to draw any definite conclusions about the initiation of shear zones. It is probable that localization on some scale is necessary to initiate the formation of the zone. This could be on a microscale where a misaligned crystal or a stress concentration around a larger or less deformable grain could be all that is required to start the propagation of a shear zone. The size and/or nature of this initial perturbation appears to be of prime importance in determining the final dimensions of the shear zone (see 5.1.7).

5.1.2 Localization versus Propagation

Once the shear zone exists as an area of locally higher strain the mechanism by which it grows becomes important. Localization on structures such as dyke margins, fold limbs or veins is commonly observed, and weaker planes in suitable orientations will be exploited in accommodating a remote stress or displacement. It is obvious however that shear zones do occur in rocks that are relatively homogeneous and so propagation through an isotropic medium must be regarded as the general case for shear zone development.

5.1.3 Relationships between the boundary conditions

The model presented allows the interrelationships between temperature, applied load stress, shear zone half-length, propagation velocity and displacement to be quantified. This illustrates the very strong influence of temperature on the other parameters. A small increase in the ambient temperature can lead to a large increase in the propagation velocity of a shear zone or the applied stress required to propagate a shear zone can be considerably reduced by increasing the temperature or the strain/displacement can be greatly increased by raising the temperature.

5.1.4 The importance of the factor n

The model predicts that shear zones will not form or propagate in materials where the n factor in the dislocation creep flow law is less than 3, as this dictates that the driving stress/stress release ratio would increase towards the shear zone tip, invalidating the model. For materials where n is greater than 3, the ratio decreases towards the tip and for $n = 3$ the ratio is a constant. The fact that shear zones do occur in materials with n values of less than 3 does not invalidate the model. In these cases the deformation may have been accommodated by means other than dislocation creep, and strain softening may also have aided localization of the deformation.

5.1.5 Variation in propagation velocity

The model predicts that the propagation velocity of a shear zone must change throughout its active life in order to maintain a constant strain profile, and hence displacement, along its length. This is due to the influence of the shear zone half-length on the development of the zone. Propagation velocity must also change if the shear zone crosses a lithological boundary, otherwise, assuming that

temperature, half-length and applied stress are constant, the displacement on the zone would have to change across the contact, which is impossible.

5.1.6 Application to natural examples

When applying the model to natural shear zones, it is assumed that the length and displacement of the zone are known. It is then possible to construct a field in terms of temperature, propagation velocity and load stress that defines the range of conditions under which the shear zone could have operated. These can then be further constrained by estimating the length of time over which the zones were operational using the propagation velocity. These are only very rough estimates as the propagation velocity changes through the lifetime of the zone, but used in conjunction with temperature estimates from geothermometry, they can narrow the range of possible values from the temperature/stress/propagation velocity diagrams. The propagation velocities estimated by this method will be an equivalent velocity for the zone at its current length, i.e. a theoretical maximum for the particular zone. The estimates for the length of time of operation of the zones used from the NW Highlands indicate that all the zones were operating for approximately the same length of time regardless of their size.

5.1.7 Final size and displacement

The final dimensions of a shear zone probably depend on the size and/or nature of the initial perturbation on which the shear zone nucleated. If all zones in an area operate for approximately the same length of time then, in order to become dominant, some must propagate faster. Assuming that temperature and load stress are approximately constant within the area, then there is only one possible propagation

velocity for a given shear zone length. Thus if a zone is to become dominant, the initial perturbation from which it grew must have provided a "head start", either in terms of the initial length, or a very local temperature rise, either of which would lead to an increase in the initial propagation velocity.

5.I.8 Displacement/width relationship

The relationship between displacement and width for the shear zones studied from the NW Highlands indicates a regional variation in the amount of movement that can be accommodated on a zone of given size. This is probably due to a temperature increase towards the N of the study area allowing the zones in the N of the area to accommodate greater displacements. This agrees closely with the conclusions from the model with respect to the relationship between temperature and displacement (see 5.I.3).

5.I.9 Tip zones

The tip zones studied all showed the development of a foliation at 45° to the shear zone in front of the shear zone tip, in close agreement with the predictions of the model. The widening of the zone of deformation around the tip is attributed to the continuation of displacement after propagation has ceased. The widening of the tip region appears to be more pronounced on the side of the zone that is displacing towards the tip (Fig 4.39) i.e. the area that is undergoing compression (Fig 1.12). The continuation of displacement when propagation has ceased followed by a resumption of propagation could lead to a curving of the shear zone that would result in the formation of a shear zone network where the initial deformation was accommodated by several sub-parallel shear zones. This is a development of the model proposed by Coward (1976).

5.I.10 Justification of the approach to modelling

All the results obtained from the model give geologically realistic values and the matching of strain profiles and foliation orientation patterns to natural examples all show a close fit. The conclusions therefore support the analogy of a propagating crack in an elastic medium, which appears to be a valid basis for a model of shear zone development.

5.II LIMITATIONS

5.II.1 Limitations of the approach

The principal limitations of the approach used in this study are the lack of suitable and reliable rheological data and the inadequacy of the field techniques available.

The published rheological data deal almost entirely with either single crystals or monomineralic aggregates; there are a few values available for natural rocks but these are scarce. Even for the comparatively simple case of quartz, there is a wide range of possible values that could be used. Any attempt to derive a mathematical flow law for the deformation of metamorphic rocks containing abundant prismatic minerals, such as hornblende and biotite, is bound to be a poor approximation for the true nature of the deformation, but until this data is available, the flow laws for plagioclase have been used.

The field and laboratory techniques available at present require near perfect examples to obtain useable results. If it were possible to determine temperature, applied stress and strain accurately for any shear zone then the model could be much more thoroughly tested and better constrained.

These limitations must be considered when applying the results of the model to any natural examples nevertheless important qualitative conclusions can be drawn from the results.

REFERENCES

- ATTFIELD, P.R. 1987. The structural history of the Canisp Shear Zone.
In: The evolution of the Lewisian and comparable Precambrian high-grade terrains. (Eds. PARK, R.G. & TARNEY, J.) Geol. Soc. Spec. Publ. 27, 165-173
- BAK, J., KORSTGARD, J.A. & SORENSEN, K. 1975. A major shear zone in the Precambrian of west Greenland. Tectonophysics 27, 191-209
- BALL, A. 1980. A theory of geological faults and shear zones. Tectonophysics 61, T1-T5
- BEACH, A. 1973. The mineralogy of high temperature shear zones at Scourie, N.W.Scotland. J. Petrol. 14, 231-248
- BEACH, A. 1974. The measurement and significance of displacements on a Laxfordian shear zone, N.W.Scotland. Proc. Geol. Ass. 85, 13-21
- BEACH, A. 1976. The interrelations of fluid transport, deformation, geochemistry and heat flow, in early Proterozoic shear zones in the Lewisian complex. Phil. Trans. R. Soc. A280, 569-604
- BEACH, A. 1978. The Scourie - Laxford region (Lewisian). In: The Lewisian and Torridonian rocks of North West Scotland. Geol. Assoc. guide 21, 14-27
- BEACH, A. & FYFE, W.S. 1972. Fluid transport and shear zones at Scourie, Sutherland: evidence of overthrusting. Contr. Min. and Pet. 36, 175-180

- BELL, T.H. 1981. Foliation development - the contribution, geometry, and significance of progressive, bulk, inhomogeneous shortening. Tectonophysics 75, 257-272
- BELL, T.H. & ETHERIDGE, M.A. 1973. Microstructures of mylonites and their descriptive terminology. Lithos 6, 337-348
- BELL, T.H. & ETHERIDGE, M.A. 1976. The deformation and recrystallization of quartz in a mylonite zone. Tectonophysics 32, 235-267
- BODINE, J.H., STECKLER, M.S. & WATTS, A.B. 1981. Observations of flexure and the rheology of the oceanic lithosphere. J. Geophys. Res. 86, 3695-3707
- BOUCHEZ, J-L. & PECHER, A. 1976. Plasticite du quartz et sans de cisaillement dans les quartzites du Grand Chevauchement, Central Himalayen. Bull. Soc. Geol. Fr. 6, 1375-1384
- BOWDEN, P.B. 1970. A criteria for inhomogeneous plastic deformation. Phil. Mag. 22, 455-462
- BRUN, J.P. & COBBOLD, P.R. 1980. Strain heating and thermal softening in continental shear zones: a review. J. Struct. Geol. 2, 149-158
- BURG, J.P. & LAURENT, Ph. 1978. Strain analysis of a shear zone in a granodiorite. Tectonophysics 47, 15-42
- BURG, J.P., WILSON, C.J.L. & MITCHELL, J.C. 1986. Dynamic recrystallization and fabric development during the simple shear deformation of ice. J. Struct. Geol. 8, 857-870

- BURROWS, S.E., HUMPHREYS, F.J. & WHITE, S.H. 1979. Dynamic recrystallization and textural development in magnesium deformed in compression at elevated temperatures. 5th. Int. Conf. of strength of metals and alloys Aachen, 607-615
- CARISTAN, Y. 1982. The transition from high temperature creep to fracture in Maryland diabase. J. Geophys. Res. **87**, 6781-6790
- CARTER, N.L. & AVE'LALLEMENT, H.G. 1970. High temperature flow of dunite and peridotite. Geol. Soc. Amer. Bull. **81**, 2181-2202
- CARTER, N.L., ANDERSON, D.A., HANSEN, F.D. & KRANZ, R.L. 1981. Creep and creep rupture of granitic rocks. In: The mechanical behaviour of crustal rocks. (Eds. CARTER, N.L., FRIEDMAN, M., LOGAN, J.M. & STEARNS, D.W.) Am. Geophys. Un. Geophysical Monograph, **24**, 61-82
- CASEY, M. 1980. Mechanics of shear zones in isotropic dilatant materials. J. Struct. Geol. **2**, 143-147
- COBBOLD, P.R. 1977(a). Description and origin of banded deformation structures. I. Regional strain, local perturbations and deformation bands. Can. J. Earth Sci. **14**, 1721-1731
- COBBOLD, P.R. 1977(b). Description and origin of banded deformation structures. II. Rheology and growth of banded perturbations. Can. J. Earth Sci. **14**, 2510-2523
- COWARD, M.P. 1976. Strain within ductile shear zones. Tectonophysics **34**, 181-197
- COWARD, M.P. 1980. Shear zones in the Precambrian crust of southern Africa. J. Struct. Geol. **2**, 19-27

- COWARD, M.P. & PARK, R.G. 1987. The role of mid-crustal shear zones in the early Proterozoic evolution of the Lewisian. In: The evolution of the Lewisian and comparable Precambrian high grade terrains. (Eds. PARK, R.G. & TARNEY, J.) Geol. Soc. Spec. Publ. 27,
- CRESSWELL, D. 1972. The structural development of the Lewisian rocks on the north shore of Loch Torridon, Ross-shire. Scott. J. Geol. 8, 293-308
- DICKINSON, B.B. & WATSON, J. 1976. Variations in crustal level and geothermal gradient during the evolution of the Lewisian complex of Northwest Scotland. Precambrian Res. 3, 363-374
- DILLAMORE, I.L., ROBERTS, J.G. & BUSH, A.C. 1979. Occurrence of shear bands in heavily rolled cubic metals. Met. Sci. J. 13, 73-77
- DIXON, J. & WILLIAMS, G. 1983. Reaction softening in mylonites from the Arnaboll Thrust, Sutherland. Scott. J. Geol. 19, 157-168
- ESCHER, A., ESCHER, J. & WATTERSON, J. 1975. The reorientation of the Kangamuit dyke swarm, West Greenland. Can. J. Earth. Sci. 12, 158-173
- EVANS, C.R. 1965. Geochronology of the Lewisian basement near Lochinver, Sutherland. Nature, London 207, 638-641
- EVANS, C.R. & LAMBERT, R. St-J. 1974. The Lewisian of Lochinver, Sutherland; the type area for the Inverian metamorphism. J. Geol. Soc. Lond. 130, 125-150
- FLIETOUT, L. & FROIDEVEAUX, C. 1980. Thermal and mechanical evolution of shear zones. J. Struct. Geol. 2, 159-164

- FLINN, D. 1977. Transcurrent faults and associated cataclasis in Shetland. J. Geol. Soc. Lond. 133, 231-248
- FRANSSEN, R.C.M.W., SPIERS, C.J. & BROCKMEIER, H.-G. 1987. Mechanical behaviour, microstructures & textures of polycrystalline halite in simple shear deformation. Terra Cognita 7, 306
- GERRARD, J.A.F., PERUTZ, M.F. & ROCH, A. 1952. Measurement of the velocity distribution along a vertical line through a glacier. Proc. R. Soc. A213, 546
- GLEN, J.W. 1953. The rate of flow of polycrystalline ice. Nature Lond. 172, 721
- GOETZE, C. 1978. The mechanisms of creep in olivine. Phil. Trans. R. Soc. Lond. A288, 99-199
- GOETZE, C. & KHOLSTEDT, D.L. 1973. Laboratory study of dislocation climb and diffusion in olivine. J. Geophys. Res. 78, 5961-71
- GOLDSTEIN, A.G. 1980. Magnetic susceptibility anisotropy of mylonites from the Lake Char mylonite zone, southeastern New England. Tectonophysics 66, 197-212
- GROCOTT, J. & WATTERSON, J. 1980. Strain profile of a boundary within a large ductile shear zone. J. Struct. Geol. 2, 111-117
- HEARD, H.C. 1976. Comparison of the flow properties of rocks at crustal conditions. Phil. Trans. R. Soc. Lond. A283, 173-186
- JAEGER, J.C. & COOK, N.G.W. 1979. Fundamentals of rock mechanics. Chapman & Hall.
- JEGOUZO, P. 1980. The South American Shear Zone. J. Struct. Geol. 2, 39-47
- JENSEN, L.N. 1984. Quartz microfabric of the Laxfordian Canisp Shear Zone, N.W.Scotland. J. Struct. Geol. 6, 293-302

- JOHNSON, M.R.W. 1967. Mylonite zones and mylonite banding. Nature Lond. 213, 246-247
- KERRICH, R., FYFE, W.S., GORMAN, B.E. & ALLISON, I. 1977. Local modification of rock chemistry by deformation. Contr. Min. and Pet. 65, 183-190
- KERRICH, R., ALLISON, I., BARNETT, R.L., MOSS, S. & STARKEY, J. 1980. Microstructural and chemical transformations accompanying deformation of a granite in a shear zone at Mieville, Switzerland; with implications for stress corrosion cracking and superplastic flow. Contr. Min. and Pet. 73, 221-242
- KHOLSTEDT, D.L. & GOETZE, C. 1974. Low stress, high temperature creep in olivine single crystals. J. Geophys. Res. 79, 2045-2051
- KHOLSTEDT, D.L., GOETZE, C. & DURHAM, W.B. 1976. Experimental deformation of single crystal olivine, with application to flow in the mantle. In: The physics and chemistry of minerals and rocks (Ed. RUNCORN, S.K.) London, John Wiley. 35-49.
- KHOURY, S.G. 1968. The structural geology and geological history of the Lewisian rocks between Kylesku and Geisgeil, Sutherland, Scotland. Krystalinikum 6, 41-78
- KNIPE, R.J. & WHITE, S.H. 1979. Deformation in low grade shear zones in the Old Red Sandstone of South Wales. J. Struct. Geol. 1, 53-66
- KOCH, P.S., CHRISTIE, J.M. & GEORGE, R.P. 1980. Flow law of 'wet' quartzite in the alpha-quartz field. Trans. Amer. Geophys. Un. 61, 376

- LAMBERT, R.St-J. & HOLLAND, G. 1972. A geochronological study of the Lewisian from Loch Laxford to Durness, Sutherland, NW Scotland
J. Geol. Soc. Lond. **128**, 3-19
- LAPWORTH, C. 1885. The Highland controversy in British geology: its causes, course and consequences. Nature Lond. **32**, 558-559
- LAURENT, P. & ETCHECOPAR, A. 1976. Mise en evidence a l'aide de la fabrique du quartz d'un cisaillement simple a deversement ouest dans le Massif de Dora Maira (Alpes Occidentales).
Bull. Soc. Geol. Fr. **18**, 1387-1393
- LAWN, B.R. & WILSHAW, T.R. 1975. Fracture of brittle solids.
Cambridge University Press.
- LISTER, G.S., WILLIAMS, P.F., ZWART, H.J. & LISLE, R.J. 1977. Fabrics, microstructures and microtectonics. Tectonophysics **39**, 1-499
- LISTER, G.S. & WILLIAMS, P.F. 1979. Fabric development in shear zones: theoretical controls and observed phenomena.
J. Struct. Geol. **1**, 283-297
- LOCKETT, J.M. & KUSZNIR, N.J. 1982. Ductile shear zones: some aspects of constant slip velocity and constant shear stress models.
Geophys. J. R. Astr. Soc. **69**, 477-494
- MITRA, G. 1979. Ductile deformation zones in Blue Ridge basement rocks and estimation of finite strains. Bull. Geol. Soc. Amer. **90**, 935-951
- NIAMATULLAH, M. 1984. The Laxfordian structure of the Kenmore Inlier, Ross-shire. Unpubl. Ph.D. thesis, Univ. Keele
- NORTON, M.G. 1982. The kinematic and microstructural development of some shear zones. Unpublished Ph.D. thesis, University of London.

- PALMER, A.C. & RICE, J.R. 1973. The growth of slip surfaces in progressive failure of overconsolidated clays. Proc. R. Soc. Lond. **A332**, 527-548
- PARIS, P.C. & SIH, G.C. 1965. Stress analysis of cracks. In: Fracture toughness testing and its applications. ASTM Spec. Tech. Publ. **381**, 30-81
- PARK, R.G. 1981. Shear zone deformation and bulk strain in granite - greenstone terrain of the Western Superior Province, Canada. Precambrian Res. **14**, 31-47
- PARK, R.G. & TARNEY, J. 1987. The Lewisian complex: a typical Precambrian high-grade terrain In: Evolution of the Lewisian and comparable Precambrian high-grade terrains. (Eds. PARK, R.G. & TARNEY, J.) Geol. Soc. Spec. Publ. **27** 13-25
- PAVLIS, T.L. 1987. The role of strain heating in the evolution of megathrusts. J. Geophys. Res. **91**, 12407-12422
- PEACH, B.N., HORNE, J., CLOUGH, C.T. & HINXMAN, L.W. 1907. The geological structure of the North West Highlands of Scotland. Mem. Geol. Surv. Gt. Britain
- POIRIER, J.P. 1980. Shear localization and shear instability in materials in the ductile field. J. Struct. Geol. **2** 135-142
- POIRIER, J.P., BOUCHEZ, J.L. & JONAS, J.J. 1979. A dynamic model for aseismic ductile shear zones. Earth and Plan. Sci. Letts. **45**, 441-453
- POST, R.L. 1977. High temperature creep of Mt. Burnett dunite. Tectonophysics **42**, 75-110

- POST, R.L. & GRIGGS, D.T. 1973. The earths mantle, evidence for non-Newtonian flow. Science 181, 1242-1244
- RAMSAY, J.G. 1980. Shear zone geometry: a review. J. Struct. Geol. 2, 175-187
- RAMSAY, J.G. & GRAHAM, R.H. 1970. Strain variation in shear belts. Can. J. Earth. Sci. 7, 786-813
- RAMSAY, J.G. & ALLISON, I. 1979. Structural analysis of shear zones in an alpinised Hercynian granite. Schweiz. Min. Pet. 59 251-279
- ROSS, J.V. 1973. Mylonitic rocks and flattened garnets in the southern Okanagai of British Columbia. Can. J. Earth Sci. 10, 1-17
- RUTTER, E.H. 1972. The influence of interstitial water on the rheological behaviour of calcite rocks. Tectonophysics 14 13-33
- SCHUBERT, G. & YUEN, D.A. 1978. Shear heating instability in the earths upper mantle. Tectonophysics 50, 197-205
- SCHWENN, M.B. & GOETZE, C. 1977. Creep of olivine during hot pressing Tectonophysics 48, 41-60
- SEGALL, P. & SIMPSON, C. 1986. Nucleation of ductile shear zones on dilatant fractures. Geology 14, 56-59
- SHELTON, G. & TULLIS, J. 1981. Experimental flow laws for crustal rocks. Trans. Amer. Geophys. Un. 62, 396
- SHERATON, J.W., SKINNER, A.C. & TARNEY, J. 1973a. The geochemistry of the Scourian gneisses of the Assynt district. In: The Early Precambrian of Scotland and related rocks of Greenland. (Eds. PARK, R.G. & TARNEY, J.) Univ. of Keele, 13-30

- SHERATON, J.W., WHEATLEY, T.J. & WRIGHT, A.E. 1973b. The structural history of the Assynt district. In: The Early Precambrian of Scotland and related rocks of Greenland. (Eds. PARK, R.G. & TARNEY, J.) Univ. of Keele, 31-44
- SIBSON, R.H. 1977. Fault rocks and fault mechanisms. J. Geol. Soc. Lond. 133, 191-213
- SIBSON, R.H. 1979. Fault rocks and structures as indicators of shallow earthquake source processes. U.S.G.S. Open File Report 79-1239, 296-303
- SIMPSON, C. 1980. Oblique girdle orientation patterns of quartz c-axes from a shear zone in the basement core of the Maggia Nappe, Ticino, Switzerland. J. Struct. Geol. 2, 243-247
- STOCKER, R.L. & ASHBY, M.F. 1973. On the rheology of the upper mantle. Rev. Geophys. 11, 391-497
- TARNEY, J. 1963. Assynt dykes and their metamorphism. Nature, London 199, 672-674
- TARNEY, J. 1973. The Scourie dyke suite and the nature of the Inverian event in Assynt. In: The Early Precambrian of Scotland and related rocks of Greenland. (Eds. PARK, R.G. & TARNEY, J.) Univ. of Keele, 105-118
- TARNEY, J. 1978. Achmelvich Bay, Assynt (Lewisian). In: The Lewisian and Torridonian rocks of North West Scotland. Geol. Assoc. Guide, 21, 35-50
- TEALL, J.J.H. 1885. The metamorphosis of dolerite into hornblende schist. J. Geol. Soc. Lond. 41, 133-145
- TURCOTTE, D.L. & SCHUBERT, G. 1982. Geodynamics John Wiley.

- WATTERSON, J. 1979. Strain and strain rate gradients at the ductile levels of faulting displacement. U.S.G.S. Open File Report 79-1239, 235-255
- WEERTMAN, J. & WEERTMAN, J.R. 1975. High temperature creep of rock and mantle viscosity. Annu. Rev. Earth and Plan. Sci. 3 293-315
- WEIJMARS, R. 1987. The Palomares brittle-ductile shear zone of southern Spain. J. Struct. Geol. 9, 139-157
- WESTWOOD, A.R.C., GOLDHEIM, D.L. & LYE, R.G. 1967. Rebinder effects in MgO. Phil. Mag. 16, 505-519
- WHEELER, J. 1987. The determination of true shear senses from the deflection of passive markers in shear zones. J. Geol. Soc. 144, 73-77
- WHITE, S.H. & KNIPE, R.J. 1978. Transformation and reaction enhanced ductility in rocks. J. Geol. Soc. Lond. 135, 513-516
- WHITE, S.H., BURROWS, S.E., CARRERAS, J., SHAW, N.D. & HUMPHREYS, F.J. 1980. On mylonites in ductile shear zones. J. Struct. Geol. 2, 175-187
- WILLIAMS, G. & DIXON, J. 1982. Reaction and geometrical softening in granitoid mylonites. Textures and Microstructures 4, 223-239
- YUEN, D.A., FLIETOUT, L., SCHUBERT, G. & FROIDEVAUX, C. 1978. Shear deformation zones along major transform faults and subducting slabs. Geophys. J. R. Astr. Soc. 54, 93-119
- ZEUCH, D.H. 1983. On the relationship between grain size sensitive creep and dynamic recrystallization of olivine. Tectonophysics 93, 151-169

APPENDIX 1

THE COMPUTER PROGRAMMES

All the programmes used for the model described in this study are written in basic and were run on the GEC 4190 mainframe at Keele. The early programmes use a finite difference method of integration to calculate stresses and strains around the shear zone tip. Later a Simpsons rule integration was used to improve the accuracy of the calculation for the driving stress/stress release ratio. The model inevitably suffers from "edge effects" caused by the necessity of integrating from a finite distance away from the tip. This is overcome by introducing a "fiddle factor" at the start of the integration. This is derived by a refining process which starts with a very "coarse" integration commencing extremely far away from the shear zone which is used to obtain a value for a point closer to the tip. This value is then introduced as a starting point for the next integration and the process is repeated until the iterative steps are small enough to give the definition required. By this method it is possible to achieve the effect of integrating from essentially infinity, with a reasonable degree of accuracy without using a vast amount of computer time.

All the models use the co-ordinate system described in figure 3.8 and integrate parallel to the shear zone.

TAURES

This programme calculates the Cartesian Stresses, the principal stresses, the differential stress and the angle of the principal stress axes around a shear zone tip. (see equations 3.1 to 3.6 and figures 3.5 to 3.12)

```

0010 REM PLOTTING PROG FOR DIFF,S1,S2,X,Y,Z,T,0.*****
0020 FILES #3,'&DUMP'
0030 PRINT "CRACK TIP STRESS INTEGRATION"
0042 PRINT "INPUT BIN WIDTH"
0044 INPUT B
0048 PRINT "INPUT I"
0050 INPUT L
0052 PRINT "INPUT SPACE STEP SIZE"
0054 INPUT S9
0056 PRINT "INPUT WIDTH"
0057 INPUT L9
0058 PRINT "INPUT PARAMETER REQD 1=DIFF 2=S1 3=S2 4=X 5=Y 6=Z 7=TMAX 8=THETA"
0059 INPUT P
0060 PRINT "INPUT VALUE FOR POINT 0,0"
0061 INPUT P1
0062 PRINT "INPUT OPTION FOR CRACK VALUE 1=DEFAULT 2=INPUT VALUE"
0063 INPUT D
0064 IF D=1 THEN GOTO 0070
0065 PRINT "INPUT CRACK VALUE"
0066 INPUT P2
0070 PRINT #3,"32"
0081 PRINT #3,"CLEAR"
0082 PRINT #3,"DATA"
0083 PRINT #3,"REG"
0085 REM SET UP XY GRID & CONVERT TO POLAR CO-ORDINATES*****
0090 FOR Y=-L9 TO L9
0100 Y1=Y*S9
0110 FOR I=-L TO L
0120 X1=I*B
0121 J=Y+L9
0130 X2=ABS(X1)
0140 Y2=ABS(Y1)
0150 IF Y2=0 THEN A=0
0155 IF Y2=0 THEN R=X2
0160 IF Y2=0 THEN GOTO 0201
0161 IF X2=0 THEN A=1.57079635
0162 IF X2=0 THEN R=Y2
0163 IF X2=0 THEN GOTO 0200
0170 A=ATN(Y2/X2)
0179 R1=Y2^2+X2^2
0180 R=SQR(R1)
0181 IF X1>0 THEN A=1.57079635-A
0190 IF X1>0 THEN A=A+1.57079635
0200 IF Y1>0 THEN A=A*(-1)
0201 REM COMPUTE ANGULAR FUNCTIONS*****
0205 IF D=2 THEN GOTO 0214
0211 IF X1=0 THEN GOTO 0213
0212 GOTO 0220
0213 IF Y=0 THEN GOTO 0562
0214 IF X1>-1 THEN GOTO 0216
0215 GOTO 0220
0216 IF Y=0 THEN GOTO 0564
0220 A4=3*A/2
0230 A5=A/2
0240 F1=SIN(A4)
0250 F2=SIN(A5)
0260 F3=COS(A4)
0270 F4=COS(A5)
0280 REM FOR XX*****
0290 E1=2+(F4*F3)
0300 X9=F2*E1*(-1)
0310 REM FOR YY*****
0320 Y9=F2*F4*F3
0330 REM FOR XY*****

```

```
0360 REM COMPUTE STANDARDISED STRESS INTENSITY FUNCTION*****
0370 C4=1^0.5
0380 C5=2*R
0390 C6=C5^0.5
0400 C7=C4/C6
0410 X8=C7*X9
0420 Y8=C7*Y9
0430 Z8=C7*Z9
0431 H1=3.1415927/2
0432 IF Y=0 THEN T2=H1
0433 IF Y=0 THEN GOTO 0440
0434 X7=X8-Y8
0435 Z7=2*Z8
0436 T1=Z7/X7
0437 T2=ATN(T1)
0440 REM COMPUTE PRINCIPAL STRESSES*****
0450 U1=(X8-Y8)^2
0460 U2=0.25*U1
0470 U3=(Z8^2)+U2
0480 U4=U3^0.5
0490 U5=0.5*(X8+Y8)
0500 U=U5+U4
0510 V=U5-U4
0520 S1=U-V
0521 T3=SIN(T2)
0522 T4=S1*T3
0523 T=T4*(-0.5)
0524 IF P=1 THEN PRINT #3,S1
0525 IF P=2 THEN PRINT #3,U
0526 IF P=3 THEN PRINT #3,V
0528 IF P=4 THEN PRINT #3,X8
0540 IF P=5 THEN PRINT #3,Y8
0550 IF P=6 THEN PRINT #3,Z8
0551 IF P=7 THEN PRINT #3,T
0561 GOTO 0570
0562 PRINT #3,P1
0563 GOTO 0570
0564 PRINT #3,P2
0570 NEXT I
0600 NEXT Y
0605 PRINT #3,"OK"
0610 STOP
0620 END
```

PLSTRAIN

This programme calculates the strain () around a crack tip for any rheology required. An artificial peak value is inputted to allow the plotter to complete the diagrams. (See equation 3.22 and figures 3.13 to 3.15)

```

0010 REM PROG TO CALCULATE STRAIN AROUND A CRACK TIP*****
0012 FILES #3,'&DUMP'
0014 PRINT "CRACK TIP STRAINS"
0018 REM INPUT VARIABLES*****
0019 REM *****
0022 PRINT "INPUT BIN WIDTH"
0024 INPUT B
0028 PRINT "INPUT I"
0030 INPUT L
0032 PRINT "INPUT SPACE STEP SIZE"
0034 INPUT S9
0036 PRINT "INPUT WIDTH"
0037 INPUT L9
0038 PRINT "INPUT POWER FOR POWER LAW"
0039 INPUT P
0042 PRINT "INPUT CRACK HALF-LENGTH IN CM."
0044 INPUT C
0046 PRINT "INPUT LOAD SHEAR STRESS IN KBARS"
0047 INPUT L5
0050 PRINT "INPUT TEMPERATURE"
0051 INPUT T
0054 PRINT "INPUT PROPOGATION VELOCITY IN CM PER SEC"
0056 INPUT V1
0060 PRINT "INPUT A"
0061 INPUT A8
0064 PRINT "INPUT B*TM "
0065 INPUT A9
0066 PRINT "INPUT PEAK VALUE FOR CRACK"
0067 INPUT Q9
0068 L6=L5*10^9
0070 V2=1/V1
0071 T1=T+273
0072 DIM D(100)
0074 PRINT #3,"32"
0075 PRINT #3,"CLEAR"
0076 PRINT #3,"DATA"
0077 PRINT #3,"REG"
0085 REM SET UP XY GRID & CONVERT TO POLAR CO-ORDINATES*****
0086 REM *****
0090 FOR Y=-L9 TO L9
0100 Y1=Y*S9
0110 FOR I=-L TO L
0120 X1=I*B
0121 J=Y+L9
0130 X2=ABS(X1)
0140 Y2=ABS(Y1)
0150 IF Y2=0 THEN A=0
0155 IF Y2=0 THEN R=X2
0160 IF Y2=0 THEN GOTO 0205
0161 IF X2=0 THEN A=1.57079635
0162 IF X2=0 THEN R=Y2
0163 IF X2=0 THEN GOTO 0200
0170 A=ATN(Y2/X2)
0179 R1=Y2^2+X2^2
0180 R=SQR(R1)
0181 IF X1>0 THEN A=1.57079635-A
0190 IF X1>0 THEN A=A+1.57079635
0200 IF Y1>0 THEN A=A*(-1)
0205 REM COMPUTE ANGULAR FUNCTIONS*****
0206 REM *****
0211 IF X1>-1 THEN GOTO 0213
0212 GOTO 0220
0213 IF Y=0 THEN GOTO 0565

```

```

0250 F2=SIN(A5)
0260 F3=COS(A4)
0270 F4=COS(A5)
0280 REM FOR XX*****
0290 E1=2+(F4*F3)
0300 X9=F2*E1*(-1)
0310 REM FOR YY*****
0320 Y9=F2*F4*F3
0330 REM FOR XY*****
0340 E2=1-(F1*F2)
0350 Z9=F4*E2
0360 REM COMPUTE STRESS INTENSITY FUNCTION*****
0361 REM *****
0370 C3=C^0.5
0375 C4=C3*L6
0380 C5=2*R
0390 C6=C5^0.5
0400 C7=C4/C6
0410 X8=C7*X9
0420 Y8=C7*Y9
0430 Z8=C7*Z9
0440 REM COMPUTE PRINCIPAL STRESSES*****
0441 REM *****
0450 U1=(X8-Y8)^2
0460 U2=0.25*U1
0470 U3=(Z8^2)+U2
0480 U4=U3^0.5
0490 U5=0.5*(X8+Y8)
0500 U=U5+U4
0502 V=U5-U4
0504 S=U-V
0505 S1=S/(10^9)
0506 S2=S1^P
0507 A7=(-A9/T1)
0508 G1=A8*EXP(A7)
0510 G2=G1*S2
0512 S3=G2*V2
0522 IF I=-L THEN GOTO 0528
0525 S4=S3*B
0526 GOTO 0540
0528 S4=S3
0540 D(J)=D(J)+S4
0542 REM OUTPUT RESULTS *****
0543 REM *****
0560 PRINT #3, D(J)
0561 GOTO 0570
0565 PRINT #3, Q9
0570 NEXT I
0600 NEXT Y
0605 PRINT #3, "OK"
0610 STOP
0620 END

```

STRESSYO

This programme calculates the differential stress along the $Y = 0$ line immediately in front of the shear zone tip (see equations 3.26 to 3.29).


```
0010 REM PROG TO CALCULATE STRESS DISTRIBUTION ON Y=0 FROM P&S
0020 FILES #3, '&TEMP'
0030 PRINT "INPUT TRAVERSE LENGTH"
0040 INPUT L
0050 PRINT "INPUT DRIVING STRESS"
0060 INPUT S
0070 PRINT "INPUT CRACK HALF LENGTH"
0080 INPUT C
0090 PRINT #3, "21"
0100 PRINT #3, "CLEAR"
0110 PRINT #3, "DATA"
0120 FOR I=L TO 1 STEP -1
0130 X1=2*I
0140 X2=C/X1
0150 X3=X2^0.5
0160 X4=2*S*X3
0170 PRINT #3, X4 I
0180 NEXT I
0190 PRINT #3, "END"
0200 PRINT #3, "OK"
0210 STOP
0220 END
```

NORSIMP

This programme calculates the dimensionless driving stress/stress release ratio along the $Y = 0$ line, it is used to provide the initial value for the refining process that is then used to initiate the integration using DIMRAT2

```

0010 REM PROG TO CALCULATE STR/STREL RATIO ALONG Y=0 USING SIMPSONS RULE*****
0012 FILES #3,'&DUMP'
0018 REM INPUT VARIABLES*****
0019 REM *****
0022 PRINT "INPUT BIN WIDTH"
0024 INPUT B
0028 PRINT "INPUT I"
0030 INPUT L
0038 PRINT "INPUT POWER FOR POWER LAW"
0039 INPUT P
0070 PRINT #3,"21"
0071 PRINT #3,"CLEAR"
0072 PRINT #3,"DATA"
0077 DIM D(5)
0078 DIM F(5)
0110 FOR I=L TO 0 STEP -2
0120 FOR J=1 TO 3
0121 IF J=1 THEN X1=I*B
0122 IF J=2 THEN X1=(I-1)*B
0123 IF J=3 THEN X1=(I-2)*B
0124 REM COMPUTE STRAINS*****
0125 REM *****
0370 C4=1^0.5
0390 C6=(2*X1)^0.5
0400 C7=C4/C6
0430 Z8=C7
0470 U3=(Z8^2)
0480 U4=U3^0.5
0500 U=U4
0502 V=-U4
0504 S=U-V
0505 F(J)=S
0506 S2=F(J)^P
0512 D(J)=S2
0525 NEXT J
0528 E9=D(1)+4*D(2)+D(3)
0530 E8=E9*((2*B)/3)
0535 R=E8+R
0540 Q7=R
0545 Q8=F(3)/Q7
0546 REM OUTPUT RESULTS *****
0547 REM *****
0548 X2=B*(I-2)
0560 PRINT #3, X2 Q8
0561 IF I=4 THEN GOTO 0571
0570 NEXT I
0571 PRINT #3,"END"
0571 PRINT #3,"OK"
0610 STOP
0620 END

```

DIMRAT2

This is essentially the same as NORSIMP only it includes the "fiddle factor" that can be derived from NORSIMP to improve the accuracy of the integration (see equation 3.32 and figure 3.18).

```

0010 REM PROG TO CALCULATE STR/STREL RATIO ALONG Y=0 USING SIMPSONS RULE*****
0012 FILES #3,'&DUMP'
0018 REM INPUT VARIABLES*****
0019 REM *****
0022 PRINT "INPUT BIN WIDTH"
0024 INPUT B
0028 PRINT "INPUT I"
0030 INPUT L
0038 PRINT "INPUT POWER FOR POWER LAW"
0039 INPUT P
0040 PRINT "INPUT FIDDLE FACTOR"
0041 INPUT F9
0070 PRINT #3,"21"
0071 PRINT #3,"CLEAR"
0072 PRINT #3,"DATA"
0077 DIM D(5)
0078 DIM F(5)
0110 FOR I=L TO 0 STEP -2
0120 FOR J=1 TO 3
0121 IF J=1 THEN X1=I*B
0122 IF J=2 THEN X1=(I-1)*B
0123 IF J=3 THEN X1=(I-2)*B
0124 REM COMPUTE STRAINS*****
0125 REM *****
0200 F(J)=X1^(-0.5)
0250 D(J)=X1^(-P/2)
0525 NEXT J
0526 IF I=L THEN R=F9
0528 E9=D(1)+4*D(2)+D(3)
0530 E8=E9*(B/3)
0535 R=E8+R
0540 Q7=R
0545 Q8=F(3)/Q7
0546 REM OUTPUT RESULTS *****
0547 REM *****
0548 X2=B*(I-2)
0549 IF X2=200 THEN GOTO 0570
0560 PRINT #3,      X2      Q8
0561 IF I=4 THEN GOTO 0571
0570 NEXT I
0571 PRINT #3,"END"
0571 PRINT #3,"OK"
0610 STOP
0620 END

```

THE INTERRELATIONSHIP PROGRAMMES

These programmes are derived from equations 3.38 to 3.40 and are used to construct figures 3.25 to 2.48. The programmes listed all use the dry quartz rheology (Koch et al. 1980) but they may be easily changed to use other rheologies.

```
0010 REM PROGRAMME TO CALCULATE THE RELATIONSHIP BETWEEN HALF-LENGTH AND
0020 REM LOAD STRESS FOR DRY QUARTZ (N=3)
0030 FILES #3,'&TEMP'
0040 PRINT "INPUT HALF-LENGTH MINIMUM"
0050 INPUT M1
0060 PRINT "INPUT HALF-LENGTH MAXIMUM"
0070 INPUT M2
0072 PRINT "INPUT STEP SIZE"
0074 INPUT S9
0080 PRINT "INPUT PROPOGATION VELOCITY"
0090 INPUT V
0100 PRINT "INPUT TEMPERATURE"
0110 INPUT T
0120 PRINT "INPUT REAL RATIO"
0130 INPUT R
0140 A=0.126
0150 B=18244.65
0160 E=100
0180 PRINT #3,"21"
0190 PRINT #3,"CLEAR"
0200 PRINT #3,"DATA"
0210 FOR C=M1 TO M2 STEP S9
0215 T1=T+273
0220 Z1=-B/T1
0230 Z2=EXP(Z1)
0240 Z3=A*E*R*Z2*(C/2)*8
0245 Z4=V/Z3
0247 S=Z4^0.5
0250 PRINT #3, S C
0260 NEXT C
0270 PRINT #3,"END"
0280 PRINT #3,"OK"
0290 STOP
0300 END
```

```
0010 REM PROGRAMME TO CALCULATE THE RELATIONSHIP BETWEEN TEMPERATURE AND
0020 REM HALF-LENGTH FOR DRY QUARTZ (N=3)
0030 FILES #3, '&TEMP'
0040 PRINT "INPUT TEMPERATURE MINIMUM"
0050 INPUT M1
0060 PRINT "INPUT TEMPERATURE MAXIMUM"
0070 INPUT M2
0072 PRINT "INPUT STEP SIZE"
0074 INPUT S9
0080 PRINT "INPUT PROPOGATION VELOCITY"
0090 INPUT V
0100 PRINT "INPUT LOAD STRESS"
0110 INPUT S
0120 PRINT "INPUT REAL RATIO"
0130 INPUT R
0140 A=0.126
0150 B=18244.65
0160 E=100
0180 PRINT #3, "21"
0190 PRINT #3, "CLEAR"
0200 PRINT #3, "DATA"
0210 FOR T=M1 TO M2 STEP S9
0211 S1=S*2
0215 T1=T+273
0220 Z1=-B/T1
0230 Z2=EXP(Z1)
0240 Z3=A*E*R*Z2*(S1^2)
0245 C=V/Z3
0250 PRINT #3, C T
0260 NEXT T
0270 PRINT #3, "END"
0280 PRINT #3, "OK"
0290 STOP
0300 END
```



```
0010 REM PROGRAMME TO CALCULATE THE RELATIONSHIP BETWEEN TEMPERATURE AND
0020 REM PROPOGATION VELOCITY FOR DRY QUARTZ (N=3)
0030 FILES #3,'&TEMP'
0040 PRINT "INPUT TEMPERATURE MINIMUM"
0050 INPUT M1
0060 PRINT "INPUT TEMPERATURE MAXIMUM"
0070 INPUT M2
0072 PRINT "INPUT STEP SIZE"
0074 INPUT S9
0080 PRINT "INPUT LOAD STRESS"
0090 INPUT S
0100 PRINT "INPUT CRACK HALF-LENGTH"
0110 INPUT C
0120 PRINT "INPUT REAL RATIO"
0130 INPUT R
0140 A=0.126
0150 B=18244.65
0160 E=100
0170 R1=R/0.5
0180 PRINT #3,"21"
0190 PRINT #3,"CLEAR"
0200 PRINT #3,"DATA"
0210 FOR T=M1 TO M2 STEP S9
0211 S1=S*2
0215 T1=T+273
0220 Z1=-B/T1
0230 Z2=EXP(Z1)
0240 V=A*E*R1*Z2*(S1^2)*(C/2)
0250 PRINT #3, V T
0260 NEXT T
0270 PRINT #3,"END"
0280 PRINT #3,"OK"
0290 STOP
0300 END
```

```
0010 REM PROGRAMME TO CALCULATE THE RELATIONSHIP BETWEEN TEMPERATURE AND
0020 REM LOAD STRESS FOR DRY QUARTZ (N=3)
0030 FILES #3, '&TEMP'
0040 PRINT "INPUT TEMPERATURE MINIMUM"
0050 INPUT M1
0060 PRINT "INPUT TEMPERATURE MAXIMUM"
0070 INPUT M2
0072 PRINT "INPUT STEP SIZE"
0074 INPUT S9
0080 PRINT "INPUT PROPOGATION VELOCITY"
0090 INPUT V
0100 PRINT "INPUT CRACK HALF-LENGTH"
0110 INPUT C
0120 PRINT "INPUT REAL RATIO"
0130 INPUT R
0140 A=0.126
0150 B=18244.65
0160 E=100
0180 PRINT #3, "21"
0190 PRINT #3, "CLEAR"
0200 PRINT #3, "DATA"
0210 FOR T=M1 TO M2 STEP S9
0215 T1=T+273
0220 Z1=-B/T1
0230 Z2=EXP(Z1)
0240 Z3=A*E*R*Z2*(C/2)*8
0245 Z4=V/Z3
0247 S=Z4*0.5
0250 PRINT #3, S T
0260 NEXT T
0270 PRINT #3, "END"
0280 PRINT #3, "OK"
0290 STOP
0300 END
```

```
0010 REM PROGRAMME TO CALCULATE THE RELATIONSHIP BETWEEN HALF-LENGTH AND
0020 REM PROPOGATION VELOCITY FOR DRY QUARTZ (N=3)
0030 FILES #3, '&TEMP'
0040 PRINT "INPUT HALF-LENGTH MINIMUM"
0050 INPUT M1
0060 PRINT "INPUT HALF-LENGTH MAXIMUM"
0070 INPUT M2
0072 PRINT "INPUT STEP SIZE"
0074 INPUT S9
0080 PRINT "INPUT TEMPERATURE"
0090 INPUT T
0100 PRINT "INPUT LOAD STRESS"
0110 INPUT S
0120 PRINT "INPUT REAL RATIO"
0130 INPUT R
0140 A=0.126
0150 B=18244.65
0160 E=100
0170 R1=R/0.5
0180 PRINT #3, "21"
0190 PRINT #3, "CLEAR"
0200 PRINT #3, "DATA"
0210 FOR C=M1 TO M2 STEP S9
0211 S1=S*2
0215 T1=T+273
0220 Z1=-B/T1
0230 Z2=EXP(Z1)
0240 V=A*E*R1*Z2*(S1^2)*(C/2)
0250 PRINT #3, V C
0260 NEXT C
0270 PRINT #3, "END"
0280 PRINT #3, "OK"
0290 STOP
0300 END
```

```
0010 REM PROGRAMME TO CALCULATE THE RELATIONSHIP BETWEEN LOAD STRESS AND
0020 REM PROPOGATION VELOCITY FOR DRY QUARTZ (N=3)
0030 FILES #3,'&TEMP'
0040 PRINT "INPUT LOAD STRESS MINIMUM"
0050 INPUT M1
0060 PRINT "INPUT LOAD STRESS MAXIMUM"
0070 INPUT M2
0072 PRINT "INPUT STEP SIZE"
0074 INPUT S9
0080 PRINT "INPUT TEMPERATURE"
0090 INPUT T
0100 PRINT "INPUT CRACK HALF-LENGTH"
0110 INPUT C
0120 PRINT "INPUT REAL RATIO"
0130 INPUT R
0140 A=0.126
0150 B=18244.65
0160 E=100
0170 R1=R/0.5
0180 PRINT #3,"21"
0190 PRINT #3,"CLEAR"
0200 PRINT #3,"DATA"
0210 FOR S=M1 TO M2 STEP S9
0211 S1=S*2
0215 T1=T+273
0220 Z1=-B/T1
0230 Z2=EXP(Z1)
0240 V=A*E*R1*Z2*(S1^2)*(C/2)
0250 PRINT #3, V S
0260 NEXT S
0270 PRINT #3,"END"
0280 PRINT #3,"OK"
0290 STOP
0300 END
```

EXY

This programme calculates the shear strain () around a shear zone tip (see equations 4.2 & 4.3 and figure 4.1).

```

0010 REM PROG TO CALCULATE SHEAR STRAIN (Exy) AROUND A CRACK TIP*****
0012 FILES #3,'&DUMP'
0014 PRINT "CRACK TIP STRAINS"
0018 REM INPUT VARIABLES*****
0019 REM *****
0022 PRINT "INPUT BIN WIDTH"
0024 INPUT B
0028 PRINT "INPUT I"
0030 INPUT L
0032 PRINT "INPUT SPACE STEP SIZE"
0034 INPUT S9
0036 PRINT "INPUT WIDTH"
0037 INPUT L9
0038 PRINT "INPUT POWER FOR POWER LAW"
0039 INPUT P
0042 PRINT "INPUT CRACK HALF-LENGTH IN CM."
0044 INPUT C
0046 PRINT "INPUT LOAD SHEAR STRESS IN KBARS"
0047 INPUT L5
0050 PRINT "INPUT TEMPERATURE"
0051 INPUT T
0054 PRINT "INPUT PROPOGATION VELOCITY IN CM PER SEC"
0056 INPUT V1
0061 A8=0.126
0065 A9=18274.112
0066 PRINT "INPUT PEAK VALUE FOR CRACK"
0067 INPUT Q9
0070 V2=1/V1
0071 T1=T+273
0072 DIM D(100)
0074 PRINT #3,"32"
0075 PRINT #3,"CLEAR"
0076 PRINT #3,"DATA"
0077 PRINT #3,"REG"
0085 REM SET UP XY GRID & CONVERT TO POLAR CO-ORDINATES*****
0086 REM *****
0090 FOR Y=-L9 TO L9
0100 Y1=Y*S9
0110 FOR I=-L TO L
0120 X1=I*B
0121 J=Y+L9
0130 X2=ABS(X1)
0140 Y2=ABS(Y1)
0150 IF Y2=0 THEN A=0
0155 IF Y2=0 THEN R=X2
0160 IF Y2=0 THEN GOTO 0205
0161 IF X2=0 THEN A=1.57079635
0162 IF X2=0 THEN R=Y2
0163 IF X2=0 THEN GOTO 0200
0170 A=ATN(Y2/X2)
0179 R1=Y2^2+X2^2
0180 R=SQR(R1)
0181 IF X1>0 THEN A=1.57079635-A
0190 IF X1>0 THEN A=A+1.57079635
0200 IF Y1>0 THEN A=A*(-1)
0205 REM COMPUTE ANGULAR FUNCTIONS*****
0206 REM *****
0211 IF X1>-1 THEN GOTO 0213
0212 GOTO 0220
0213 IF Y=0 THEN GOTO 0565
0220 A4=3*A/2
0230 A5=A/2
0240 F1=SIN(A4)

```

```
0280 REM FOR XX*****
0290 E1=2+(F4*F3)
0300 X9=F2*E1*(-1)
0310 REM FOR YY*****
0320 Y9=F2*F4*F3
0330 REM FOR XY*****
0340 E2=1-(F1*F2)
0350 Z9=F4*E2
0360 REM COMPUTE STRESS INTENSITY FUNCTION*****
0361 REM *****
0370 C3=C^0.5
0375 C4=C3*L5
0380 C5=2*R
0390 C6=C5^0.5
0400 C7=C4/C6
0410 X8=C7*X9
0420 Y8=C7*Y9
0430 Z8=C7*Z9
0506 S2=Z8^P
0507 A7=(-A9/T1)
0508 G1=A8*EXP(A7)
0510 G2=G1*S2
0512 S3=G2*V2
0522 IF I=-L THEN GOTO 0528
0525 S4=S3*B
0526 GOTO 0540
0528 S4=S3
0540 D(J)=D(J)+S4
0542 REM OUTPUT RESULTS *****
0543 REM *****
0560 PRINT #3, D(J)
0561 GOTO 0570
0565 PRINT #3, Q9
0570 NEXT I
0600 NEXT Y
0605 PRINT #3, "OK"
0610 STOP
0620 END
```

PROFILE

This programme calculates a theoretical strain profile for a given set of boundary conditions at any point along the length of a shear zone. The version listed uses a dry quartz rheology (Koch et al. 1980) but this may easily be changed (see figures 4.2 to 4.5).


```

0010 REM PROG TO CALCULATE STRAIN PROFILES FROM Exy*****
0012 FILES #3,'&DUMP'
0014 PRINT "CRACK TIP STRAINS"
0018 REM INPUT VARIABLES*****
0019 REM *****
0022 PRINT "INPUT BIN WIDTH"
0024 INPUT B
0028 PRINT "INPUT I"
0030 INPUT L
0032 PRINT "INPUT SPACE STEP SIZE"
0034 INPUT S9
0036 PRINT "INPUT WIDTH"
0037 INPUT L9
0038 PRINT "INPUT POWER FOR POWER LAW"
0039 INPUT P
0042 PRINT "INPUT CRACK HALF-LENGTH IN CM."
0044 INPUT C
0046 PRINT "INPUT LOAD SHEAR STRESS IN KBARS"
0047 INPUT L5
0050 PRINT "INPUT TEMPERATURE"
0051 INPUT T
0054 PRINT "INPUT PROPOGATION VELOCITY IN CM PER SEC"
0056 INPUT V1
0061 A8=0.126
0065 A9=18274.112
0066 PRINT "INPUT PEAK VALUE FOR CRACK"
0067 INPUT Q9
0068 PRINT "INPUT X VALUE FOR PROFILE SECTION"
0069 INPUT H
0070 V2=1/V1
0071 T1=T+273
0072 DIM D(100)
0074 PRINT #3,"21"
0075 PRINT #3,"CLEAR"
0076 PRINT #3,"DATA"
0085 REM SET UP XY GRID & CONVERT TO POLAR CO-ORDINATES*****
0086 REM *****
0090 FOR Y=-L9 TO L9
0100 Y1=Y*S9
0110 FOR I=-L TO L
0120 X1=I*B
0121 J=Y+L9
0130 X2=ABS(X1)
0140 Y2=ABS(Y1)
0150 IF Y2=0 THEN A=0
0155 IF Y2=0 THEN R=X2
0160 IF Y2=0 THEN GOTO 0205
0161 IF X2=0 THEN A=1.57079635
0162 IF X2=0 THEN R=Y2
0163 IF X2=0 THEN GOTO 0200
0170 A=ATN(Y2/X2)
0179 R1=Y2^2+X2^2
0180 R=SQR(R1)
0181 IF X1>0 THEN A=1.57079635-A
0190 IF X1>0 THEN A=A+1.57079635
0200 IF Y1>0 THEN A=A*(-1)
0205 REM COMPUTE ANGULAR FUNCTIONS*****
0206 REM *****
0211 IF X1>-1 THEN GOTO 0213
0212 GOTO 0220
0213 IF Y=0 THEN GOTO 0565
0220 A4=3*A/2
0230 A5=A/2

```

```

0270 F4=COS(A5)
0280 REM FOR XX*****
0290 E1=2+(F4*F3)
0300 X9=F2*E1*(-1)
0310 REM FOR YY*****
0320 Y9=F2*F4*F3
0330 REM FOR XY*****
0340 E2=1-(F1*F2)
0350 Z9=F4*E2
0360 REM COMPUTE STRESS INTENSITY FUNCTION*****
0361 REM *****
0370 C3=C^0.5
0375 C4=C3*L5
0380 C5=2*R
0390 C6=C5^0.5
0400 C7=C4/C6
0410 X8=C7*X9
0420 Y8=C7*Y9
0430 Z8=C7*Z9
0506 S2=Z8^P
0507 A7=(-A9/T1)
0508 G1=A8*EXP(A7)
0510 G2=G1*S2
0512 S3=G2*V2
0522 IF I=-L THEN GOTO 0528
0525 S4=S3*B
0526 GOTO 0540
0528 S4=S3
0540 D(J)=D(J)+S4
0542 REM OUTPUT RESULTS *****
0543 REM *****
0545 IF I=H THEN GOTO 0550
0547 GOTO 0570
0550 PRINT #3, J      D(J)
0552 GOTO 0600
0565 IF I=H THEN GOTO 0567
0566 GOTO 0570
0567 PRINT #3, J      Q9
0568 GOTO 0600
0570 NEXT I
0600 NEXT Y
0602 PRINT #3,"END"
0605 PRINT #3,"OK"
0610 STOP
0620 END

```

THETA

This programme calculates the theoretical foliation orientations around a shear zone tip, again this listing uses the dry quartz parameters. (see equation 4.6 and figures 4.8 & 4.9).

```

0001 REM PROG TO CALCULATE FABRIC ORIENTATION FROM Exy *****
0002 FILES #3,'&DUMP'
0005 PRINT "INPUT BIN WIDTH"
0006 INPUT B
0007 PRINT "INPUT I"
0008 INPUT L
0009 PRINT "INPUT SPACE STEP SIZE"
0010 INPUT S9
0011 PRINT "INPUT WIDTH"
0012 INPUT L9
0015 PRINT "INPUT CRACK HALF-LENGTH"
0016 INPUT C
0019 PRINT "INPUT LOAD STRESS"
0020 INPUT L5
0023 PRINT "INPUT TEMPERATURE"
0024 INPUT T1
0025 T=T1+273
0027 PRINT "INPUT PROPAGATION VELOCITY"
0028 INPUT V1
0029 V2=1/V1
0030 P9=3
0031 A1=0.126
0032 Q=18274.112
0033 DIM D(105)
0070 PRINT #3,"32"
0081 PRINT #3,"CLEAR"
0082 PRINT #3,"DATA"
0083 PRINT #3,"REG"
0085 REM SET UP XY GRID & CONVERT TO POLAR CO-ORDINATES*****
0091 FOR Y=0 TO -L9 STEP -1
0092 J=ABS(Y)
0094 Y1=Y*S9
0095 FOR I=-L TO L
0097 X1=I*B
0130 X2=ABS(X1)
0140 Y2=ABS(Y1)
0150 IF Y2=0 THEN A=0
0155 IF Y2=0 THEN R=X2
0160 IF Y2=0 THEN GOTO 0201
0161 IF X2=0 THEN A=1.57079635
0162 IF X2=0 THEN R=Y2
0163 IF X2=0 THEN GOTO 0200
0170 A=ATN(Y2/X2)
0179 R1=Y2^2+X2^2
0180 R=SQR(R1)
0181 IF X1>0 THEN A=1.57079635-A
0190 IF X1>0 THEN A=A+1.57079635
0200 IF Y1>0 THEN A=A*(-1)
0201 REM COMPUTE ANGULAR FUNCTIONS*****
0202 IF I=0 THEN GOTO 0204
0203 GOTO 0205
0204 IF Y=0 THEN GOTO 0520
0205 A4=3*A/2
0230 A5=A/2
0240 F1=SIN(A4)
0250 F2=SIN(A5)
0260 F3=COS(A4)
0270 F4=COS(A5)
0330 REM FOR XY*****
0340 E2=1-(F1*F2)
0350 Z9=F4*E2
0360 REM COMPUTE STRESS INTENSITY FUNCTION*****
0365 C3=C^0.5

```

```
0400 C7=C4/C6
0435 Z8=C7*Z9
0440 S2=Z8^P9
0445 A7=-Q/T
0450 G1=A1*EXP(A7)
0455 G2=G1*S2
0460 S3=V2*G2
0465 IF I=-L THEN GOTO 0480
0470 S4=S3*B
0475 GOTO 0485
0480 S4=S3
0485 D(J)=D(J)+S4
0490 H1=2/D(J)
0491 H2=H1*0.0174533
0492 H3=ATN(H2)
0493 H4=H3/0.0174533
0494 H5=H4/2
0510 REM OUTPUT RESULTS*****
0515 PRINT #3, D(J)      X1      Y1      H5
0520 NEXT I
0550 PRINT #3, "*****"
0555 NEXT Y
0570 STOP
```

PLDISPL

This programme integrates the shear strain around a shear zone tip to give the displacement field from equation 4.9, this listing uses a plagioclase rheology (see figures 4.10 to 4.12).

```

0001 REM PROG FOR INTEGRATING Txy TO GIVE DISPLACEMENT FIELD*****
0002 FILES #3,'&DUMP'
0005 PRINT "INPUT BIN WIDTH"
0006 INPUT B
0007 PRINT "INPUT I"
0008 INPUT L
0009 PRINT "INPUT SPACE STEP SIZE"
0010 INPUT S9
0011 PRINT "INPUT WIDTH"
0012 INPUT L9
0015 PRINT "INPUT CRACK HALF-LENGTH"
0016 INPUT C
0019 PRINT "INPUT LOAD STRESS"
0020 INPUT L5
0023 PRINT "INPUT TEMPERATURE"
0024 INPUT T1
0025 T=T1+273
0027 PRINT "INPUT PROPAGATION VELOCITY"
0028 INPUT V1
0029 V2=1/V1
0030 P9=3
0031 A1=8.2E+02
0032 Q=28788
0033 DIM D(105)
0034 DIM H(105)
0070 PRINT #3,"32"
0081 PRINT #3,"CLEAR"
0082 PRINT #3,"DATA"
0083 PRINT #3,"REG"
0085 REM SET UP XY GRID & CONVERT TO POLAR CO-ORDINATES*****
0086 M5=(2*L)
0087 FOR P=0 TO M5
0089 P1=P-L
0091 FOR Y=0 TO -L9 STEP -1
0092 J=ABS(Y)
0094 Y1=Y*S9
0095 FOR I=-L TO P1
0097 X1=I*B
0130 X2=ABS(X1)
0140 Y2=ABS(Y1)
0145 IF Y=0 THEN GOTO 0487
0150 IF Y2=0 THEN A=0
0155 IF Y2=0 THEN R=X2
0160 IF Y2=0 THEN GOTO 0201
0161 IF X2=0 THEN A=1.57079635
0162 IF X2=0 THEN R=Y2
0163 IF X2=0 THEN GOTO 0200
0170 A=ATN(Y2/X2)
0179 R1=Y2^2+X2^2
0180 R=SQR(R1)
0181 IF X1>0 THEN A=1.57079635-A
0190 IF X1>0 THEN A=A+1.57079635
0200 IF Y1>0 THEN A=A*(-1)
0201 REM COMPUTE ANGULAR FUNCTIONS*****
0220 A4=3*A/2
0230 A5=A/2
0240 F1=SIN(A4)
0250 F2=SIN(A5)
0260 F3=COS(A4)
0270 F4=COS(A5)
0330 REM FOR XY*****
0340 E2=1-(F1*F2)
0350 Z9=F4*E2

```

```
0380 C5=2*R
0390 C6=C5^0.5
0400 C7=C4/C6
0435 Z8=C7*Z9
0440 S2=Z8^P9
0445 A7=-Q/T
0450 G1=A1*EXP(A7)
0455 G2=G1*S2
0460 S3=V2*G2
0465 IF I=-L THEN GOTO 0480
0470 S4=S3*B
0475 GOTO 0485
0480 S4=S3
0485 D(J)=D(J)+S4
0486 GOTO 490
0487 D(J)=0
0490 NEXT I
0500 D(J)=D(J)*S9
0510 H(P)=H(P)+D(J)
0530 PRINT #3, H(P)    P    J    X1    Y1    D(J)
0535 D(J)=0
0540 NEXT Y
0550 PRINT #3, "*****"
0560 NEXT P
0570 STOP
```


STRESS/TEMPERATURE/VELOCITY PROGRAMMES

These are the programmes used to construct the stress/temperature/velocity diagrams (Figs 4.30 to 4.32). They use a standard displacement from PLDISPL to compare with the measured displacement, this allows the values of stress/temperature/velocity that would be required to produce the measured displacement to be calculated.

```
0010 REM PROG TO WORK OUT THE RELATIONSHIP BETWEEN STRESS/TEMP AND VEL
0020 REM USING THE STANDARD DISPLACEMENT FROM PLDISPL FOR A GIVEN SET OF
0021 REM BOUNDARY CONDITIONS,NS.
0025 PRINT "INPUT DISPLACEMENT FROM PLDISPL"
0026 INPUT X
0030 PRINT "INPUT PROPAGATION VELOCITY USED IN PLDISPL"
0040 INPUT V1
0050 PRINT "INPUT TEMPERATURE USED IN PLDISPL"
0060 INPUT T1
0061 PRINT "INPUT LOAD STRESS USED IN PLDISPL"
0062 INPUT S9
0063 PRINT "INPUT TEMPERATURE REQUIRED"
0064 INPUT T2
0065 PRINT "INPUT LOAD STRESS REQUIRED"
0066 INPUT S7
0070 PRINT "INPUT HALF LENGTH"
0080 INPUT C
0090 PRINT "INPUT MEASURED DISPLACEMENT"
0100 INPUT S
0130 A9=-28788/(T1+273)
0140 A8=8.2E+02*EXP(A9)
0150 C9=(C/2)^1.5
0155 S8=S9^3
0156 A7=A8*S8*C9
0157 Q1=(V1*X)/A7
0158 A5=-28788/(T2+273)
0159 A4=8.2E+02*EXP(A5)
0160 S6=S7^3
0161 A3=A4*S6*C9*Q1
0162 V3=A3/S
0190 PRINT V3
0200 STOP
0210 END
```

```
0010 REM PROG TO WORK OUT THE RELATIONSHIP BETWEEN VEL/TEMP AND LOAD STRESS
0020 REM USING THE STANDARD DISPLACEMENT FROM PLDISPL FOR A GIVEN SET OF
0021 REM BOUNDARY CONDITIONS,NS.
0025 PRINT "INPUT DISPLACEMENT FROM PLDISPL"
0026 INPUT X
0030 PRINT "INPUT PROPAGATION VELOCITY USED IN PLDISPL"
0040 INPUT V1
0050 PRINT "INPUT TEMPERATURE USED IN PLDISPL"
0060 INPUT T1
0061 PRINT "INPUT LOAD STRESS USED IN PLDISPL"
0062 INPUT S9
0063 PRINT "INPUT TEMPERATURE REQUIRED"
0064 INPUT T2
0065 PRINT "INPUT PROPAGATION VELOCITY REQUIRED"
0066 INPUT V2
0070 PRINT "INPUT HALF LENGTH"
0080 INPUT C
0090 PRINT "INPUT MEASURED DISPLACEMENT"
0100 INPUT S
0130 A9=-28788/(T1+273)
0140 A8=8.2E+02*EXP(A9)
0150 C9=(C/2)^1.5
0155 S8=S9^3
0156 A7=A8*S8*C9
0157 Q1=(V1*X)/A7
0158 A5=-28788/(T2+273)
0159 A4=8.2E+02*EXP(A5)
0160 A6=Q1*A4*C9
0170 S1=(S*V2)/A6
0180 S2=S1^(1/3)
0190 PRINT S2
0200 STOP
0210 END
```

profile at lower strains (Fig 4.37). Figure 4.38 has been constructed by extrapolating the strain profile for shear zone 22 at lower strains, recalculating the displacement and using this to draw a revised calculated profile. This takes account of the low strains that are impossible to measure in the field and consequently improves the match of the profiles.

Changing the rheology used to calculate the strain profile does not alter the shape of the profile as this is dictated by the displacement, which is used to constrain the temperature, stress and propagation velocity.

4.II.2.c Foliation orientations.

Comparing the theoretical foliation orientation patterns with observed field examples shows a close agreement between the calculated and the measured orientations around shear zone tip zones. Figure 4.39 shows the measured foliation orientations at the tip of shear zone 11 which is very similar to the calculated pattern for a shear zone in plagioclase at 550 C, 0.5 Kb and 1×10^{-11} cm/sec propagation velocity, the foliation in front of the zone being at approximately 45° to the shear zone walls. Figure 4.39 also shows a shear zone tip from an alpinised Hercynian granite from the Pennine Zone of the Central Alps (Ramsay & Allison 1979), which is also very similar to the calculated pattern. The model predicts that at very low strains there will still be a foliation at 45° to the shear zone, whereas in natural examples the foliation will disappear at low strains, thus the model has a foliation at 45° to the zone even at some distance from the zone as it cannot predict 'undeformed' rock.